

The Cataclysmic Variables from the Palomar-Green Survey

A Thesis

Submitted to the Faculty

in partial fulfillment of the requirements for the

degree of

Doctor of Philosophy

by

F. A. Ringwald

DARTMOUTH COLLEGE

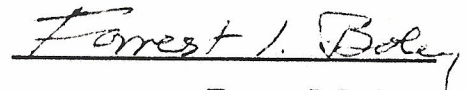
Hanover, New Hampshire

March 1993

Examining Committee:



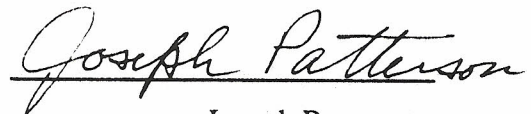
Chairman John R. Thorstensen



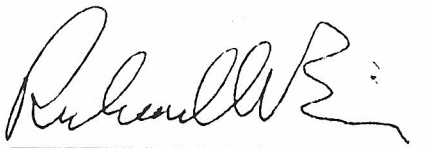
Forrest I. Boley



Robert A. Fesen



Joseph Patterson



Dean of Graduate Studies

Copyright by
Frederick Arthur Ringwald
1993

ABSTRACT

This thesis explores the cataclysmic variables (CVs) found by the Palomar-Green (PG) survey. This is the first compilation of a statistically complete sample of CVs found by ultraviolet color excess, and not outburst behavior. Blue and red follow-up spectrophotometry suggests that 22 of 68 objects classified originally as CVs are hot subdwarfs. Cool companions may be mimicking CVs' flat energy distributions, although the possibility remains that some are face-on CVs. Spectra taken with the *International Ultraviolet Explorer* satellite prove useful for distinguishing difficult cases.

With the CV sample defined, the orbital periods for eleven systems are investigated with radial velocity studies. At 16th magnitude, CV number counts increase by 2.3 mag^{-1} , although this may level off. The luminosity function is examined for the first time, and a trend toward higher space density at low luminosity is suspected. Outburst properties are compiled, and low-luminosity dwarf novæ inflate the total space density to $6 \times 10^{-6} \text{ pc}^{-3}$. I describe all the PG CVs and candidate objects, and show spectra for most. This sample should be useful for population studies, such as measuring the space density with trigonometric parallaxes, or finding the fraction of eclipsing CVs.

A new class of nova-likes, the SW Sextans stars, is characterized by absorption events of the emission lines at spectroscopic phase 0.5, accompanied by large phase lags between the lightcurves and the radial velocity curves and strong high-excitation emission. There are at least six such CVs in this sample of 33, so this mysterious behavior must be common and not peculiar, as previously thought. Five of these six objects eclipse.

Serendipitous results for individual CVs include finding low-frequency quasi-periodic variations in the radial velocity curve of the dwarf nova BZ Ursa Majoris. While erratic from epoch to epoch, these are too coherent to be pure noise. Another dwarf nova, HX Pegasi, is caught with time-resolved spectrophotometry on the rise to outburst. This is the second-ever such observation, and the first with red spectra. HX Pegasi is also confirmed as having a novel subdwarf-K red star.

Acknowledgements

Throughout this work, I was supported by a Dartmouth Fellowship. NASA grant NAG 5 1410, involving the *IUE* observations, was also helpful.

I wish to thank John Thorstensen, foremost for making good on his promise that Dartmouth is “very generous with observing time for graduate students.” His data analysis software also helped greatly, and he also obtained the blue(r) spectrum of PG 2300+166.

Frosty Boley and Gary Wegner wrote lots of letters, necessary in this time of keen job competition. They have also been excellent teachers and inspirational fellow observers.

I am also pleased to have had Joe Patterson on my committee. When new to CVs, I discovered his large 1984 *Astrophysical Journal Supplement* paper, and believe it or not, I read it from start to finish. His phone discussions are always interesting, and I admire his freedom from electronic mail, a paradise lost. Rob Fesen was also on my committee.

Bob Barr, Larry Breuer, Matt Johns, and Peter Mack provided expert observatory support on the many observing runs I had at Michigan-Dartmouth-MIT Observatory (formerly McGraw-Hill Observatory), Kitt Peak, Arizona, which is owned and operated by a consortium of the University of Michigan, Dartmouth College, and the Massachusetts Institute of Technology. I’m going to miss that facility, and the magnificent view from it.

Richard Green was also an enormous help, throughout this work, and particularly generous with his time for digging up many original spectrometer traces from the Palomar-Green survey. The PG catalog includes some 1874 objects, so this was no small task!

Andy Silber just finished his Ph.D. thesis last year, on an X-ray-selected sample of CVs. I guess that makes me his optical counterpart. In a series of electronic mail messages back and forth in early 1992 April, much of the real work of this thesis—poring over the object list line by line, and thrashing out each object carefully—was carried out.

I am grateful for discussions with Graham Berriman, Donald Ferguson, Ronald

Kaitchuck, Steve Howell, Cathy Mansperger, Ron Remillard, Allen Shafter, Mike Shara, Paula Szkody, David Tytler, and Brian Warner. I am especially indebted to Richard Wade, who made the offhand comment about “complete samples” that started my enthusiasm for this project. This comment was perhaps meant in the context of the desirability for complete samples of CV progenitors, though, since months later, when I asked just what he had meant by a complete sample of CVs, he denied ever having discussed one! He did, however, quote Mahatma Gandhi on what he thought of western civilization: “It would be a good idea.”

I thank all those who provided data I have used in this thesis, including two of my fellow students Monica Davis and Bob Hamwey, for the spectra of PG 1136+581 and BZ UMa, respectively. I certainly appreciate the tireless efforts of the AAVSO observers, and of the AAVSO Director, Janet A. Mattei, who sent us their data on BZ UMa. Al Grauer, Jim Liebert, Gary Schmidt, and Gary Wegner sent pre-publication spectra, lightcurves, and the ephemeris of PG 0859+415, Ron Remillard sent pre-publication catalog from the HEAO-1 MC-LASS X-ray survey, and Ron Webbink sent his list of highly evolved close binaries with known or suspected orbital periods. Special thanks go to Janusz Kaluzny for his CCD photometry, and to Paula Szkody, for her infrared photometry, of BZ UMa.

Too many astronomers know too little about statistics. To remedy this situation, Eric Feigelson and G. J. Babu hosted the Statistical Challenges in Modern Astronomy meeting at Penn State University, in 1991 August, and I am grateful to them, and to the National Science Foundation, for a travel grant for me to attend.

I was a Guest Observer the *International Ultraviolet Explorer* satellite, operated by the NASA Goddard Space Flight Center. Lyla Taylor helped me remotely access the Regional Data Analysis Facility there. I should also acknowledge Dr. John C. Raymond, the Principal Investigator of the project that took the *IUE* archive spectra of PG 2300+166.

Joyce Watson introduced me to SIMBAD, which is so useful, I am surprised that

every astronomical paper these days doesn't have the acknowledgement: "This research has made use of the SIMBAD database, operated at CDS, Strasbourg, France."

Martha Hazen and Allison Doane introduced me to the Harvard Plate Archive, while I stayed at Steve Saar's place. Elizabeth Bohlen and Fred Seward helped me use the measuring engine at the Smithsonian Astrophysical Observatory's High Energy Division. I thank Lola Eachus Chaisson and William Liller, for writing me on their study of HX Peg.

I owe my research career to Ron Taam, who introduced me to it, and to the literature. Pat McDermott actually supervised me during this crucial first stage, though, and I guess his patient efforts worked. George Corso taught me how to observe, and importantly, how to conduct myself in the presence of a large telescope. He also introduced me to my first observational research, much of which was carried out with Ron Harris.

I also thank Phyllis Pitluga, for hiring me as an Astronomy Assistant at the Adler Planetarium in Chicago. That job was a dream come true. Eric Carlson also taught me a lot.

I thank all my friends, over the years, all the musicians, artists, and teachers, who helped me along my way. I finally wish to especially thank my beloved Mother and Father, who when I was five, used to take me to see the dinosaur fossils at the American Museum of Natural History in New York. One day, we were early and we couldn't find a place to park—fancy that, in New York—but the Hayden Planetarium next door had a parking lot, so we went there. I immediately sensed the exhibits were interesting, somehow special and important, particularly the fluorescent murals of the Solar eclipse and the moonscape. When the show started in the large orrery room, beneath the sky theater, I was beside myself with amazement—I just couldn't believe my eyes. I can still remember my Father looking interested, smiling at me. It was then that I decided to go into astronomy. Some time later, when I was in the second or third grade and noticed my writing assignments were getting longer, I asked my Mother, "in school, do you ever have to write a book?" She said "Yes, dear—it's called a thesis."

Contents

Abstract	ii
Acknowledgements	iii
Contents	vi
List of Tables	viii
List of Illustrations	x
1. Introduction	
1.1. What are Cataclysmic Variables?	1
1.2. Evolution	3
1.3. Classification Scheme	5
1.4. Thesis Objectives	10
2. Observations and Reductions	
2.1. Optical Spectroscopy	12
2.2. Ultraviolet Spectroscopy	14
2.3. The Harvard College Observatory Plate Archive	14
3. The Palomar-Green Catalog's Sample of Cataclysmic Variables and its Completeness	
3.1. Defining a Sample	18
3.2. Estimating Completeness	19
3.3. The Palomar-Green Cataclysmic Variable Sample	20
3.4. External Checks	21
4. The Space Density of the Palomar-Green Cataclysmic Variables	26
5. The Orbital Periods	
5.1. Introduction	35
5.2. Measuring Orbital Periods	35

5.3.	The Periods of the Individual Objects	37
5.4.	Implications for Sample	40
6.	The Individual Stars Found by the Survey	72
6.1.	The Cataclysmic Variables	74
6.2.	Objects Previously Thought to be Cataclysmic Variables	90
7.	Aggregate Properties of the Stars	117
8.	The SW Sextans Stars	120
9.	BZ Ursa Majoris and its Ringing Radial Velocity Curve	
9.1.	Introduction	126
9.2.	Observations	127
9.3.	Spectrum and Red Star	127
9.4.	Orbit	130
9.5.	Blue and Infrared Time-Resolved Photometry	131
9.6.	Discussion	133
9.7.	Conclusions	137
10.	HX Pegasi, Caught on the Rise to a Dwarf Nova Outburst	
10.1.	Introduction	168
10.2.	Observations	169
10.3.	Quiescent Spectrum and Red Star	170
10.4.	Radial Velocities and Orbital Period	171
10.5.	Outburst	173
10.6.	Discussion	176
Appendix A.	Cataclysmic Variable Spectra,	
	presented in order of Right Ascension	198
Appendix B.	Spectra of Other Objects, presented in order of Right Ascension	225
References		275

List of Tables

Table 2.1.	Instrument Setups	16
Table 4.1.	The Space Density and Luminosity Function of the PG CVs	31
Table 5.1.	Derived Orbital Parameters, for H α velocities (for PG 0917+342, PG 0943+521, PG 1000+667, PG 1002+502, PG 1341-079 = HS Vir, PG 1524+622, PG 1543+145 = CT Ser, PG 1717+413 = V825 Her, and PG 2133+115)	41
Table 5.2.	H α Emission Radial Velocities (for PG 0917+342)	42
Table 5.3.	H α Emission Radial Velocities (for PG 0943+521)	43
Table 5.4.	H α Emission Radial Velocities (for PG 1000+667)	44
Table 5.5.	H α Emission Radial Velocities (for PG 1002+506)	45
Table 5.6.	H α Emission Radial Velocities (for PG 1341-079 = HS Vir)	46
Table 5.7.	H α Emission Radial Velocities (for PG 1524+622)	47
Table 5.8.	H α Emission Radial Velocities (for PG 1543+145 = CT Ser = N Ser 1948)	48
Table 5.9.	H α Emission Radial Velocities (for PG 1717+413 = V825 Her)	49
Table 5.10.	H α Emission Radial Velocities (for PG 2133+115)	50
Table 5.11.	Orbital Periods of the Cataclysmic Variables in the Complete Sample of the Palomar-Green Survey	51
Table 6.1.	Cataclysmic Variables from the Palomar-Green Catalog	101
Table 6.2.	Suspected Palomar-Green CVs, but not in Complete Sample (Blim = 0)	103
Table 6.3.	NON-CVs, from the Palomar-Green Catalog	104

Table 6.4.	H α Emission Radial Velocities (for PG 0134+070 = AY Psc)	105
Table 9.1.	Emission Lines in Summed Spectra	138
Table 9.2.	Instrument Setups	139
Table 9.3.	H α Emission Radial Velocities	140
Table 9.4.	H α Emission Radial Velocities	141
Table 9.5.	H α Emission Radial Velocities	142
Table 9.6.	BZ UMa – Derived Orbital Parameters	143
Table 10.1.	H α Emission Radial Velocities (for HX Peg)	180
Table 10.2.	HX Peg – Derived Orbital Parameters	181

List of Illustrations

Fig. 1.1.	Portrait of a cataclysmic variable	11
Fig. 2.1.	Red calibration for 1990 June 14	17
Fig. 3.1.	CV color-color diagram (cf. Bruch 1984)	24
Fig. 3.2.	Cumulative surface density for the PG CVs	25
Fig. 4.1.	PG CV Period vs. Space Density	33
Fig. 4.2.	Luminosity Function for PG CVs	34
Fig. 5.1.	Periodogram of H α Velocities – PG 0917+342	52
Fig. 5.2.	H α Radial Velocities – PG 0917+342	53
Fig. 5.3.	Periodogram of H α Velocities – PG 0943+521	54
Fig. 5.4.	H α Radial Velocities – PG 0943+521	55
Fig. 5.5.	Periodogram of H α Velocities – PG 1000+667	56
Fig. 5.6.	H α Radial Velocities – PG 1000+667	57
Fig. 5.7.	Periodogram of H α Velocities – PG 1002+506	58
Fig. 5.8.	H α Radial Velocities – PG 1002+506	59
Fig. 5.9.	Periodogram of H α Velocities – PG 1341–079 = HS Vir	60
Fig. 5.10.	H α Radial Velocities – PG 1341–079 = HS Vir	61
Fig. 5.11.	Periodogram of H α Velocities – PG 1524+622	62
Fig. 5.12.	H α Radial Velocities – PG 1524+622	63
Fig. 5.13.	Periodogram of H α Velocities – PG 1543 + 145 = CT Ser = N Ser 1948	64
Fig. 5.14.	H α Radial Velocities – PG 1543 + 145 = CT Ser = N Ser 1948	65
Fig. 5.15.	Periodogram of H α Velocities – PG 1717+413 = V825 Her	66
Fig. 5.16.	H α Radial Velocities – PG 1717+413 = V825 Her	67

Fig. 5.17.	Periodogram of $H\alpha$ Velocities – PG 2133+115	68
Fig. 5.18.	$H\alpha$ Radial Velocities – PG 2133+115	69
Fig. 5.19.	The Orbital Period Distribution of the Palomar-Green Cataclysmic Variables	70
Fig. 5.20.	Orbital Period Distributions	71
Fig. 6.1.	PG 0859+415 – 1991 March 3 (red spectrum)	106
Fig. 6.2.	PG 0859+415 – $H\alpha$ Radial Velocities	107
Fig. 6.3.	PG 0859+415 – $H\alpha$ profiles (1991)	108
Fig. 6.4.	PG 0935+075 – <i>IUE</i> Short and Long Wavelength Spectra	109
Fig. 6.5.	PG 0943+521 – <i>IUE</i> Short and Long Wavelength Spectra	110
Fig. 6.6.	PG 1000+667 – <i>IUE</i> Short and Long Wavelength Spectra	111
Fig. 6.7.	PG 0948+344 = RZ LMi – 1991 October 19 & 20 UT	112
Fig. 6.8.	PG 0948+344 = RZ LMi – <i>IUE</i> Short and Long Wavelength Spectra	113
Fig. 6.9.	PG 2300+166 – <i>IUE</i> Short and Long Wavelength Spectra	114
Fig. 6.10.	PG 1002+506 – <i>IUE</i> Short Wavelength Spectrum	115
Fig. 6.11.	PG 1002+506 – $H\alpha$ equivalent widths	116
Fig. 9.1.	BZ UMa – 1989 Grand Sum Spectrum	144
Fig. 9.2.	BZ UMa – 1991 Red Average Spectrum	146
Fig. 9.3.	BZ UMa – 1991 Far Red Spectrum	148
Fig. 9.4.	BZ UMa – $H\alpha$ profiles (1988)	150
Fig. 9.5.	BZ UMa – Periodograms of $H\alpha$ Velocities	152
Fig. 9.6.	BZ UMa – Periodograms of $H\alpha$ Velocities	154
Fig. 9.7.	BZ UMa – Periodograms of $H\alpha$ Velocities	156
Fig. 9.8.	BZ UMa – $H\alpha$ Radial Velocities	158
Fig. 9.9.	BZ UMa – Periodograms of He I $\lambda 6678$ Velocities	160

Fig. 9.10.	Kaluzny's BZ UMa photometry (in B)	162
Fig. 9.11.	BZ UMa – $H\alpha$ Radial Velocities (orbit subtracted)	164
Fig. 9.12.	BZ UMa – $H\alpha$ Radial Velocities (orbit subtracted)	166
Fig. 10.1.	HX Peg – Spectra of rise to outburst	182
Fig. 10.2.	HX Peg – Periodogram of $H\alpha$ Radial Velocities	184
Fig. 10.3.	HX Peg – $H\alpha$ Radial Velocities	186
Fig. 10.4.	HX Peg outburst – $H\alpha$ equivalent widths	188
Fig. 10.5.	HX Peg outburst– $H\alpha$ equivalent widths (1991 October 19 UT)	190
Fig. 10.6.	HX Peg red continuum fits	192
Fig. 10.7.	HX Peg EWs and continuum fits	194
Fig. 10.8.	HX Peg red continuum fits (1991 October 19 UT)	196
Appendix A.	Cataclysmic Variable Spectra,	
	presented in order of Right Ascension	198 – 224
Appendix B.	Spectra of Other Objects,	
	presented in order of Right Ascension	225 – 274

Chapter 1

Introduction

1.1. What are Cataclysmic Variables?

Cataclysmic variables (CVs) are close binary stars in which a red K – M dwarf star overfills its gravitational equipotential, or Roche lobe, and spills gas onto a white dwarf star, via the cosmic whirlpool of an accretion disk (see Fig. 1.1). CVs are widely touted as the best natural laboratories for studying accretion disk physics, since their light is dominated by their geometrically thin disks, their basic geometry and component stars are reasonably well-understood, and they rotate and often eclipse, giving spatially resolved information on the disk. Even though CVs are faint stars, humble creatures in the grand scheme of things, accretion is the ubiquitous gravitational aggregation of matter, essential in binary stellar evolution, star and galaxy formation, and active galactic nuclei and quasars. Recent CV reviews are by Wade & Ward (1985), King (1988), and Livio (1992).

This general picture of CVs has been held over the past twenty years, since all CVs are observed to be short-period spectroscopic binaries (Kraft 1963), and also since eclipses can reveal a CV's geometry (Warner & Nather 1971). However, despite hundreds of observational and theoretical papers, many of even the basic details are still uncertain. For example, reliable estimates of stellar masses, for both white dwarfs and red stars, are hard to come by (Wade & Horne 1988), as are distances (Berriman 1987). The mechanism of viscosity in the accretion disk—what makes it a disk in the first place—is still uncertain (Frank, King, & Raine 1992). The origin of CVs is still obscure, with only a handful of observations to constrain theory (Ritter 1986b; Webbink 1989).

Radiative processes in accretion disks are poorly understood, and disk spectra still cannot be calculated reliably (Horne & Marsh 1986; Wade 1988), as can those of normal stellar atmospheres. CV spectra often show Balmer lines in strong, broad emission, with

flat Balmer decrements and blue, power-law continua. The white dwarf spectrum is rarely seen, except in the ultraviolet spectra of less-luminous CVs; the red star's optical spectrum is also often overwhelmed. He I lines are often present in broad emission, but are never as strong as the Balmer lines. Sometimes high-excitation lines such as He II $\lambda 4686$ and C III /N III $\lambda\lambda 4640 - 4650$ are present in broad emission, which can be stronger than the Balmer lines in old novæ and magnetic CVs (see below). When CVs are relatively luminous, their lines often go into strong, broad absorption, especially their higher Balmer lines.

Cataclysmic variables have many components, including the accretion disk, the white dwarf, the red star, the gas stream, the bright spot where the gas stream hits the disk, and the disk/white dwarf boundary layer (see Fig 1.1). The mass transfer rate and inclination of the disk will no doubt affect its appearance. Excluding metallicity, at least five independent parameters are required for physical modeling of a disk and calculating its spectrum: the white dwarf mass, mass transfer rate, inner radius, outer radius, and viscosity parameter (Adam et al. 1989). This is inherently more complex than a stellar atmospheres calculation, which requires just temperature and gravity. Selection effects will no doubt bias which CVs one sees, as well as what one sees. So, to obtain a reasonable empirical assessment of the nature of CV accretion disks, an unbiased sample is desirable. Certain programs require it, such as measuring the space densities of CVs by trigonometric parallaxes, or determining the fraction of eclipsing CVs, to learn about radiative processes in accretion disks.

CVs are idiosyncratic objects, but they always show a strong ultraviolet excess. Luminous CVs have power-law continua, and intrinsically faint CVs have flat energy distributions, but with strong emission lines and Balmer jumps in emission. Bruch (1984) compiles a list of CV colors, and 95% of them have $U - B < -0.46$. The highly successful Palomar-Green survey (Green, Schmidt, & Liebert 1986; hereafter GSL86) has this same color criterion, so for an unbiased sample, it is natural to turn to it.

1.2. Evolution

A CVs' evolution is driven by its red star. An evolving CV cannot conserve both angular momentum and mass. If it did, mass transfer would switch off as soon as it started (Patterson 1984). Most CV evolution theory assumes that mass loss is negligible. Some mass loss does occur, in the form of nova shells and stellar winds, but the total amount is small. Nova shells expel, very roughly, $10^{-4} M_{\odot}$, each 10^4 years (Cohen 1985). Mass loss from a disk wind is estimated to be two orders of magnitude less than the mass transfer rate (Córdova & Howarth 1987). Angular momentum loss is thought to occur by at least two mechanisms: gravitational radiation, which must always work for all CVs, and magnetic stellar wind braking, where a small amount of plasma flows down the magnetic field lines and decouples at the Alfvén radius, typically several solar radii away (Verbunt & Zwann 1981). This acts as a long torque arm, so only a small amount of mass outflow is needed to produce a large braking torque. This process is thought responsible for the observed spin-down of low-mass stars that advances with age (e.g., Kawaler 1989).

CVs therefore evolve from long to short periods, over timescales from 10^7 to 10^{10} years, the timescales of angular momentum loss from magnetic braking and gravitational radiation, respectively. Lifetimes are thought to exceed 10^8 years, which the observed cool-down of the white dwarf of Z Cha suggests (Marsh, Horne, & Shipman 1987). Nuclear evolution in the red star can also affect a CV's evolution for CVs with orbital periods exceeding eight hours, but the timescale for this normally exceeds a Hubble time. While CV red stars are for the most part unevolved (Patterson 1984), sometimes an evolved red star will turn up in longer-period systems, such as in CH UMa (Friend et al. 1990).

The CV orbital period distribution shows three distinct features: the long-period cutoff at ten hours, the short-period cutoff at 80 minutes, and the period gap, or significant dearth of CVs between two and three hours (e.g., see Figs. 5.19 and 5.20). The long-

period cutoff occurs since CVs must have mass ratio $q = M_2/M_1 < 4/3$ for Roche lobe overflow from a main sequence star to be thermally stable (King 1988). Since $M_1 < 1.4 M_\odot$, the Chandrasekhar limit, this imposes a mass limit on any main sequence companion. Roche geometry and Kepler's Third Law then impose a maximum period such a system can have; CVs may have longer orbital periods, but the evolved red stars this requires have shorter lifetimes. The short-period cutoff occurs because, at a period of 80 minutes, any main-sequence dwarf that could fit inside such a small Roche lobe would have insufficient mass to sustain nuclear burning. Since it is losing mass, it is pushed out of thermal equilibrium, and without nuclear burning becomes degenerate and expands. Since it is so strongly tidally coupled to the white dwarf, this causes the orbital period to increase, reducing the accretion flow and luminosity to nearly zero, and becoming undetectable as the white dwarf cools (see King 1988 and references therein).

The period gap is thought to be caused by disrupted magnetic braking (Robinson 1983; Rappaport, Verbunt, & Joss 1983; Taam & Spruit 1989; McDermott & Taam 1989). At an orbital period of about three hours, the red star becomes fully convective. Its magnetic dynamo can no longer be anchored to the base of its convective envelope, so the field transforms from a dipole to a bunched-up, higher-order multipole. This is not unlike what happens to the Sun during Solar maximum, which prevents the formation of coronal holes, so the stellar wind cannot get out and presumably cause magnetic braking. The angular momentum loss rate then drops to that of gravitational radiation. The now-fully convective red star also shrinks by about 10%. These two effects keep the CV detached until it can lose enough angular momentum to reattach, at an orbital period of about two hours.

A carefully determined CV period distribution, unbiased by selection effects, would be a powerful probe of CV evolution. CV periods corresponding to the edges of the period gap and the minimum are still uncertain. An unbiased distribution would also give CV modelers a template to match large numbers of CV evolutionary calculations with, in order

to reconstruct the initial CV period distribution and shed light on CVs' origin, given an initial period distribution such as the one of Politano (1988). Another evolutionary constraint could be to match the lower main sequence mass function (e.g., Reid 1987; Kroupa, Tout, & Gilmore 1990) against the CV period distribution: a glance at the present CV period distribution (see King 1988, his Fig. 1, with data from Ritter 1990; or Figs. 5.19 and 5.20) suggests the evolution is strong. If the period gap is interpolated over, the CV period distribution rises much faster with decreasing period than the lower main sequence mass function with decreasing mass.

1.3. Classification Scheme

Cataclysmic variables get their name from their outbursts, so it is not surprising that they are commonly classified by outburst behavior. These have a complex phenomenology, having wide ranges of magnitude extremes, duration, recurrence times, and physics (Robinson 1976; Mattei 1990). The three basic types are classical novæ, dwarf novæ, and nova-likes. There are provisional models for most outburst types, which I discuss in turn.

Novæ, often called classical novæ since they have been observed since ancient times, are by definition observed to erupt only once. The visual outburst amplitudes are typically 10 – 12 magnitudes, and the outbursts last from days to years. They are thought to be nuclear-powered: hydrogen-rich matter accretes onto the degenerate white dwarf surface, and the pressure and temperature build up until sudden detonation, or thermo-nuclear runaway. This has been extensively modeled, and is a rich astrophysical subject in its own right, particularly for studies of nucleosynthesis. For a review, see Shara (1989).

Novæ which are observed to erupt more than once, over a timescale of decades, are termed recurrent novæ. These are heterogeneous and rare, and involve evolved red stars, white dwarfs near the Chandrasekhar limit. Two of the four mentioned by Webbink et al. (1987) are actually symbiotic stars (Kenyon 1986), not CVs.

Ordinary dwarf novæ, or U Gem stars, have 2 – 5-magnitude outbursts, which last several days and recur over weeks to months, often unpredictably. These outbursts are commonly thought to be caused by thermal instability in the accretion flow (Osaki 1974). The outer accretion disk is cool, convective, and inviscid, and matter builds up here. Viscous heating ionizes the hydrogen, increasing the viscosity until it avalanches inward. Eventually the eruption stops, starved for matter to accrete. Dwarf nova outbursts therefore display a limit cycle, pitting the accretion disk's surface density and viscosity against its temperature and mass throughput. For a review, see Smak (1984). A minority view on the cause of dwarf nova outbursts that has never been disproved definitively is that the mass flow from the red star is modulated, by an ill-understood process involving the thermal disequilibrium of the red star's envelope (Bath 1973). Whatever the case, quiescent U Gem stars have typical absolute magnitudes $M_V \approx 8$, measurable since the red stars' spectra are sometimes detectable (Warner 1987).

The Z Cam stars are dwarf novæ similar to the U Gem stars, except that every few years, an outburst gets stuck in a bright state, about one magnitude below maximum. Smak (1984) noticed that the Z Cam stars tend to be relatively luminous, for quiescent dwarf novæ. They may therefore have average mass transfer rates close to the critical mass flow rate which would ionize the disk, increasing the viscosity and preventing dwarf nova outbursts from occurring. Meyer & Meyer-Hofmeister (1983) have proposed that, in Z Cam stars, a normal outburst illuminates the red star, causing its low-gravity atmosphere to expand and raise the mass transfer rate into a positive feedback cycle. The outburst stops when the red star can no longer expand fast enough to maintain this enhanced flow, so the standstill dies of starvation. Problems with this have been pointed out by King (1989), in that there may not be enough hard flux to puff up the red star's atmosphere.

The SU UMa stars are dwarf novæ that, in addition to normal outbursts like those of the U Gem stars, have superoutbursts, of 5 – 6-magnitude amplitude. These last for

weeks and recur over a timescale of about six months to a year, and seem to be precipitated by normal outbursts. Osaki (1989) has proposed a combination of thermal and tidal instability to explain superoutbursts, in which the disk mass grows in successive normal outbursts until it reaches a critical mass above which the disk is tidally unstable. During superoutbursts, there are periodic modulations in the lightcurve of several percent amplitude, called superhumps. Superhumps have very regular periods, a few percent longer than the orbital periods, and these periods are “remembered” from outburst to outburst (Warner 1985). SU UMa stars normally have orbital periods less than three hours, which imply extreme ($> 4:1$) mass ratios. Tides therefore become important: during the enhanced mass transfer of a superoutburst, the disk’s viscosity may cause it to expand until it reaches the radius of tidal instability, which lies within the white dwarf’s Roche lobe. The disk then develops a tidal bulge that slowly precesses about the white dwarf, producing superhumps (Whitehurst 1988). It may not even be necessary to have an outburst to produce superhumps. An extreme mass ratio might give a CV permanent superhumps, as inferred from the many CVs having photometric and spectroscopic periods which are both well-determined, but slightly incommensurate (Patterson & Richman 1991).

Dwarf novæ with interoutburst intervals exceeding 400 days have only superoutbursts (Warner 1987). These are sometimes called WZ Sge dwarf novæ (Bailey 1979), although this prototype is highly idiosyncratic. These stars tend to have short orbital periods, near the period minimum (O’Donoghue et al. 1991), which imply low-mass red stars. Having only superoutbursts may mean there is insufficient mass transfer for normal dwarf nova outbursts to occur often, so that it takes years for a disk to build up sufficient mass for an outburst; and whenever one does, at these short orbital periods, tides are so strong, it turns into a superoutburst. These can be among the intrinsically faintest of quiescent CVs, with BC UMa at $M_V = 11.0 - 13.5$ (Mukai et al. 1990).

Unfortunately, because of extreme photometric variability resembling classical nova

outbursts, the term “nova-like” is sometimes applied to stars not even remotely physically similar to CVs, such as P Cyg or Eta Car. Throughout this thesis, I will use the term “nova-like” to designate CVs which do not have outbursts. Photometrically and spectroscopically, nova-likes resemble dwarf novæ in outburst, or Z Cam stars in perpetual standstill, or old classical novæ, many years after an eruption. These may be old classical novæ, the outbursts of which were missed, or possibly novæ about to erupt (Robinson 1975). Even with the CVs called “nova-likes,” though, there is confusion on terminology, as it is not a homogeneous class. Warner (1976) designates a subclass, the prototype being UX UMa, with broad, absorption lines as well as the emission lines, which are often weak, relative to the bright continuum.

Another subclass of nova-likes, the VY Scl stars, are sometimes called “anti-dwarf novæ.” They unpredictably decrease in brightness, for days to many months. The dynamical studies of Kraft & Luyten (1965) show that nova-likes have $M_V \approx 4.2$, so the red stars are almost never detectable in their spectra. VY Scl stars can therefore be valuable for studies of the component stars of nova-likes, since sometimes the mass transfer can turn almost completely off (Shafter et al. 1985; Hessman 1990).

About a third of all CVs show signs of strong magnetic fields generated by the white dwarfs. For reviews, see Wickramasinghe (1988) and Cropper (1990). Two subclasses, the AM Her and DQ Her stars, are also called the polars and intermediate polars, respectively. They differ primarily in white dwarf rotation period, as inferred by coherent optical and X-ray lightcurve modulations. The AM Her stars’ white dwarfs rotate synchronously with the red stars; the DQ Her stars’ do not. The AM Her stars can also undergo high and low states, not unlike those of the VY Scl stars. Some DQ Her stars are suspected also of having dwarf nova outbursts (Szkody & Mateo 1983; Shafter, Szkody, & Thorstensen 1986; Hazen 1986; Silber 1992). The AM Her stars are thought to possess magnetic fields strong enough to have Alfvén radii extending beyond their Roche lobes; the

DQ Her stars are thought to possess only partially disrupted accretion disks. In both cases, plasma accretes onto the white dwarfs magnetic poles through columns.

In addition to their outbursts—or lack of them—all CVs show erratic photometric variations of a few percent amplitude over timescales of minutes, called flickering (see Warner 1988, p. 139). The cause of flickering is unknown, although it is commonly taken as a sign of accretion. Another photometric variation often seen is an orbital hump. This is a brightening when the bright spot, where the gas stream from the red star hits the disk, is in inferior conjunction. This is modulated at the orbital period, but is erratic and only a few tenths of a magnitude in amplitude, so it is not a preferred way of finding orbital periods.

A curious aspect of the various CV classes is their strong correlation with orbital period (Shafter 1983a; Patterson 1984; Shafter, Wheeler, & Cannizzo 1986). U Gem stars are generally found above the period gap, and nova-likes nearly always are. The orbital period distributions of the SU UMa stars and the Z Cam stars do not overlap. There is a strong spike of AM Her stars with orbital periods near 114 minutes, which is thought to be from adiabatic expansion of the red stars as the CVs evolve out of the period gap (Hameury et al. 1988). Since most DQ Her stars have orbital periods longer than this, idea that the DQ Hers evolve into AM Hers seems plausible. Also, why do faint dwarf novæ and luminous nova-likes occupy the same period regimes, if their component stars are so similar?

If we wish to understand CVs physically well-enough for a definitive classification scheme, it would help to have an unbiased sample. This is complicated by using outburst behavior: dwarf novæ call attention to themselves with their outbursts, and therefore will probably be over-represented in catalogs. So will classical novæ, bright enough to be seen across the Galaxy. Magnetic CVs have strong X-ray emission, and so they dominate X-ray-selected samples (Remillard et al. 1992; Silber 1992).

1.4. Thesis Objectives

This thesis has three overall goals, as follows.

1) Definitive identifications of all the CVs in the complete sample of the Palomar-Green (hereafter PG) catalog must be made. This entails obtaining blue and red spectra. A useful by-product would be spectroscopic classification of the CV “related,” or detached, objects, interesting in their own right (Ferguson, Green, & Liebert 1984; Ritter 1986b; Downes 1987).

2) Once the PG CVs have been identified, the orbital periods should be measured, by radial velocity studies, drawing on the precepts of Thorstensen & Freed (1985).

3) Since measuring CV orbital periods is a telescope time-intensive activity, ways to optimize the scientific return of these spectra should be sought. Ultimately, I wish to find the outburst behavior and distances for as many PG CVs as possible.

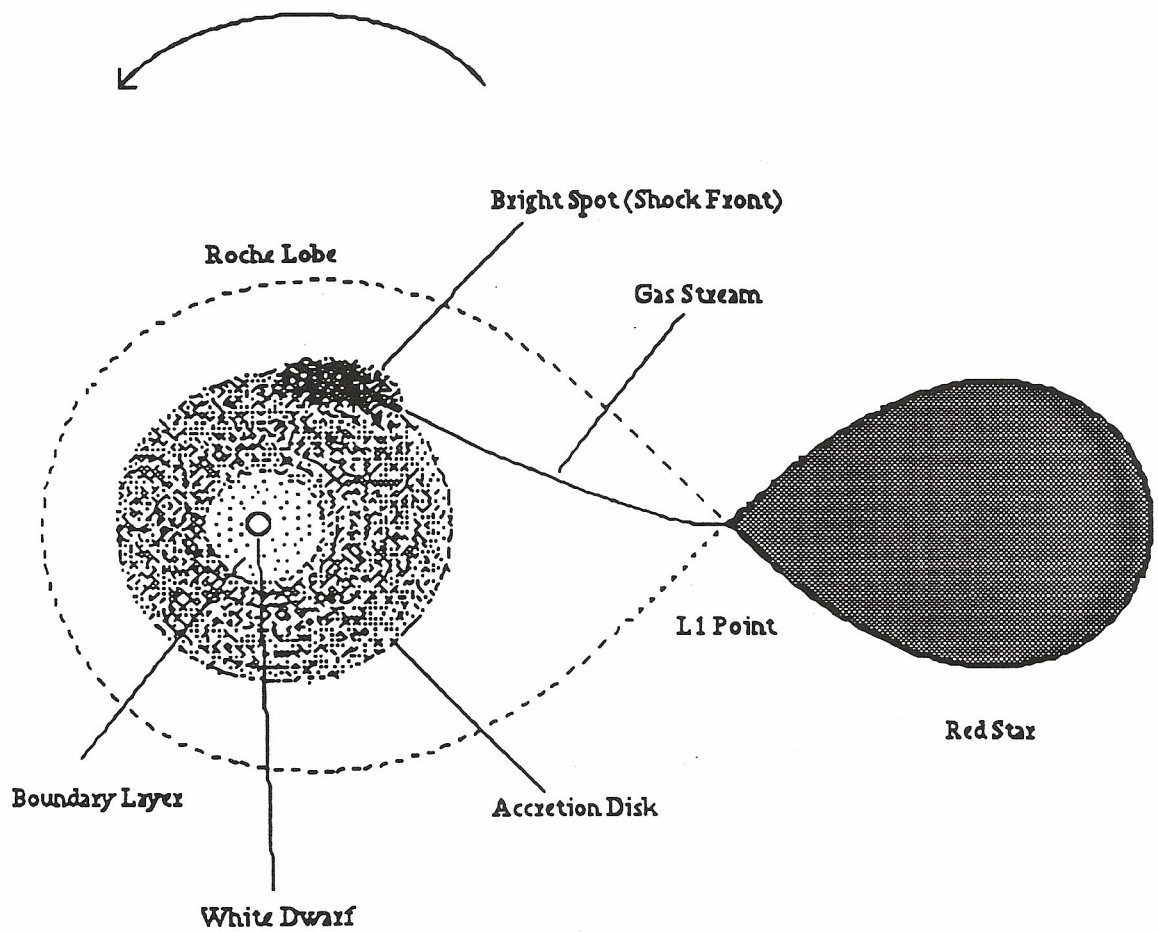


Fig. 1.1. Schematic cataclysmic variable.

The Roche lobe, red star, gas stream, and disk are roughly to scale.

Chapter 2

Observations and Reductions

2.1. Optical Spectroscopy

Table 2.1 is a list of instrumental setups used on each observing run. The follow-up spectroscopy and radial velocity studies were carried out at Michigan-Dartmouth-MIT Observatory, with both the Hiltner 2.4-m telescope and McGraw-Hill 1.3-m telescope. Both the nearly identical Mark IIIa and Mark IIIb spectrographs were used. These all-transmission instruments have high throughput and are stiff and stable. The long-slit spectra normally permit accurate sky subtraction, although absolute spectrophotometry can be trusted only to 30% because of slit losses through the 2.2" slit, used for all exposures. The detector was either a TI-4849 CCD in the BRICC camera (Luppino 1989) or a Thomson-CSF CCD, both chips being geometrically nearly identical.

For the red follow-up spectroscopy and all the radial velocity studies except for the 1989 March run (see Chapter 9), I used a 300 line/mm grism blazed at $\lambda 6400$, for high throughput in the red. All the red setups used a Hoya Y-50 order-sorting filter in the spectrograph, important since CVs have very blue continua. The wavelength coverage spanned about $\lambda\lambda 6200 - 9000$ at 11-Å resolution (with 5 Å per channel). The blue spectra covered about $\lambda\lambda 4400 - 7000$, again at 11-Å resolution, and used gratings with 300 lines/mm blazed at either $\lambda 5400$ or $\lambda 6400$. Exposure times were usually 900 seconds.

Several exposures of Ne, Ar, and Xe lamps, taken at the beginning of each night, were used to determine the wavelength scales. The rms residuals of fifth-order polynomial fits set wavelength scales accurate to within 0.10 Å, and reproducible within 0.05 Å, for all spectra. I show a typical solution for a red setup in Fig. 2.1. Wavelength shifts were measured with Ne lamp exposures, taken every half hour, for all blue spectra, and Ne–Ar spectra (both lamps on) for most red spectra. Slit-viewing TV autoguiding helped minimize

velocity drifts.

Not all observations were made in photometric conditions, but flux standards from Oke (1974) were taken usually at least once per night, to calibrate out the instrumental response. Red spectra of hot stars, such as sdO stars from Stone (1977) or metal-deficient sdF stars from Oke & Gunn (1983), were also taken, for mapping and dividing out atmospheric absorption bands (see Wade & Horne 1988).

All data are reduced and analyzed as in Thorstensen & Freed (1985), and Thorstensen et al. (1989). Briefly, the reduction involved bias removal and flat-fielding. Bias was removed by overscanning with the TI-4849, and with an erase line for the Thomson chip. Flat fields used from 9 to 81 median-filtered frames of a tungsten filament lamp inside the spectrograph, each frame exposed about halfway to saturation, or 8000 counts. Dark frame subtraction was carried out during the BRICC runs, since during 1990 this camera had cryogenic problems. The Thomson chip was normally pre-flashed to an average of 20 – 30 counts, to prevent charge transfer problems at low light levels. All times and velocities were heliocentrically corrected, and all times written as the time of mid-exposure.

Extraction of the data from the frames was done in two ways. First, I weighted the individual columns by their total amount of signal and then summed them. Second, I simply summed the columns together, unweighted. The first extraction was to optimize S/N, for use with measuring velocities and equivalent widths. The second extraction was to preserve accurate fluxes, for spectroscopic classification. The few cosmic rays not rejected by the software were manually interpolated over, although spectra taken with a cosmic ray hit near or on the H α line were discarded.

Most of the follow-up spectra are presented in order of right ascension, for the cataclysmic variables in Appendix A, and of the other objects in Appendix B. See also Chapter 6, for descriptions of the objects.

2.2. Ultraviolet Spectroscopy

Since most of the light of a CV accretion disk is emitted in the UV, spectra from the *International Ultraviolet Explorer (IUE)* satellite have made many contributions to this field, among the most important being the discovery of CV winds. Córdova & Howarth (1987) review observing CVs with *IUE*, and other papers in this volume describe *IUE* in detail.

In two US2 shifts in 1991 February and May, low-resolution (6 \AA) spectra were taken through the large-aperture of several PG CVs. Spectra with the SWP camera, covering $\lambda\lambda 1150 - 2000$, were taken of PG 0935+075, PG 0943+521, PG 0948+344 = RZ LMi, PG 1000+667, and PG 1002+506. Low-resolution, large-aperture spectra with the LWP camera, covering $\lambda\lambda 1825 - 3300$, were taken for all but PG 1002+506. Because of *IUE*'s is a small telescope, the spectra are not time-resolved.

PG 0935+075 is a dwarf nova found in quiescence, with maximum flux near $\lambda 1800$. PG 0943+521 and PG 1000+667 are confirmed as high-luminosity nova-likes, with lines with P Cygni profiles indicating strong, optically thick winds from the accretion disks. PG 1002+506 shows no lines that CVs usually show: it instead has a spectrum typical of a white dwarf, which is discussed in Chapter 6. PG 0948+344 = RZ LMi shows a spectrum more typical of a subdwarf B star, as does PG 2300+166, the spectra for which I obtained from the *IUE* archive.

2.3. The Harvard College Observatory Plate Archive

A valuable and cost-effective method of learning about CV outburst types is looking at archive data. In 1991 June and September, I traveled to the Harvard/Smithsonian Center for Astrophysics to use the HCO plate archive. This archive has about 400,000 photographic plates, taken from 1885 to 1990 with many different telescopes for various programs. Some series plates go as deep as $m_{pg} \approx 17$, although it is rare that any given field will have one taken. The sky patrol plates cover a wide area and are grouped by field

and filed in chronological order. This makes them useful for variability studies, although they are generally taken many days apart, so detailed study of dwarf nova sub-classes can be difficult. The RH and RB series were taken from 1928 to 1952 and generally go down to $m_{pg} \approx 13 - 14$, as do the Damon series, taken from 1965 to 1990. The quiescent magnitudes of many PG CVs are below this, but with the survey's average limiting magnitude at $B = 16.1$, even modest PG dwarf nova outbursts should be detectable. A measuring engine belonging to the Smithsonian Astrophysical Observatory's High Energy Division was used with Palomar Observatory Sky Survey prints to improve positional measurements for most of the PG CVs to within 2", which I will show in Table 6.1.

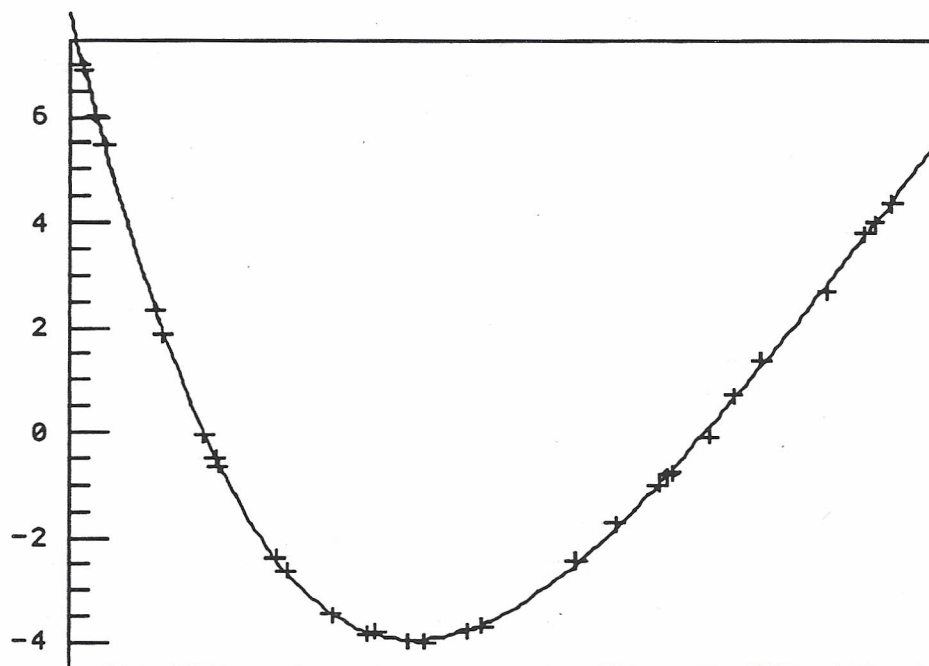
Table 2.1. Instrument Setups

Epoch	Telescope	Mk III	CCD	Range (\AA)
1990 April 26 – 29	1.3	b	TI-4849	4320 – 7350
1990 May 3	1.3	b	Thomson	4200 – 7180
1990 May 4 – 7	2.4	a	TI-4849	6200 – 9000
1990 June 1 – 6	1.3	b	Thomson	6200 – 8940
1991 February 24 – March 8	1.3	a	TI-4849	6200 – 9000
1991 May 23 – 30	1.3	a	TI-4849	6200 – 9000
1991 June 1 – 3	1.3	a	TI-4849	4200 – 6950
1991 October 16 – 21	1.3	a	TI-4849	6200 – 8940
1991 October 26 – 29	1.3	a	Thomson	6300 – 9100
1992 February 17 – 20	1.3	a	TI-4849	6300 – 9100

rms residual = 6.0273431E-02
 variance of fit = 4.5805960E-03
 coeffs (constant term first):
 6.2185000E+03 4.8970728E+00
 3.3004215E-04 -2.0970683E-07
 -1.8510665E-10 2.2036585E-13

Fig. 2.1

Red calibration for 1990 June 14



fifth-order polynomial fit to lamp wavelengths

WLN	CHAN	LAMP	RESIDUAL
6266.495	9.792	NE	1.2207031E-02
6304.789	17.601	NE	-7.8125000E-03
6334.428	23.632	NE	1.9042969E-02
6506.528	58.595	NE	-4.3945313E-03
6532.882	63.946	NE	-5.8105469E-02
6678.277	93.340	NE	-8.7890625E-03
6717.043	101.160	NE	1.3671875E-02
6728.010	103.378	XE	-1.5625000E-02
6929.468	143.915	NE	6.2500000E-02
6965.431	151.140	AR	4.9316406E-02
7119.600	182.069	XE	-2.1484375E-02
7245.167	207.196	NE	-3.4667969E-02
7272.936	212.728	AR	5.5664063E-02
7383.980	234.919	AR	-2.4902344E-02
7438.899	245.879	NE	-4.6875000E-02

WLN	CHAN	LAMP	RESIDUAL
7438.899	245.879	NE	-4.6875000E-02
7584.680	274.924	XE	-1.9531250E-02
7635.106	284.969	AR	-4.8339844E-02
7948.176	347.181	AR	7.5683594E-02
8082.458	373.835	XX	1.0009766E-01
8231.635	403.449	XE	1.3671875E-02
8264.522	409.980	AR	-2.6367188E-02
8280.116	413.079	XE	-5.8593750E-02
8409.190	438.693	XE	-1.6015625E-01
8495.360	455.733	XX	5.6640625E-02
8591.259	474.727	XX	1.2988281E-01
8819.410	519.989	XE	-1.1328125E-01
8952.250	546.273	XE	7.2265625E-02
8988.570	553.482	XX	2.9296875E-03
9045.450	564.755	XE	-2.0507813E-02

Chapter 3

The Palomar-Green Catalog's Sample of Cataclysmic Variables and its Completeness

3.1. Defining a Sample

In Chapter 1, I referred to CV selection effects. Some causes of selection effects are not difficult to guess, such as the presence of dwarf nova outbursts. Unknown selection effects, however, make a statistically-complete sample desirable, for an unbiased look at CV properties and for population studies.

What I mean by a "complete sample" is a sample which includes all the CVs in a specified area of the sky, down to a certain magnitude limit. In astronomy one can almost never obtain a non-trivial complete sample of anything, so the degree of incompleteness should be estimable, which makes it a statistically complete sample. The causes of incompleteness should be insensitive to the selection criteria, too. Even if the losses are large, they should be Gaussian-distributed with respect to the parameters of interest. A complete sample of CVs should not depend on outburst characteristics, since they can be complex and different from object to object, even within each subclass (Szkody & Mattei 1984).

The Palomar-Green catalog of UV-excess stellar objects (GSL86) should provide such a sample. Its color criterion, $U - B \leq -0.46$, includes nearly all CVs. Bruch (1984) has compiled 85 mean colors of 38 CVs of all types, corrected for reddening, and excluding the truly peculiar recurrent novæ (see Fig. 3.1). The PG color criterion is met by the mean colors of all but two of these dereddened CVs (of AR And and AB Dra, both in quiescence, out of 15 dwarf novæ). All the colors for Bruch's dwarf novæ in outburst (including AR And and AB Dra), classical novæ, and nova-likes have $(U - B)_0 \leq -0.46$. All but nine CVs, evenly drawn from all types, have $(U - B)_0 < -0.75$, away from this limit as much as the uncertainty of the B magnitudes of GSL86, $\sigma_B = 0.29$. In the larger

UBVRI catalog of Echevarría (1984), 877 $U - B$ measurements for 75 dwarf novæ in all outburst stages are presented as measured—they are not dereddened, averaged, or otherwise manipulated. Of these, 807/887 (91%) have $U - B < -0.46$. I therefore estimate that losses in the PG catalog from CVs not meeting the color criterion are 5 – 10%.

The PG survey used the 18" Palomar Schmidt telescope to photograph 266 circular fields, of diameter 8.7° . All field centers lie within $|b| > 30^\circ$ and $\delta > -10^\circ$, covering 10,714 square degrees in total, about quarter of the sky. At these high latitudes, interstellar extinction is so small, the effect on $U - B$ color will be minimal, with $E_{U-B} < 0.04$ and $A_V = 0.19$ at $b = 30^\circ$ (Woltjer 1975). Not the entire area of the sky for which $|b| > 30^\circ$ and $\delta > -10^\circ$ was covered. The magnitude limit varies from field to field, from $B = 15.49$ to $B = 16.67$, with $B = 16.1$ being the average limit. For $B \leq 15.8$, 95.9% of the survey area was covered, for $B \leq 16.0$, 79.1% was covered, and for $B \leq 16.1$, 64.3% was covered. The images were scanned automatically (Green & Morrill 1976), and some 1874 point-like objects are included in the catalog, 1715 of which comprise a statistically-complete sample of objects of various spectroscopic classes.

3.2. Estimating Completeness

Incompleteness in any survey comes from measurement and accidental errors. GSL86 estimate an overall completeness of 84%, but stress that completeness should be checked for each spectroscopic subsample. This overall completeness was estimated internally. Since 46.8% of the area of the fields are surveyed twice, the number of objects observed twice in overlapping fields was counted, giving the overall incompleteness of 16%. This incompleteness can have three causes: color errors near the limiting color, magnitude errors near the magnitude limit, and accidental detection losses, which can be due to plate flaws, overlapping adjacent star images, etc.

While one can correct for measurement losses, accidental losses must be estimated

by comparing detections with comparisons with an external list of known objects. For the overall survey, GSL86 used white dwarfs. This may raise suspicion, since the completeness of white dwarfs from the PG catalog has become controversial (Reid, Wickramasinghe, & Bessell 1983), but GSL86 took a completely empirical approach, taking known hot white dwarfs with measured photoelectric colors from the catalog of McCook & Sion (1984) and checking to see if they were in the PG sample. This resulted in estimate of an accidental error rate of $5.3 \pm 2.6\%$, independent of subsample color and magnitude distribution. An additional correction must be made for the measurement errors of the particular spectroscopic subsample, which I will estimate for CVs below.

3.3. The Palomar-Green Cataclysmic Variable Sample

In Chapter 6, I find 33 CVs in the complete sample of the PG survey. Defining a complete sample is not helped by these objects being variable. I will ignore flickering variations, as they would be averaged out by the time exposure of the films. I will also take the B -magnitudes of GSL86 as snapshot values, being wary that a Malmquist bias may result from brightness variations from epoch to epoch, although these are small and slow.

I should exclude dwarf novæ that were in outburst when Green was exposing his films, since these are large-amplitude brightness variations. There are three such dwarf novæ, PG 0911-066, PG 0935+075, and PG 1551+719 = SS UMi. All have quiescent magnitudes (i.e., spend most of their time) fainter than the faintest of the survey limiting magnitudes. I should also throw out the only classical nova in the sample, PG 1543+145 = CT Ser. It had only been about 25 years since its 1948 eruption when Green photographed that region, and at $B = 14.1$, it was much brighter than its pre-outburst level of $m_{pg} = 16.6$ (Bode, Duerbeck, & Evans 1987). In 1991, it was at $V = 16.3$ (Howell et al. 1990).

Over 10,714 square degrees, the surface density of the 29 PG CVs with $B < 16$ is $N(< B = 16.0) = 2.7 \times 10^{-3}$ CVs per square degree. This compares with 2.7×10^{-2} white

dwarfs per square degree and 1.4×10^{-2} sdO stars per square degree in the same B -magnitude range (GSL86). Using the magnitudes in Table 6.1, I plot this cumulative surface density of CVs in Fig. 3.2. Following GSL86, the count slope for CVs between $B = 14.4$ and 16.4 is $d(\log N)/dB = 0.358 \pm 0.080$, or about 2.3 mag^{-1} . This means that at $B = 18.0$, one might expect to see 0.014 ± 0.006 CVs per square degree. The slope for CVs is very similar to that for sdO and sdB stars, interesting since some detached binaries thought to be “precataclysmic” have similar hot stars (Ritter 1986b). Are they from a similar population? This may point to a disk population for CVs, especially since there is some evidence of the count slope leveling off within the range $B = 15.4 - 16.4$, in which case the slope $d(\log N)/dB = 0.177 \pm 0.034$, or about 1.5 mag^{-1} . In this case, at $B = 18.0$, one would expect to see $6.1 \pm 1.0 \times 10^{-3}$ CVs per square degree.

Eddington (1940) gives a correction for measuring errors, which can be applied to the PG sample since inclusion depends only on magnitude and color measurements and spectroscopic classification as CVs. This correction is equal to $-(\sigma^2/2)(d^2N/dB^2)$ where $N(B)$ is as above. The magnitude error of the films used is $\sigma_B = 0.29 \text{ mag}$ (GSL86). With the above count slope, this gives an additional -2.5% incompleteness to CV counts, since more CVs are included from outside the magnitude limit than are lost from within the limit because of measuring errors. This results in an incompleteness for CVs due to measuring errors of 81.5% .

3.4. External Checks

The ideal way to check for losses would be to take a deeper sample covering the same area of the sky, and count how many of the initial sample was represented. Such a list is hard to come by for CVs, however.

The Kiso Schmidt camera survey (Noguchi, Maehara, & Kondo 1980; Kondo et al. 1982; Kondo, Noguchi, & Maehara 1984) went to $B \approx 17.4$, fainter than the PG survey,

but so far (Wegner & McMahan 1985, 1986, 1988; Wegner, McMahan, & Boley 1987; Wegner & Swanson 1990 a,b) the spectroscopic follow-up has found only two definite CVs: K345-57 = PG 0859+415 (Wegner & McMahan 1985) and KUV 15506+1905 = PG 1550+191 = MR Ser (Wegner & Swanson 1990a). Both are also PG CVs.

The catalog of northern dwarf novæ of Bruch, Fischer, & Wilmsen (1987) includes four dwarf novæ within one of the PG fields (GSL86) and having minimum $m_{pg} < 16.2$. These are AF Cam, BZ UMa, CH UMa, and SU UMa. All but AF Cam are PG CVs.

The Kitt Peak-Downes survey (Downes 1986a) recovered six of seven CVs (86%). Although the methods were similar to the PG survey, the color criterion, magnitude limit, and region of the sky covered all were different. Furthermore, the scanning process was done by eye, not automatically.

Howell & Szkody (1990) have a CV sample for $|b| > 40^\circ$, selected from the General Catalogue of Variable Stars (Kholopov et al. 1985). This study was originally intended to find halo CVs, but these CVs' red stars seem unexpectedly easy to detect, so this sample probably has many nearby low-luminosity CVs such as BC UMa or BZ UMa. Of the eight CVs with $V \approx B < 16.2$, seven are in the PG catalog (88%). However, the list of Green et al. (1982) was explicitly used in the selection process. Care should be taken anyway, since the GCVS is an assortment from a variety of sources, not a homogeneous sample.

The census of nova-like variables of Vogt (1989) is largely taken from the GCVS, too, so similar considerations apply. Of 28 objects thought to be CVs that occupy PG fields and have $B < 16.2$, 20 are in the PG catalog (71%). However, several of these objects, such as BE UMa and NN Ser, are known not to be CVs (see Chapter 6). Several others, such as PG 0911-066 and SS UMi, are in fact dwarf novæ in outburst, and so will spend most of their time in a faint state. Permitting only objects known to be nova-likes (Ritter 1990; this work), the ratio of objects in the PG catalog to nova-likes in this census within PG fields and with $B < 16.2$ drops sharply, to $12/19 = 63\%$. Many of the nova-likes

missed are bright, with $B < 13$, including TT Ari, RW Sex, UX UMa, and PHL 227. GSL86 note that the PG survey was designed to work at the plate limit, so bright objects may have a non-linear response on their photographs. This may not be as serious for the PG CVs, though, because of their apparent faintness (see Fig. 3.2).

The catalog of Ritter (1990) includes only CVs with known orbital periods. It is an inhomogeneous sample, and will probably be biased toward including bright CVs, CVs with strong emission lines such as dwarf novæ, and eclipsing CVs, although it does list both large- and small-scale variability. There were no classical novæ in the Ritter catalog in PG fields. (Since I will only get to measuring the orbital period of PG 1543+145 = CT Ser = N Ser 1948 in Chapter 5, it is not yet in the Ritter catalog...) I selected the CVs occupying PG fields having $B < 16.2$ as the minimum brightness for quiescent dwarf novæ, and for the minimum brightness for nova-likes, excluding VY Scl low states. I found 18/29, or 62%, of such CVs included in the PG catalog.

Although crude, all estimates are 62% complete or better. This is somewhat lower than the 71.5% rate one might expect from a sample having a 18.5% loss rate from magnitude and color errors and accidental causes, plus a 10% loss from the few CVs that are not blue enough. The agreement with the Vogt (1989) census may be completely fortuitous, although objects now known not to be CVs were thought to be CVs because of their photometric and spectroscopic similarity to them. And of course one must beware of small numbers and inhomogeneous samples. An additional source of losses might be from the low states of the VY Scl stars, although the timescales over which these objects vary is not well-studied, nor is the fraction of nova-likes which have these low states known. A rigorous external check will require a large sample which goes fainter, such as from the Edinburgh-Cape (Stobie et al. 1987) or Montreal-Cambridge surveys (Demers et al. 1987). The lists are not yet available, though, since their spectroscopic follow-up will take years.

Fig. 3.1. CV color-color diagram (Bruch 1984)

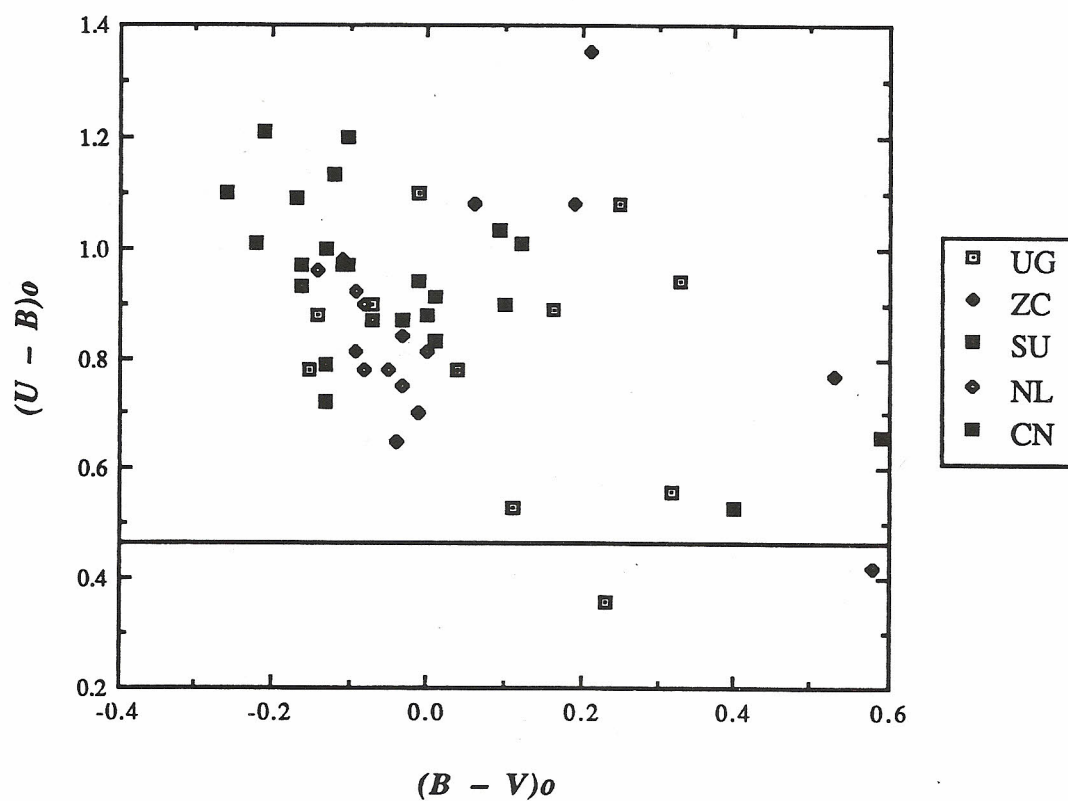
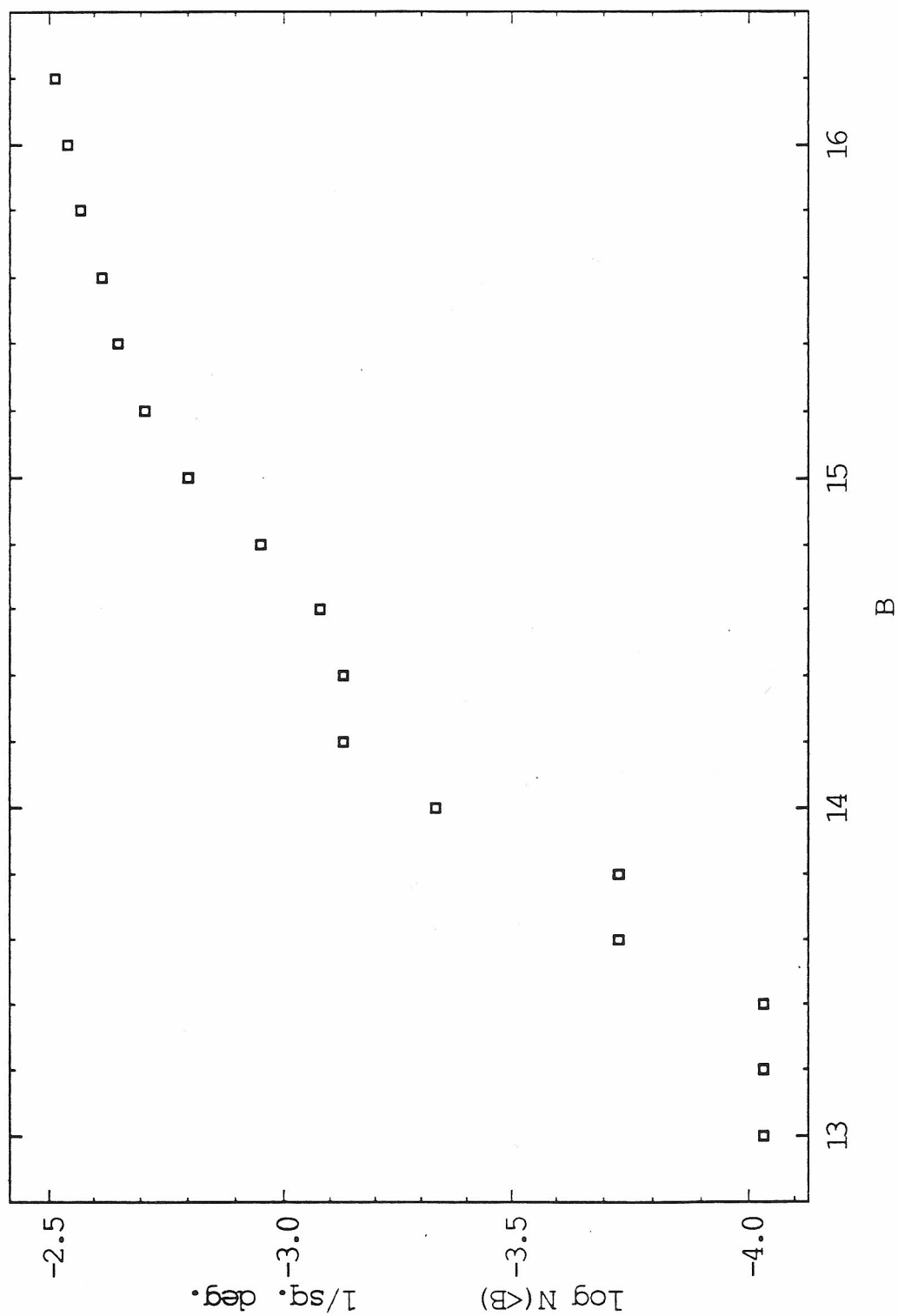


Fig. 3.2. Cumulative surface density for the PG CVs



Chapter 4

The Space Density of the Palomar-Green Cataclysmic Variables

CV distances are “not at all well determined” (Berriman 1987). Expansion parallaxes of classical nova shells show that quiescent novæ have $M_V \approx 4.2$ (Warner 1987). The proper motion study of dwarf novæ of Kraft & Luyten (1965) indicates $M_V \approx 8$. Although typical distances of 100 – 1000 parsecs are expected, direct observational determination by trigonometric parallax has been attempted for few CVs, because of their faintness.

CV space densities have been controversial for some years. The observed nova rate of M31 (Ciardullo et al. 1987) shows that novæ must have many outbursts, since if sustained over a Hubble time, every star in the galaxy would have to be a nova. Ford (1978) estimated the stellar death rate by observing the space density of planetary nebulae in M31, and, dividing the nova rate by it, found that novæ must have at least several hundred outbursts throughout their lives. That every white dwarf is not a nova shows that this number must be even higher: Ford estimated 10^4 . Bath & Shaviv (1978) note that if

$$n \approx \frac{N_0}{\alpha \dot{N}_{WD} \Delta t}$$

where n is the number of outburst recurrences, $N_0/\Delta t$ is the observed nova rate, \dot{N}_{WD} is the white dwarf formation rate, and α is the fraction of white dwarfs that are in novæ, then $\alpha \approx 0.02 - 0.07$. Multiplying this by the space density of white dwarfs in the Solar neighborhood, they found an expected space density of CVs of $n = 10^{-4}$ parsecs $^{-3}$. This would imply a large number of bright novæ in the sky (400 with $m_V < 9.5$) (Patterson 1984), a seemingly absurd result. Shara et al. (1986) invented the hypothesis of nova hibernation: that novæ remain luminous for only a few decades after an outburst, and then, as the white dwarfs cool, become detached, remaining so until angular momentum loss

reattaches the red star. This may explain the low observed space densities. It may also explain why different cataclysmic variables of the same orbital period seem to have different mass transfer rates, although different white dwarf masses may explain differing accretion luminosities, too.

It is therefore desirable to measure the space density of CVs. Space densities and orbital periods together would constrain CV evolution with dn/dP , the space density per period interval. This would be useful for finding the absolute magnitude limits and evolutionary timescales (Patterson 1984).

Depending on the Galactic scale height of CVs, the PG survey's average limiting magnitude of $B = 16.1$ may show nearly all the luminous ones, but miss many of the intrinsically faint ones, if their space density is too low. But, with the Schmidt estimator, also called the V/V_m method (Schmidt 1968), how one defines "complete sample" dodges this. The detection efficiency everywhere is assumed equal to one, and the volume in which one is complete to shrinks. This has its limitations, of course: no one is interested in a flux-limited complete sample of three or four objects.

The Schmidt estimator is also valuable as a test for completeness of a sample. The volume V is defined by the actual distance to the object in question, and V_m is the volume containing a similar object, far enough away to be on the threshold of detection. For a complete sample, $\langle V/V_m \rangle = 0.5$.

Assuming an isotropic distribution in space, having constructed a volume element to account for the Galactic scale height dropoff, $dV' = dV \exp[-z/z_0]$, with $z_0 = 150$ parsecs-for CVs (Patterson 1984) (since there are too few PG CVs for me to find one myself), one can find the limiting magnitude the sample is complete to, by adjusting the limiting magnitude adopted for the survey until $\langle V'/V'_m \rangle = 0.5$. The sum of $1/V'_m$ for all objects within an absolute magnitude bin is the luminosity function, $1/V'_m$ for each object being its contribution to the space density.

I carry out this test for the PG CVs, and show the results in Table 4.1. Of course, doing this properly requires reliable absolute magnitudes, which for CVs are hard to come by. For the purpose of illustration in this thesis alone, I will assign estimates of statistical averages of $M_V = 4.2$ for the nova-likes, $M_V = 8$ for most dwarf novæ, $M_V = 10$ for the AM Her stars, and $M_V = 10 - 11$ for the low-luminosity dwarf novæ, which I call WZ* Sge stars (because spectroscopically, they do not really resemble this peculiar prototype: see Chapter 1). This is crude, but even spectroscopic parallaxes of the red stars give distances to perhaps only $\pm 40\%$ (see Chapter 9), and spectroscopic parallax is regarded as the most reliable distance determination method for CVs, aside from trigonometric parallaxes or expansion parallaxes for novæ (Berriman 1987; Warner 1987). Photometric parallaxes in *JHK* (Bailey 1981) do not have the disadvantage of being applicable to only about 40% of the CVs, but they give only lower limits for distances. For luminous nova-likes, which completely overwhelm their red stars, this may give an overestimate of the distance by as much as a factor of three (see Warner 1987).

Trying various limiting magnitudes to set $\langle V/V_m \rangle = 0.5$ shows the PG CV sample is complete to a limiting magnitude of $B = 15.93$ (see Table 4.1). I have neglected differences in limiting magnitudes between fields, though, and a rigorous test should take this into account. Still, 84.9% of the area covered by the PG survey has a limiting magnitude brighter than this (GSL86), so this loss is probably not serious.

For space density estimates for the dwarf novæ and nova-likes (see Table 4.1, bottom), I use only the objects with $B < 15.93$. Even so, these estimates are several times higher than those in the literature (Warner 1974; Patterson 1984; Downes 1986b). If the space density of the lowest-luminosity dwarf novæ is subtracted from the space density of all dwarf novæ, it makes up for much of the difference. Also, since inclusion does not depend on outburst properties, the PG sample should see the nova-likes systematically missed in the past. One might expect this estimate to err on the side of nova-likes being less

common, since I assume $M_V = 4.2$, the high end of the known range, for all. The SW Sex stars (see Chapter 8) comprise most of this space density, too. These star's nature is poorly understood, and their luminosities are still highly uncertain.

For the magnetic AM Her stars, I find a value within a factor of two of that of Patterson (1984), although this uses only two stars. This is also not included into the total space density, since GSL86 lists both AM Her stars with $B > 15.93$.

CT Ser is the only nova present in the PG survey, and I exclude it from the complete sample because an outburst, and not color excess alone, got it into the PG survey (see Chapter 3). It can be used to find a very crude upper limit on the space density of novæ—which at $6.7 \times 10^{-5} \text{ pc}^{-3}$, is still less than the controversial theoretical value of 10^{-4} pc^{-3} of Bath & Shaviv (1978). Any serious attempt at this, though, really ought to use more than one nova.

A surprising aspect of this exercise is the unexpectedly high space density for the lowest-luminosity dwarf novæ. Some caution is in order with only a small number of stars, but still, does this suggest a large population of low-luminosity CVs? What about related, detached stars? Also, what comes in between these and CVs; what is the nature of the lowest-luminosity CVs? Unfortunately, the PG survey seems not to have gone faint enough to answer these questions.

I plot period versus space density in Fig. 4.1, and note a large dispersion everywhere. There is no obvious increase with period, in contradiction to the mass transfer rate versus period relation of Patterson (1984). Three objects with periods just under four hours, PG 1140+678 = YY Dra, PG 0818+513 = BH Lyn, and PG 0027+260, appear noticeably above the trend, and it is tempting to read some significance into these last two being SW Sex stars (see Chapter 8). It is easy to see why YY Dra is above the trend, however, with its low luminosity: perhaps the firmest trend one can assess from Fig. 4.1 is a rise in space density of CVs below the period gap.

I next make a first attempt at plotting the luminosity function for CVs (see Fig. 4.2). This involves only very rough estimates of CV absolute magnitude, and only a few bins with small numbers of objects in them, so it must be regarded as preliminary. The relatively high $1/V'_m$ and its wide dispersion for the more luminous CVs could be just the result of putting all them into one bin. What is interesting to note is a trend toward higher space density at low luminosity. Does this imply a population of low-luminosity CVs, which increase in number as they go fainter? If so, it would be interesting to find the count slopes for CVs for ongoing, fainter ultraviolet-excess surveys (see Chapter 3). All one needs to find count slopes is the photometry from the survey itself and the follow-up spectroscopy, both of which would be done anyway in such surveys, so such a project could be carried out with very little extra effort.

Table 4.1. The Space Density and Luminosity Function of the PG CVs

address	b	B	M(B)	d(pc)	z(pc)	V'(pc ³)	rmax	Vm'(pc ³)	1/Vm'	V/Vm'
0027+260	-36.3	15.41	4.2	1.7E+03	1.4E+03	4.9E+05	2.2E+03	1.0E+06	9.9E-07	0.488
0134+070	-53.9	15.41	4.2	1.7E+03	1.0E+03	6.1E+06	2.2E+03	1.2E+07	8.0E-08	0.488
0244+104	-42.9	15.1	4.2	1.5E+03	1.1E+03	2.3E+06	2.2E+03	7.3E+06	1.4E-07	0.318
0808+627	33.1	15.27	8	2.8E+02	2.4E+02	5.1E+06	3.9E+02	1.3E+07	7.9E-08	0.402
0818+513	34.8	15.29	4.2	1.7E+03	1.4E+03	5.8E+05	2.2E+03	1.4E+06	7.1E-07	0.413
0834+488	37.4	14.83	8	2.3E+02	1.8E+02	4.0E+06	3.9E+02	1.8E+07	5.5E-08	0.219
0849+580	38.8	16.32	11	1.2E+02	9.0E+01	9.3E+05	9.7E+01	5.4E+05	1.8E-06	1.714
0858+181	36.4	14.18	8	1.7E+02	1.4E+02	2.2E+06	3.9E+02	2.5E+07	4.0E-08	0.089
0859+415	41.6	14.19	4.2	1.0E+03	7.4E+02	7.5E+06	2.2E+03	8.3E+07	1.2E-08	0.090
0917+342	44.5	15.09	8	2.6E+02	1.9E+02	5.6E+06	3.9E+02	1.8E+07	5.6E-08	0.313
0943+521	47.7	14.16	4.2	9.8E+02	6.6E+02	1.3E+07	2.2E+03	1.5E+08	6.9E-09	0.087
1000+667	43.1	15.09	4.2	1.5E+03	1.1E+03	2.4E+06	2.2E+03	7.7E+06	1.3E-07	0.313
1003+678	42.7	15.97	8	3.9E+02	2.9E+02	9.6E+06	3.9E+02	9.1E+06	1.1E-07	1.057
1012-029	41.7	14.75	4.2	1.3E+03	9.6E+02	3.8E+06	2.2E+03	1.9E+07	5.1E-08	0.196
1030+590	50.4	15.02	4.2	1.5E+03	9.3E+02	6.9E+06	2.2E+03	2.4E+07	4.1E-08	0.284
1038+155	57.4	15.75	4.2	2.0E+03	1.1E+03	6.1E+06	2.2E+03	7.8E+06	1.3E-07	0.780
1101+453	62.1	16.08	10	1.6E+02	7.7E+01	2.9E+06	1.5E+02	2.4E+06	4.2E-07	1.230
1114+187	66.6	15.22	4.2	1.6E+03	6.3E+02	6.5E+07	2.2E+03	1.7E+08	5.8E-09	0.375
1119+147	65.7	15.91	4.2	2.2E+03	9.1E+02	2.8E+07	2.2E+03	2.8E+07	3.5E-08	0.973
1135+036	60.5	14.82	11	5.8E+01	2.9E+01	1.8E+05	9.7E+01	8.2E+05	1.2E-06	0.216
1140+719	44.5	15.85	11	9.3E+01	6.7E+01	5.7E+05	9.7E+01	6.3E+05	1.6E-06	0.895
1142-041	54.6	15.39	8	3.0E+02	1.7E+02	9.3E+06	3.9E+02	2.0E+07	5.1E-08	0.474
1316+677	49.4	16.02	4.2	2.3E+03	1.5E+03	5.9E+05	2.2E+03	5.2E+05	1.9E-06	1.132
1341-079	52.4	15.76	8	3.6E+02	2.2E+02	1.2E+07	3.9E+02	1.5E+07	6.8E-08	0.791
1510+234	57.8	15.12	8	2.7E+02	1.4E+02	7.9E+06	3.9E+02	2.4E+07	4.1E-08	0.327
1524+622	46.8	15.44	8	3.1E+02	2.1E+02	7.8E+06	3.9E+02	1.5E+07	6.5E-08	0.508
1550+191	47.7	16.27	10	1.8E+02	1.2E+02	2.8E+06	1.5E+02	1.8E+06	5.7E-07	1.600
1633+115	35.2	14.92	8	2.4E+02	2.0E+02	4.1E+06	3.9E+02	1.7E+07	6.0E-08	0.248

1642+253	38.2	14.34	8	1.9E+02	1.5E+02	2.6E+06	3.9E+02	2.4E+07	4.2E-08	0.111
1711+336	34.1	12.68	4.2	5.0E+02	4.1E+02	8.6E+06	2.2E+03	7.7E+08	1.3E-09	0.011
1717+413	34.4	13.79	4.2	8.3E+02	6.8E+02	6.5E+06	2.2E+03	1.2E+08	8.0E-09	0.052
2133+115	-28.8	14.3	4.2	1.0E+03	9.2E+02	2.8E+06	2.2E+03	2.6E+07	3.8E-08	0.105
2337+123	-46.7	14.29	10	7.2E+01	4.9E+01	2.9E+05	1.5E+02	2.8E+06	3.5E-07	0.104

LIMITING B for CVs = 15.93

address	b	B	M(B)	d(pc)	z(pc)	V' (pc^3)	rmax	Vm' (pc^3)	1/Vm'	V/Vm'
CT Ser	47.6	16.6	4.2	3.0E+03	2.0E+03	3.8E+04	2.2E+03	1.5E+04	6.7E-05	2.523

Previous Work:

n(DN)	Downes 1986	2.4E-07	n(DN) (all)	3.7E-06
	Patterson 1984	3.0E-07	n(WZ*)	2.8E-06
	Warner 1974	4.0E-07	n(DN-WZ)	9.1E-07

This work:

n(NL)	Downes 1986	4.4E-07	n(NL) (all)	2.4E-06
	Warner 1974	5.0E-07	n(SW)	1.9E-06

n(AM)	Patterson 1984	5.0E-07	n(AM)	9.9E-07
-------	----------------	---------	-------	---------

n(CN)	Bath & Shaviv	1.0E-04	n(CN)	< 6.7E-5
-------	---------------	---------	-------	----------

Downes 1986

Duerbeck 1984

Warner 1974

6.1E-06

n(all)	Downes 1986	8.2E-07
--------	-------------	---------

Patterson 1984

Luminosity function (pc^-3)

M(B)	4.2	2.4E-06
------	-----	---------

8

5.6E-07

10

3.5E-07

11

2.8E-06

Fig. 4.1. PG CV Period vs. Space Density

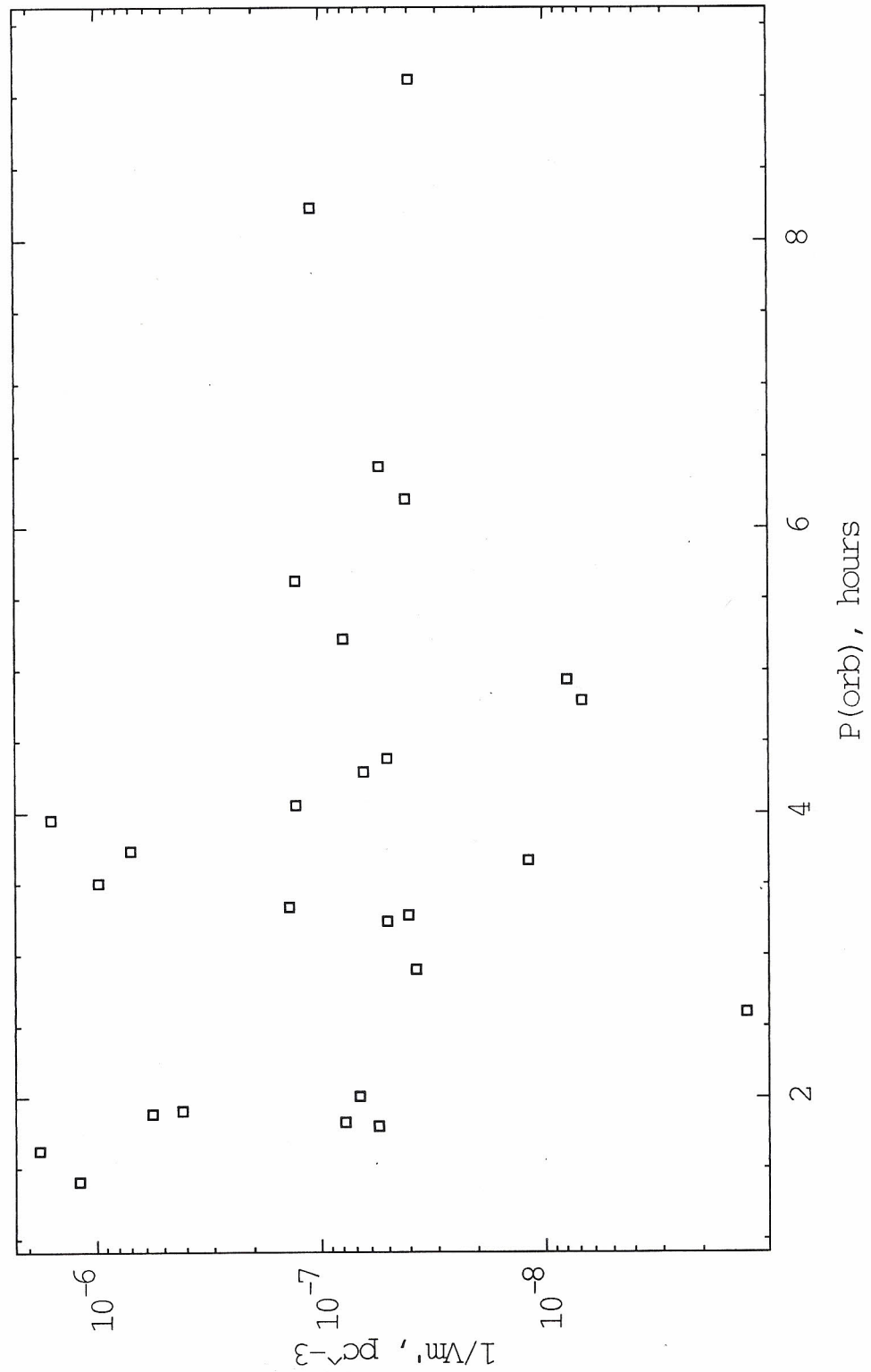
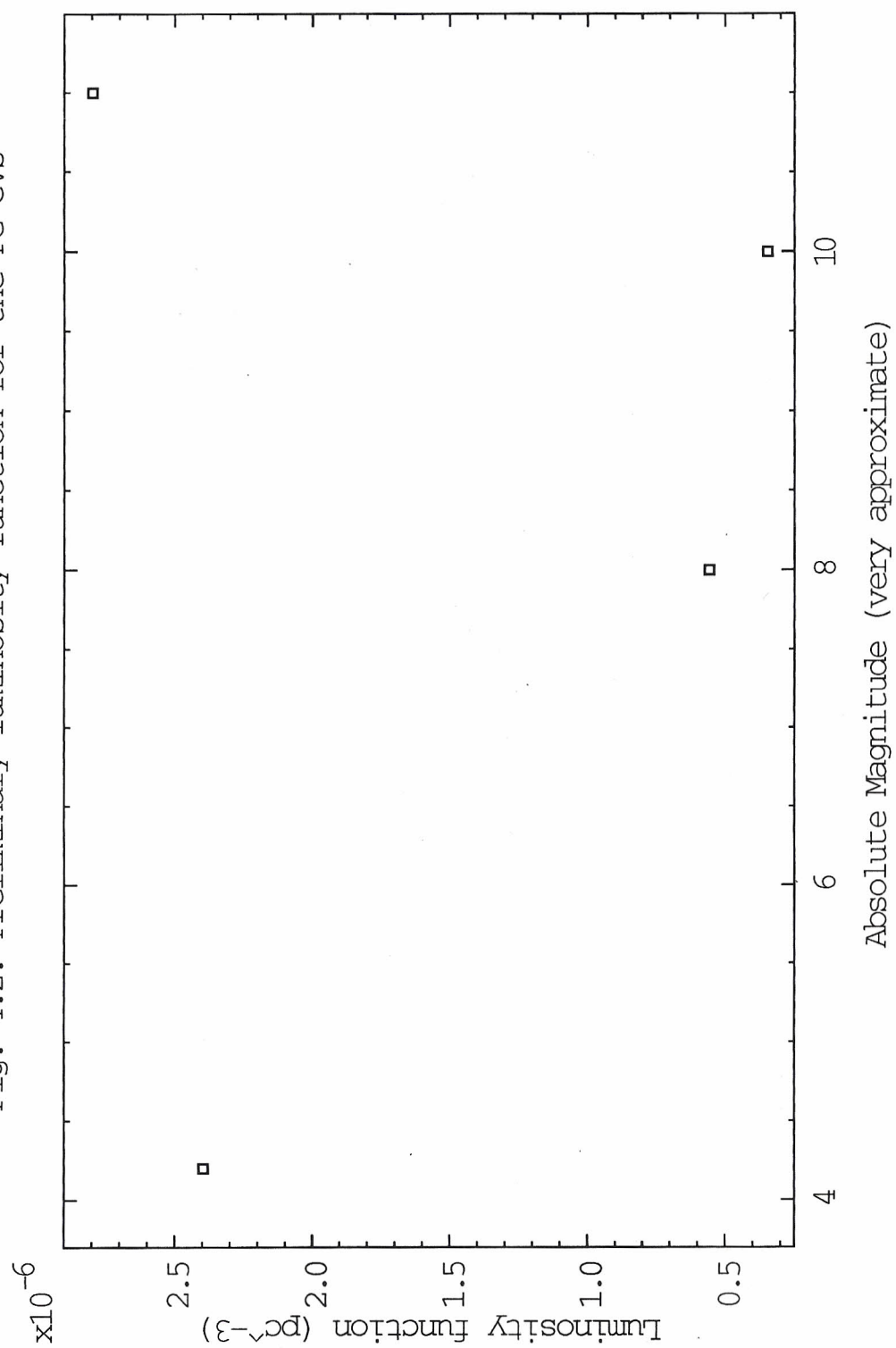


Fig. 4.2. Preliminary luminosity function for the PG CVs



Chapter 5

The Orbital Periods

5.1. Introduction

The orbital period (P_{orb}) of a CV is among the few directly measurable parameters that is not model-dependent. Without it, one knows little of consequence about the CV, since the period influences its secular evolution, luminosity, and outbursts (Shafter, Wheeler, & Cannizzo 1986). The catalogs of Patterson (1984), Webbink (1990), and Ritter (1990) include only CVs of known period, emphasizing its importance.

Radial velocity studies determine periods more reliably than do photometric modulations, save for eclipses, but are not without problems. Orbital semi-amplitudes, or K -velocities, are notoriously hard to determine *reliably*. The emission lines one measures form in the accretion disk, and not necessarily about the white dwarf's center of mass: $K_{\text{em}} \neq K_{\text{WD}}$, necessarily. Since one finds K_{em} by fitting sinusoids to the measured velocities, the same problem applies to γ_{em} , the emission line mean velocity, and T_0 , the epoch, or time of spectroscopic phase zero. Eclipsing CVs sometimes show T_0 lagging the eclipse by over 70° in phase (e.g., Thorstensen et al. 1991b), and dwarf novæ show K_{em} which varies during outbursts (Robinson, Zhang, & Stover 1986; Hessman 1989).

5.2. Measuring Orbital Periods

At the telescope, one should sample the velocities (take the spectra) evenly throughout the orbital phase. The mathematics involved is similar to that of diffraction: a narrow window in time will have little frequency resolution, just as a small telescope aperture will have a large diffraction limit. If many measurements are taken in multiple intervals, fringing will result, and erratic sampling will make for fierce, confusing fringes.

The best policy for time series analysis is to take as long a series of time-resolved

spectra as possible modulo one day, during at least one night of the observing run. If a continuous series is not possible, then the spectra should at least be taken at as many different times of the night as possible. This is to avoid miscounting cycles from night to night, and so avoid confusion among one cycle/day aliases. Other spectra should also be taken throughout the observing run, to improve the precision of the ephemeris by stretching measurements over as long a time baseline and sampling as many cycles as possible.

I measure velocity shifts in the H α emission line in two ways, as described by Thorstensen & Freed (1985). The Gaussian-derivative width (FWHM) algorithm of Schneider & Young (1980) detects the line core's motion. The double-Gaussian separation algorithm of Shafter (1983a) lets us ignore the line core and measure the line wings' motion. Throughout this work, whenever using the Shafter method, I use Gaussian widths of 2.8 channels, or 640 km s⁻¹. This should be wide enough to average out spurious velocity shifts from noise variations.

Periodograms (Lomb 1976; Scargle 1982) show periodicities in the unevenly-sampled velocities as peaks in a frequency spectrum. This is essentially a discrete Fourier transform, modified to accept discrete data that are unevenly sampled, and to return a graphical result equivalent to a least-squares fit for many trial frequencies, stretching across the horizontal axis. I usually use 4000 trial frequencies, to span from 51 minutes to 10 days and so cover all expected orbital periods (Ritter 1990) and greatly oversample them.

But is this best fit really the correct alias? Aliasing, due to miscounting cycles during interruptions in data acquisition (daylight, etc.), creates spurious periodogram peaks, but the Monte Carlo analysis of Thorstensen & Freed (1985) estimates the *correctness likelihood* of choosing the correct alias and the *discriminatory power* of the time series to make the proper choice. I emphasize that this analysis tests the quality of the time series, not the velocity measurements, but this is crucial: the highest-quality spectra are *useless* for finding P_{orb} if *sampled* in time poorly.

In another test, of my own, I generate an artificial sinusoid with the orbital period and the parameters derived from a least-squares fit to the measured velocities, T_0 , K_{em} , and γ_{em} , as defined in Table 5.1. I give this artificial sinusoid enough random noise to set σ , its standard deviation from a true sinusoid, to 10 – 15% more than the σ of the data, since without noise, orbital period determination would be trivial. Sampling the artificial sinusoid at the observation times, I measure velocities and generate a periodogram. If this “fake” periodogram looks like the real one, derived from the spectra, it increases confidence that the form of the real periodogram results only from the sampling.

When measuring velocities with the Shafter (1983a) method, varying the Gaussian separation is useful to maximize K_{em}/σ . This shows how far to measure into the line wings, to avoid both low-velocity jitter and contamination by the continuum. This careful procedure can still produce weird results for white dwarf dynamics (e.g., Shafter, Hessman, & Zhang 1988; O’Donoghue et al. 1989), but it is nonetheless valuable to ensure the highest S/N possible in the radial velocity curve. Errors in the orbital parameters are estimated internally, using the likelihood ratio test of Cash (1979).

5.3. The Periods of the Individual Objects

Orbital period determinations for nine stars are presented in Table 5.1, with Gaussian separations shown as well. Periodograms and least squares fits to sinusoids are shown for each in Figures 5.1 – 5.18. The fits are given in Table 5.1, including second aliases, if they are likely. Journals of times versus velocities are given in Tables 5.2 – 5.10. Some period determinations were clear and unambiguous. Others were noisy, because of the weak lines and small amplitudes involved. I carried out radial velocity studies for PG 0849+580 = BZ UMa and PG 2337+123 = HX Peg as well, and will discuss them in Chapters 9 and 10, respectively. The objects will be discussed in Chapter 6; the individual period determinations for the nine objects will be commented upon here:

- PG 0917+342 – The alias choice is in some doubt. The problem was not as much with measuring velocities as it was with a short (5.3-hour) timebase, modulo one day. This gave problems with discriminating between one cycle/day aliases. A Monte Carlo simulation was run, and the resulting correctness likelihood of 89% and discriminatory power of only 76% are less than compelling. I prefer the alias of 0.0751 days (108 minutes), since it fits a sinusoid better, as its σ in Table 5.1 shows. The two aliases bracket the period of 104 minutes found by Dobrzycka & Howell (1992).

- PG 0943+521 – This determination is based on a noisy signal, with $K_{\text{em}}/\sigma = 1.19$. It is no wonder, since the lines are so weak, and K_{em} small. The false alarm probability (Press et al. 1992) for these velocities is 3%, so the signal probably is being seen.

- PG 1000+667 – The periodogram (Fig. 5.5) shows one alias towering over the others. Curiously, though, the correctness likelihood is only 74%, and the discriminatory power is only 68%. $K_{\text{em}}/\sigma = 0.99$, also surprisingly low. The problem here may be shown by the “fake” periodogram in Fig. 5.5: there appears to be high-frequency noise in the period regime of about one hour. This is too short to represent an orbital period. It is reminiscent of the low-frequency quasi-periodic variability I find in the radial velocity curve of BZ UMa and PG 1711+336 = V795 Her (see Chapter 9). This spells trouble for the Monte Carlo statistics, since they both assume uncorrelated noise in the velocity curve.

- PG 1002+506 – The signal is clear, with $K_{\text{em}}/\sigma = 1.88$, and the periodogram is clean. This object, however, turns out not to be a CV (see Chapter 6). Also, at 30 km s^{-1} , K_{em} is remarkably low, although the fit to a sinusoid was among the best in this work. Then again, this is not a CV. Noise sources in astronomy always include instrumental effects, effects of the Earth’s atmosphere, and effects intrinsic to the object—which is often

called signal, not noise. The methodology that found this was developed to find the orbital periods of CVs (Thorstensen & Freed 1985) and so far has not been used for any other kind of binary star system. It is interesting to have stumbled onto a test case. Particularly interesting is seeing how precisely velocities really can be measured with this setup: are the noise variations in CVs all intrinsic velocity variations of the lines, brought about by small-scale motion in the accretion disks? That other erratic phenomena are known to be associated with disks, such as flickering and QPOs, makes this idea plausible.

Cutting out the three outlying points near phase 0.3 and $O - C \approx +35 \text{ km s}^{-1}$ affects the periodogram only in increasing the likelihood of the next likely one cycle/day alias, at 0.475 days. It still does not dominate, and the “fake” periodogram in Fig. 5.7 suggests this enhancement is just an affect of uneven sampling about the phase.

- PG 1341–079 = HS Vir – This may have aliasing problems, although it is reasonably certain that one of two aliases is correct. I prefer the alias at 0.0836 days, since it fits a sinusoid better, and also since co-adding the spectra into twos, to give effective exposure times of twice as long, does not affect the velocity measurements or the alias choice significantly.

- PG 1524+622 – This was the best period determination, with a strong signal with $K_{\text{em}}/\sigma = 2.79$. The correct alias is obvious, and both Monte Carlo statistics exceed 99%.

- PG 1543+145 = CT Ser – The periodogram (Fig. 5.13) shows a clear alias choice, even though the signal is noisy, with $K_{\text{em}}/\sigma = 0.97$. K_{em} is small, at 55 km s^{-1} .

- PG 1717+413 = V825 Her – Interpretation of the periodogram in Fig. 5.15 is straightforward, and the alias choice is secure. At $K_{\text{em}}/\sigma = 1.49$, the signal is fairly strong.

- PG 2133+115 – This is the only orbital period determination which gave a significant false-alarm probability, at 17.4%. This means there is a non-negligible chance that the velocity measurements themselves are showing a false signal, regardless of how they are sampled. This might not be unexpected with such a noisy periodogram (Fig. 5.17), although when other velocity measurements are taken by varying the Gaussian separation with the Shafter method (see Chapter 2), the periodicity at 0.121 days remains. Binning the spectra by two, effectively doubling the time exposures, has no noticeable effect on the periodogram.

5.4. Implications for Sample

I compile a table of all known PG CV orbital periods, to full precision, in Table 5.11, and plot the resulting orbital period distribution in Fig. 5.19. I caution that at least five of the 33 CVs still need orbital periods to be measured. The long- and short-period cutoffs are obvious, as well as the relative paucity of CVs in the 2 – 3-hour period gap. The AM Her spike is still present, even though there are only two of them, plus there is a preponderance of objects in the one-hour bin just above the period gap. These are nearly all SW Sex stars, a class of nova-likes discussed in Chapter 8.

Even though there is one anomalous CV in the period gap (PG 1711+336 = V795 Her; see Shafter et al. 1990), I note the similarity to the CV sample of Silber (1992) (see Fig. 5.20). This is an X-ray-selected sample of CVs from the HEAO-1 Modulation Collimator (MC) survey. A Kolmogoroff-Smirnoff test (see Press et al. 1992) was carried out to find whether the period distributions are the same. They are: drawing randomly from the same parent distribution, over 99% of the draws would result in a distribution which differ by at least as much as observed.

Table 5.1. Derived Orbital Parameters, for H α velocities^a

Object	P_{orb} (days)	K_{em} (km s ⁻¹)	γ_{em} (km s ⁻¹)	T_0 (HJD - 2440000)	σ (km s ⁻¹)
PG 0917+342 ^b	0.0751 \pm 0.0002	73 \pm 13	-55 \pm 9	8313.834 \pm 0.002	48
Alias 2	0.0702 \pm 0.0004	71 \pm 14	-55 \pm 9	8313.823 \pm 0.002	52
PG 0943+521 ^c	0.1997 \pm 0.0022	57 \pm 11	-5 \pm 8	8320.794 \pm 0.006	48
PG 1000+667 ^d	0.169 \pm 0.001	94 \pm 17	27 \pm 13	8322.822 \pm 0.005	95
PG 1002+506 ^e	0.318 \pm 0.002	30 \pm 3	39 \pm 3	8671.799 \pm 0.006	16
PG 1341-079 ^f	0.0836 \pm 0.0004	107 \pm 21	63 \pm 15	8404.689 \pm 0.003	88
Alias 2	0.0909 \pm 0.0004	105 \pm 21	61 \pm 15	8404.681 \pm 0.003	90
PG 1524+622 ^g	0.17660 \pm 0.00006	134 \pm 11	-75 \pm 8	8411.024 \pm 0.002	48
PG 1543+145 ^h	0.195 \pm 0.002	55 \pm 10	2 \pm 7	8400.790 \pm 0.006	57
PG 1717+413 ⁱ	0.206 \pm 0.002	67 \pm 10	177 \pm 7	8406.676 \pm 0.005	45
PG 2133+115 ^j	0.121 \pm 0.001	51 \pm 14	-75 \pm 10	8546.652 \pm 0.005	60
Alias 2	0.138 \pm 0.001	76 \pm 21	-60 \pm 15	8546.654 \pm 0.006	92

^a Velocities fit to $V(t) = \gamma_{em} + K_{em} \sin[2\pi(t - T_0)/P_{orb}]$. All measurements use Shafter (1983a) double-Gaussian method. Gaussian widths are 640 km s⁻¹. All errors are estimated to 68% confidence (see Thorstensen & Freed 1985).

^b Gaussian separation 650 km s⁻¹

^c Gaussian separation 1300 km s⁻¹

^d Gaussian separation 1950 km s⁻¹

^e Gaussian separation 650 km s⁻¹

^f PG 1341-079 = HS Vir; Gaussian separation 650 km s⁻¹

^g Gaussian separation 1300 km s⁻¹

^h PG 1543+145 = CT Ser = N Ser 1948; Gaussian separation 650 km s⁻¹

ⁱ PG 1717+413 = V825 Her; Gaussian separation 1500 km s⁻¹

^j Gaussian separation 1500 km s⁻¹

Table 5.2. H α Emission Radial Velocities

HJD ^a	<i>V</i>	HJD ^a	<i>V</i>	HJD ^a	<i>V</i>	HJD ^a	<i>V</i>
(km s ⁻¹)		(km s ⁻¹)		(km s ⁻¹)		(km s ⁻¹)	
PG 0917+342 (1991 February) ^b							
8313.614	34	8313.704	58	8314.619	-70	8314.731	-105
8313.625	83	8313.715	15	8314.630	-109	8314.742	-59
8313.636	-12	8313.727	-43	8314.642	-124	8314.754	27
8313.647	2	8313.738	-74	8314.653	-83	8314.765	26
8313.659	-90	8313.749	-66	8314.664	-96	8314.777	-130
8313.670	-60	8313.760	-27	8314.675	-30	8314.788	-182
8313.681	-97	8314.597	-10	8314.709	-157	8314.799	-123
8313.692	26	8314.608	-86	8314.720	-205	8314.810	-29

^a Heliocentric Julian Date of mid-integration, minus 2 440 000.

^b Shafter (1983a) algorithm, Gaussian separation 650 km s⁻¹.

Table 5.3. H α Emission Radial Velocities

HJD ^a	V	HJD ^a	V	HJD ^a	V	HJD ^a	V
(km s ⁻¹)	(km s ⁻¹)	(km s ⁻¹)	(km s ⁻¹)	(km s ⁻¹)	(km s ⁻¹)	(km s ⁻¹)	(km s ⁻¹)
PG 0943+521 (1991 March) ^c							
8320.700	-6	8320.777	-22	8320.854	1	8321.606	85
8320.711	-68	8320.788	-30	8320.865	37	8321.618	27
8320.722	-69	8320.799	-19	8320.887	70	8321.629	27
8320.733	-57	8320.810	35	8320.899	63	8321.651	66
8320.744	-73	8320.821	-21	8320.910	-92	8321.663	17
8320.753	-106	8320.832	44	8320.921	-149	8321.673	23
8320.766	0	8320.843	29	8321.596	78	8321.685	15
8320.777	-22	8320.854	1				

^a Heliocentric Julian Date of mid-integration, minus 2 440 000.

^c Shafter (1983a) algorithm, Gaussian separation 1300 km s⁻¹.

Table 5.4. H α Emission Radial Velocities

HJD ^a	V	HJD ^a	V	HJD ^a	V	HJD ^a	V
(km s ⁻¹)	(km s ⁻¹)	(km s ⁻¹)	(km s ⁻¹)	(km s ⁻¹)	(km s ⁻¹)	(km s ⁻¹)	(km s ⁻¹)
PG 1000+667 (1991 March) ^d							
8320.938	-45	8322.938	-48	8323.679	-59	8323.793	10
8320.949	-38	8322.949	102	8323.690	87	8323.804	-135
8322.845	156	8322.961	-72	8323.701	90	8323.815	25
8322.855	184	8322.971	-58	8323.714	-69	8323.827	63
8322.868	111	8322.984	-102	8323.724	114	8323.838	99
8322.878	194	8323.623	-109	8323.736	177	8323.850	31
8322.890	109	8323.634	-203	8323.747	189	8323.860	147
8322.901	83	8323.645	115	8323.759	-203	8323.872	12
8322.913	-103	8323.656	41	8323.769	-26	8323.883	218
8322.927	-178	8323.668	11	8323.781	1		

^a Heliocentric Julian Date of mid-integration, minus 2 440 000.

^d Shafter (1983a) algorithm, Gaussian separation 1950 km s⁻¹.

Table 5.5. H α Emission Radial Velocities

HJD ^a	V	HJD ^a	V	HJD ^a	V	HJD ^a	V
(km s ⁻¹)	(km s ⁻¹)	(km s ⁻¹)	(km s ⁻¹)	(km s ⁻¹)	(km s ⁻¹)	(km s ⁻¹)	(km s ⁻¹)
PG 1002+506 (1992 February) ^e							
8671.701	-1	8671.850	58	8671.998	17	8672.788	79
8671.712	0	8671.862	55	8672.009	36	8672.812	74
8671.724	12	8671.873	62	8672.021	28	8672.826	108
8671.735	4	8671.885	38	8672.670	-8	8672.838	103
8671.747	-7	8671.896	49	8672.683	21	8672.851	60
8671.759	5	8671.907	42	8672.694	8	8672.861	105
8671.772	20	8671.918	38	8672.707	40	8672.973	23
8671.783	35	8671.930	59	8672.719	26	8672.984	21
8671.794	32	8671.941	45	8672.732	33	8672.996	-2
8671.805	41	8671.953	27	8672.743	46	8673.007	14
8671.817	51	8671.964	31	8672.754	27	8673.019	5
8671.828	47	8671.975	40	8672.765	41	8673.030	4
8671.839	62	8671.986	29	8672.777	57		

^a Heliocentric Julian Date of mid-integration, minus 2 440 000.

^e Shafter (1983a) algorithm, Gaussian separation 650 km s⁻¹.

Table 5.6. H α Emission Radial Velocities

HJD ^a	V	HJD ^a	V	HJD ^a	V	HJD ^a	V
(km s ⁻¹)	(km s ⁻¹)	(km s ⁻¹)	(km s ⁻¹)	(km s ⁻¹)	(km s ⁻¹)	(km s ⁻¹)	(km s ⁻¹)
HS Vir = PG 1341-079 (1991 May) ^f							
8403.664	-22	8403.757	-93	8404.656	115	8404.760	-51
8403.675	-116	8403.768	66	8404.667	-25	8404.773	-36
8403.687	166	8403.781	131	8404.679	118	8404.784	-4
8403.698	194	8403.791	63	8404.690	232	8404.796	136
8403.710	51	8403.804	254	8404.713	251	8404.807	92
8403.721	60	8403.814	139	8404.726	214	8404.821	-70
8403.733	35	8403.826	-146	8404.737	43	8404.832	-136
8403.744	-52	8403.837	-29	8404.749	-105	8404.844	43
8403.757	-93	8404.656	115				

^a Heliocentric Julian Date of mid-integration, minus 2 440 000.

^f Shafter (1983a) algorithm, Gaussian separation 650 km s⁻¹.

Table 5.7. H α Emission Radial Velocities

HJD ^a	V	HJD ^a	V	HJD ^a	V	HJD ^a	V
(km s ⁻¹)	(km s ⁻¹)	(km s ⁻¹)	(km s ⁻¹)	(km s ⁻¹)	(km s ⁻¹)	(km s ⁻¹)	(km s ⁻¹)
PG 1524+622 (1991 May) ^g							
8401.839	-59	8401.940	-122	8402.761	17	8402.866	-176
8401.850	-31	8401.952	-173	8402.772	-2	8402.878	-121
8401.862	-76	8401.963	-173	8402.784	43	8402.889	-106
8401.873	8	8402.693	-205	8402.795	-22	8402.901	-60
8401.884	55	8402.704	-193	8402.806	-30	8402.912	43
8401.895	-34	8402.716	-50	8402.817	-129	8402.924	35
8401.907	-46	8402.727	-62	8402.829	-191	8402.935	107
8401.918	-70	8402.738	23	8402.840	-232	8402.946	193
8401.929	-117	8402.749	6	8402.853	-219	8402.957	143
8401.940	-122	8402.761	17				

^a Heliocentric Julian Date of mid-integration, minus 2 440 000.

^g Shafter (1983a) algorithm, Gaussian separation 1300 km s⁻¹.

Table 5.8. H α Emission Radial Velocities

HJD ^a	V	HJD ^a	V	HJD ^a	V	HJD ^a	V
(km s ⁻¹)	(km s ⁻¹)	(km s ⁻¹)	(km s ⁻¹)	(km s ⁻¹)	(km s ⁻¹)	(km s ⁻¹)	(km s ⁻¹)
PG 1543+145 = CT Ser = Nova Ser 1948 (1991 May) ^h							
8399.669	138	8399.859	131	8400.766	-13	8400.945	-79
8399.680	11	8399.870	83	8400.777	-17	8400.956	-70
8399.692	71	8399.881	134	8400.789	3	8400.968	-30
8399.714	-6	8399.892	39	8400.799	-4	8401.699	-134
8399.724	-8	8399.903	72	8400.811	39	8401.710	-155
8399.736	72	8399.914	27	8400.822	50	8401.722	-44
8399.747	21	8399.925	-39	8400.833	-6	8401.732	-65
8399.758	-38	8399.936	56	8400.844	7	8401.744	-56
8399.769	-97	8399.947	-41	8400.856	122	8401.755	-40
8399.781	-89	8399.958	24	8400.866	104	8401.767	-14
8399.791	-12	8399.969	101	8400.878	-29	8401.777	19
8399.803	-48	8399.979	44	8400.889	-60	8401.790	-27
8399.814	92	8400.721	-59	8400.901	-80	8401.800	2
8399.825	60	8400.732	-57	8400.912	-70	8401.812	-20
8399.836	13	8400.744	-125	8400.923	-65	8401.823	-54
8399.848	102	8400.755	-10	8400.934	-96		

^a Heliocentric Julian Date of mid-integration, minus 2 440 000.

^h Shafter (1983a) algorithm, Gaussian separation 650 km s⁻¹.

Table 5.9. H α Emission Radial Velocities

HJD ^a	V	HJD ^a	V	HJD ^a	V	HJD ^a	V
(km s ⁻¹)	(km s ⁻¹)	(km s ⁻¹)	(km s ⁻¹)	(km s ⁻¹)	(km s ⁻¹)	(km s ⁻¹)	(km s ⁻¹)
V825 Her = PG 1717+413 (1991 May) ⁱ							
8405.769	155	8405.891	193	8406.715	256	8406.835	124
8405.780	120	8405.902	166	8406.727	251	8406.847	123
8405.792	122	8405.915	189	8406.739	281	8406.859	151
8405.804	112	8405.926	207	8406.752	256	8406.872	131
8405.816	119	8405.959	144	8406.763	265	8406.884	129
8405.827	122	8405.970	36	8406.776	193	8406.896	150
8405.839	102	8405.981	88	8406.787	183	8406.908	157
8405.851	153	8406.680	195	8406.800	165	8406.919	196
8405.864	157	8406.691	245	8406.811	122	8406.944	250
8405.875	199	8406.703	265	8406.824	108	8406.956	195
8405.891	193	8406.715	256				

^a Heliocentric Julian Date of mid-integration, minus 2 440 000.

ⁱ Shafter (1983a) algorithm, Gaussian separation 1500 km s⁻¹.

Table 5.10. H α Emission Radial Velocities

HJD ^a	V	HJD ^a	V	HJD ^a	V	HJD ^a	V
(km s ⁻¹)		(km s ⁻¹)		(km s ⁻¹)		(km s ⁻¹)	
PG 2133+115 (1991 October) ^j							
8545.649	-263	8545.746	-51	8546.606	-252	8546.707	-47
8545.657	-162	8545.758	-18	8546.617	-153	8546.719	-35
8545.668	-155	8545.769	-67	8546.628	-190	8546.730	-118
8545.679	-104	8545.780	-120	8546.639	-51	8546.742	-40
8545.691	-90	8545.791	-30	8546.651	-102	8546.753	-84
8545.701	-20	8545.803	-39	8546.661	-113	8546.765	-110
8545.713	-98	8545.814	21	8546.673	-33	8546.775	-33
8545.724	31	8546.584	-130	8546.684	-61	8546.787	-88
8545.735	-51	8546.594	-27	8546.696	-72	8546.798	15
8545.746	-51	8546.606	-252				

^a Heliocentric Julian Date of mid-integration, minus 2 440 000.

^j Shafter (1983a) algorithm, Gaussian separation 1500 km s⁻¹.

Table 5.11. Orbital Periods of the Cataclysmic Variables
in the Complete Sample of the Palomar-Green Survey
(spectroscopic period, unless noted otherwise)

"Address"	Name	P_{orb}	References
0027 + 260		0.1463533	Thorstensen et al. 1991b
0134 + 070	AY Psc	0.2173209	Diaz & Steiner 1990; from eclipse
0244 + 104	WX Ari	0.13934	Beuermann et al. 1992
0808 + 627	SU UMa	0.07635	Thorstensen et al. 1986
0818 + 513	BH Lyn	0.15587490	Andronov et al. 1989; from eclipse
0834 + 488	EI UMa	0.26810	Thorstensen 1986
0849 + 580	BZ UMa	0.0679	this work
0858 + 181	SY Cnc	0.380	Shafter 1983b
0859 + 415		0.15281265	Grauer et al. 1993; from eclipse
0917 + 342		0.0751:	this work
0943 + 521		0.1997:	this work
1000 + 667		0.169	this work
1003 + 678	CH UMa	0.343	Friend et al. 1990; from red star
1012 - 029	SW Sex	0.134938	Penning et al. 1984; from eclipse
1030 + 590	DW UMa	0.13660653	Shafter et al. 1988; from eclipse
1038 + 155	DO Leo	0.2345147	Abbott et al. 1989; from eclipse
1101 + 453	AN UMa	0.079753	Schneider & Young 1980b
1114 + 187		?	
1119 + 147		?	
1135 + 036	T Leo	0.058819	Shafter & Szkody 1984
1140 + 719	YY Dra	0.1650	Mateo et al. 1991
1142 - 041	TW Vir	0.18267	Shafter 1983b
1316 + 677		?	
1341 - 079	HS Vir	0.0836:	this work
1510 + 234		?	
1524 + 622		0.1766	this work
1550 + 191	MR Ser	0.078871	Szkody 1988
1633 + 115		?	
1642 + 253	AH Her	0.258116	Horne et al. 1986
1711 + 336	V795 Her	0.108265	Shafter et al. 1990
1717 + 413	V825 Her	0.206	this work
2133 + 115		0.121:	this work
2337 + 123	HX Peg	0.2008	this work

Fig. 5.1 - Periodogram of H α Velocities

PG 0917+342

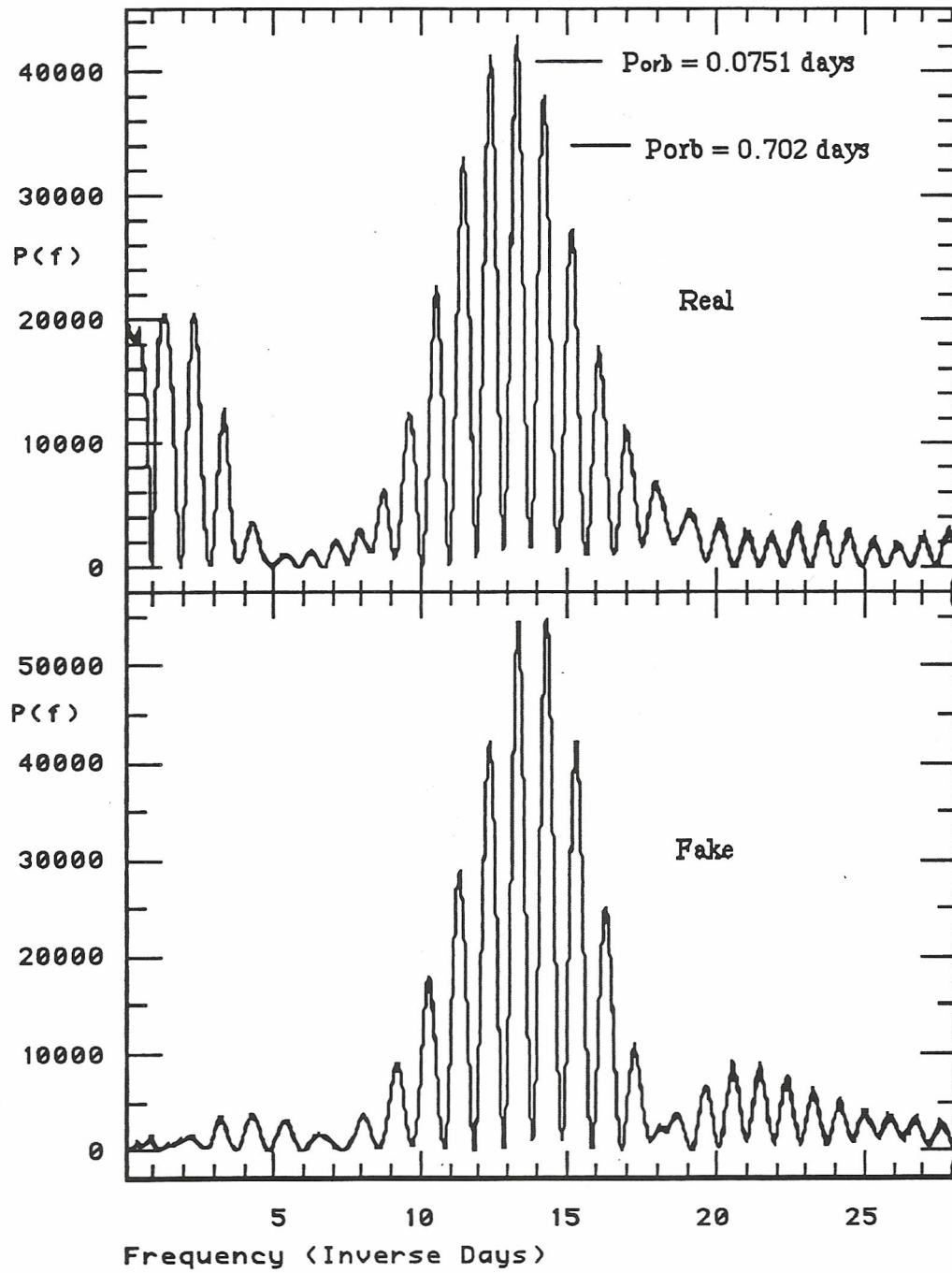


Fig. 5.2 - H α Radial Velocities

PG 0917+342

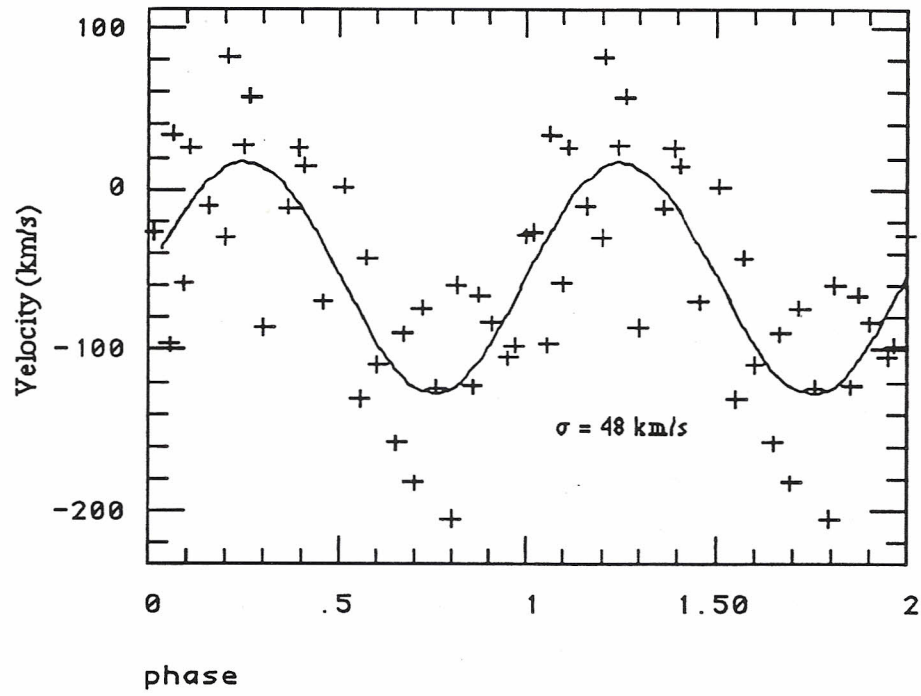


Fig. 5.3 - Periodogram of H α Velocities

PG 0943+521

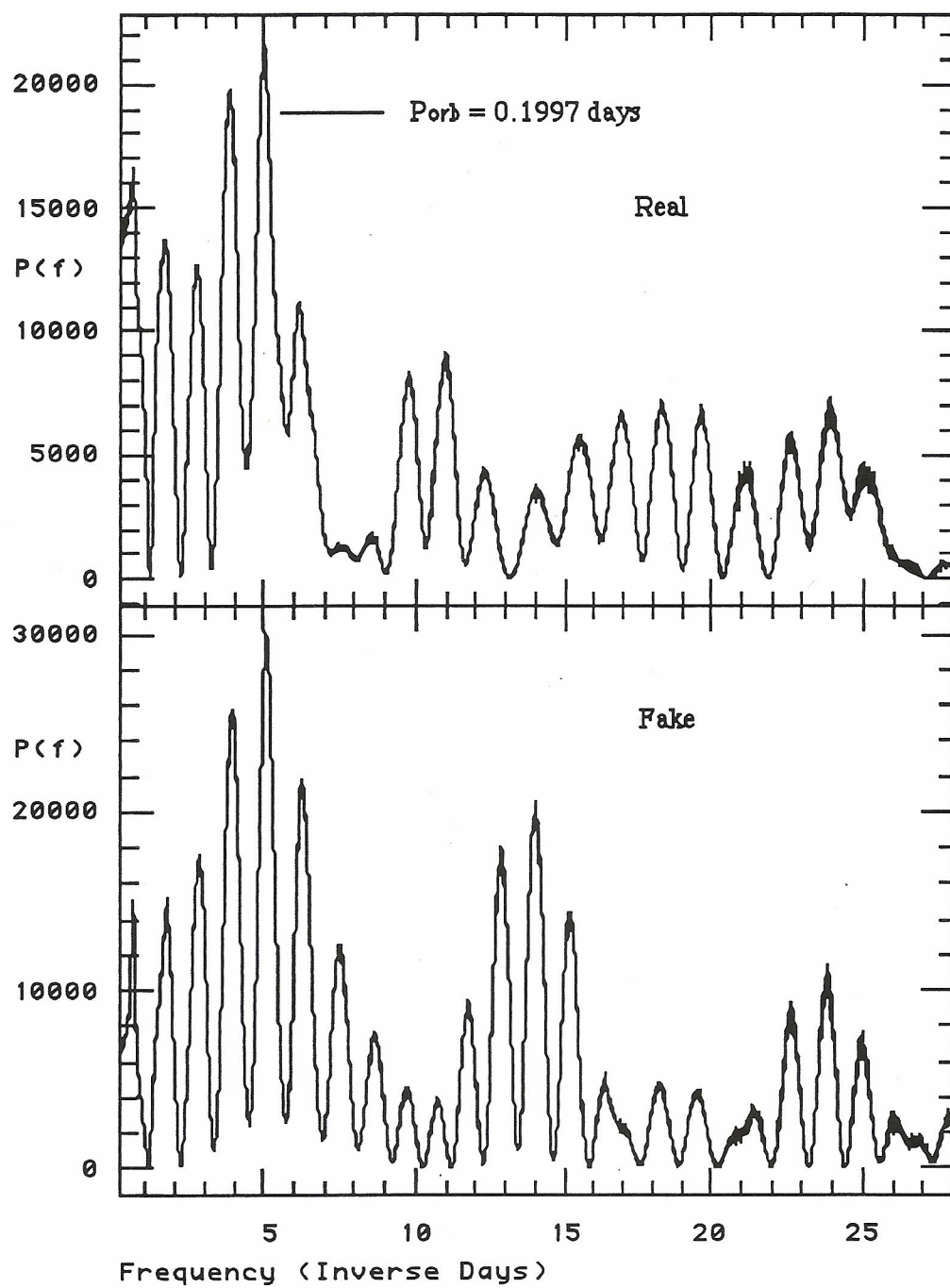


Fig. 5.4 - H α Radial Velocities

PG 0943+521

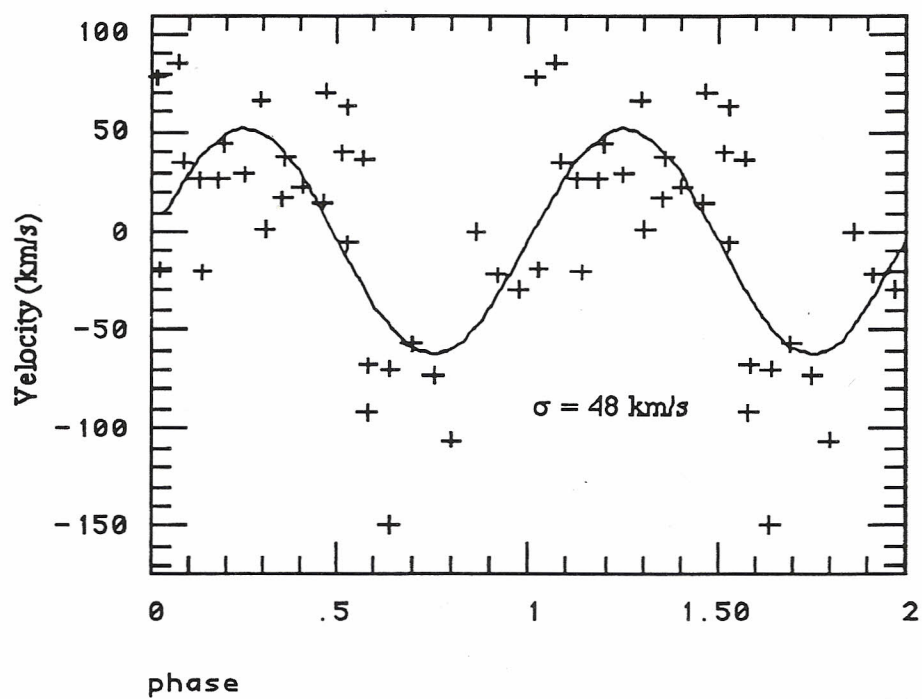


Fig. 5.5 - Periodogram of H α Velocities

PG 1000+667

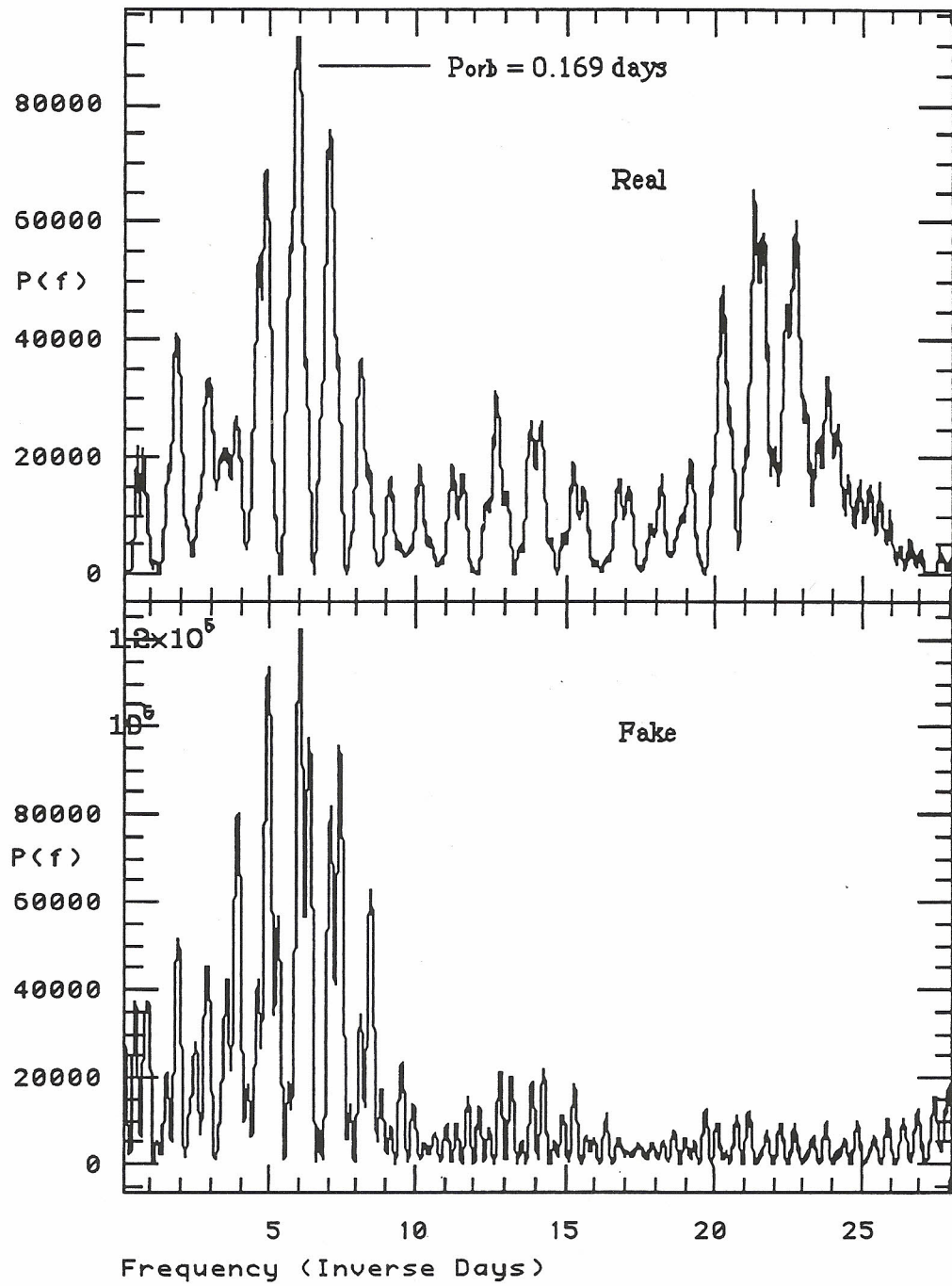


Fig. 5.6 - H α Radial Velocities

PG 1000+667

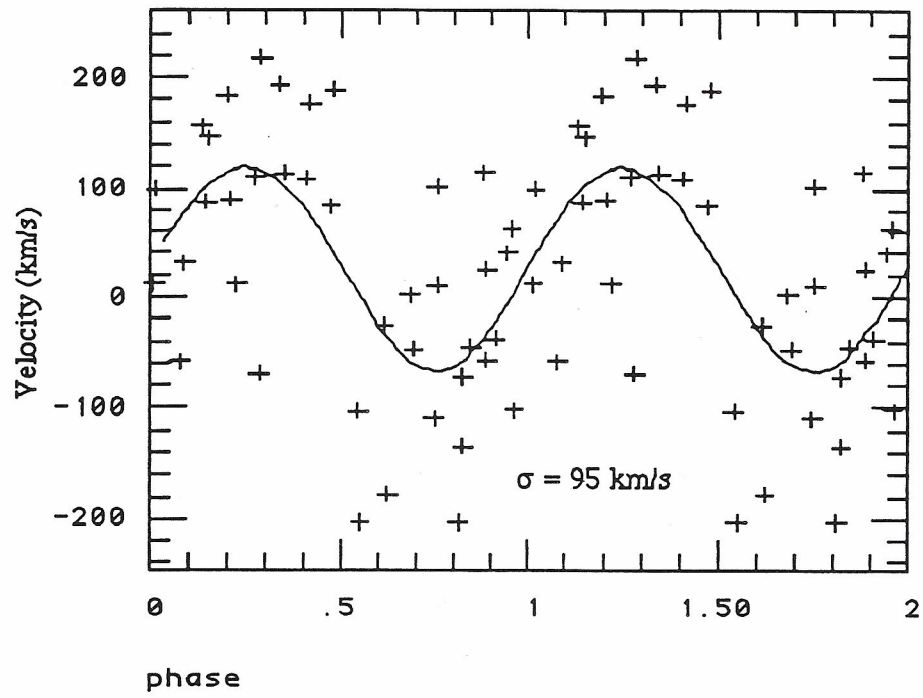


Fig. 5.7 - Periodogram of H α Velocities

PG 1002+506

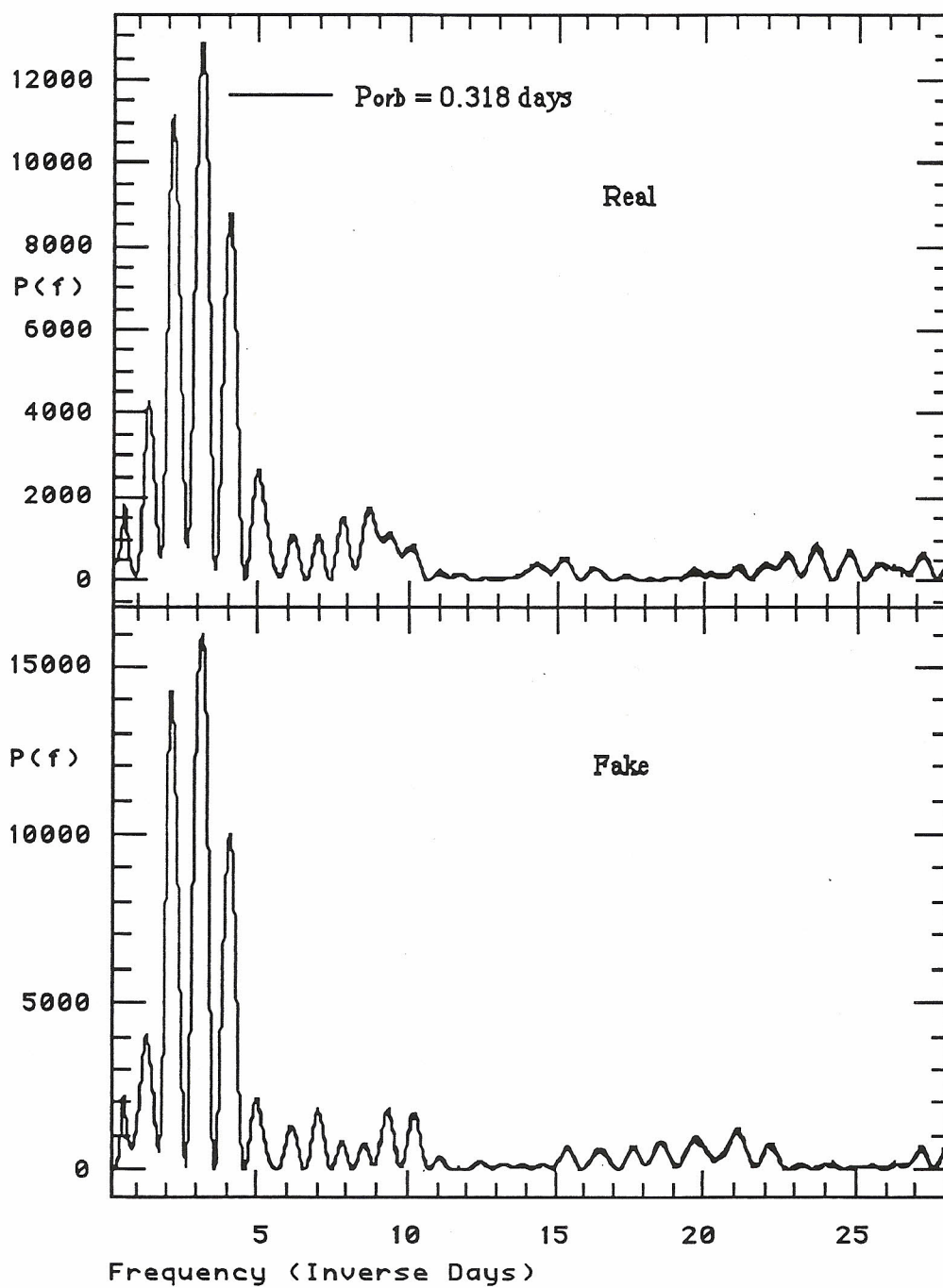


Fig. 5.8 - H α Radial Velocities

PG 1002+506

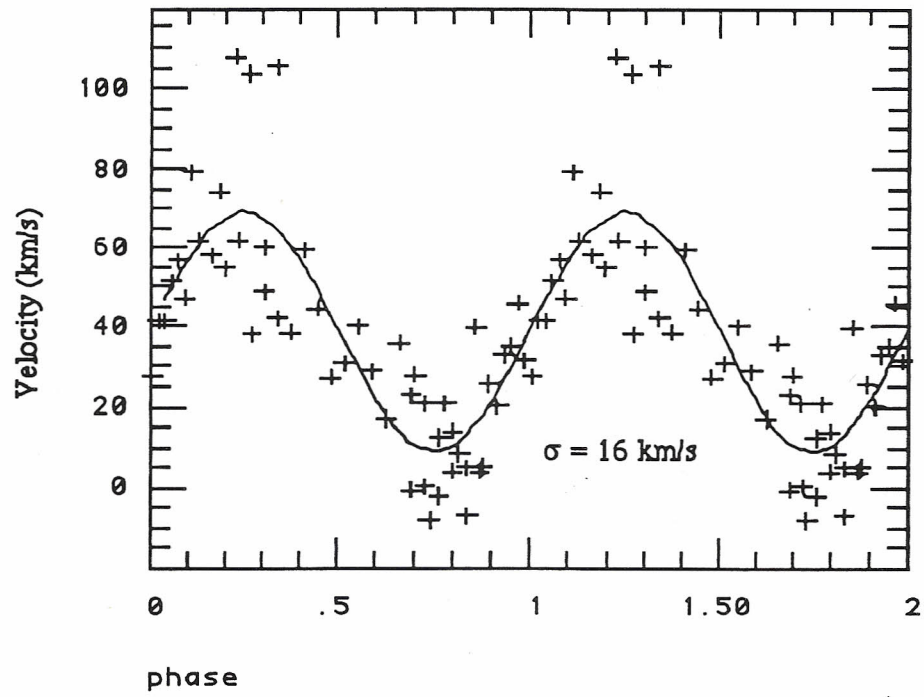


Fig. 5.9 - Periodogram of H α Velocities

PG 1341-079 = HS Vir

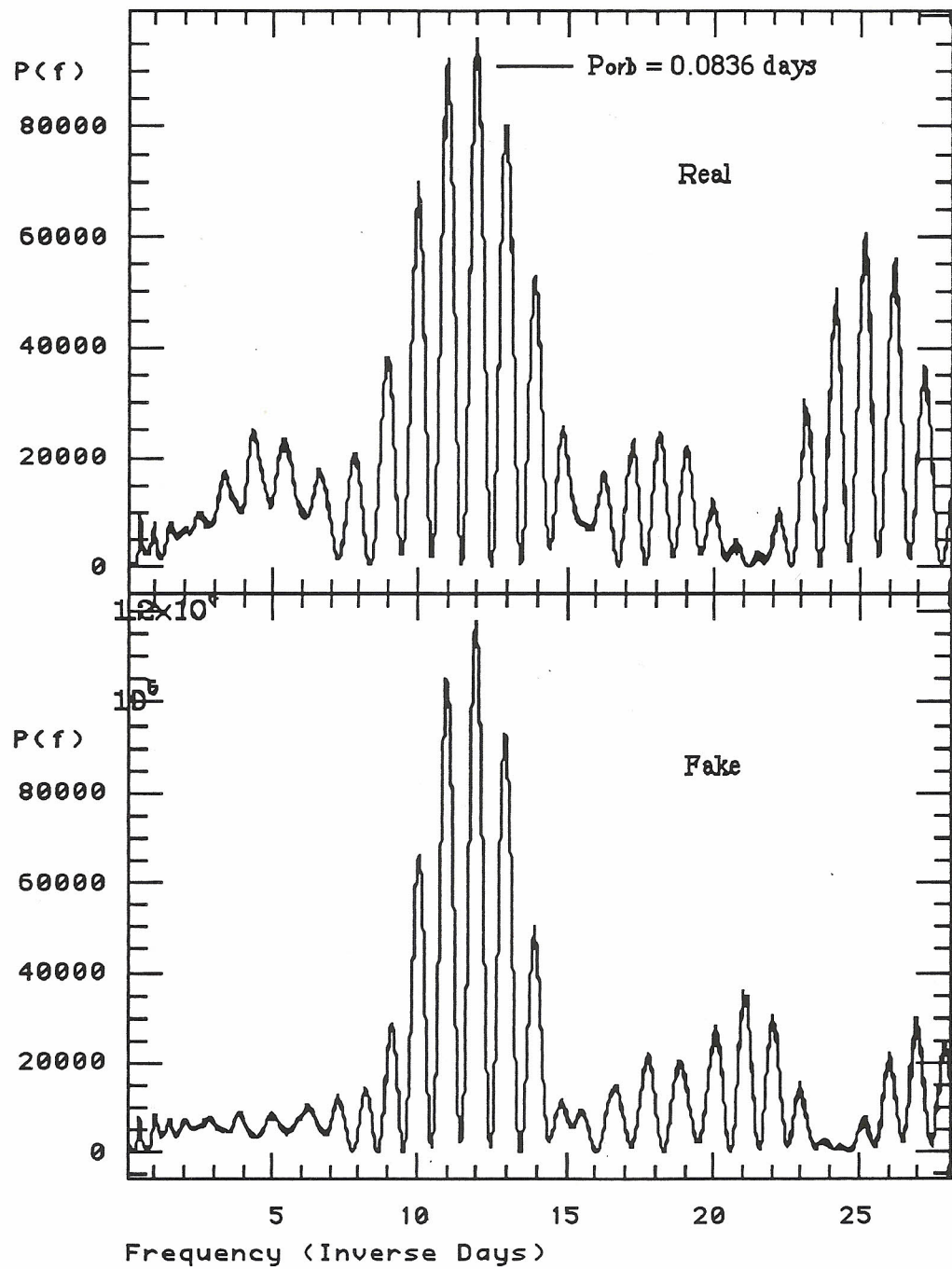


Fig. 5.10 - H α Radial Velocities

PG 1341-079 = HS Vir

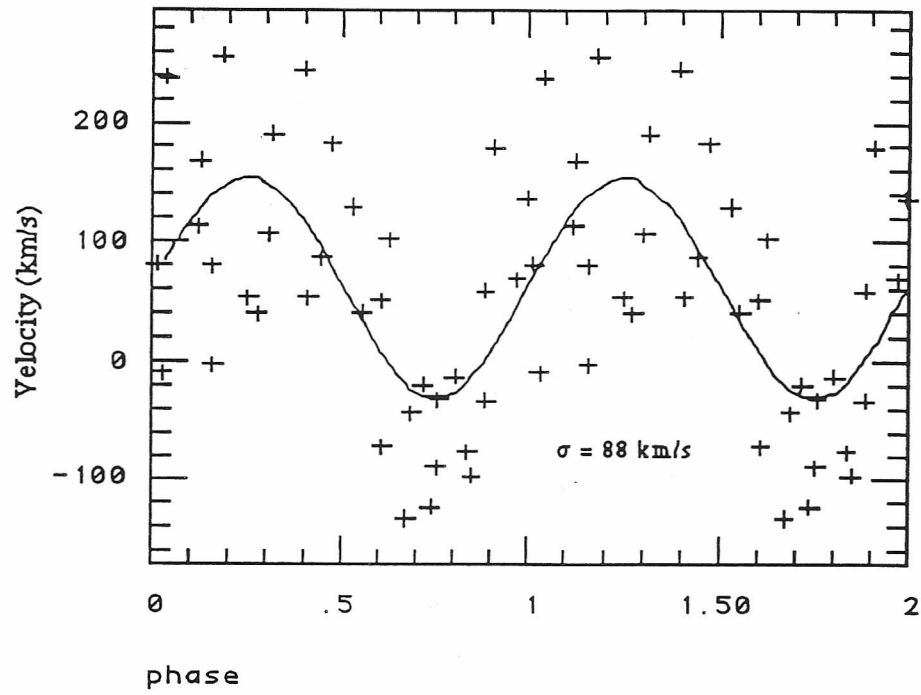


Fig. 5.11 - Periodogram of H α Velocities

PG 1524+622

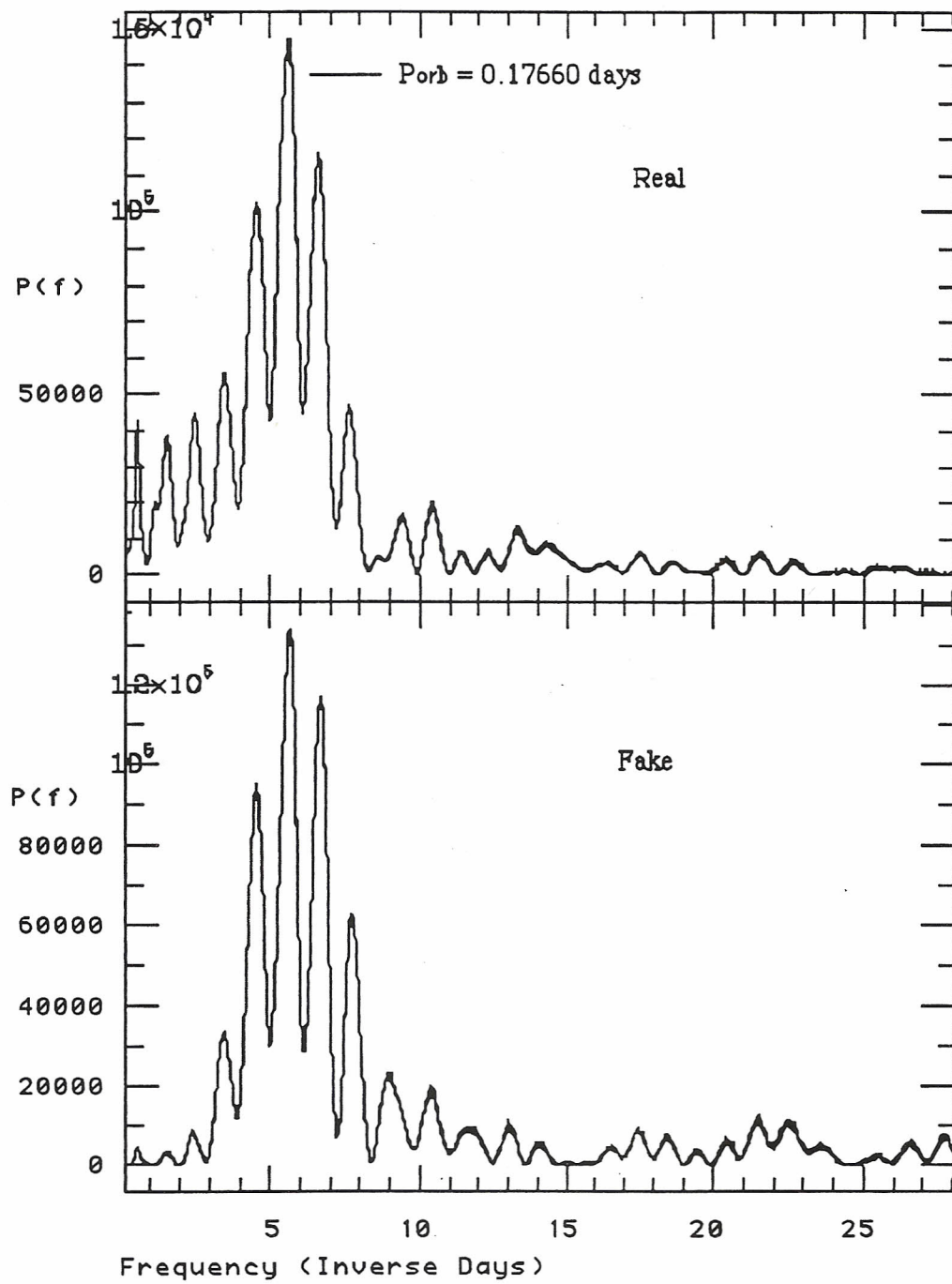


Fig. 5.12 - Periodogram of H α Velocities

PG 1524+622

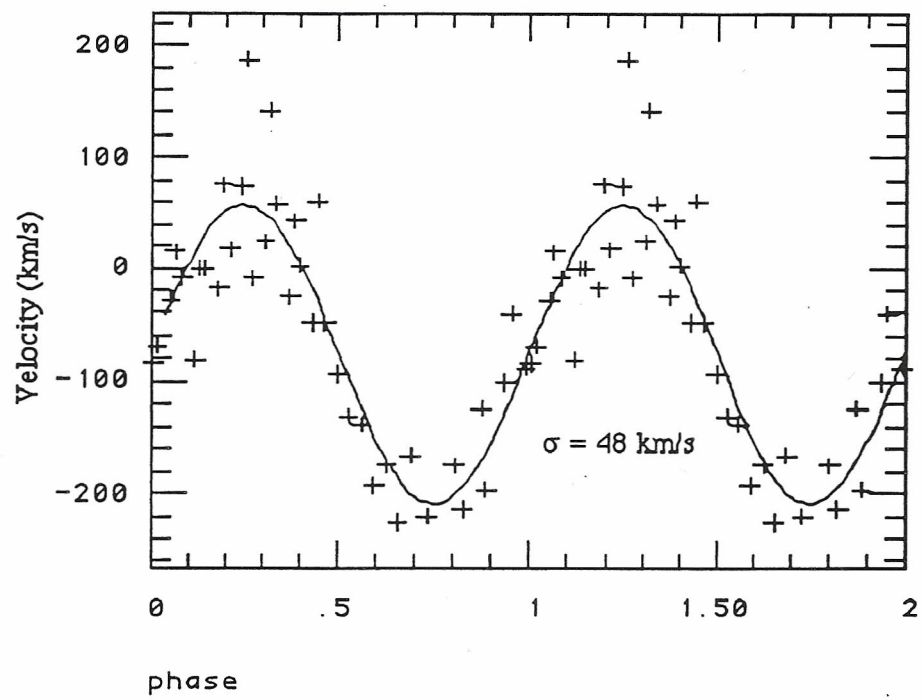


Fig. 5.13 - Periodogram of H α Velocities

PG 1543+145 = CT Ser = N Ser 1948

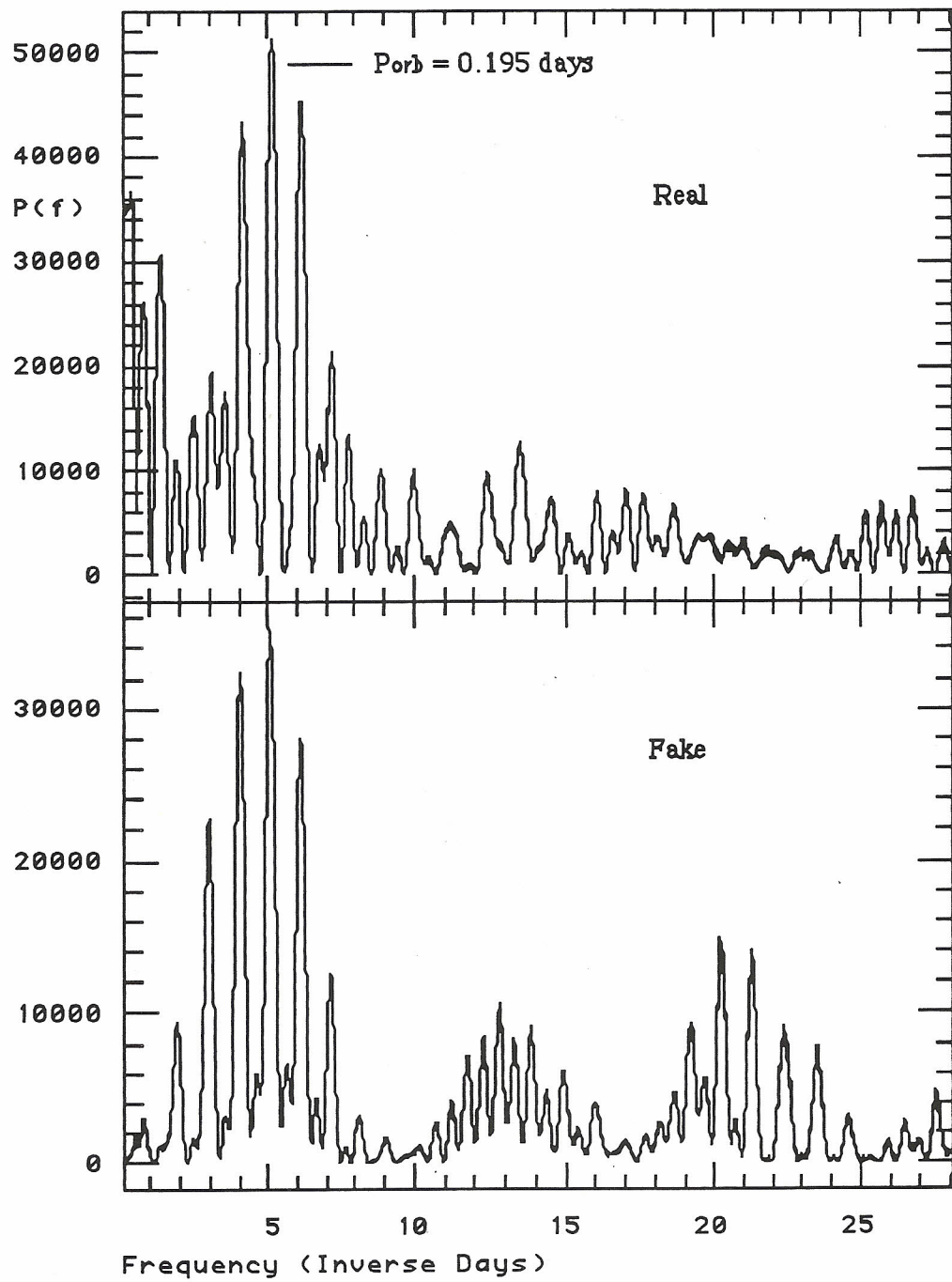


Fig. 5.14 - H α Radial Velocities

PG 1543+145 = CT Ser = N Ser 1948

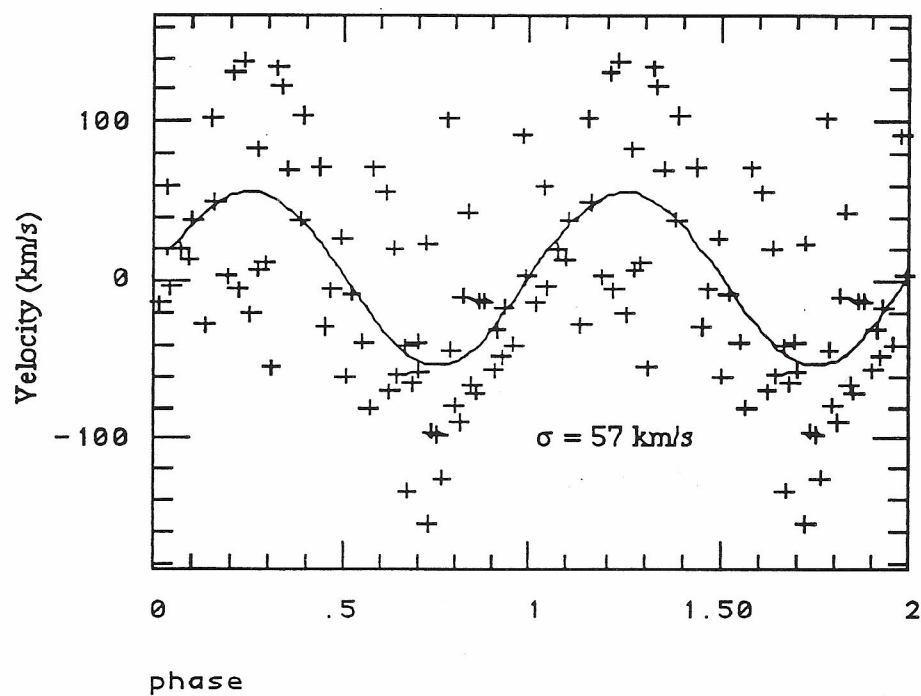


Fig. 5.15 - Periodogram of Ha Velocities

PG 1717+413 = V825 Her

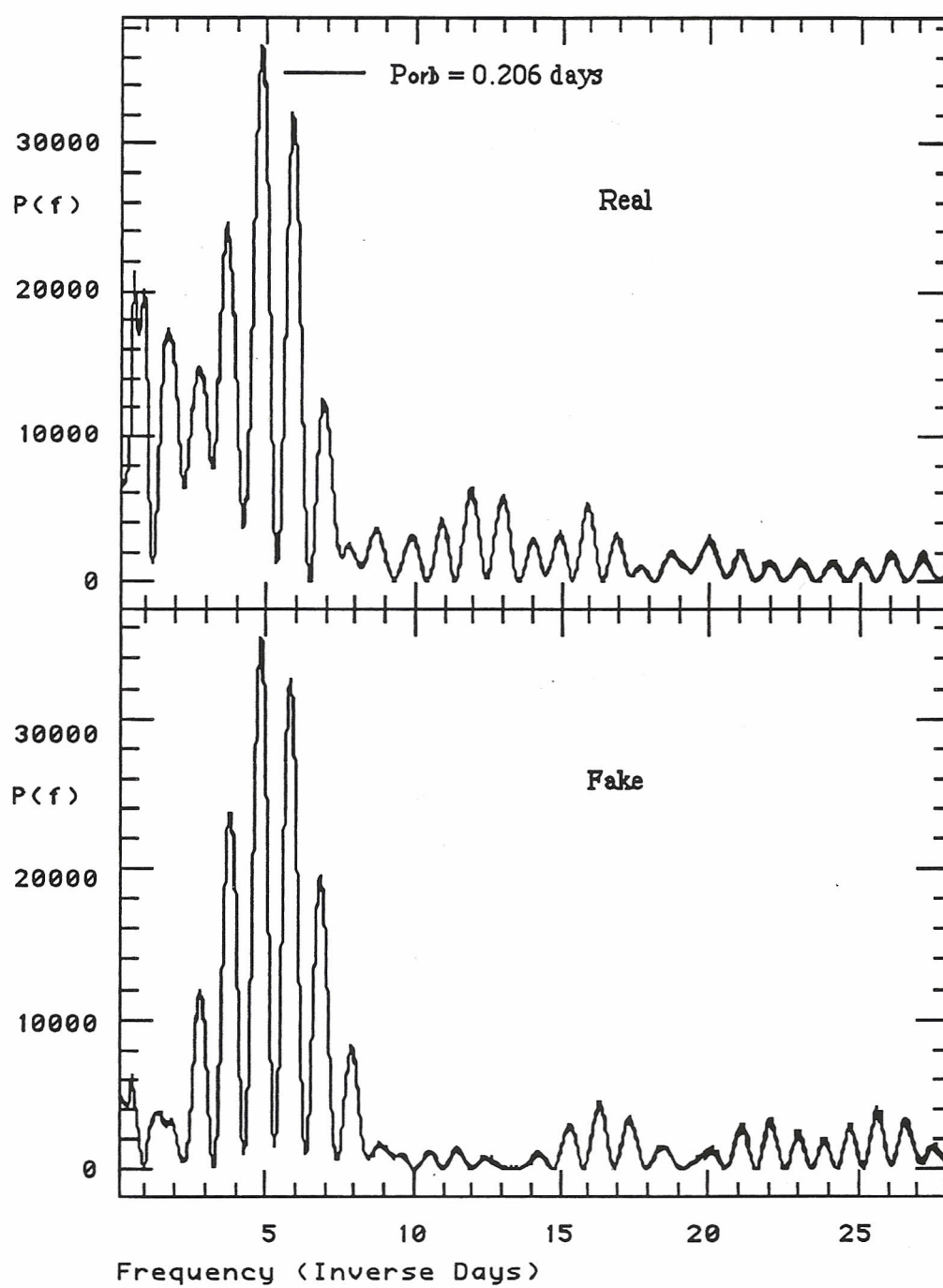


Fig. 5.16 - H α Radial Velocities

PG 1717+413 = V825 Her

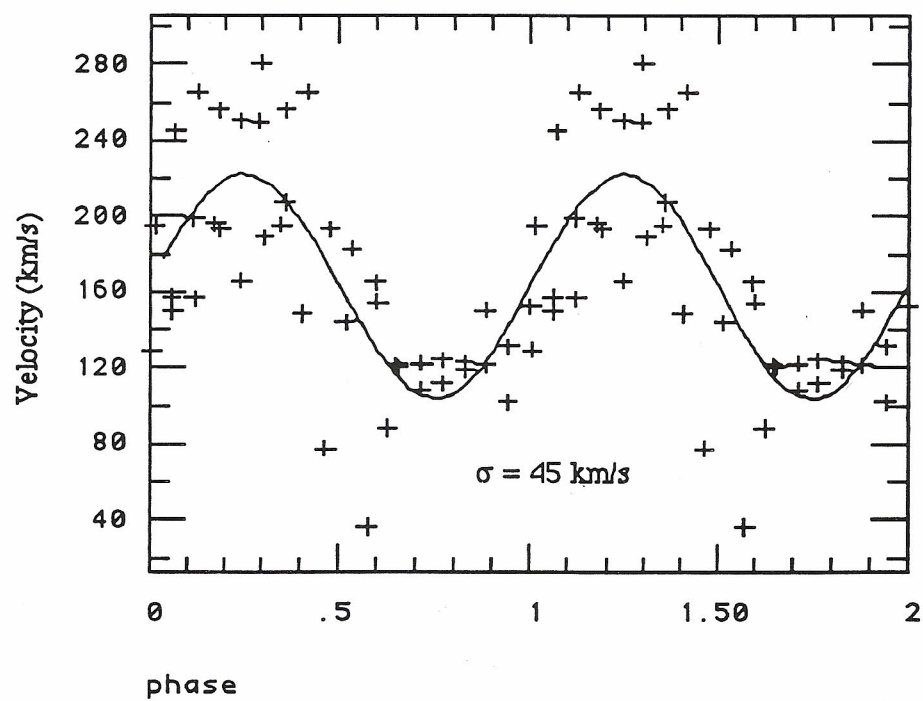


Fig. 5.17 - Periodogram of H α Velocities

PG 2133+115

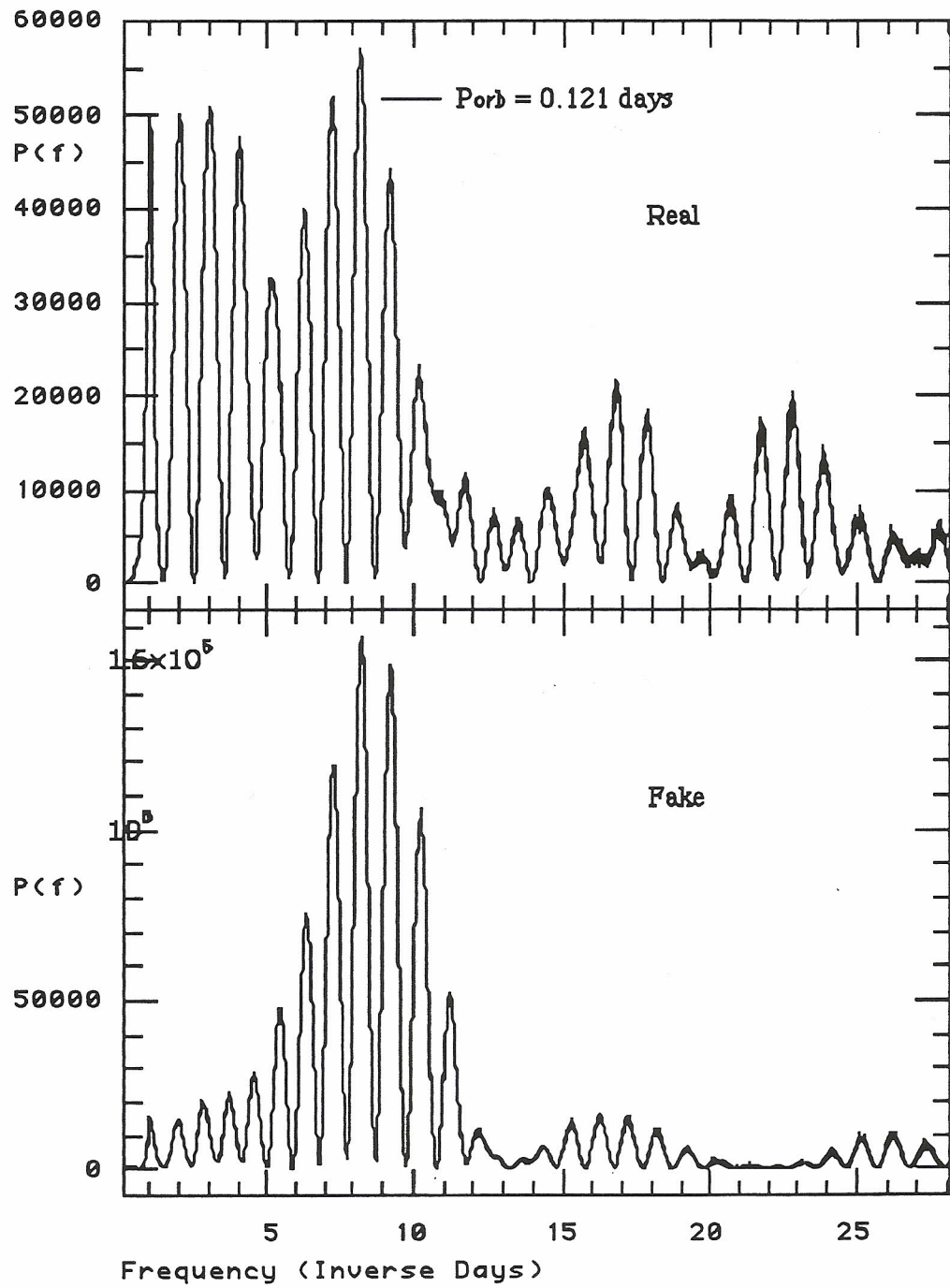
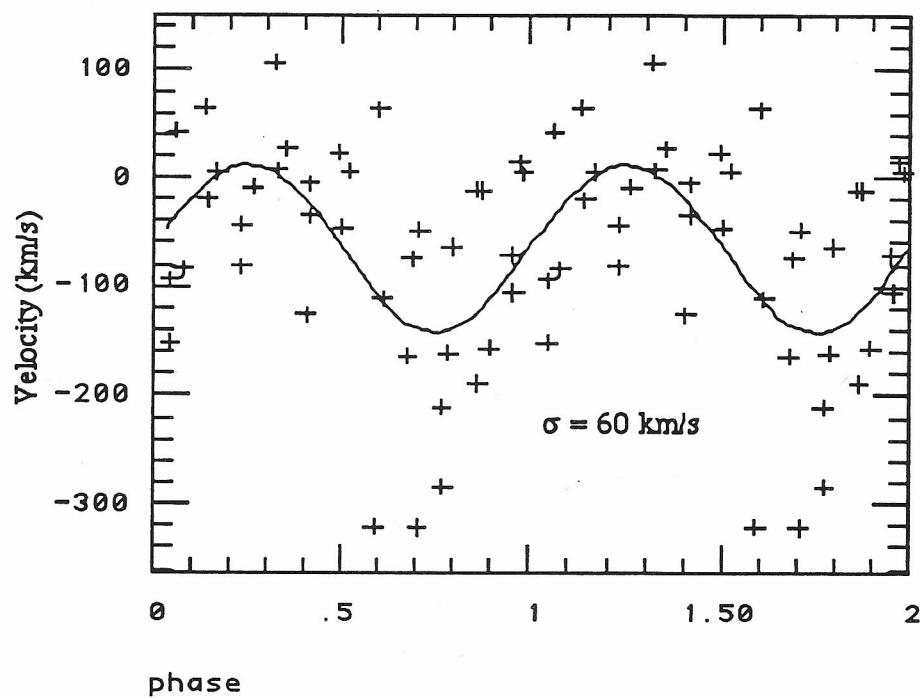


Fig. 5.18 - H α Radial Velocities

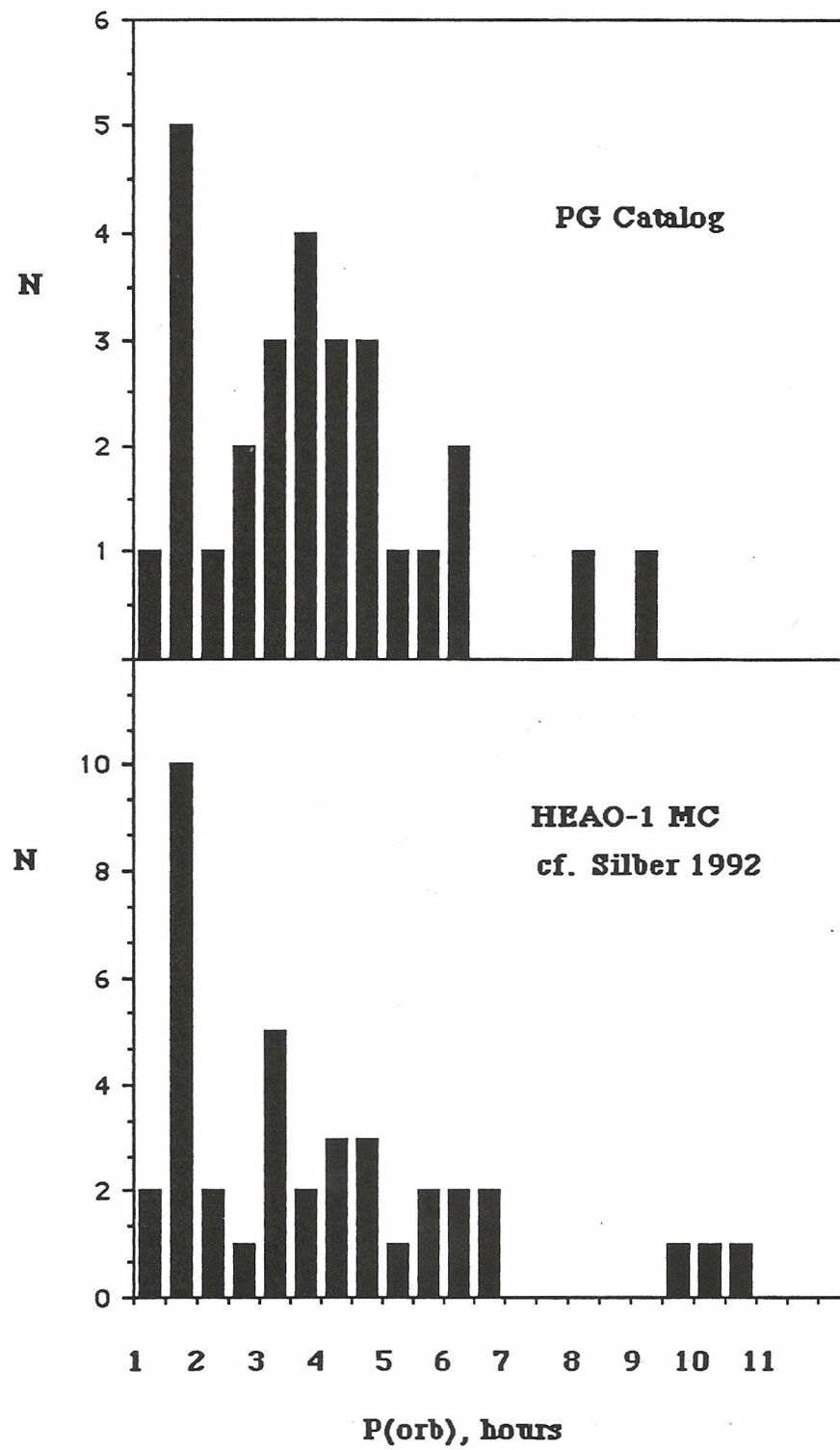
PG 2133+115



70

Z

Fig. 5.20 - CV Orbital Period Distributions from the PG and HEAO-1 MC surveys



Chapter 6

The Individual Stars Found by the Survey

Table 6.1 summarizes the properties of the PG CVs. Column 1 is the “address,” or designation of GSL86. Column 2 is the star’s name. Columns 3 and 4 are the most precise 1950.0 coordinates available, with references in the notes on the page following Table 6.1. Column 5 lists *B* magnitudes from GSL86. The four CVs I excluded from the sample in Chapter 3 because they are normally fainter than the faintest limiting magnitude of the PG catalog are listed separately at the bottom of Table 6.1. I also revised their listed *B*-magnitudes to reflect their normal brightness, referenced below, although since these are cataclysmic variable stars, this is necessarily somewhat arbitrary. Column 6 lists the orbital periods, not quoted to full precision, which are quoted to full precision and referenced in Table 5.11. Column 7 lists comments on the outburst type and other properties. The notation for these comments is explained in the notes on the page following Table 6.1.

Explanations for why I made these comments will make up the rest of this chapter. For “completeness,” I include in Table 6.2 a list of 11 CV candidates, classified as CV, CV?, or ?? by GSL86, but not in their complete sample. This could occur in one of three ways: they were selected from fields taken before a limiting magnitude was decided upon; they were found by eye, and not with the scanner; or they were in whole fields that were rejected because of too-bright limiting magnitudes.

There are 55 objects listed as CV, 6 as CV:, 7 as CV? and 5 as ?? in the complete sample of GSL86. My follow-up blue and red spectroscopy, described in Chapter 2, shows that 33 of these 73 objects are CVs, and that 36 turn out not to be CVs. Table 6.3 lists my spectroscopic reclassifications for these other objects, in a format similar to the PG catalog. Most of these objects appear to be subdwarf B stars, identifiable by their uniform blue continua and deep, V-shaped Balmer lines, as opposed to the broad, shallow,

Gaussian absorption lines of CVs. Green (1991) has noted that GSL86 listed some objects as CVs because they have flux distributions that are flat in F_{ν} , and not only because they have Galactic-velocity emission lines, as stated by GSL86. They were not all clear CV candidates, as with the list of Green et al. (1982; hereafter GFLS82). Many PG stars taken originally as CVs are studied by Ferguson, Green, & Liebert (1984; hereafter FGL84), who interpret their spectra as those of hot subdwarfs with cool companions. Downes (1987), in his own UV-excess survey, finds stars with spectra resembling those of sdB stars, but with weak or “missing” H α . He attributes this to filling by H α emission, raised on a companion by the hot subdwarf, and I find several examples in this sample.

Why these 36 objects were misclassified is a matter of conjecture. Many original classifications of were based on MCSP scans, which have accurate energy distributions but very low spectral resolution. Others used Reticon scans, which are often noisy for the short classification exposures, especially in the red. Probably the best explanation, however, is that distinguishing CVs from detached objects can often be difficult. FGL84 suggest that a hot degenerate and a cool companion may mimic the optical energy distribution of a CV, flat in F_{ν} . To make matters worse, illumination of the cool companion may raise emission lines in its temperature-inverted chromosphere (Thorstensen et al. 1978; Ferguson et al. 1987). A tidally-locked cool companion to a hot subdwarf would rotate rapidly, increasing magnetic activity and raising emission lines, as in several classes of close binaries (Linsky 1988; Bianchini 1990; Maceroni et al. 1990). A blue continuum sporting emission lines could be taken for a CV, especially in the absence of time-resolved photometry to reveal flickering—or in its presence, which unless meticulously calibrated and of high S/N, can mislead one to thinking that any erratic variations detected are flickering. For example, the light curves of Wilson et al. (1986) could be taken to show flickering, even though neither NN Ser (Haefner 1989) nor PG 2240+193 (Szkody & Howell 1992) flicker.

Another, intriguing idea for why these objects are misclassified is that they are not.

Perhaps GSL86 are right, and these are CVs, after all: Warner (1976) and Garrison (1987) have raised the idea that face-on CVs, with steady, optically thick disks, may have weak emission lines and relatively strong, high-gravity absorption lines. With roughly Solar composition, such a disk spectrum might closely resemble that of an sdB, with strong hydrogen and weaker He I lines. This idea would be supported if optically thick accretion disks show limb darkening (Paczynski & Schwarzenberg-Czerny 1980), which might be expected on the basis of disk geometry alone. Even if all sdB stars are face-on CVs, however, it still will not solve the problem of the observed space density of CVs being much lower than expected from the nova rate (Patterson 1984), since at $2 - 4 \times 10^{-6} \text{ pc}^{-3}$ (Downes 1986a; Heber 1986), the space density of sdB stars is still too low.

Whatever the case, these "PG non-CVs" in Table 6.3 deserve further study, even to confirm the hypothesis of binarity. Patient time-resolved photometry and spectroscopy have shown this for BE UMa (Margon, Downes, & Katz 1981) and NN Ser (Haefner 1989), and radial velocity study has shown this for PG 1002+506, in Chapter 5 and below.

I now include short notes on all CVs in the complete sample of GSL86, although I will go into more detail with objects barely studied or newly brought to attention. I include in § 6.2 notes on the "non-CVs." Spectra for the CVs covered by the follow-up are in order of right ascension, in Appendix A, as are those of other objects, in Appendix B.

6.1. The Cataclysmic Variables

PG 0027+260

This is one of the SW Sex stars, a class of nova-likes considered in detail in Chapter 8. PG 0027+260 was the object of an intensive optical spectroscopic and photometric and *IUE* study by Thorstensen et al. (1991b). It has two intriguing peculiarities: relatively shallow eclipses, the V-shaped profiles of which vary perhaps the most of any of

the SW Sex stars; and phase-0.5 absorption events in the metal lines. These mysterious events are characteristic of the class, although they have only been noticed so far in the Balmer and helium lines. This star was seen in 1984 by Thorstensen to be in a faint state, with $V > 17$, reminiscent of the low states of VY Scl and similar nova-likes with periods in the 3 – 4 hour range (see Ritter 1990).

PG 0134+070 = AY Psc

This nova-like has eclipses with a period of 313 minutes, found by Szkody et al. (1989) and with a refined ephemeris by Diaz & Steiner (1990) (see Table 5.11). I observed this object with a red setup described in Chapter 2 on 1991 October 29 UT, and obtained 33 spectra with 600-second exposures (see Table 6.4). With a least-squares fit to a sinusoid with the photometric period, I find a spectroscopic ephemeris of $\text{MHJD} = 8558.8195 \pm 0.0031$ days, $K_{\text{em}} = 106 \pm 14 \text{ km s}^{-1}$, and $\gamma_{\text{em}} = 21 \pm 10 \text{ km s}^{-1}$, with $\sigma = 58 \text{ km s}^{-1}$. Allowing the spectroscopic period to vary does not produce a significantly different fit. The radial velocities were measured with the double-Gaussian method of Shafter (1983a), with a separation of 1300 km s^{-1} , which maximizes K_{em}/σ for orbital periods both fixed and allowed to vary.

When extrapolated to 1991 October 29 UT, the photometric ephemeris accumulates a $2\text{-}\sigma$ error of 0.0017 days = 0.008 cycles, or about 3° . The photometric ephemeris also predicts an eclipse at $\text{MHJD} = 8558.91278 \pm 0.0018$ days, which is spectroscopic phase 0.429—but an eclipse should occur at spectroscopic phase 0.5, when the red star is in inferior conjunction. This implies a phase lag of 0.071 cycles, or $26 \pm 3^\circ$. This is consistent with the value found by Szkody & Howell (1993), of $18 \pm 11^\circ$. Such phase lags are not uncommon for nova-likes (Shafter 1991), although the SW Sex stars (Chapter 8) have the largest phase lags, up to 76° . The phase-resolved spectra of Szkody & Howell (1993), of 3-Å resolution, do not show the phase-0.5 absorption characteristic of the SW Sex stars.

Instead, they show a narrow emission component moving back and forth in the H β and H γ emission lines. This is reminiscent of that seen in V1193 Ori (Ringwald, Thorstensen, & Hamwey 1993), in IP Peg (Hessman 1989), in RW Tri and UX UMa (Honeycutt, Kaitchuck, & Schlegel 1987), in IX Vel (Beuermann & Thomas 1990). All these are UX UMa stars, except IP Peg, which was a dwarf nova just coming out of outburst. AY Psc has not so far been seen to show absorption wings about its emission lines, though, but neither is a red star obvious.

PG 0244+104 = WX Ari

This star was the object of blue and H α radial velocity studies, by Beuermann et al. (1992). It is the only SW Sex star (see Chapter 8) not showing obvious eclipses. Another peculiarity, for an SW Sex star, is that it shows double-peaked He I emission lines. That WX Ari is an SW Sex star is shown by the periodic absorption events in the otherwise single-peaked Balmer emission lines (Beuermann et al. 1992, their Figs. 5 and 6). These also occur strongly in the He I lines, contributing to its double-peaked appearance in the summed spectrum. He II $\lambda 4686$ and C III / N III $\lambda\lambda 4640 - 4650$ are in relatively weak emission, O I $\lambda 7773$ is in very weak absorption, if present at all, and there are no obvious TiO bands to show the red star.

Even without an eclipse, there is evidence of brightness asymmetry in the disk, as the equivalent widths of both H β and H γ (but not He I $\lambda 4471$) dip abruptly at spectroscopic phase 0.8. This often occurs in SW Sex stars opposite the eclipse (see Chapter 8). If this really is the red star's superior conjunction, it implies a phase lag between the light curve and radial velocity curve of $\approx 72^\circ$. Such a large phase lag would not be unusual for an SW Sex star, although it would for any other type of CV (Shafter 1991).

PG 0808+627 = SU UMa

This is the well-studied prototype of the SU UMa stars, a sub-class of dwarf novæ. With the discovery of superhumps while in superoutburst, it became the perfect prototype (Udalski 1990a). Many papers have been published on it, including the orbital period determination (Thorstensen, Wade, & Oke 1986). Patterson & Richman (1991) note that its photometric period is slightly longer than its spectroscopic period, and so may exhibit permanent superhumps.

PG 0818+513 = BH Lyn

BH Lyn is another SW Sex star. Dhillon et al. (1992) caught it when it was faint, with the continuum level a factor of ≈ 6 lower than that of Thorstensen, Davis, & Ringwald (1991a). Intriguingly, in this low state, several properties characteristic of the SW Sex stars (see Chapter 8) were diminished: the Balmer and He I lines were deeply eclipsed, the high-excitation lines of C III / N III $\lambda\lambda 4640 - 4650$ nearly disappeared, and the eclipse became somewhat less V-shaped. The O I $\lambda 7773$ feature was also in deep absorption, although it nearly disappeared in eclipse; in the brighter state observed by Thorstensen et al. (1991a), it had also disappeared.

PG 0834+488 = EI UMa

At first glance, the spectrum of EI UMa resembles that of a dwarf nova, with H α and other Balmer emission lines towering over the continuum (GFLS82; Thorstensen 1986; Silber 1992). High-excitation emission lines are strong, too, with He II $\lambda 4686$ emission half as high as H β above the continuum, or higher. Although the only published *IUE* spectrum, SWP 19038 (la Dous 1991), is noisy, C IV $\lambda 1549$ is clearly in emission, with no obvious P Cygni profile. This star is also an X-ray source, 1H 0832+488 (Wood et al. 1984). An *EXOSAT* observation (Cook 1985) showed a hard spectrum with temperature,

column density, luminosity (with an assumed distance), and X-ray-to-optical ratio all consistent with this CV being a dwarf nova. No coherent X-ray pulsations were found. This and the 6.43-hour orbital period might make one think it was similar to SS Cyg or EM Cyg. No red star is obvious in the spectrum, though, which is surprising, since the orbital period is so long. The optical variability is not well studied, either, with only about 40 photographic observations over about 800 days by Andronov (1986a). They show about one magnitude of variation, which is large for random flickering, but the sampling is too sparse to show convincingly it has ever actually had a dwarf nova outburst.

PG 0849+580 = BZ UMa

This dwarf nova is the object of an intensive study in Chapter 9.

PG 0858+181 = SY Cnc

This is a well-studied dwarf nova, with outburst statistics compiled from AAVSO data by Szkody & Mattei (1984). It is one of two PG dwarf novæ of the Z Cam subclass, which show standstills; the other is PG 1642+253 = AH Her (see below).

PG 0859+415

This star is the object of a detailed study by Grauer et al. (1993). High-speed photometry reveals an orbital hump and shallow eclipses, with a period of 220 minutes. I obtained time-resolved spectra of this object with a red setup (see Chapter 2) on 1991 March 3 UT, for just over one orbital cycle. Fig. 6.1 is the grand-average of these spectra. There are broad, strong, emission lines, one of high excitation (C II $\lambda 7234$, from continuum fluorescence: see Williams & Ferguson 1983). There is also a blue continuum, with a power-law slope of -2.5 in F_λ , and no obvious TiO band at $\lambda 7600$, normally the strongest CV red star feature. Broad, shallow O I $\lambda 7773$ may be present, but only barely so, even despite a S/N

of 80 in this part of the spectrum. The red spectrum is therefore consistent with this object being a nova-like having a luminous, steady-state disk, although no observations over time are available, to check for outbursts or their lack.

Velocities of $H\alpha$ were measured with a Shafter (1983a) double-Gaussian technique, with a Gaussian separation of 1400 km s^{-1} , about 80% of the FWZI of the line (FWHM is 1300 km s^{-1}) (see Chapter 2). These were fit to a sinusoid with the photometric period (see Table 5.11). After achieving a good fit, the period was allowed to vary, and did not change significantly when allowed to do so, but then again only one cycle was observed. The derived parameters and their errors are: $T_0 = 8318.6585 \pm 0.0050$ (MHJD), $K_{\text{em}} = 130 \pm 22 \text{ km s}^{-1}$, $\gamma_{\text{em}} = 53 \pm 16 \text{ km s}^{-1}$, with $\sigma = 59 \text{ km s}^{-1}$. The photometric ephemeris of Grauer et al. (1993) was built up over 8482 cycles, ending in 1992, so the spectroscopic ephemeris can be matched and plotted over the photometric cycle (see Fig. 6.2). The eclipse, at photometric phase 0, should occur at spectroscopic phase 0.5. In fact it occurs at phase 0.402, so there is obviously a phase lag of $35 \pm 1^\circ$.

When the $H\alpha$ line from the time-resolved spectra is plotted on an expanded scale, a phase-0.5 absorption event becomes apparent (see Fig. 6.3). This is defining characteristic of the SW Sex stars (see Chapter 8). Classification as an SW Sex star is consistent with this star's high-excitation spectrum: a blue spectrum taken with the MMT by J. Liebert and G. Schmidt (Grauer et al. 1993) shows a He II $\lambda 4686$ emission comparable in height to $H\beta$. This is high excitation even for an SW Sex star, as only DW UMa can match this (Shafter, Hessman, & Zhang 1988). However, PG 0859+415 also shows broad absorption wings flanking $H\beta$ and the higher Balmer lines—characteristic of UX UMa nova-like, and previously unknown in any SW Sex star. Also, Grauer et al. (1993) suspect the presence of a 25.5-second periodicity in the high-speed photometry. This period is more typical of those of dwarf nova oscillations than of magnetic CVs (Warner 1988, p. 139; Ritter 1990), and so, if real at all, may come from an optically-thick disk, such as those of

UX UMa stars. This star, then, is the first CV known to show defining characteristics common to both the SW Sex stars and the UX UMa stars. It is interesting that this stars' phase lag of 35° is intermediate the maximum values known so far for UX UMa stars (22° , ranging up from zero) and the minimum for SW Sex stars (48° , ranging up to 76°) (Shafter 1991). This curious hybrid tends to support an interpretation of the SW Sex stars' mysterious effects being from disk asymmetries and stream-disk interactions, and not white dwarf magnetism (for a review, see Dhillon, Marsh, & Jones 1990).

PG 0911-066

This object is at $B \approx 18.7$ on the Palomar Observatory Sky Survey (hereafter *POSS*) O print, and was at $B > 15.5$ in several times I attempted to find it in 1990 and 1991. At the Harvard archive I examined fourteen A-series plates, with limiting magnitudes near $m_{pg} = 16$, and twelve MC-series plates, with limiting magnitudes between $m_{pg} = 15.5$ and 17.5, and never saw it once. It is clearly fainter than $B = 14.3$ listed by GSL86. GFLS82 describe a spectrum with "emission peaks centered in absorption troughs." A rare, optically thick high state implies that this object is a dwarf nova, which just happened to be in outburst when the exposure for that field in the PG survey was being taken, so I exclude it from my sample.

PG 0917+342

Dobrzycka & Howell (1992) claim this is the first UX UMa star to be found beneath the period gap, with a spectroscopic period of 104 minutes. Chapter 5 of this work does concur roughly with this period, although a cycle-count ambiguity still needs to be resolved. Both spectra in Appendix A, taken a week apart, do resemble that of a UX UMa star, with the absorption wings flanking the Balmer lines and no obvious red star. This may not necessarily be a nova-like, however, as it has large continuum variations, similar to

those of a dwarf nova (Szkody & Howell 1992).

Dobrzycka & Howell (1992) also find peculiar, blue-shifted line profiles. This nova-like roughly coincides in position with the nova of 101 A.D. Perhaps this is just a coincidence, since ancient position measurements were poor, but it is 29' from the third magnitude star α Lyn, which one might think would act as a fiducial (Hertzog 1986). The chance of two CVs this close together in the sky is tiny, considering their low space density (Patterson 1984). May this be the most ancient nova ever recovered, by over a millennium?

PG 0935+075

This “new” CV is one of the six objects classified in the PG catalog as “??”, with an additional listing of “VAR?” in the comments column. Its magnitude is listed as $B = 14.3$, although this star is at $B \approx 17.5$ and $R \approx 17.5$ on the *POSS*. A search of 41 Harvard RB and RH sky patrol plates, which reach $m_{pg} \approx 13 - 14$, found nothing. Using 11 MC-series plates, however, I found it twice, at $m_{pg} \approx 16.9$. I attempted to observe this object with *IUE*, but the spectrum is greatly underexposed (see Fig. 6.4). I did obtain two quiescent optical spectra, however (see Appendix A). The blue spectrum shows strong, broad H α and H β of nearly equal height. The red spectrum shows TiO bands from the red star, at $\lambda\lambda 7150$ and 7600 . This star probably is a dwarf nova that happened to in outburst when Green observed it, so I exclude it from the sample.

PG 0943+521

This “new” $B \approx 14$ nova-like went unnoticed until now. The blue spectrum reveals it to be a UX UMa (see Appendix A). *IUE* spectra (Fig. 6.5), taken in 1991 February, show a predominantly absorption line spectrum, indicating an optically thick disk. A strong P Cygni profile in C IV $\lambda 1549$ is also present. If this indicates a bipolar wind (Córdova & Howarth 1987), then this CV should be at low inclination. My radial velocity study in

Chapter 5 had difficulty finding a period. $H\alpha$ is weak and narrow, and K_{em} is small, consistent with this being a face-on CV. That this is a nova-like, and not a dwarf nova in outburst, is supported only by its lack of variability during the survey and *IUE* spectra and radial velocity study.

PG 1000+667

I have found an orbital period of 4.06 ± 0.02 hours for this “new” CV (see Chapter 5). *IUE* spectra (Fig. 6.6) show only a flat continuum and C IV $\lambda 1549$ in emission, with a P Cygni profile. This could be from most any type of face-on CV, either nova-like or a dwarf nova in outburst. The optical spectrum more resembles that of a nova-like, with narrow $H\alpha$ and $H\beta$ emission lines, a strong continuum, and no obvious red star. He II $\lambda 4686$ may be present, but the blue spectrum is noisy. Surprisingly, O I $\lambda 7773$ is in emission, as more often occurs in quiescent dwarf novæ (Friend et al. 1988). There is no obvious variability during the eight days between the blue and red follow-up spectra, although dwarf novæ can have interoutburst intervals much longer than this (Szkody & Mattei 1984).

PG 1003+678 = CH UMa

This orbital period of this dwarf nova was found by Thorstensen (1986). Bruch (1989) shows blue spectra in outburst and in quiescence. The red spectra of Friend et al. (1990) suggest it has an evolved red star, since its spectral type appears “too cool for credibility” to fit inside its Roche lobe, assuming the main sequence mass-radius relation of Patterson (1984). Friend et al. (1990) also carried out a radial velocity study by cross-correlating absorption features of the red star with a K7 dwarf. This study resolved a cycle-count ambiguity in the previous orbital period determination. A significant eccentricity, $e = 0.10 \pm 0.03$, was also found, and was attributed to illumination of the red star by the disk (Davey & Smith 1992), and not to actual eccentricity of the orbit.

PG 1012-029 = SW Sex

This is the prototype of the SW Sextans class of nova-likes, discussed in Chapter 8, and is among the brightest. The high-excitation C III /N III $\lambda\lambda 4640 - 4650$ and He II $\lambda 4686$ emission lines are shown by Williams & Ferguson (1982) to be highly variable in SW Sex. These lines are usually eclipsed most strongly of any lines in the SW Sex stars (e.g., Dhillon, Marsh, & Jones 1991). While in SW Sex they do decrease in flux in eclipse, they rival H β in strength when just coming out of eclipse.

PG 1030+590 = DW UMa

This SW Sex star is the object of a spectroscopic and photometric study by Shafter et al. (1988). Its eclipse profile is variable, not unlike that of PG 0027+260. This star was observed by Hessman (1990) in a low state. Also like PG 0027+260, at one epoch it showed what may have been an orbital hump, from the bright spot swinging in front of the star—except both are in patently the wrong place in the phase, slightly *after* the eclipse! A peculiarity of this star is that its He II $\lambda 4686$ emission rivals H β in strength.

PG 1038+155 = DO Leo

Nearly all that is known about this faint nova-like comes from the description of the spectrum by GFLS82 and the time-resolved photometry of Abbott et al. (1990), who find V-shaped eclipses with a 5.63-hour period. Abbott et al. also show a low-resolution CCD spectrum. They do not see the red continuum reported by GFLS82, although this spectrum only goes to $\lambda 6800$. They find a strong-lined nova-like spectrum, with He II $\lambda 4686$ in emission, about one-third the height of H β . The C III /N III feature at $\lambda\lambda 4640 - 4650$ may also be present, although S/N is low. A radial velocity study may be interesting: the spectrum and eclipses resemble those of an SW Sex star (see Chapter 8), although the period is in excess of five hours.

PG 1101+453 = AN UMa

This is a well-studied magnetic CV, similar to AM Her. Two papers recommended by Ritter (1990) as “jumping-off places” are by Szkody, Downes, & Mateo (1988) and by Cropper et al. (1989). As with PG 1550+191 = MR Ser, the other AM Her star in the PG catalog, this star has ill-understood “low states,” reminiscent of, but not necessarily related to, the low states seen in VY Scl stars, or in certain X-ray binaries, such as Her X-1.

PG 1114+187

This object went unnoticed until now. The orbital period is unknown, and flickering should be searched for, to confirm that it is a CV. This is not the same object as the faint ($V \approx 17.8$) AM Her star, DP Leo = 1E 1114+18, a finding chart for which is given by Bierman et al. (1985). I took this originally to be a Be star, the only one found by the PG survey, because of the He I $\lambda 4471$ in absorption. $H\beta$ has a narrow emission core, though, with almost as much flux as $H\alpha$ (see Appendix A). CVs are noted for their flat Balmer decrements, as well as for their variability: a week after my blue follow-up spectrum was taken, the red spectrum shows a blue continuum with TiO bands at $\lambda\lambda 6800$ and 7150 , although not 7600 , so perhaps the red star is a K-type. The narrow $H\alpha$ emission had weakened, and the continuum level at $H\alpha$ is 50% lower than in the blue spectrum. This resembles a dwarf nova outburst or the low state of a VY Scl star, with a bright, optically thick state and a faint, optically thin state.

PG 1119+147 = SA79-B1

Both $H\alpha$ and $H\beta$ are in broad absorption, like those of a sdB, but they are filled with emission. He I $\lambda 4471$ is distinctly present in absorption. There is some indication there is also He II $\lambda\lambda 4686$ and 5411 absorption. Both spectra are noisy, but I tentatively classify this as a CV, although this needs confirmation.

PG 1135+036 = T Leo

This well-studied dwarf nova has the shortest orbital period of the PG CVs, near the 80-minute period minimum. It has rare outbursts, X-rays, superhumps, and a very low luminosity (see Warner 1987 and references therein).

PG 1140+719 = YY Dra

This star has a curious history. It was probably confused with DO Dra (Patterson & Eisenmann 1987), and is often referred to by that name. It has one of the lowest accretion luminosities of any of the PG CVs, and its red star is surprisingly easy to detect. A radial velocity study was done with the absorption lines, although it does not eclipse (Mateo, Szkody, & Garnavich 1991). Recently, coherent optical pulsations were found, showing that it is a DQ Her star (Patterson et al. 1992). Long thought to be a nova-like, since no outbursts were observed, Hazen (1986) searched the Harvard plate archive and found evidence for rare dwarf nova outbursts, with years between them.

PG 1142-041 = TW Vir

This is a well-known U Gem star, with its outburst statistics compiled by Szkody & Mattei (1984). Mateo, Szkody, & Bolte (1985) discovered ellipsoidal variations with time-resolved *H* Photometry. It was also the first dwarf nova caught spectroscopically on the rise to outburst (Mansperger & Kaitchuck 1990; see Chapter 10).

PG 1316+677

There is some doubt about whether this star is a CV. Weak, unresolved H α emission, and little or no H β on a noisy continuum do not tell much. There may be a trace of He I λ 5876 emission, but this may just noise. A bluer spectrum would be helpful here. There is no obvious red star, but this could use higher S/N. The orbital period is unknown.

PG 1341-079 = HS Vir

This CV has double-peaked H α emission, even in my low-resolution spectra, and a strong S-wave. The other Balmer lines are also in strong, broad emission, and He I is in weak emission (GFLS82; Bruch 1989). Although H α is strong, the orbital period determination was not as easy as one might have expected (see Chapter 5). With the first alias at 2.01 hours (see Table 5.1), this object defines the lower edge of the period gap for the PG CVs, but this orbital period should be confirmed before this is used in any analysis of the width of the period gap. Over two magnitudes of variability was noted by GFLS82 and by Osminkin (1985), so this object is probably a dwarf nova, especially since two red spectra, taken three days apart, show a continuum brightening of nearly a magnitude (see Appendix A). Howell et al. (1990) found a dip in its lightcurve with $\Delta R \approx 0.2$, although it does not occur in the next cycle, so the presence of eclipses is doubtful.

PG 1510+234

This is probably a dwarf nova, since its spectrum has the characteristic strong, broad Balmer lines. There is also evidence for continuum variability (see Appendix A). The blue spectrum of 1990 April 27 was taken when it was probably in outburst, since H α is weak and the continuum is strong and blue. The red spectrum of 1990 May 5 was taken after it appeared to fade into quiescence, as H α had strengthened and broadened and the continuum had flattened. All this occurred in the plausible time of eight days. This is the first time attention has been paid to this object. The orbital period is unknown.

PG 1524+622

This CV has a spectrum of a dwarf nova, with Balmer lines in strong, broad emission, a flat continuum, and hints of TiO bands at $\lambda\lambda 6800, 7150$, and 7600 (see Appendix A). The radial velocity curve is among the least noisy I measured (see Fig. 5.12), although

H α shows a curious velocity pop-up near phase 0.3. This is unlike a Z-wave, indicating eclipses, since there is no corresponding downward excursion of the lines from a rotational disturbance. If it were, it would suggest a 72° phase lag, quite unexpected in a dwarf nova at an orbital period of 4.29 hours (see Shafter 1991). He I $\lambda 5876$ emission is also present. Andronov (1991) examined 57 archival plates and found variability between $m_{pg} = 13.9$ and 16.3, with one variation of 1.3 mag in one day. Photographic photometry is notoriously imprecise, but variations this large are probably real: this CV is probably a dwarf nova, although follow-up observations will be necessary to characterize any outbursts present.

PG 1543+145 = CT Ser = N Ser 1948

Comparing the nova atlas of Bode, Duerbeck, & Evans (1989) with GSL86 reveals only one classical nova, PG 1543+145 = CT Ser = Nova Ser 1948. See the discussions in Chapter 3 (excluding it from the complete sample, since it had a nova outburst in 1948 and was still bright in 1973 – 1974, when the PG survey photographs were taken), Chapter 4 (putting an upper limit on the space density of classical novæ with just it), and Chapter 5 (the orbital period determination).

PG 1550+191 = MR Ser

This is a well-studied magnetic CV, similar to AM Her, as is PG 1101+453 = AN UMa. Recognized by Liebert et al. (1982), MR Ser has occasional low states (Szkody et al. 1988; Szkody 1988), in which the red star was detected (Mukai & Charles 1986).

PG 1551+719 = SS UMi

This faint SU UMa star has a quiescent level near $V = 17$, falling below the limiting magnitude of the PG survey, although it rises to $V \approx 13$ in outburst. Discovered as an X-ray source (Mason et al. 1982), its spectrum was described by GFLS82. It has been ob-

served in quiescence and in outburst by Andronov (1986b), Richter (1989), and in outburst by Udalski (1990b). It was caught in superoutburst by Chen, Liu, & Wei (1991), who found superhumps with a 101-minute period.

PG 1633+115

This star is on the list of white dwarfs of Fleming, Liebert, & Green (1986; hereafter FLG86), although I find it quite different from a white dwarf. My blue spectrum in Appendix A shows weak, narrow H α emission, and weak, broad H β absorption, and perhaps also He I λ 5876. The corresponding red spectrum, taken six days later, shows weak, but broad H α emission on a noticeably fainter continuum. I suspect this object is a dwarf nova, although more photometric observations are needed to confirm this. Silber (1992, private communication) notes this star as a possible marginally-detected HEAO-1 X-ray source, and suspects activity on Harvard archive plates. The orbital period is unknown.

PG 1642+253 = AH Her

This is a bright, well-studied dwarf nova. It is one of two dwarf novae in the PG catalog of the Z Cam subclass, which show standstills. A study of its outburst photometry was done by Szkody & Mattei (1984), using AAVSO data. Horne, Wade, & Szkody (1986) made a serious attempt at mass-radius determination of the component stars, using high-resolution radial velocities measured from the absorption lines.

PG 1711+336 = V795 Her

This CV, described by GFLS82, is in the CV period gap, shown by the extensive radial velocity study of Shafter et al. (1990). Its photometric period is slightly less than the spectroscopic period. Patterson & Richman (1991) suggest this might be from permanent superhumps in the accretion disk. Being in the period gap does suggest an extreme mass

ratio (Hameury, King, & Lasota 1991), an essential agreement for superhumps (Whitehurst 1988; Molnar & Kobulnicky 1992), particularly since this CV is a luminous nova-like with no obvious red star. Zhang et al. (1991) find a tight correlation between orbital period and superhump period for SU UMa star, which extends to V795 Her (see their Fig. 1).

However, Zhang et al. (1991) also show the photometric period of V795 Her to be stable over a timescale of years, with $\dot{P} < 1.7 \times 10^{-9}$. This is much longer than any expected disk viscous timescale, and much stabler than ever observed in superhumps, which are observed to decrease on a timescale of weeks, with $\dot{P} \approx 5 \times 10^{-5}$ (Warner 1985; Udalski 1990a). This suggests that V795 Her is a DQ Her star, although it lacks strong X-ray emission (Rosen et al. 1989), and the correlation with the superhump periods is puzzling.

PG 1717+413 = V825 Her

This nova-like was the first of two found by FGL84, in their search for “thick disk” systems. I carried out a time-resolved radial velocity study in 1991 May, and found an orbital period of 4.94 hours (see Table 5.1). A separate 14.5 hours of observing produced a possible flare event, with a sudden brightening and broadening of H α (Ringwald 1991). In a study of X-ray-selected CVs, Silber (1992) found no coherent optical pulsations, so this is probably not a magnetic CV. The red and blue spectra in Appendix A show no obvious cyclotron or red star features, and weak H α emission. If He II $\lambda 4686$ is present, it is weak. H β is in filled-in absorption, and the He I lines are in absorption, as is the O I $\lambda 7773$ feature.

PG 2133+115

This nova-like was the second of two found by FGL84 in a search for “thick disk” systems. Its spectrum is similar to that of UX UMa, with often only H α in emission. I carried out a radial velocity study (see Chapter 5) and found its orbital period to be 2.90

hours, just at the upper edge of the period gap, although the line was weak, which made velocity measurements uncertain. A confirmation should be done before this period is used for statistical purposes on the width of the period gap (Hameury et al. 1991), especially since this was the only one of my radial velocity curves with a significant false alarm probability.

PG 2337+123 = HX Peg

This dwarf nova is the object of an intensive study in Chapter 10.

6.2. Objects Previously Thought to be Cataclysmic Variables

I doubt if these are CVs, but they should be checked for flickering, anyway. More interestingly, if these are detached binary stars, time-resolved photometry might uncover sinusoidal illumination variations, or ellipsoidal variations, not to mention the odd eclipse. I should emphasize that while many may be binaries, time-resolved photometry, radial velocity studies, or even just sightings of spectral features from both stars in static spectra exist for only a handful. All spectra, unless otherwise noted, are in Appendix B.

PG 0023+298

Balmer and He I $\lambda\lambda 4026$ and 4471 absorption lines are present in a spectrum kindly provided by Green (1991), which justifies the classification by GSL86 as sdOA. A noisy red spectrum shows only a blue continuum, convincingly, and maybe H α absorption. The spectra show no other obvious resemblance to a CV, such as emission lines, except the continuum, which is relatively flat in F_{ν} .

PG 0048+091

This star is on the white dwarf list of Green (1980), but not of FLG86. It is classified by GSL86 as a CV, although my red spectrum has H α in broad, deep absorption, and on a blue continuum that closely matches that of an sdB. There are also no He I lines and possibly also some Paschen absorption lines.

PG 0051+169

Another unpublished Reticon scan from Green (1991) shows an sdB spectrum with an energy distribution flat in F_{ν} . An absorption feature from the G-band, the CH absorption feature at $\lambda\lambda 4290 - 4314$ often used as an indicator for G stars, may be present, but the scan is noisy. My red spectrum shows just H α absorption, which may have filled-in emission, although I caution that this spectrum is noisy, too.

PG 0914+120

In two separate epochs, the H α line in this object is weak, probably filled in by emission, even though both spectra are noisy. This effect is not uncommon in sdB stars (Downes 1987). H β probably suffered a cosmic ray or some other electronic glitch, since the line dips below zero. The continuum matches that of an sdB, as GSL86 classify it; there are no signs of it being a CV, however.

PG 0935+087

This star was classified by GSL86 as ??. It shows only faint helium absorption lines, the strongest being He II $\lambda\lambda 4686$ and 5411 . I therefore classify it as a DO.

PG 0947+462

This object is classified as ?? by GSL86. I identify it as the blue compact emission-line galaxy Markarian 125, by comparing the finding charts of Markarian (1969) and GSL86. Inspecting blue and red *POSS* prints shows no other blue object with $B < 15.8$ within several arc minutes. The coordinates of GSL86 and of Peterson (1973) match to within 1.1 seconds of time and arc, but such good agreement is perhaps fortuitous, since PG coordinates are precise only to $5 - 10''$.

PG 0948+344 = RZ LMi

GFLS82 describe this star as having an emission line spectrum with an inverted Balmer decrement. Wegner & Swanson (1990a) show such a spectrum, with the Balmer lines in narrow emission. On the other hand, Szkody & Howell (1992) show a spectrum quite like that of a subdwarf B star, although they note $H\alpha$ has an emission core. He I $\lambda 4471$ is also weakly present, so I infer that the proper spectral type is sdB-O. Kopylov et al. (1988) show an absorption spectrum.

Fig. 6.7 shows that the $H\alpha$ line can vary from weak, narrow emission to shallow, broad absorption rapidly, between 15-minute exposures. This line can appear completely filled in low-dispersion spectra: note the difference in $H\alpha$ line profiles between the spectra in Appendix B. This kind of phenomenon was attributed by Downes (1987) as the cause of "the stars with $H\alpha$ missing." A pair of *IUE* spectra show a subdwarf spectrum (Fig. 6.8), not unlike that of PG 2300+166 (Fig. 6.9). Weak Si III $\lambda 1300$ and Si IV $\lambda 1400$ features are in absorption, and there is no obvious C IV $\lambda 1549$.

This star is probably like Feige 24 (Thorstensen et al. 1978), BE UMa (Margon et al. 1981), or NN Ser (Haefner 1989), with a hot degenerate heating a cool companion and raising emission lines in its temperature-inverted atmosphere. The orbital period could be days long, though (see Ritter 1986b; Ritter 1990), so finding it may require patient time-re-

solved spectroscopic follow-up. Since GFLS82 report a magnitude range of $B = 14.4 - 16.8$. Since it is usually easier to get time on a small telescope than on a large telescope, it may be useful to carry out time-resolved photometry first, to find any eclipses present. If the reported $\Delta B = 2.4$ range is due to an illumination effect on the cool star, it will be among the strongest known. Observing this photometrically may also be useful for characterizing the cool companion, using the method of Russell (1945) as implemented by Szkody & Feinswog (1988), since a fourth-magnitude subdwarf could well overwhelm a cool companion's spectrum.

PG 1002+506

This star has a spectrum resembling an sdB star, with $H\beta$ in broad, V-shaped absorption on a blue continuum. There is also a trace of He I $\lambda 4471$, so its spectral type is sdB-O. However, $H\alpha$ is in very strong, narrow emission (see Appendix B). An *IUE* short-wavelength spectrum (Fig. 6.10) shows none of the usual lines that CVs show, except for perhaps Si III $\lambda 1300$ absorption, but Lyman α appears to be in absorption. It appears more like a white dwarf spectrum (see Wegner & Swanson 1991). A radial velocity study, summarized in Chapter 5, shows a relatively clean sinusoidal variation with a 7.65-hour period that is probably the orbit. Such a period is relatively short for a detached binary with a hot degenerate and a cool companion, but it is not unheard of (Ritter 1986b).

This star deserves detailed follow-up. It is probably not a CV, but in the light of the suggestion by Warner (1976) that face-on CVs may resemble sdBs, it would be interesting to do time-resolved photometry, to see if it flickers. Finding ellipsoidal or illumination variations would help constrain the binary parameters, too. This is not necessarily another BE UMa, however (see below), since the equivalent width of $H\alpha$ changes relatively little about the orbit (Fig 6.11).

PG 1038+270

This star is one of the five listed as ?? by GSL86. While there is no blue spectrum, the red spectrum resembles that of a horizontal branch B (HBB) star, with a blue continuum similar to those of the sdBs, and unresolved $H\alpha$ in deep absorption.

PG 1104+022

$H\alpha$ and $H\beta$ in deep, wide absorption and no He I $\lambda 4471$ show this to be an sdB star. He II $\lambda 4686$ may be present in weak absorption, although the spectrum is noisy. There are no other traces of a binary companion, or similarities to a CV.

PG 1128+098

In addition to $H\alpha$ and $H\beta$ absorption, this star shows wide, pronounced He I $\lambda 4471$ absorption. I therefore classify it as an sdOA.

PG 1136+581

Monica K. Davis kindly provided the unfluxed spectrum in Appendix B. It covers $\lambda\lambda 4800 - 7600$, and was taken with 1.3-m telescope, one of the Mark III spectrographs, and the BRICC and its TI-4849 CCD, the multilayer coating of which produces bumps in raw spectra. I identify this object as a blue compact galaxy, as it looks like a fuzzy point on the *POSS* blue print. It is coincident with 7 ZW 415 and LB 2070, as well as Markarian 1450, as the finding chart of Markarian, Lipovetskii, & Stepanyan (1981) and precise coordinates of Kojoian, Chute, & Aumann (1984) show. As a starburst galaxy, its spectrum is of interest, since even in this unfluxed spectrum, it is obvious that [N II] $\lambda 6583$ is unusually weak, compared with $H\alpha$ (Veilleux & Osterbrock 1987). $H\beta$ also appears unusually weak, compared to the [O III] lines, but a flux-calibrated spectrum will be necessary to take this analysis further.

PG 1146+228

This star shows H α and H β in absorption and a trace of He I λ 4471, so I classify it as an sdB-O. There are no features to suggest it is a CV, though.

PG 1155+492 = BE UMa

This star was for some time thought to be similar to a CV, but uniquely peculiar (Ferguson et al. 1981). Patient time-resolved studies showed it to be a detached binary (Margon et al. 1981), with a DO white dwarf illuminating an M1 – M5 dwarf, and producing a rich emission-line spectrum of extreme variability (Ferguson et al. 1987), not to mention many papers, including the discovery of eclipses by Ando, Okazaki, & Nishimura (1982), detailed atmospheric fitting by Wesemael, Green, & Liebert (1985), and time-resolved *IUE* spectroscopy by Hutchings & Cowley (1985).

PG 1156-037

This star is in the white dwarf list of Green (1980), but not of FLG86. Its bright sdB spectrum (see Appendix B) may have been taken for a white dwarf, but shows little similarity to a CV. He I λ 4471 absorption may be present, but very faintly.

PG 1157+004

I identify this star as a DA white dwarf, because of its broadened H α and H β lines. The red spectrum shows H α has a distinctly Lorentzian profile, showing pressure broadening. No other lines are obvious, nor are any characteristics of CVs such as a red star.

PG 1217-067

This star is on the white dwarf list of Green (1980), but not of FLG86. It has an sdB spectrum, with unusually narrow H β , which is still resolved and so this probably is

not an HBB.

PG 1257+010

This is the only star I have no spectra of, nor are there any published. If GSL86 could classify it as an sdB-O, though, it is probably not a CV.

PG 1314+041

This star has the spectrum of an sdB star. He I $\lambda 4471$ may be present, but the spectrum is noisy. The spectrum does not otherwise resemble that of a CV.

PG 1315-123

This star is in the white dwarf list of FLG86, but not of Green (1980). Its relatively narrow H α and H β lines lead me to reclassify it as an sdB.

PG 1443+337

This star is in the white dwarf list of FLG86, but not of Green (1980). It is also CBS 200, from the Case Low-Dispersion Northern Sky Survey (Pesch & Sanduleak 1989). It is a composite spectrum object, with broad H β absorption from a white dwarf, as well as strong Na D and TiO at $\lambda\lambda 6800, 7150$, and 7600 , from a cool dwarf companion. H α is weak, probably filled with emission from the cool star. Other such spectrum composites will be discussed in Chapter 7.

PG 1445+584

Andronov (1991) examined archival plates of this star, with inconclusive results. I find an sdB spectrum, with H α and H β in absorption and no other features.

PG 1459-026

This star shows an sdB spectrum, with $H\alpha$ and $H\beta$ in absorption. Mg b and Na D absorption may also be present, although higher S/N is needed to confirm this.

PG 1517+265

This star was studied by FGL84, who show a blue spectrum and judge it to be a subdwarf binary. From its energy distribution, they infer the presence of a K3.5 companion to an sdB of $T = 28,000$ K.

PG 1520-050

This star has faint $H\alpha$ and $H\beta$ absorption on a very blue continuum, resembling an sdB. No other features are present, but S/N is low.

PG 1522+122

This star has an sdB spectrum. Higher S/N in the blue would be useful, though, since noise variations there may be hiding He I $\lambda 4471$ and other features.

PG 1550+131 = NN Ser

GFLS82 describe this star's emission spectrum. Haefner (1989) shows it to be an eclipsing detached binary with a strong illumination effect by a hot degenerate of a cool companion. Very deep (≈ 4.8 mag) eclipses were also discovered, along with a variable spectrum, with absorption lines going into emission during superior conjunction of the cool companion. *IUE* spectra were taken and analyzed in detail by Wood & Marsh (1991).

PG 1617+150

This sdB shows a broad absorption feature near $\lambda 5174$, which may be Mg b, since Na D is also present in absorption. While the red continuum is redder than most other sdBs, no obvious red star features are present. I therefore designate this object peculiar in Table 6.3, in the unexpected event it is a metal-rich subdwarf. No helium lines are obvious.

PG 1639+338

This object was found by the Kiso survey, KUV 433-6 = KUV 16395+3351, with spectroscopic follow-up by Wegner, McMahan, & Boley (1987), who classify it as NHB: either normal, horizontal branch, or subdwarf B. I find a spectrum like other sdBs, though.

PG 1657+656

GSL86 classify this as an sdB-O, and it does have a spectrum resembling an sdB with a trace of He I $\lambda 4471$. No other features are obvious, though.

PG 1710+567

A high S/N spectrum covering $\lambda\lambda 4000 - 5000$ is shown by Moehler et al. (1990), who classify it as an sdOB. My red spectrum shows H α on a blue continuum and no other obvious features, except perhaps Paschen lines.

PG 1712+493

Comparing the finding charts of Sanduleak (1983) and GSL86 will show this is the nucleus of the well-studied planetary nebula, PK 075+35 1 = PN Sa 4-1. Its peculiar *IUE* and optical spectra were discussed by Feibelman (1987) and Feibelman & Bruhweiler (1989), which lacks certain nebular emission lines, particularly C III] $\lambda 1909$.

PG 2200+085

The is the fifth object in the complete sample of GSL86 classified as ??. Blue spectra of Green (1991) show no hydrogen features, although they do show a Balmer jump in absorption, the G-band (λ 4304), and Mg b and Na D absorption lines, although not strong Ca II H and K lines. My red spectrum (Appendix B) shows faint H α , the only hydrogen line obvious in any of the spectra, as well as K I and Ca II. Comparison with the spectra of Silva & Cornell (1992) shows this object has a K5 spectral type. It is not obvious why this star is in the PG catalog, though, since it is not particularly blue. Perhaps it is a flare star, which flared when the Schmidt film for this field was being exposed. Whatever this object is, it is not a subdwarf or a CV.

PG 2240+193 = KQ Peg

GFLS82 list this star as a CV candidate, with H α and H β in emission and the higher Balmer lines in absorption, and with a Balmer decrement unusually steep for a CV. Szkody & Howell (1992) show a spectrum, in which V-shaped H α and H β lines in deep absorption. There is also a trace of He I λ 4471 absorption: this is an sdB-O spectrum. Howell et al. (1991) show a lightcurve constant to within $V \approx \pm 0.05$ mag over 3.5 hours. If this is a subdwarf heating a cool companion, the apparent lack of continuum variation may suggest an orbital period of many days.

PG 2300+166

This star was described by GFLS82 as having H α and He II λ 4686 in emission and the rest of the Balmer lines in absorption, with a decrement suggestive of emission-line filling. A 600-second Mark IIIa exposure taken on 1989 November 8 – 9 with the 1.3-m McGraw-Hill telescope and BRICC, provided by J. R. Thorstensen, shows a bright ($V \approx 13.0$) subdwarf spectrum (see Appendix B). This and my red spectrum show the Balmer

and Paschen lines in absorption. The He I lines are strong, with He I $\lambda\lambda$ 4921, 5015, 5876, and 6678, so I classify this star as an sdOA. There is also evidence for metal absorption, such as an indent in the He I λ 5876 line that may be Na D, and a broad absorption feature that may be Fe II λ 4954, although there is no obvious Fe II λ 5169 absorption, as suspected by GFLS82. It may instead be Ba II λ 4957. Barium stars do come disproportionately in binaries (McClure, Fletcher, & Nemec 1980; McClure 1983), and the companions are suspected of being white dwarfs (Böhm-Vitense, Nemec, & Proffitt 1984). Normally the G giant dominates the spectrum, though, and the degenerate component is much less easy to detect. Might this represent a previously-unseen evolutionary link?

If PG 2300+166 does have strong Ba II lines, then Ba II λ 4554 should be obvious in a high S/N blue spectrum. High-resolution spectroscopy would also be interesting, especially with H α , since this star may be a close binary with a variable spectrum from the illuminated face of a cool companion. *IUE* archive spectra SWP 24779 and LWP 5101, taken by John C. Raymond, show an sdB spectrum, with the characteristic continuum bump at $\lambda\lambda$ 1400 – 1500, and with metal absorption lines (see Fig. 6.9).

PG 2315+071

An unpublished scan from Green (1991) shows a flat, composite spectrum over $\lambda\lambda$ 3700 – 6600, with Balmer lines and a G-band. Green commented it is probably an sdB+sdG.

Table 6.1.

Cataclysmic Variables from the Palomar-Green Catalog

"Address"	Name	RA(1950)	DEC(1950)	B	P(hr)	Type
0027+260		00 27 28.1	+26 00 54	2	15.41	3.51 ecl SW VY
0134+070	AY Psc	01 34 18.3	+07 01 14	2	15.41	5.22 ecl NL
0244+104	WX Ari	02 44 54.2	+10 23 07	2	15.10	3.34 SW
0808+627	SU UMa	08 08 05.5	+62 45 23	B	15.27	1.83 SU PSH XR AAVSO
0818+513	BH Lyn	08 18 54.0	+51 15 02	2	15.29	3.74 ecl SW VY
0834+488	EI UMa	08 34 49.3	+48 48 37	2	14.83	6.43 DN: XR
0849+580	BZ UMa	08 49 52.5	+58 00 04	B	16.32	1.63 WZ* XR AAVSO
0858+181	SY Cnc	08 58 14.3	+18 05 44	W	14.18	9.12 ZC AAVSO
0859+415		08 59 53.7	+41 29 41	2	14.19	3.67 ecl UX SW
0917+342		09 17 08.3	+34 09 24	2	15.09	1.80: DN:
0943+521		09 43 50.6	+52 08 03	2	14.16	4.79 New - UX
1000+667		10 00 45.3	+66 43 48	2	15.09	4.06 New - NL:
1003+678	CH UMa	10 03 08.9	+67 47 26	B	15.97	8.23 UG AAVSO
1012-029	SW Sex	10 12 37.2	-02 53 35	M	14.75	3.24 ecl SW
1030+590	DW UMa	10 30 38.0	+59 02 24	2	15.02	3.28 ecl SW VY
1038+155	DO Leo	10 38 11.2	+15 27 14	2	15.75	5.63 ecl NL
1101+453	AN UMa	11 01 35.2	+45 19 27	2	16.08	1.91 AM AAVSO
1114+187		11 14 26.0	+18 42 24	5	15.22	? New - CV:
1119+147	SA79-B1	11 19 36.3	+14 42 45	5	15.91	? New - CV:
1135+036	T Leo	11 35 53.1	+03 38 43	2	14.82	1.41 WZ* XR AAVSO
1140+719	YY Dra	11 40 48.8	+71 57 59	W	15.85	3.96 WZ* DQ XR
1142-041	TW Vir	11 42 47.7	-04 09 25	W	15.39	4.38 UG AAVSO
1316+678		13 16 11.2	+67 47 46	5	16.02	? New - CV:
1341-079	HS Vir	13 41 00.6	-07 59 00	2	15.76	2.01: DN:
1510+234		15 10 50.0	+23 26 12	5	15.12	? New - DN:
1524+622		15 24 36.4	+62 11 28	2	15.44	4.29 New - DN:
1550+191	MR Ser	15 50 33.1	+19 05 18	L	16.27	1.89 AM
1633+115		16 33 24.6	+11 30 59	5	14.92	? New - DN: XR:
1642+253	AH Her	16 42 06.1	+25 20 31	W	14.34	6.20 ZC AAVSO
1711+336	V795 Her	17 11 05.7	+33 34 46	M	12.68	2.60 UX PSH/DQ:
1717+413	V825 Her	17 17 00.8	+41 18 51	2	13.79	4.94 UX XR
2133+115		21 33 53.4	+11 27 27	2	14.30	2.90: UX
2337+123	HX Peg	23 37 51.3	+12 21 03	2	14.29	4.82 DN
(33, total)						

Exclude from sample: CNe or DNe that were in outburst during survey

0911-066		09 11 45.4	-06 35 17	2	18	? DN
0935+075		09 35 57.9	+07 28 33	2	17	? New - DN
1543+145	CT Ser	15 43 19.6	+14 31 52	2	17.4	4.68 CN 1948 AAVSO
1551+719	SS UMi	15 51 40.6	+71 55 05	2	16.7	? SU
(4, total)						

Notes to Table 6.1:

Uncertainty is denoted by a colon (:)

(Column 4) Position references follow DEC(1950):

B Bruch, A. Fischer, F.-J., & Wilmsen, U. 1987, A&AS, 70, 481

M McNaught, R. H. 1986, IBVS, No. 2926

L Liebert, J., et al. 1982, ApJ, 256, 594

W Williams, G. 1983, ApJS, 53, 523

2 Measured to within 2" by the author with SAO High Energy measuring engine

5 PG catalog coordinates (Green, Schmidt, & Liebert 1986, ApJS, 61, 305)

(Column 5) B - B magnitude from Green, Schmidt, & Liebert (1986)

(Column 6) P(hr) - Orbital period, not quoted to full precision

? Orbital period unknown

(Column 7) Type:

ecl = eclipsing

PSH = photometric period exceeds spectroscopic period; may have permanent
superhumps (Patterson, J., & Richman, H. 1991, PASP, 103, 735)

XR = HEAO-1 MC-LASS X-ray source (Silber, A. D. 1992, Ph.D. thesis, M.I.T.)

AAVSO = monitored by AAVSO (Mattei, J. A. 1991, private communication)

DN = generic dwarf nova, subclass uncertain

UG = U Gem dwarf nova, with only normal outbursts

ZC = Z Cam dwarf nova, with standstills

SU = SU UMa dwarf nova, with normal outbursts, superoutbursts, & superhumps

WZ = WZ Sge dwarf nova, with only superoutbursts (subset of SU); only T Leo
has shown superhumps, others not well-enough observed

WZ* = Similar photometrically to WZ Sge, but not spectroscopically: red
star present

NL = generic nova-like, with no outbursts, bright continuum with no red
star obvious (called RW Tri stars by Warner, B. 1987, MNRAS, 227, 23)

UX = UX UMa nova-like, with absorption wings about Balmer and other lines
(subset of NL)

SW = SW Sex nova-like, with intermittent absorption events near phase 0.5
and large spectroscopic phase offsets (new class, subset of NL: see
Thorstensen et al. 1991, AJ, 102, 272)

VY = anti-dwarf nova; NL with unpredictable low states, excluding AM Hers

DQ = DQ Her star, with magnetized white dwarf

AM = AM Her star, with strongly magnetized white dwarf and no disk

CN = Classical nova; the only one found by PG is CT Ser = Nova Ser 1948

Table 6.2.

Suspected Palomar-Green CVs, but not in Complete Sample (Blim = 0). I did not take spectra of these objects: they may not necessarily be CVs.

"Address"	Name	RA(1950)	DEC(1950)	B	Comment	Class
0008+186		00 08 58.4	+18 33 05	5 16.21	PHL 719	CV
0240+066		02 40 15.8	+06 34 43	5 16.46		CV
0248+054		02 48 39.1	+05 25 35	5 16.19		CV
0322+078		03 22 52.6	+07 49 20	5 16.01	CV?	sd
0947+036		09 47 05.2	+03 38 13	5 16.76		CV
1116+349		11 16 48.6	+34 56 36	5 13.49	CBS 138	CV
1200-095		12 00 50.5	-09 31 32	5 16.35		??
1403-111		14 03 15.1	-11 03 22	5 15.92	COMP	sdB
2254+075		22 54 45.8	+07 27 17	5 16.01	PKS	BLL
2357+027		23 57 02.8	+02 39 11	5 16.41	PB 5660	??
2357+125		23 57 25.4	+12 28 06	5 16.44	COMP	CV
(11)						

Notes:

(Column 7) Comment and Class, with designations of Green, Schmidt, & Liebert (1986), with some reclassified by me.

Table 6.3.

NON-CVs, from the Palomar-Green Catalog (Green, Schmidt, & Liebert 1986)
Most may be hot/cool binaries (see Ferguson, Green, & Liebert 1984)

"Address"	Name	RA(1950)	DEC(1950)	B	Comment	Class
0023+298		00 23 15.5	+29 48 36	5 15.44		sdOA
0048+091		00 48 50.5	+09 05 16	5 14.95		sdB
0051+169		00 51 01.8	+16 53 24	5 15.64		sdB
0914+120		09 14 55.3	+12 02 33	5 16.19	NO HA	sdB
0935+087		09 35 40.9	+08 45 15	2 16.27		DO
0947+462		09 47 03.2	+46 11 29	5 15.76	Mrk 125	Gal
0948+344	RZ LMi	09 48 50.9	+34 21 30	2 14.57	VAR HA	Bin
1002+506		10 02 16.5	+50 35 15	2 15.36		Bin
1038+270		10 38 11.7	+27 00 40	5 16.01		HBB
1104+022		11 04 05.8	+02 11 12	5 14.07		sdB
1128+098		11 28 39.0	+09 48 49	5 14.60		sdOA
1136+581		11 36 06.2	+58 07 45	5 16.24	Mrk 1450	Gal
1146+228		11 46 25.6	+22 47 44	5 15.01		sdB-O
1155+492	BE UMa	11 55 09.8	+49 13 01	5 15.15		Bin
1156-037		11 56 48.3	-03 44 40	5 13.79		sdB
1157+004		11 57 18.1	+00 24 40	5 15.88		DA
1217-067		12 17 23.0	-06 43 04	5 14.85		sdB
1257+010		12 57 52.0	+01 01 39	5 15.80	CV?	sdB-O
1314+041		13 14 06.1	+04 04 07	5 15.37		sdB
1315-123		13 15 01.0	-12 17 05	5 15.25		sdB
1443+337	CBS 200	14 43 55.9	+33 41 28	5 16.01	COMP	DA2
1445+584		14 45 34.5	+58 21 46	5 15.84		sdB
1459-026		14 59 36.2	-02 34 11	5 14.92		sdB
1517+265		15 17 05.1	+26 28 10	5 15.80	Ton 228	Bin
1520-050		15 20 40.1	-05 01 03	5 15.29		sdB
1522+122		15 22 04.6	+12 12 38	5 15.78		sdB
1550+131	NN Ser	15 50 35.8	+13 03 35	5 16.03		Bin
1617+150		16 17 31.8	+15 00 20	5 15.41	PEC	sdB
1639+338		16 39 30.9	+33 50 33	5 15.34	K433-6	sdB
1657+656		16 57 14.4	+65 36 15	5 15.95		sdB-O
1710+567		17 10 26.7	+56 39 01	5 15.99		sdB
1712+493		17 12 32.4	+49 19 26	5 13.38	075+35 1	PNN
2200+085		22 00 51.9	+08 31 06	5 15.50	COMP	Bin
2240+193	KQ Peg	22 40 01.1	+19 16 34	5 15.71		sdB-O
2300+166		23 00 51.9	+16 33 30	5 15.29		sdOA
2315+071		23 15 15.9	+07 06 20	5 14.67	PB 5322	K
(36, total)						

Notes:

(Column 7) Comment and Class, with designations of Green, Schmidt, & Liebert (1986), but reclassified by me, and with new comments:

NO HA = sdB with H alpha weak or "missing" (Downes, R. A. 1987, ApJ, 316, 763)

VAR HA = variable H alpha line profile

Table 6.4. H α Emission Radial Velocities

HJD ^a	V	HJD ^a	V	HJD ^a	V	HJD ^a	V
(km s ⁻¹)		(km s ⁻¹)		(km s ⁻¹)		(km s ⁻¹)	
PG 0134+070 = AY Psc (1991 October) ^b							
8558.689	-36	8558.750	-28	8558.811	39	8558.872	148
8558.696	0	8558.758	-125	8558.819	-25	8558.880	128
8558.704	-25	8558.766	-106	8558.826	-8	8558.888	226
8558.711	70	8558.773	-98	8558.834	70	8558.896	219
8558.720	-61	8558.781	-116	8558.841	83	8558.903	144
8558.727	-84	8558.788	-79	8558.850	116	8558.911	40
8558.735	1	8558.795	-90	8558.857	98	8558.919	-63
8558.742	-71	8558.803	25	8558.865	127	8558.927	21
8558.750	-28						

^a Heliocentric Julian Date of mid-integration, minus 2 440 000.

^b Shafter (1983a) algorithm, Gaussian separation 1300 km s⁻¹.

Fig. 6.1. PG 0859+415 - 1991 March 3 UT

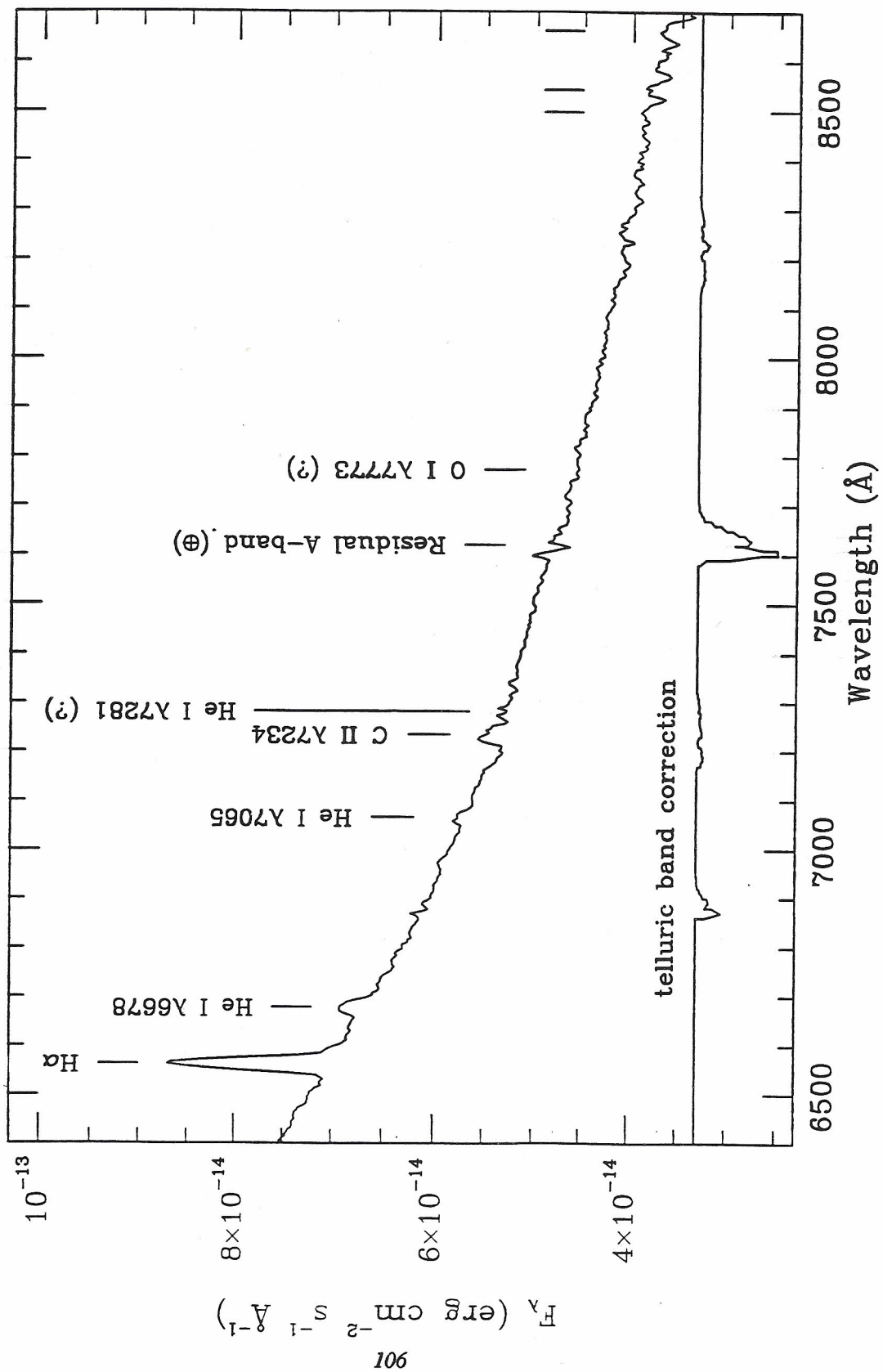


Fig. 6.2. PG 0859+415 - H α Radial Velocities

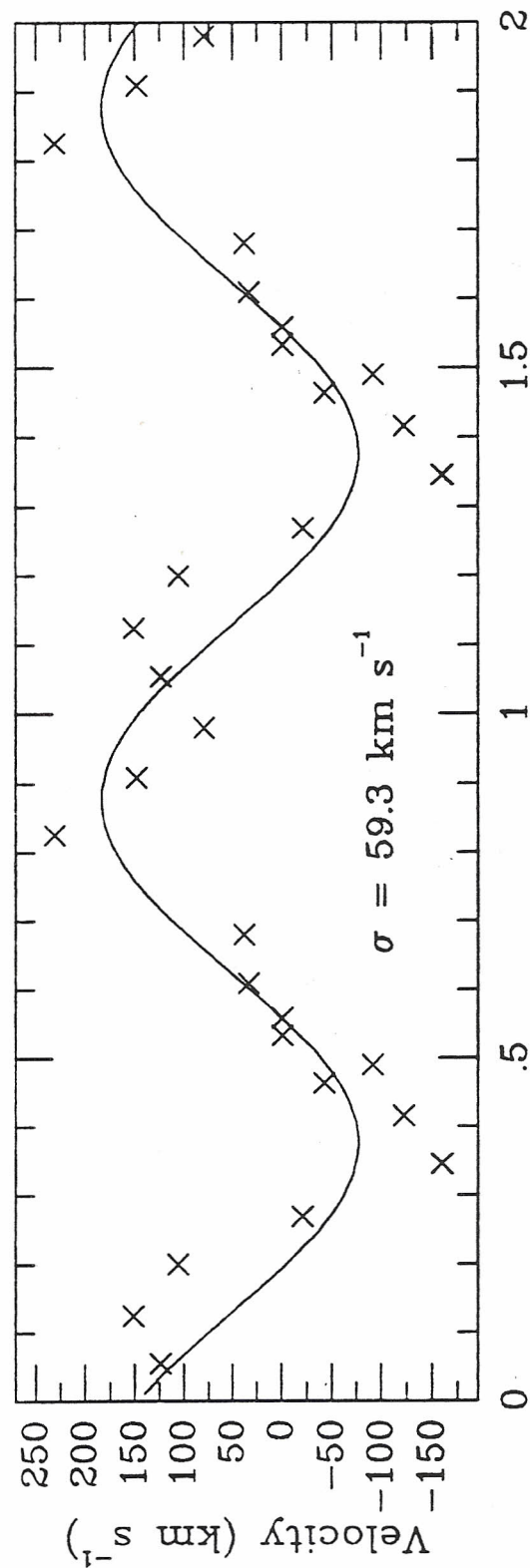


Fig. 6.3.

PG 0859+415 - H α profiles (1991)

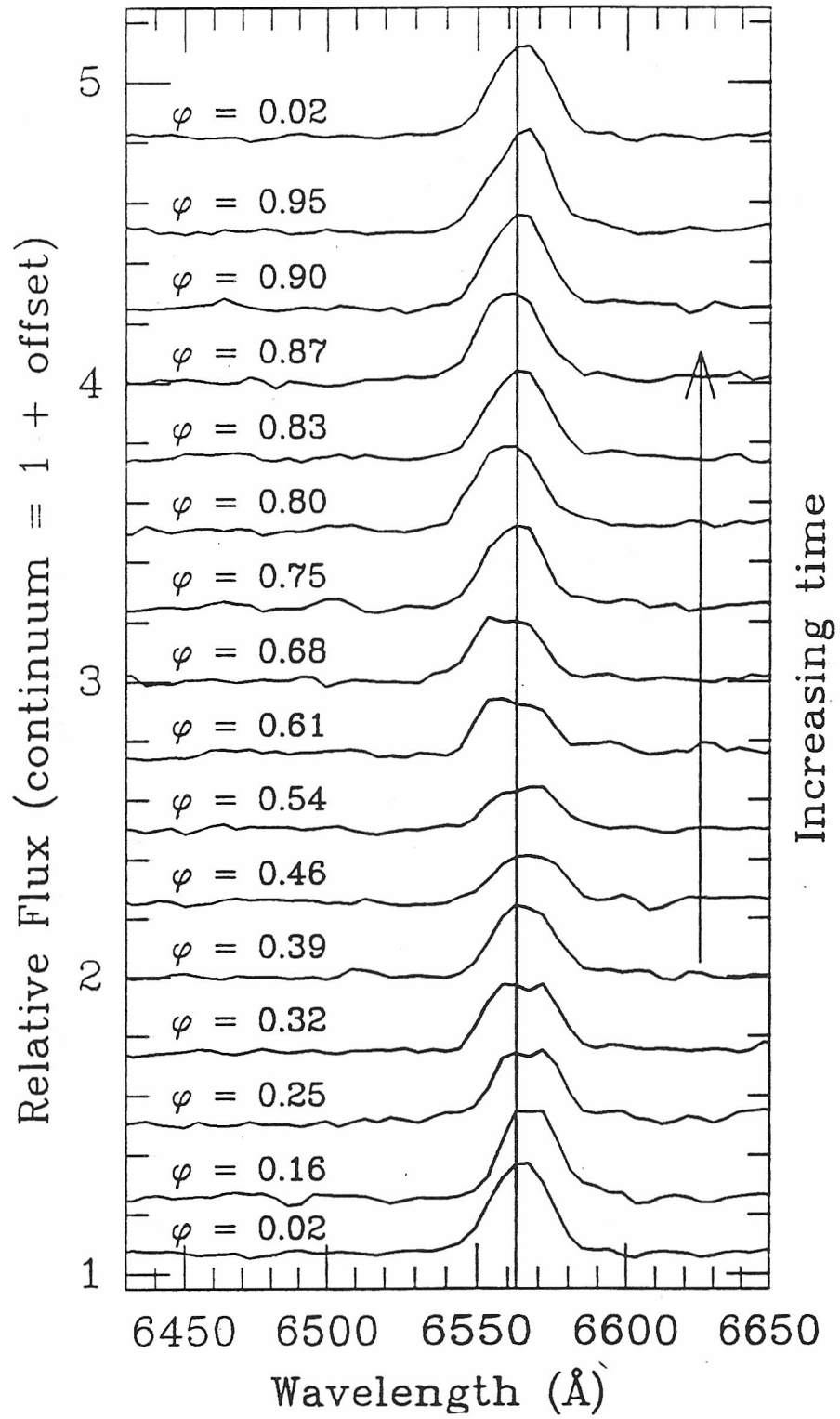


Fig. 6.4. PG 0935+075 - IUE Short and Long Wavelength Spectra

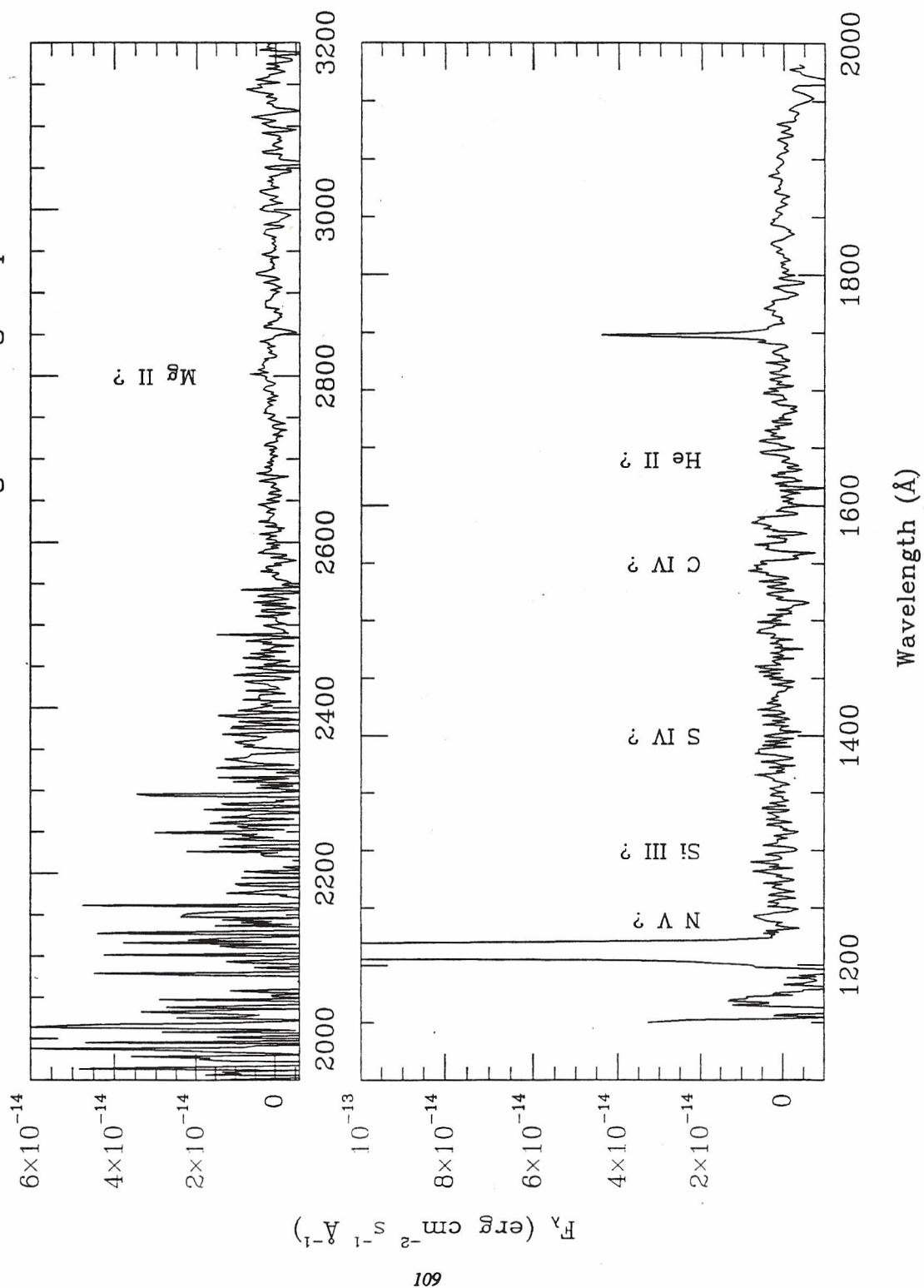


Fig. 6.5. PG 0943+521 - *IUE* Short and Long Wavelength Spectra

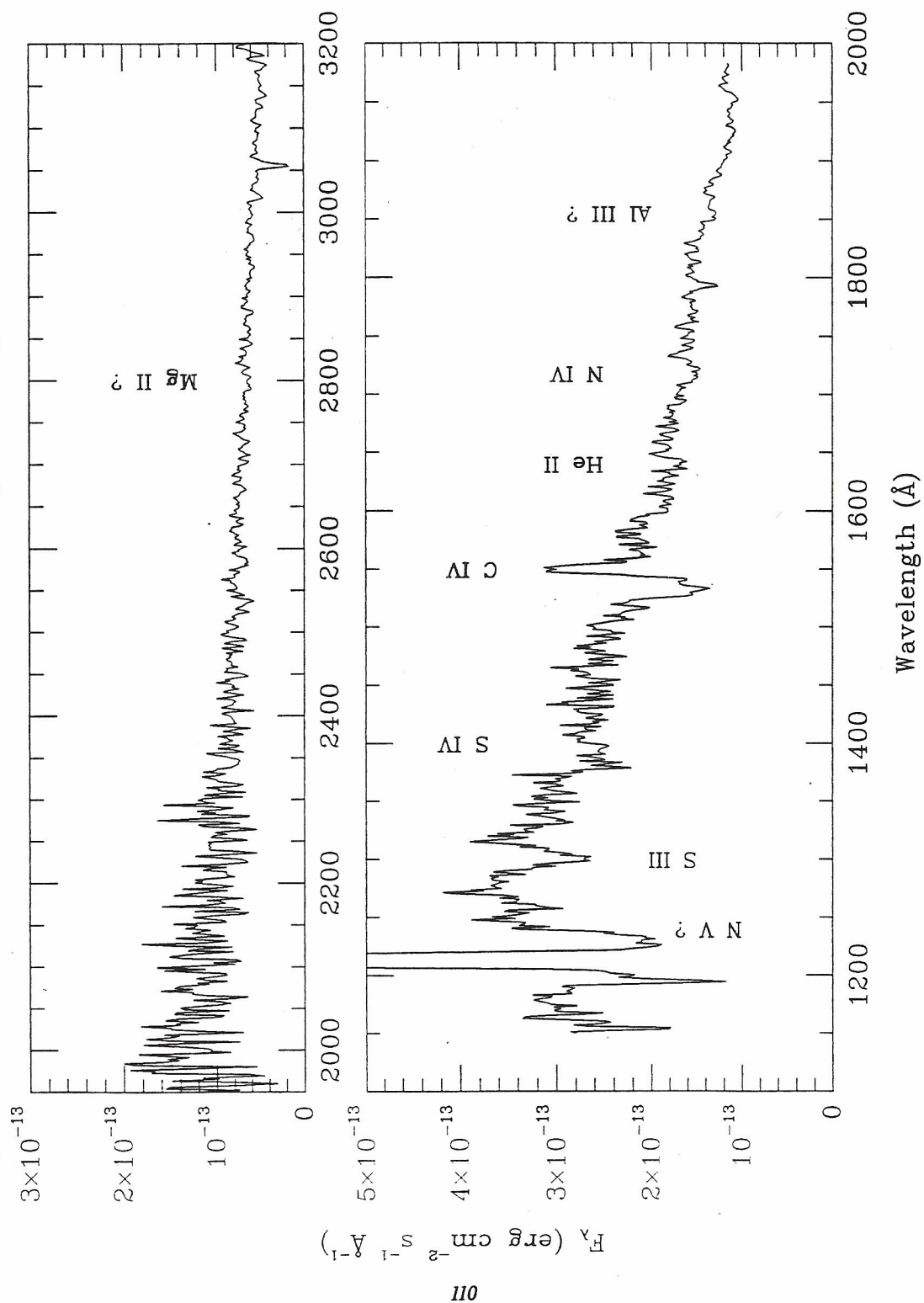


Fig. 6.6. PG 1000+667 - IUE Short and Long Wavelength Spectra

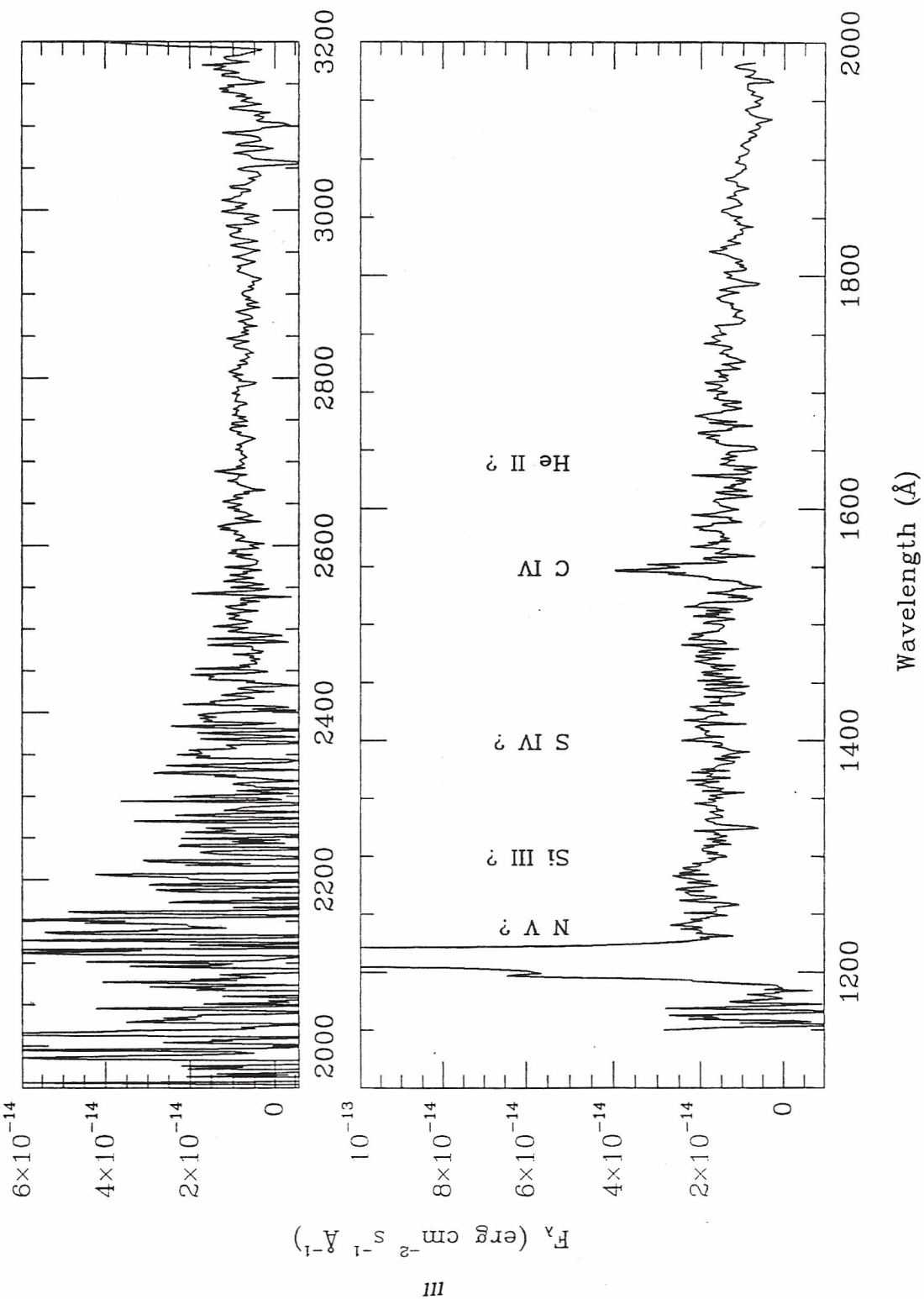


Fig. 6.7. PG 0948+344 = RZ LMi - 1991 October 19 & 20 UT

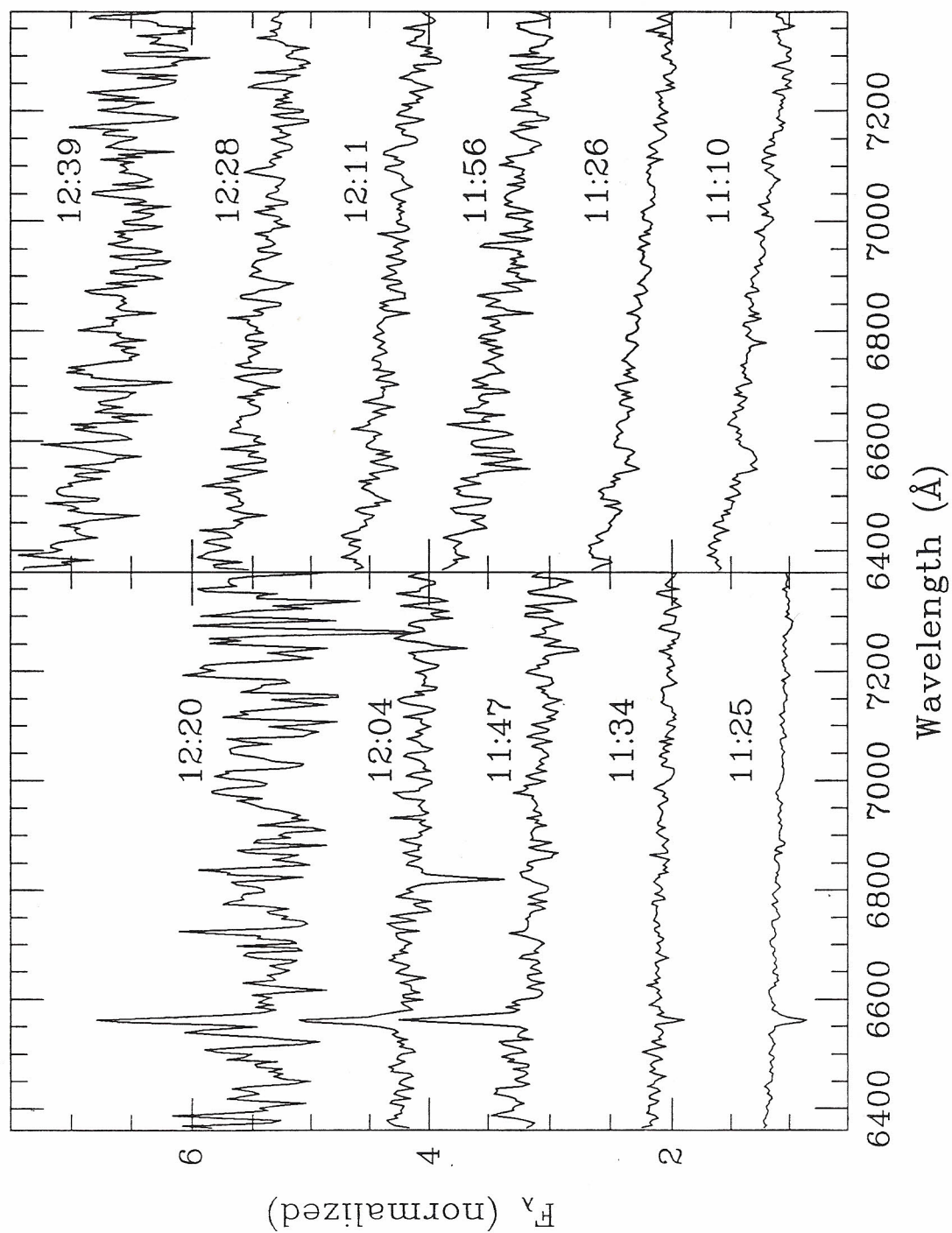
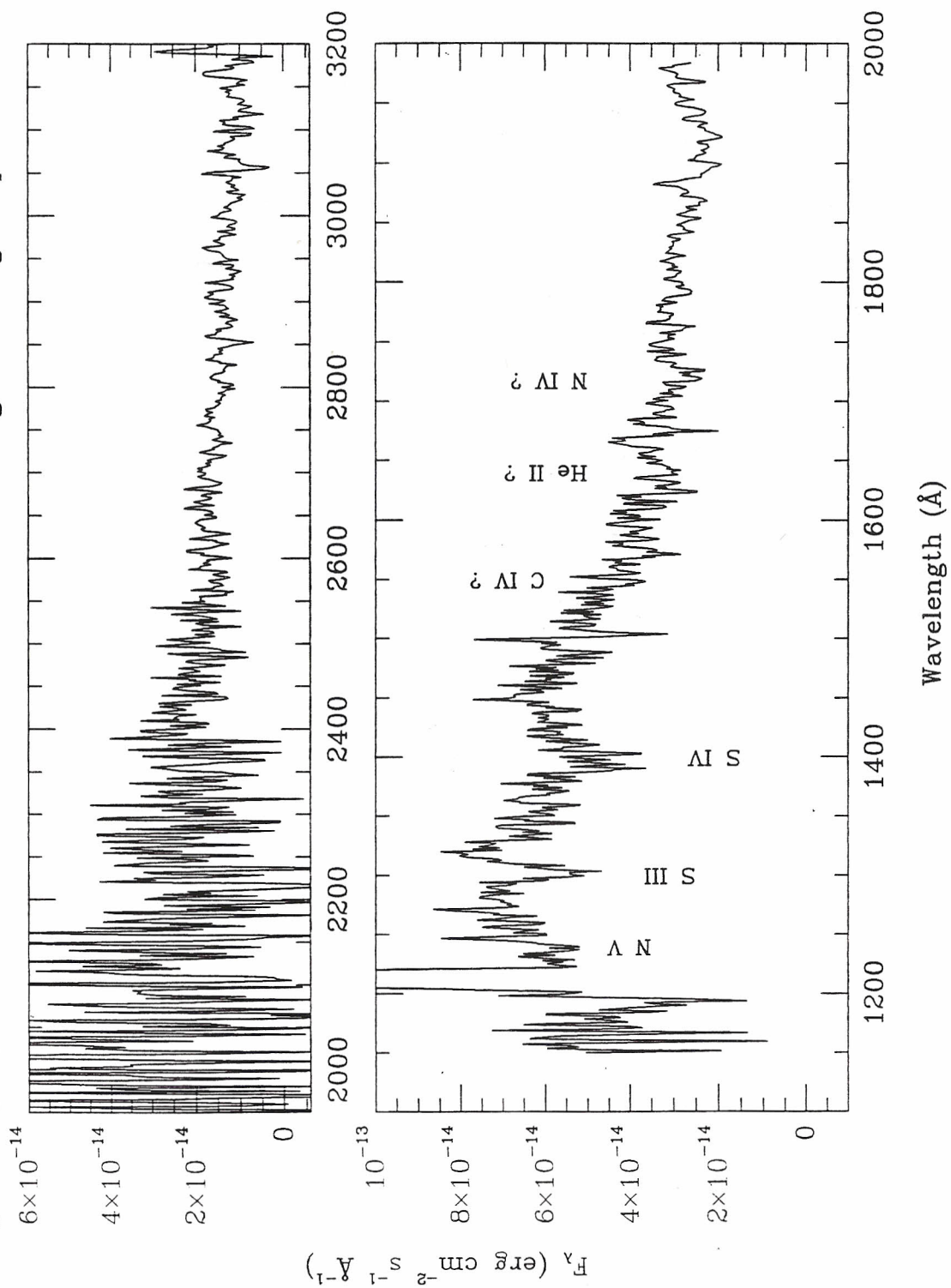


Fig. 6.8. PG 0948+344 = RZ LMi - IUE Short and Long Wavelength Spectra



PG 2300+166 - IUE Long and Short Wavelength Spectra

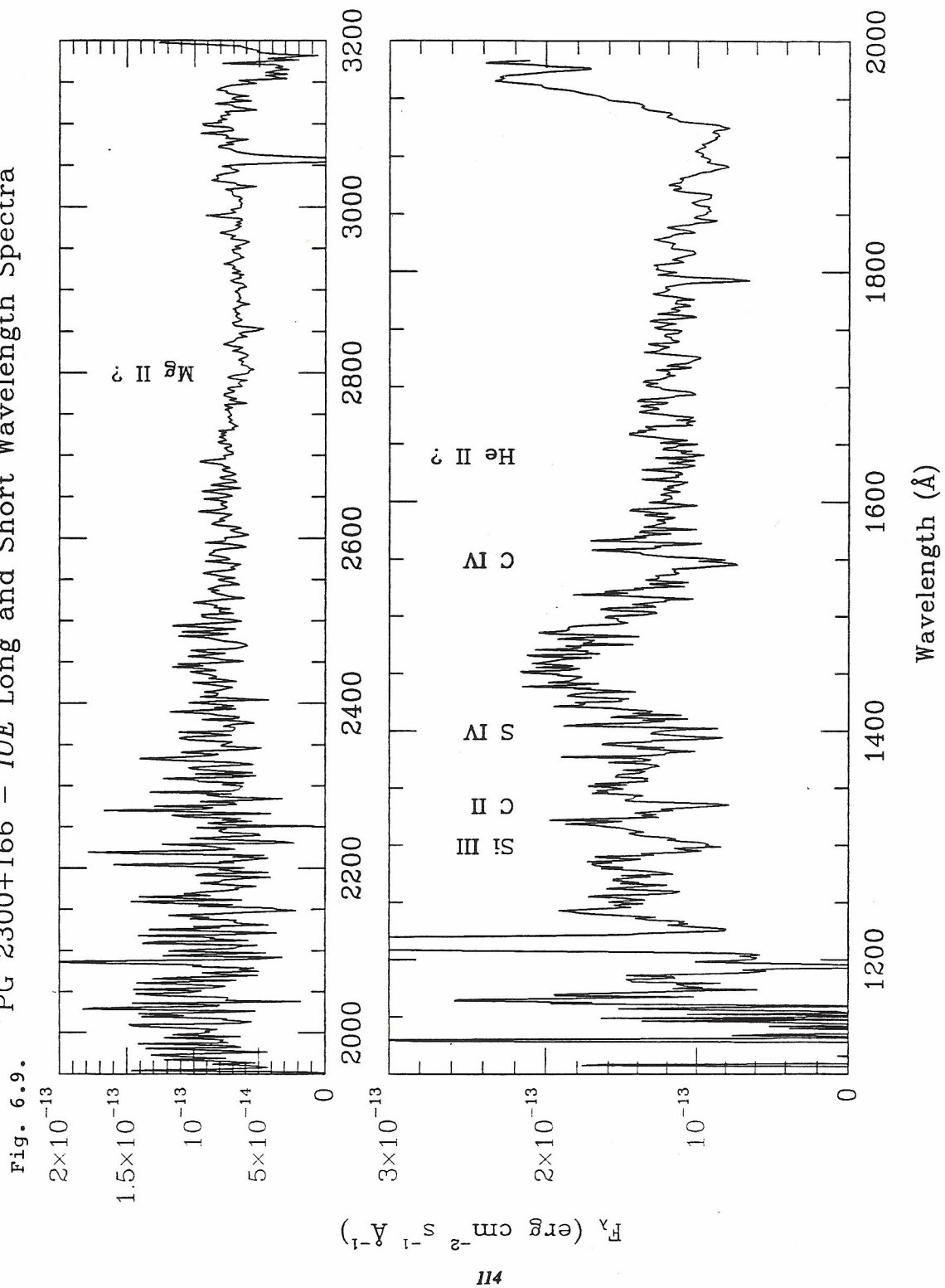


Fig. 6.10. PG 1002+506 - *IUE* Short Wavelength Spectrum

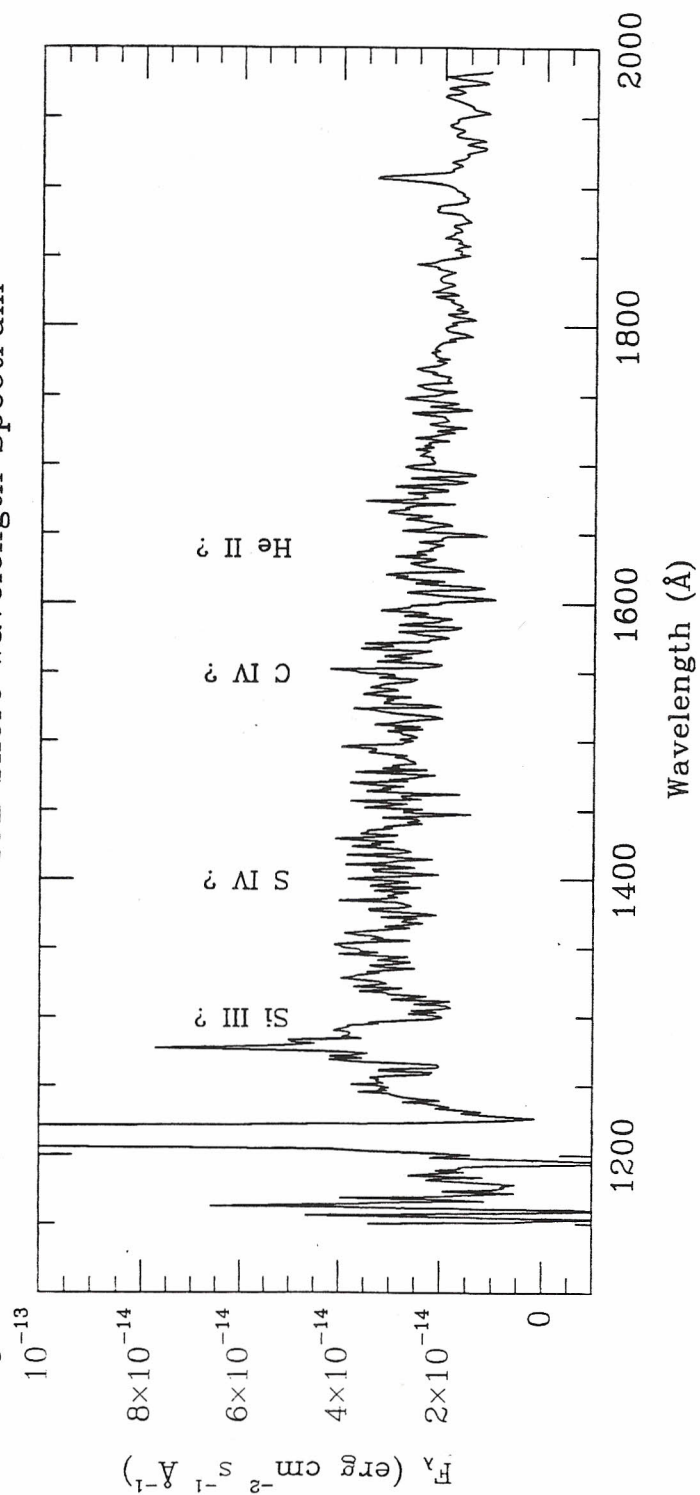
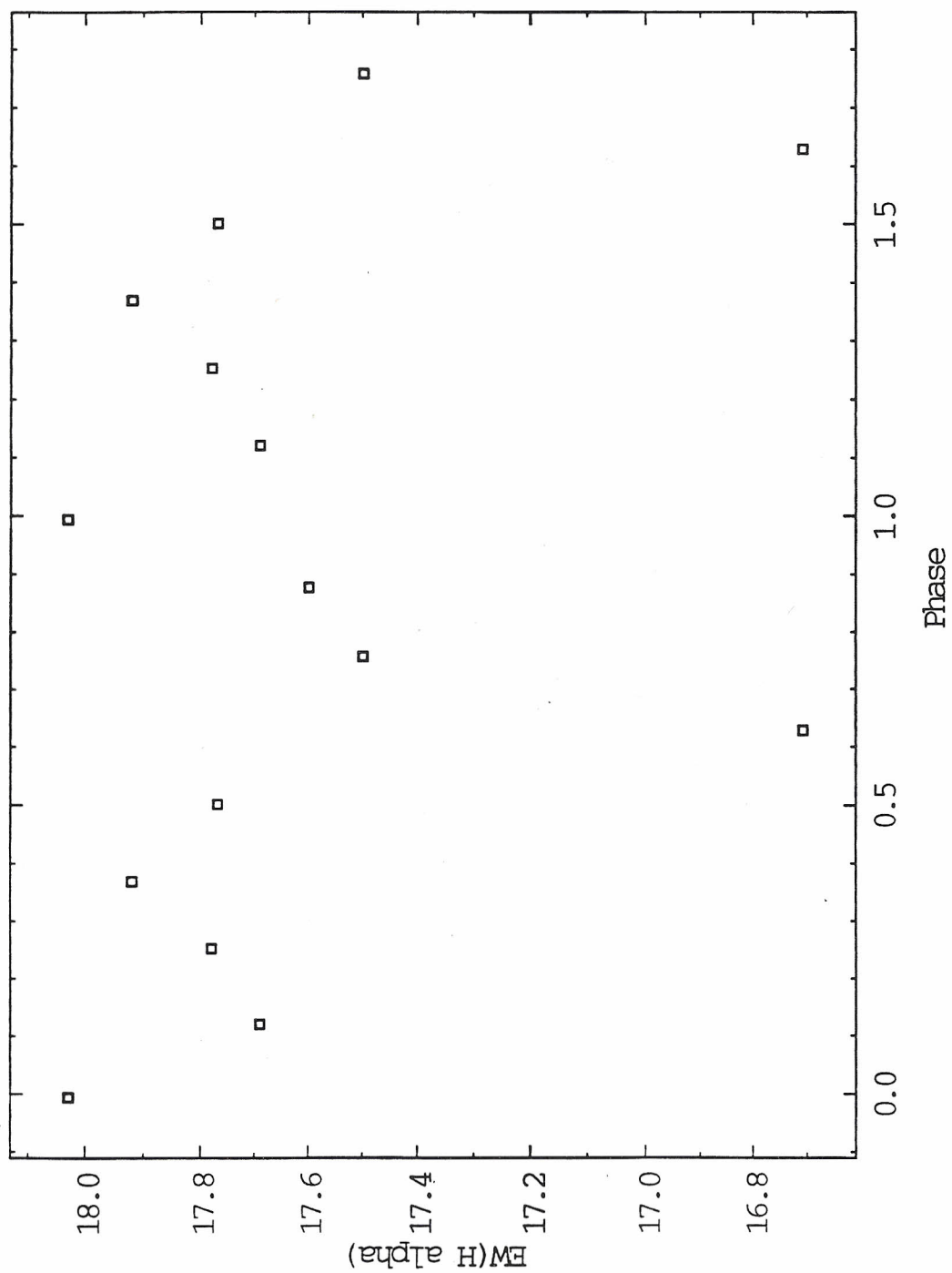


Fig. 6.11. PG 1002+506 - H alpha equivalent widths



Chapter 7

Aggregate Properties of the Stars

CVs are idiosyncratic. This is a small sample, so one must be careful not to read too much into what one or two objects say. One might wonder how common CVs in the period gap are, since PG 1711+336 = V795 Her is there. Although I suspect it is a dwarf nova, if PG 0917+342 is a nova-like, it is among the first found below the period gap (Dobrzycka & Howell 1992). The nature of PG 0834+344 = EI UMa is unclear: it is a dwarf nova? The red star of HX Peg is probably a subdwarf K star, which has not been seen elsewhere.

Nevertheless, one might wonder about trends apparently emerging from the spectroscopic follow-up, orbital period distribution, and outburst properties:

- In the PG sample, only nova-likes similar to SW Sex (see Chapter 8) have low states, similar to those of VY Scl. This may just be because of the small sample size, plus the difficulty of observing these faint low states.

- Magnetic CVs appear to be relatively uncommon. They take up fully one-third of the Ritter (1990) catalog, and they dominate the X-ray-selected sample of Silber (1992). While I have not searched them all for coherent optical pulsations, few PG CVs have strong He II $\lambda 4686$, as most magnetic CVs do (e.g., Williams 1983).

- Nova-likes of a dazzling variety show up. I have listed many of the previously unknown PG CVs as NLs mainly because of their spectra: strong power-law continua and weak emission lines which sometimes go into absorption, up the Balmer series. With no red star features are visible, the absolute magnitudes should be bright, about $R < 6$. In the Kitt Peak-Downes survey, Downes (1986b) found two blue stars with strong, narrow emission lines with a flat Balmer decrement, namely KPD 2032+5037 and KPD 2302+4910. He concluded they were either nova-likes or Be stars. The Kitt Peak-Downes survey (1986a), however, was at low latitude, and so one might expect Be stars to be

heavily reddened. One of them also flickers (Patterson 1986), suggesting accretion is present. PG 1000+667 resembles this, too, with its narrow H α . It has measurable radial velocity variations, so this is definitely a binary star.

- The only two Z Cam stars, SY Cnc and AH Her, appear near the long end of the period distribution. CVs with longer periods tend to have higher luminosities than those of lower luminosities (Patterson 1984; Warner 1987). This may be at least consistent with the idea that they are relatively luminous dwarf novæ, with average accretion rates near the critical rate above which disk viscosity prevents dwarf nova outbursts, allowing only steady accretion as in nova-likes. A larger sample, with better-determined absolute magnitudes, would be helpful here.

- Dwarf novæ with long interoutburst intervals are surprisingly common. These include T Leo, BZ UMa, and YY Dra. EI UMa might perhaps be one of these, since it does have very strong emission lines and X-rays. Although often referred to as WZ Sge stars (Bailey 1979; O'Donoghue et al. 1991), none really resemble WZ Sge spectroscopically. Generally, red stars are visible, because of the low accretion luminosity. With only three stars, it may be hasty to conjecture about the significance of two of them being near the period minimum, but with 3/33 stars in the entire sample, does this point to a large population at the low end of the CV luminosity function? If so, and if these stars can be found throughout the orbital period distribution, this might be of interest to nova hibernation theory (Shara et al. 1986), which explains both the apparent low space density of CVs (Patterson 1984), and also why CVs with such similar component stars can have such similar accretion luminosities.

- Most of the stars in Table 6.3 and Appendix B are similar to the stars of Ferguson, Green, & Liebert (1984), who suggest they might be detached binaries. Hot subdwarfs or white dwarfs may produce most of the light, although the presence of cooler companions is suggested by their flat energy distributions.

PG 1443+337 is the only white dwarf /red dwarf composite found in this thesis. There are 26 white dwarf composites listed by GSL86 in their complete sample, not including PG 1443+337 or any other objects in Tables 6.1 – 6.3, except for PG 2200+085, which may be just a K-star (Chapter 6). The abundances of such composites and of subdwarf binaries are of interest for the theory of CV formation (de Kool & Ritter 1993), although this is beyond the scope of this work. Although the PG catalog's average limiting magnitude of $B = 16.1$ may still be too bright to see the low end of the CV luminosity function and the transition to detached white dwarf /red dwarf binaries, this remains to be seen by deeper ultraviolet-excess surveys, e.g., the APM survey (Berg et al. 1992), the Edinburgh-Cape Blue Object Survey (Stobie et al. 1987), the Kiso survey (Noguchi et al. 1980; Kondo et al. 1984), and the Montreal-Cambridge survey (Demers et al. 1987).

- What is striking about the orbital period distribution for the PG CVs (Fig. 5.19) is that, only in the 3 – 4-hour bin, six of the seven stars share mysterious, but consistent, characteristics with PG 1012–029 = SW Sex. Five of these six eclipse. I will discuss these in Chapter 8, although it is worth noting that these five eclipsing CVs, plus the nova-likes AY Psc = PG 0134+070 and DO Leo = PG 1038+155, comprise the seven of the 33 PG CVs known to eclipse. This fraction of 21% is consistent with an isotropic distribution of inclinations, found for the X-ray-selected sample of Silber (1992, his Chapter 4.2), but this agreement is perhaps fortuitous: few of the PG CVs have been carefully checked for eclipses, using time-resolved photometry over several cycles. (I should have explained this more carefully in my referenced private communication to A. D. Silber.) The fraction of eclipsing CVs, essential for constraining models for selection effects (Ritter & Özkan 1986; Ritter 1986a; Ritter et al. 1990) still needs to be determined for the PG CVs. If significantly more are found to have eclipses, this would show they are preferentially seen at high inclination, in contradiction to the idea that limb darkening in optically-thick disks causes face-on CVs to be more noticeable (Paczynski & Schwarzenberg-Czerny 1980; Warner 1987).

Chapter 8

The SW Sextans Stars

Recently, a new class of CVs has been recognized, the SW Sextans stars (Thorstensen et al. 1991b). These stars are too common and too similar to each other to be peculiar cases, as previously thought. They must arise naturally, under conditions occurring frequently. The list keeps growing, with PG 1012-029 = SW Sex, PG 0027+260, PG 0859+415, PG 0244+103 = WX Ari, V1315 Aql, Lanning 90 = V1776 Cyg, PG 0818+513 = BH Lyn, Stepanyan's star = LX Ser, and PG 1030+590 = DW UMa. All show similar unexplained behavior:

- Absorption events in the Balmer and He I emission lines' cores, appearing near phase 0.5 (see Szkody & Piché 1990; Szkody 1991). These phase-0.5 absorption events tend to be stronger in the He I lines, and have been seen in the metal lines of PG 0027+260 (Thorstensen et al. 1991b);

- A dip in the equivalent widths of the Balmer lines, opposite the eclipse (PG 0027+260: Thorstensen et al. 1991b; BH Lyn: Thorstensen, Davis, & Ringwald 1991a; V1315 Aql: Dhillon, Marsh, & Jones 1991; V1776 Cyg: Garnavich et al. 1990; SW Sex: Honeycutt, Schlegel, & Kaitchuck 1986);

- Large ($50 - 76^\circ$) phase lags of the radial velocity curve, relative to the eclipses, as plotted by Shafter (1991). While these are common in CVs of all types, they are significantly larger here;

- Continuum eclipses much deeper than those of the lines. All the SW Sex stars show obvious eclipses, except for WX Ari (Beuermann et al. 1992);

- Eclipses that are V-shaped, as opposed to U-shaped (as with U Gem: Warner & Nather 1971; HT Cas: Zhang, Robinson, & Nather 1986), or otherwise showing structure from the white dwarf (e.g., Wood 1986). These V-shaped eclipses are often asymmetrical,

with eclipse maps showing significant brightness asymmetries in the disks (Rutten, van Paradijs, & Tinbergen 1992a). Sometimes the eclipses have variable profiles (PG 0027+260: Thorstensen et al. 1991b; DW UMa: Shafter, Hessman, & Zhang 1988);

- Orbital humps in the wrong places in the orbits, such as *after* the eclipses (PG 0027+260: Thorstensen et al. 1991b; DW UMa: Shafter et al. 1988);

- No obvious rotational disturbances in the lines, as they eclipse (Williams 1989). Dhillon et al. (1991), however, suspected having seen a rotational disturbance in He II $\lambda 4686$, at the same time the Balmer lines were undisturbed;

- Single-peaked emission lines, even though the stars are highly inclined and eclipse. He I in WX Ari is an exception, but it is helped by strong phase-0.5 absorption;

- Strong high-excitation lines, with C III /N III $\lambda\lambda 4640 - 4650$ and He II $\lambda 4686$ typically half the height of H β above the continuum (GFLS82), although sometimes brighter (PG 0859+415: Grauer et al. 1993; DW UMa: Shafter et al. 1988);

Perhaps the most striking property of the SW Sex stars is their homogeneity. Most show all these characteristics, and show them together. It is rare to find *two* stars among the idiosyncratic CVs that are so similar.

Many of these behaviors, while unexplained, are common in CVs, such as the single-peaked lines in highly inclined systems, and the phase lags between the eclipse cycles and radial velocity curves. The phase-0.5 absorption events, however, are unique to the class (Szkody 1991), and so I will use them as the defining feature of the class of SW Sex stars. So far invariably also, the phase-0.5 absorption events are accompanied by uncommonly large phase lags. Phase lags larger than 40° are exclusively found in SW Sex stars, with the exception of WZ Sge. An increase in phase lag versus orbital period at shorter orbital periods, below the period gap, perhaps presages more short-period CVs turning out to have large phase lags. In CVs above the period gap, however, these phase lags are generally less than 30° . With the SW Sex stars, they usually exceed 50° (see

Shafter 1991, his Fig. 2).

The PG survey's sample is selected by $U - B$, not by outburst variability or X-ray flux, which ordinarily call attention to CVs. An important consequence of this sample is to show just how common the SW Sex stars are. Of 33 PG CVs (see Table 6.1), at least five are SW Sex stars. There are only two AM Her stars, and only six-to-twelve dwarf novæ. All six nova-likes with orbital periods between three and four hours all show phase-0.5 absorption events. To be fair, the sixth, PG 0859+415, also shows the absorption wings about its Balmer lines, characteristic of the UX UMa nova-likes. It is the only object so far common to both classes. Interestingly, its phase lag is intermediate that typical of the two classes, at $35 \pm 1^\circ$ (see Chapter 6; Grauer et al. 1993).

So far, all SW Sex stars occupy the 3–4-hour period regime, in which dwarf novæ are rare. Is this a coincidence, or a clue? Is this telling us about how CVs enter the period gap? Other CVs outside this period regime share some of the SW Sex stars' properties, though. These include H1752+081, which has a large phase offset (Silber 1992); LB 1800, which has transient absorption events at phases 0.8 – 0.9 (Buckley et al. 1990); and perhaps DO Leo, which has high-excitation lines and a spectrum similar to the SW Sex stars (Abbott et al. 1990; Chapter 6). H1752+081 is below the period gap, and its optically-thin spectrum resembles that of a dwarf nova, although the Harvard archive plates show no outbursts (Silber 1992). Worst of all, it has no phase-0.5 absorption events, so by definition it cannot be an SW Sex star, although interestingly, eclipse maps do show a "bright stripe," perhaps responsible for the large phase lag. This may indicate that the phase lags and the phase-0.5 absorption events really are from two separate components, as suggested by Szkody & Piché (1990). LB 1800 and DO Leo both have periods exceeding five hours. H1752+081 and LB 1800 are strong X-ray sources, detected by HEAO-1, unlike any of the SW Sex stars (Silber 1992). All three of these stars eclipse, so perhaps at least some of the SW Sex stars' properties result from high inclination. If two components

really are involved, might they both be effects of the high inclination?

The phase lags of the emission lines are actually common among CVs of all types (Shafter 1991). But why are they so large here? Marsh, Horne, & Shipman (1987) invoke disk brightness asymmetries and velocity field distortions to explain phase lags, but such large values may strongly constrain these models. Interestingly, the eclipse maps of Rutten et al. (1992a) shows an obviously asymmetrical disk for SW Sex, and a less-extreme but noticeable asymmetry for LX Ser, a borderline object, which shows a strong *S*-wave in its line profiles (Young, Schneider, & Shectman 1981; Hantzios 1992).

Doppler maps might be expected to clarify the curious stream-disk-wind interactions the variable line profiles suggest, but velocity mapping of one SW Sex star, V1315 Aql, was inconclusive (Dhillon et al. 1991). There was some evidence, though, for a slight rotational disturbance in the He II $\lambda 4686$ line. This should be confirmed, since it bears on the disturbing question of whether these stars contain disks at all (Williams 1989). PG 0859+415 probably does contain a disk, however, since it shows optically thick line profiles in the blue (Grauer et al. 1993). It may also be useful to map individual eclipses, to help model their changing profiles.

Winds are turning out to be essential parts of accretion disks of all kinds, from protostars to AGNs. The variable eclipses of the SW Sex stars may be telling us about strong, optically thick winds (or thick disks?). Even so, it is essential to disprove (or prove) that the SW Sex stars are magnetic, with both X-ray observations and high-speed optical photometry, to search for coherent pulsations. Searches so far include those of LX Ser by Eason et al. (1984), with no convincing detection, and of PG 0859+415 by Grauer et al. (1993), with a tentative detection of a 25.5-second periodicity. If real, this variation's period is more typical of dwarf nova oscillations than the spin periods of magnetic CVs, however (Warner 1988, p. 136; Ritter 1990), and so may be from an optically thick disk.

In some SW Sex stars, the O I $\lambda 7773$ feature is in the deepest absorption seen in

CVs (Friend et al. 1988; Thorstensen et al. 1991b; Dhillon et al. 1992). This feature is sensitive to CV outburst state (Friend et al. 1988; Chapter 10), as are the higher Balmer lines. Does this say that the SW Sex stars are among the most luminous CVs? The Balmer jumps for the SW Sex stars are in emission, though (GFLS82). Is it a manifestation of their high inclination? O I $\lambda 7773$ was seen in absorption by Wade & Horne (1988) in Z Cha, an SU UMa star, while quiescent. Intriguingly, WX Ari has O I $\lambda 7773$ in shallow absorption (Beuermann et al. 1992), but the shallowest O I $\lambda 7773$ absorption so far seen of any SW Sex star is that of BH Lyn, in which it is undetectable (Thorstensen et al. 1991a). Also intriguingly, time-resolved spectra show O I $\lambda 7773$ absorption to be variable, decreasing in strength near phase zero (Dhillon et al. 1992).

All but one of these stars, WX Ari, are known to eclipse (Beuermann et al. 1992). Assuming isotropically distributed inclinations and Roche geometry, the probability that a CV will have eclipses is about 20 – 25% (Silber 1992, his Chapter 4.2). But for the seven PG CVs with orbital periods between three and four hours, five are eclipsing, and four of these five are SW Sex stars. Also, of these seven, six are SW Sex stars, specifically meaning they show the phase-0.5 absorption events in their Balmer lines. They all show large phase lags, too, and high-excitation emission lines, which other SW Sex stars generally do, too. Assuming the CVs are isotropically inclined, randomly drawing five out of seven, and finding all five are eclipsing seems improbable, namely

$$\frac{7!}{(5!)(2!)} (0.2 - 0.25)^5 (0.8 - 0.75)^2 + \frac{7!}{6!} (0.2 - 0.25)^6 (0.8 - 0.75) = 0.5 - 1.3 \times 10^{-2}$$

or about one chance in a hundred. So, where are the face-on SW Sex stars?

Does this indicate limb brightening, from a a bright corona or wind with a temperature inversion perpendicular to the spin axis? Although this may increase the surface brightness of a highly-inclined disk, CVs are unresolved sources, and so limb brightening above the disk would probably not increase the absolute flux we receive. A limb-darkened

disk continuum may be fainter when highly inclined, and allow the light from the stream-disk interaction to shine through, but this does not explain why five of seven PG CVs with periods between three and four hours are eclipsing. Also, the gas is moving, so the photons may radiate preferentially in directions oblique to the midplane (Adam 1990).

Further observations of WX Ari will be essential. A thorough check, to see if eclipses really are absent, should be carried out. If WX Ari does not eclipse, seeing P Cygni profiles in the UV emission lines would be a first among the SW Sex stars (Penning et al. 1984; Szkody 1987; Thorstensen et al. 1991b), and would support the idea that these stars' strange properties are indeed from material at great vertical height from the disk. The possibility of material above and below the disk causing these stars' strange properties was raised as early as the initial recognition of these properties (Honeycutt et al. 1986). Dhillon et al. (1990) have pointed out problems with this interpretation, although alternative ideas such as magnetic accretion also run into trouble. Although the SW Sex stars do show high-excitation lines in their spectra, as magnetic CVs do, they show neither significant circular polarization (Liebert & Stockman 1980; Stockman et al. 1992) nor strong X-rays (Silber 1992). Although eclipse mapping has shown the stream-disk interaction to cause significant brightness asymmetries in these stars' disks (Rutten et al. 1992a), the hypothesis that these stars' peculiar properties are caused by winds or coronæ must be regarded as wanting of confirmation.

It is not obvious what we are dealing with, except perhaps a revision of the canonical thin-disk CV model. What are they, football-shaped fountains, with midplanes bisected by accretion disks? These objects do flicker, so accretion should be present. Also, their emission lines do show gross sinusoidal velocity variations, presumably from binary star orbits: they eclipse, too. Most after that is up for examination, and a serious modeling effort is due.

Chapter 9

BZ Ursa Majoris and its Ringing Radial Velocity Curve

9.1. Introduction

BZ UMa (= PG 0849+580) was serendipitously discovered in outburst by Markarian (1968), who gives a finding chart and coordinates, as do Bruch, Fischer, & Wilmsen (1987). The compilation of CVs found by this survey of Green et al. (1982) shows and describes a blue spectrum. The Balmer jump is in emission, the broad H and He I emission lines are doubled, and a weak, broad He II $\lambda 4686$ emission line is blended with C III/N III at $\lambda\lambda 4640 - 4650$. Bruch (1989) also presents a spectrum and describes it as “a textbook example for a spectrum of a dwarf nova.” The lines are unusually strong, though: the equivalent width of H α is about 200 Å (see Table 9.1).

BZ UMa has very infrequent outbursts, with mean intervals longer than 5.2 years (Wenzel 1982). The last outburst recorded reliably was in 1974 (Mattei 1989), although there have been recent outburst reports (Hurst & Lubbock 1988; Schmeer 1990). The outbursts are slow, lasting 10 – 20 days, with large amplitudes of $\Delta V \approx 6$. These are energetic enough to be superoutbursts, which would suggest BZ UMa is a dwarf nova like SU UMa. Superhumps, the defining property of this class, have eluded detection but may well exist, since to my knowledge, there has been no published time-resolved photometry of an outburst. Dwarf novæ with interoutburst intervals exceeding 400 days only have outbursts with the amplitudes and durations of superoutbursts (Warner 1987; Ritter 1990), and BZ UMa is no exception.

Observations of BZ UMa are described in § 9.2. I describe the spectrum and find the red star in § 9.3, and with it estimate absolute magnitude and distance. Radial velocity studies are presented in § 9.4, wherein I find the orbital period plus a mysterious ringing in the radial velocity curve. I reanalyze other observers’ time-resolved *B*- and *J*-band photom-

etry § 9.5, with overall discussion in § 9.6 and conclusions in § 9.7.

9.2. Observations

The instrument setups and journals of observations appear in Tables 9.2 and 9.3, respectively. Observations are similar to that described in Thorstensen & Freed (1985), this work (Chapter 2), with exceptions noted here, and data reductions were carried out as by Thorstensen et al. (1989). All observations used MDM Observatory's 1.3-m McGraw-Hill telescope, both Mark III all-transmission Cassegrain spectrographs, and either a Thomson or a TI-4849 CCD (Luppino 1989), both being geometrically similar. The spectra taken in 1988 were kindly provided by R. M. Hamwey, who used a 600 line/mm grism, blazed at $\lambda 5800$, delivering 5.5-Å resolution at 2.5 Å/channel. For all other observations, I used a 300 line/mm grism, blazed at $\lambda 6400$, obtaining 11-Å resolution at 5.0 Å/channel. The reddest setup, in 1991 June, used a Hoya Y-50 order-blocking filter, and during this run, spectra of hot stars were taken, to calibrate out the telluric absorption bands. Flux standards (Oke 1974) were observed, to remove the instrumental response. The narrow slit (2.2") precludes absolute spectrophotometry to within 30%, although allows accurate digital sky subtraction. Instrument rotation was deemed unnecessary for the red setups.

9.3. Spectrum and Red Star

Dwarf novæ with rare outbursts are sometimes called WZ Sge stars, after a CV with mean interoutburst intervals of 32.5 years. (For a review, see O'Donoghue et al. 1991.) Wenzel (1982) calls BZ UMa an intermediate case between WZ Sge and U Gem, because of its outbursts, but its spectrum (Figs. 9.1 – 9.3 and Table 9.1) more resembles that of U Gem (Oke & Wade 1982). WZ Sge shows Balmer lines in emission with broad absorption wings, perhaps from its white dwarf, and no trace of a red star.

In the blue spectrum (Fig. 9.1 and Table 9.1), the Balmer and He I lines are broad

and in strong emission, with no trace of absorption wings. H β is double-peaked, with a peak-to-peak separation of $560 \pm 50 \text{ km s}^{-1}$. In the higher-resolution 1988 spectra, He I $\lambda\lambda$ 5876, 6678, and 7065 are doubled, with peak-to-peak separations of 1000, 950, and $1100 \pm 50 \text{ km s}^{-1}$, respectively. He II λ 4686 is in weak, broad emission, and the presence of the C III/N III blend at $\lambda\lambda$ 4640 – 4650 is not obvious. Even in the far infrared, there is a suggestion of strong line emission, with a detection in the *IRAS* 100- μ channel by Harrison & Gehrz (1992), who note that most of the surprisingly many dwarf novæ and nova-likes detected by *IRAS* do not follow any plausible disk or dust continuum.

As Fig. 9.2 shows, the red star is visible. I scale several M dwarf spectra, using as fiducials K I λ 7665 and a faint, unidentified line at λ 7565, which I note becomes more prominent in later M dwarfs (see Wade & Horne 1988, their Fig. 3). These fiducials are free of telluric absorption, and straddle the steep λ 7600 TiO bandhead. An M5 dwarf, in the system of Boeshaar (1976) revised by Kirkpatrick, Henry, & McCarthy (1991), subtracts out to leave the smoothest disk spectrum (Fig. 9.2, middle trace), although not quite perfectly. Using an M6 dwarf leaves even more noticeable residual traces of the red star, so I infer a spectral type of $M5.5 \pm 0.5$. Correcting for an M5.5 dwarf's color (Bessell 1986), the effective wavelength of Kron-Cousins R is λ 7000, adopting a mean error of $\pm 100 \text{ \AA}$. An M5.5 dwarf has an absolute magnitude in R_{KC} of 14.06 (Bessell 1991). Since the red star of BZ UMa contributes 4.5% of the light at λ 7000 $\pm 100 \text{ \AA}$, in quiescence, BZ UMa has an absolute magnitude in R_{KC} of 10.69 (+0.66/–0.85). This lies near the empirical ZAMS of Patterson (1984, his Fig. 4).

The fraction of light from the red star at λ 8000 is 9.7%. A check for the I -band, which is at an effective wavelength λ 8000 for an M5.5 dwarf (Bessell 1986), gives an absolute magnitude in I_{KC} of 9.47 (+0.50/–0.70), giving an $R - I$ of 1.22 (+0.16/–0.15). This is even redder than the $R - I$ of 0.97 of U Gem (Echevarría 1984).

So far, this avoids error in absolute spectrophotometry due to slit losses, but to turn

this absolute magnitude into a distance, this error cannot be helped. Assuming an accurate absolute flux level at $\lambda 7000$ of $8.7 \times 10^{-16} \text{ erg cm}^{-2} \text{ s}^{-1} \text{ \AA}^{-1}$, an M5.5 dwarf with the observed fraction of the light has $R_{\text{KC}} = 15.9$, and a distance of 110 (+44/-51) parsecs. This distance is probably systematically overestimated by up to 30%, as experience with this narrow slit on flux standards shows.

The O I $\lambda 7773$ line is in strong emission, and appears doubled even in my low-resolution spectra, with a peak-to-peak separation of $840 \pm 70 \text{ km s}^{-1}$. The Na I $\lambda 8190$ feature and the He II $\lambda 8236$ lines are not obviously present, overwhelmed by perhaps the strongest “ $\lambda 8200$ bump” yet seen in any CV (Friend et al. 1988). This feature cannot be from telluric water vapor absorption, as Fig. 9.3 shows it both with and without the telluric band correction. Fig. 9.3 also shows Paschen and Ca II lines in strong emission, and double-peaked. The Ca II lines have separations ranging from 600 to 700 km s^{-1} , and the Paschen lines range from 600 to 850 km s^{-1} , although blending confuses them.

The $\lambda 8200$ bump, thought to be unresolved H Paschen lines in emission, is all the more unusual as it is normally seen in high-luminosity CVs (Friend et al. 1988). Then again, BZ UMa has strong emission lines of most kinds, including high excitation lines, normally seen only in luminous CVs. This $\lambda 8200$ bump makes it difficult to find, much less fit, the continuum just to the red of $\lambda 8200$, and this complicates precise spectral typing of the red star by measuring the flux deficits of the TiO bands (Wade & Horne 1988). I tried this, and it gave a spectral type of M6.5+, clearly too red: I caution against trusting this method to excessive precision. Contamination by emission features may explain the unexpected illumination asymmetry found in maps of CV red stars’ Na I $\lambda 8190$ absorption by Davey & Smith (1992).

9.4. Orbit

Periodogram analyses of H α velocities measured with both line-measuring algorithms show a periodicity of 97.8 minutes. I take this to be the orbital period, since an *S*-wave is apparent in the H α line profile, upon binning the 1988 spectra in phase about this period and co-adding them (see Fig. 9.4). The peak of this *S*-wave has a semi-amplitude $K_S \approx 300 \pm 50 \text{ km sec}^{-1}$, estimated by eye and cursor. There is also an independent spectroscopic confirmation of P_{orb} of BZ UMa by Claudi, Bianchini, & Munari (1990), although they do not give many details.

To measure velocities of different parts of the H α line, I use the Shafter (1983a) algorithm and vary the separation of the Gaussians, to avoid the *S*-wave by measuring far into the line wings. In all cases (Fig. 9.5, top three panels), periodogram peaks appear at low frequencies, below 10 cycles/day. These are not aliases of the orbital period, which clearly cluster at 1 cycle/day intervals about the orbital periodicity. Neither do they arise from the sampling in any way: an artificial sinusoid test, using the orbital period and parameters from a least-squares fit to the velocities, shows no excess power at low frequencies (Fig. 9.5, bottom panel). These peaks have higher significance than those of the *orbit*, except when evaluated using velocities measured from the core of the line, and they increase in power farther out into the wings.

These low-frequency variations appear to be sinusoids, since they make discrete peaks in the periodogram, not bands or smears. The most significant peaks correspond to periods of 17.8 and 38.4 hours, both accompanied by patterns of 1 cycle/day aliases from the day-night cycle (Fig. 9.6, bottom). I adopt a separation of 1300 km s^{-1} for the remaining analysis, to compromise between the core velocities, which follow the orbit but may be contaminated by the *S*-wave, and wing velocities, which exhibit these mysterious low-frequency variations most strongly. The velocities measured are listed in Table 9.3; I also include the 1989 velocities measured in the line core, at 650 km s^{-1} , and in the line wings, at

1950 km s⁻¹, in Tables 9.4 and 9.5, respectively.

I fit a least-squares sinusoid to the 17.8-hour velocity variation of the orbit, subtract it from the radial velocity curve, and calculate a periodogram (Fig. 9.6, top). I also do so for the 38.4-hour variation (Fig. 9.6, middle), and show the resulting fit parameters in Table 9.6. In both cases, the measured orbital variation does not change significantly. After subtracting both long periodicities from the original velocities, the resulting periodogram looks like the artificial sinusoid's (see Fig. 9.7), although a third quasi-periodic variation at 3.13 hours, at the threshold of significance and perhaps only noise, can be fit and subtracted, too. Subtracting sinusoids that fit these low-frequency quasi-periodicities from the radial velocity curve gives it a much better fit to a sinusoid, halving σ at least (see Fig. 9.8).

Velocities measured from H β give only noise, but this is probably due to the weak signal from this setup's low blue throughput. So do He I λ 5876 velocities, but He I λ 6678 velocities give interesting results, basically the same periodogram as for H α , with both the orbit and the quasi-periodic variations (see Fig. 9.9 and Table 9.6). The periodogram is noisier, but the He I λ 6678 line is weaker. I worried that problems with calibrating the wavelength scale might give similar periodogram patterns for two closely spaced lines, but curiously, the strength of the low-frequency variations of He I λ 6678 does not increase farther into the wings, as with H α . If anything, it is strongest at about 1300 km s⁻¹, and then decreases in both the line wings and core.

9.5. Blue and Infrared Time-Resolved Photometry

Four hours of time-resolved CCD photometry by Kaluzny (1986) shows flickering variations in B of about 0.1 mag, with BZ UMa at $B = 17.8$, much fainter than the $B = 15.3$ seen by Green et al. (1982). With a periodogram analysis down to the Nyquist limit of 90 seconds, I find no obvious coherent optical pulsations to indicate a magnetic white dwarf. The only sign of eclipses is a single discrepant point in the lightcurve, when binned

on my orbital period (see Fig. 9.10). Although this does lie just after what may be a shallow orbital hump of 0.02 ± 0.02 mag semi-amplitude, it seems too narrow for a genuine eclipse. Without eclipses, one can still place limits on the orbital inclination i , although since the disk radius is uncertain, one must be content with a limit precluding white dwarf eclipses. For grazing eclipses, assuming the red star fills its Roche lobe,

$$\cos i = \frac{R_L}{a} = \frac{0.49q^{2/3}}{0.6q^{2/3} + \ln(1 + q^{1/3})}$$

using the approximation of Eggleton (1983), where $4\pi R_L^3/3$ is the volume of the lobe, a is the semi-major axis of the circular orbit and q is the binary mass ratio, $q \equiv M_2/M_{\text{WD}}$, where M_{WD} is the white dwarf mass and M_2 is the red star mass. I take the red star mass to be $0.13 M_{\odot}$, from the approximation $M_2/M_{\odot} = 0.38 (P_{\text{orb}}/4 \text{ hr})^{1.22}$ (Patterson 1984). The white dwarf mass is problematical, difficult to measure even in the best circumstances (Wade & Horne 1988), so I consider the entire plausible range of masses, from 0.3 to $1.4 M_{\odot}$. These values constrain i to be $< 72^\circ$ to 78° , respectively, with $i < 76^\circ$ for $M_{\text{WD}} = 0.65 M_{\odot}$. If one uses the gas stream's circularization radius (Plavec & Kratochvil 1964; Livio 1992) as a minimum disk radius, one obtains $i < 68.4^\circ$, 73° , and 71° , respectively.

Szkody & Feinswog (1988) obtained *JHK* colors and a *J* lightcurve, based on just over three hours of continuous observations. They find a period of 107 ± 11 minutes, which agrees with mine, although I attribute this variation to the bright spot and not to ellipsoidal variations of the red star. Again, no eclipse is obvious. With the average *JHK* magnitudes of Szkody & Feinswog (1988), I estimate the red star contributes $< 30\%$ of the light in *K* and so the red star has $K > 14.3$. Using the photometric parallax method of Bailey (1981), I find a distance of > 160 parsecs. This seems high, compared to my spectroscopic parallax, but this disk is so faint, the red star may well contribute a greater fraction of the light in *K*.

9.6. Discussion

A consistent picture of BZ UMa is emerging, of a dwarf nova with a very low accretion luminosity. This is shown by the infrequent outbursts, extremely strong lines in the optical and near-IR, weak disk continuum and detectable late-M dwarf, and X-ray emission (see below). The rare outbursts and short orbital period might explain why the outbursts have large amplitudes: they might all be tidally-driven superoutbursts, so any outburst should be searched for superhumps. A surprise, perhaps having little to do with this picture, is its wandering radial velocity curve.

BZ UMa's radial velocity curve clearly shows excess power at low frequencies. I am confident of having identified the orbital period, because an *S*-wave is superimposed on it. Periodograms show the effect is strongest in the high velocity material, although the low-velocity material is also affected, since the whole H α line shifts. I consider explanations for this curious behavior:

i) The reduction or analysis is wrong — How the slit is illuminated may introduce a velocity error, but this should be unimportant in the red. Guiding errors should be small since the guiding TV camera is red-sensitive. The mysterious velocity variations do not correspond to any obvious artificial timescale, such as 60 Hz, or to the diurnal cycle.

Measuring velocities of the $\lambda 5577$ night sky line should uncover problems with the wavelength scale or its stability, and none are found in the 1989 spectra (see Fig. 9.11). There is some shifting in this line, but it occurs on the diurnal timescale, and its semi-amplitude is about 10 km sec^{-1} . The semi-amplitude of the anomalous velocity variation exceeds 40 km sec^{-1} . The standard deviation of the velocities measured from the $\lambda 5577$ line is 7.4 km s^{-1} . That of the $\lambda 6300$ night sky line is 14.6 km s^{-1} , although experience shows that this line is usually less precise for this test, being surrounded by variable absorption. The standard deviation of the H α velocities, with the orbit fit and subtracted, is 37.9 km s^{-1} , and without subtracting the orbit, it is 45.6 km s^{-1} .

Furthermore, one need not rely on statistics to see this effect: every part of the cycle is manifest. Night 1 shows a net decrease in γ_{em} , night 2 shows a smooth increase, night 5 shows a minimum, and night 6 shows a maximum. If something were wrong due to atmospheric dispersion or spectrograph flexure, one might expect whatever effect to be similar from night to night. If something were wrong due to a loose CCD or some other mechanical failure in the instrument, one might expect the mysterious velocity variations to be erratic, not to vary smoothly, as on night 1 and especially night 2.

I also find anomalous velocity variations during two other epochs (see Fig. 9.12). Neither run had the frequency resolution of the 1989 run, but even so, whenever a sinusoid with the orbital period is fit to the radial velocity curve and subtracted from the radial velocities, rumbling of similar amplitude persists. Curiously, the rumbling might change period (if indeed it is periodic) between epochs (see Table 9.6). Since the wavelength scale for the 1989 spectra was calibrated to the red of $\text{H}\alpha$ by only three neon lamp lines, I had worried that the wavelength solution was in error, but since three different instrumental setups at different epochs show some rumbling, it is probably not from the wavelength solutions.

BZ UMa's $\text{H}\alpha$ emission line is very strong, so this effect is perhaps not entirely due to noisy velocity measurements. Besides, the anomalous variations in 1989 are not noise: Figs. 9.6 and 9.7 show that when fit to sinusoids, they subtract out cleanly.

Nevertheless, it is impossible to exclude categorically some unknown instrumental effect. But at least one other non-eclipsing CV, V795 Her (= PG 1711+336), shows similar behavior, in observations taken by different instruments and observers (Shafter et al. 1990), who note line profile variations causing a noisy radial velocity curve. In one epoch, a low-frequency velocity variation was so strong it completely masked this CV's orbit (Thorstensen 1986).

ii) *A magnetic white dwarf*— Here, BZ UMa's inner disk would be disrupted into one or two columns that accrete onto the white dwarf's magnetic pole(s). The timescale for

this seems too long, though, and it may be difficult to explain more than one low-frequency quasi-periodicity in this way. Also, magnetic CVs have high-excitation optical spectra, unlike those of dwarf novæ (see Williams 1983). This possibility still should not be dismissed, however, since V795 Her has been suspected of harboring a magnetic white dwarf (Shafter et al. 1990; see their Figs. 6 and 7). V795 Her is unusual for another reason: it is in the well-known CV period gap. This may contradict white dwarf magnetism, though, since it might be explained by an extreme mass ratio (Hameury, King, & Lasota 1991). This may also produce permanent superhumps (Patterson & Richman 1991) giving the observed photometric variability, although the stability of these photometric variations observed by Zhang et al. (1991) may be difficult to explain in this way.

If the rumbling of BZ UMa does indicate white dwarf magnetism, it may be possible to detect coherent optical oscillations with high-speed optical photometry. BZ UMa is an X-ray source (1H 0849+578; Remillard et al. 1992), albeit a faint one at $f_X = 0.3 \mu\text{Jy}$ at 5 keV, assuming a Crab-like spectrum (Wood et al. 1984), so that if magnetic, it should have coherent X-ray variations. BZ UMa also has negligible circular polarization (Liebert & Stockman 1980; Stockman et al. 1992).

iii) Inner disk oscillations — Recently, several authors have considered waves in accretion disks. Honey et al. (1988) detected a variable γ_{em} from a CV disk, thought due to disk waves horizontal to the midplane (although associated with superhumps: see Whitehurst 1988). BZ UMa is not edge-on, but one may wonder, does its disk have vertical waves?

Spiral bending waves, seen in the rings of Saturn (Shu, Cuzzi, & Lissauer 1983), are at least superficially similar to this. One would not see quasi-periodic behavior at any epoch if unless such waves had a non-zero pattern speed. If these really are bending waves, they should be seen more often in low-inclination CVs, and less in eclipsing CVs.

Other types of accretion disk waves may warrant consideration. I tried binning the

1988 spectra on both the periodicities, to check for a V/R variation from an $m = 1$ one-armed spiral wave (Kato 1989). Results were inconclusive, since the S -wave muddies the line profile. Interestingly, though, a low frequency V/R variation *is* present in V795 Her (Thorstensen 1986; see his Fig. 14).

Judging from the width of the oversampled periodogram peaks of about 0.1 cycles/day (Fig. 9.6, bottom), I estimate $Q \equiv f/\Delta f \approx 15$ for the 1989 quasi-periodicities, although the observations sample only 9.4 or 11.3 long periods, over a seven-day baseline, so this estimate is limited by frequency resolution. Because of this lack of frequency resolution over such a long timescale, I stress that the “long periodicities” in 1988 and 1991 could be just stochastic variations: they need not be sinusoidal or even periodic.

I caution that no proper statistical analysis for unevenly-sampled, multiply-periodic (or quasi-periodic) data is in common use in astronomy. The closest is that of Horne & Baliunas (1986), which treats two periodicities plus noise. A problem with the periodogram (Lomb 1976; Scargle 1982) is that it assumes the signal to be sinusoidal and the noise to be Gaussian-distributed. If two or more periodicities exist, this assumption no longer holds: the noise can no longer be considered to be uncorrelated. This approach of subtracting one periodicity at a time and then measuring the parameters of what is left, sometimes called “prewhitening,” leaves me with reservations about its strict statistical validity—it does change the data. It may well force γ_{em} for the anomalous velocity variations to zero, as Table 9.6 shows, even though I have by trial and error subtracted the periodicities in all orders possible, and find no significant changes in the parameters in Table 9.6. It would be desirable to have a rigorous technique, though, since the lack of one leaves doubts. Beats of any small modulation of the radial velocity curve may give the velocities their observed low frequency quasi-periodicities, and noise variations in the velocities may well cause the apparent variability in period.

9.7. Conclusions

BZ Ursa Majoris displays a 97.8-minute spectroscopic period I interpret as the orbital period. There is also significant low-frequency variation in velocities measured from the H α line. While it is impossible to rule out completely an instrumental origin for this, I suggest the accretion disk may oscillate, or perhaps there is column accretion onto a magnetic white dwarf. Either case is interesting: the first would illuminate disk physics, the second would indicate a new type of magnetic CV. No explanation is satisfactory in present form, however, and I stress the need to confirm this finding with other instruments. A fiber-fed spectrograph with a circular aperture, for example, should reduce atmospheric dispersion and flexure effects.

A troubling thought arises: if this is right, how many other times were these velocity variations measured and interpreted as orbital periods? I therefore advise caution in interpreting the radial velocity curves of apparent long-period CVs, such as V795 Her (Thorstensen 1986). If some long-period CVs have their radial velocity curves remeasured, will they change?

I also deconvolve an $M5.5 \pm 0.5$ red star from spectra of BZ UMa, and find an absolute magnitude for this CV in R_{KC} of 10.7 (+0.66/−0.85), and estimate a distance of 110 (+44/−51) parsecs. A *JHK* photometric parallax gives a distance of > 160 parsecs, but even so, BZ UMa is a good candidate for a trigonometric parallax measurement.

Table 9.1. Emission Lines in Summed Spectra

	H γ 4340	He I 4471	He II 4686	H β 4861	He I 4921	He I (5015)	Fe II 5169	He I 5876	H α 6563	He I 6678		
BZ UMa – 1989 March												
$W(\text{\AA})$	71	29	13	118	14	28	–	69	198	29		
FWHM (km s ^{−1})	1790	1960	3570	1600	1690	blend	blend	1550	1340	1550		
FWZI (km s ^{−1})	4900	3600	5200	4100	2800	blend	blend	4200	3800	2900		
I/I _{cont}	4.2	2.1	1.3	6.0	1.5	1.6	1.4	3.0	7.2	1.8		
	H α 6563	He I 6678	He I 7065	He I 7281	O I 7773	8200 bump	Pa18 8438	Ca II blend	Pa14 8598	Ca II 8662	Pa12 8750	Pa11 8862
1991 June												
$W(\text{\AA})$	235	34	28	7.2	6.0	5:	1.3	33	2.2	32	15	21
FWHM	1250	1550	1650	1970	1650	3000	1250	blend	1100	1450	1680	1540
FWZI	4050	4100	3700	3100	1650	3870	1750	blend	1600	2800	2760	2730
I/I _{cont}	9.2	2.0	1.7	1.2	1.15	1.09	1.08	1.6	1.8	1.8	1.3	1.6

Table 9.2. Instrument Setups

Epoch	CCD	Observer	Range (Å)	$\Delta\lambda$ (Å)
1988 January	Thomson	RMH	5900–7100	4.5
1989 March	Thomson	FAR	4200–6750	9.0
1991 June	TI-4849	FAR	6200–8940	9.0

Table 9.3. H α Emission Radial Velocities

HJD ^a	V	HJD ^a	V	HJD ^a	V	HJD ^a	V
(km s ⁻¹)		(km s ⁻¹)		(km s ⁻¹)		(km s ⁻¹)	
BZ UMa (1988 January) ^d							
7167.974	16	7169.012	-17	7170.972	48	7173.001	63
7167.995	15	7169.027	44	7170.995	14	7173.012	41
7168.017	17	7169.951	52	7171.018	73	7173.023	11
7168.951	20	7169.974	27	7171.038	91	7173.035	4
7168.969	24	7169.996	6	7172.966	21	7173.045	53
7168.983	47	7170.018	17	7172.976	41		
7168.998	20	7170.950	22	7172.989	76		
BZ UMa (1989 March) ^d							
7600.751	11	7601.794	42	7603.685	37	7605.784	8
7600.762	15	7601.807	74	7603.696	67	7605.795	56
7600.775	31	7601.819	23	7603.708	69	7605.807	111
7600.788	76	7601.831	11	7603.720	72	7605.819	77
7600.800	34	7601.842	22	7603.731	31	7605.831	40
7600.812	6	7601.854	43	7603.743	24	7605.842	16
7600.822	30	7601.866	81	7604.661	10	7605.854	23
7600.832	5	7601.878	96	7604.677	79	7605.866	51
7600.845	24	7601.890	58	7604.690	100	7605.877	54
7600.858	45	7601.901	26	7604.702	79	7605.889	42
7600.870	6	7601.913	54	7604.713	11	7605.901	5
7600.883	29	7601.925	79	7604.725	27	7605.908	54
7600.895	23	7602.630	67	7604.737	20	7605.915	22
7600.907	12	7602.642	15	7604.749	70	7605.928	19
7600.919	25	7602.654	17	7605.634	40	7607.662	41
7600.932	0	7602.666	43	7605.645	36	7607.674	61
7601.683	30	7602.678	87	7605.658	63	7607.686	65
7601.695	66	7602.690	69	7605.670	77	7607.698	38
7601.708	64	7602.702	40	7605.682	107	7607.709	24
7601.720	20	7602.714	2	7605.696	62	7607.721	11
7601.732	30	7602.726	33	7605.724	48	7607.733	6
7601.746	41	7602.738	26	7605.736	78	7607.745	49
7601.758	21	7603.649	86	7605.747	87		
7601.770	40	7603.661	36	7605.760	40		
7601.782	0	7603.673	29	7605.772	14		
BZ UMa (1991 June) ^d							
8318.863	-85	8318.941	-75	8319.807	-35	8319.885	-15
8318.874	50	8318.952	-30	8319.819	-25	8319.896	23
8318.886	84	8318.963	4	8319.830	2	8323.899	-35
8318.896	19	8318.980	105	8319.841	38	8323.909	3
8318.908	-59	8319.774	30	8319.852	49	8323.923	46
8318.918	-85	8319.785	44	8319.863	27	8323.933	33
8318.930	-114	8319.796	13	8319.874	7	8323.945	13

^d Shafter (1983a) algorithm, Gaussian separation 970 km s⁻¹

Table 9.4. H α Emission Radial Velocities

HJD ^a	V	HJD ^a	V	HJD ^a	V	HJD ^a	V
(km s ⁻¹)		(km s ⁻¹)		(km s ⁻¹)		(km s ⁻¹)	
BZ UMa (1989 March) ^e							
7600.751	-16	7601.794	55	7603.685	55	7605.784	3
7600.762	26	7601.807	86	7603.696	85	7605.795	79
7600.775	50	7601.819	1	7603.708	65	7605.807	129
7600.788	86	7601.831	-33	7603.720	51	7605.819	53
7600.800	-1	7601.842	-20	7603.731	-3	7605.831	7
7600.812	-38	7601.854	56	7603.743	27	7605.842	-4
7600.822	33	7601.866	91	7604.661	11	7605.854	35
7600.832	9	7601.878	89	7604.677	-113	7605.866	73
7600.845	50	7601.889	37	7604.690	-117	7605.877	58
7600.858	46	7601.901	14	7604.702	-67	7605.889	31
7600.870	-25	7601.913	72	7604.713	19	7605.901	-28
7600.883	-50	7601.925	85	7604.725	-5	7605.908	15
7600.895	-16	7602.630	50	7604.737	-33	7605.915	-34
7600.907	1	7602.642	-31	7604.749	-100	7605.928	28
7600.919	43	7602.654	-5	7605.634	7	7607.662	-63
7600.932	-19	7602.666	39	7605.645	20	7607.674	-74
7601.682	-47	7602.678	115	7605.658	86	7607.686	-60
7601.695	-79	7602.690	84	7605.670	91	7607.698	-35
7601.708	-66	7602.702	7	7605.682	104	7607.709	36
7601.720	-9	7602.714	-38	7605.696	21	7607.721	0
7601.732	46	7602.726	-44	7605.724	55	7607.733	-24
7601.746	17	7602.738	36	7605.736	92	7607.745	-64
7601.758	-52	7603.649	77	7605.747	84		
7601.770	-53	7603.661	5	7605.760	7		
7601.782	5	7603.673	32	7605.772	-7		

^e Shafter (1983a) algorithm, Gaussian separation 650 km s⁻¹

Table 9.5. H α Emission Radial Velocities

HJD ^a	V	HJD ^a	V	HJD ^a	V	HJD ^a	V
(km s ⁻¹)	(km s ⁻¹)	(km s ⁻¹)	(km s ⁻¹)	(km s ⁻¹)	(km s ⁻¹)	(km s ⁻¹)	(km s ⁻¹)
BZ UMa (1989 March) ^f							
7600.751	32	7601.794	31	7603.685	27	7605.784	10
7600.762	4	7601.807	68	7603.696	47	7605.795	38
7600.775	16	7601.819	41	7603.708	84	7605.807	99
7600.788	80	7601.831	7	7603.720	93	7605.819	99
7600.800	65	7601.842	-16	7603.731	56	7605.831	61
7600.812	17	7601.854	37	7603.743	24	7605.842	27
7600.822	43	7601.866	79	7604.661	10	7605.854	11
7600.832	-16	7601.878	101	7604.677	-58	7605.866	30
7600.845	1	7601.889	76	7604.690	-92	7605.877	49
7600.858	45	7601.901	40	7604.702	-82	7605.889	51
7600.870	14	7601.913	41	7604.713	-36	7605.901	32
7600.883	-13	7601.925	83	7604.725	-40	7605.908	80
7600.895	-24	7602.630	95	7604.737	-9	7605.915	-11
7600.907	-28	7602.642	51	7604.749	-53	7605.928	13
7600.919	9	7602.654	33	7605.634	81	7607.662	-27
7600.932	17	7602.666	53	7605.645	44	7607.674	-54
7601.683	-14	7602.678	82	7605.658	61	7607.686	-66
7601.695	-50	7602.690	65	7605.670	82	7607.698	-38
7601.708	-65	7602.702	69	7605.682	111	7607.709	9
7601.720	-29	7602.714	34	7605.696	115	7607.721	18
7601.732	9	7602.726	-10	7605.724	44	7607.733	8
7601.746	63	7602.738	23	7605.736	73	7607.745	-35
7601.758	9	7603.649	97	7605.747	103		
7601.770	-25	7603.661	44	7605.760	68		
7601.782	-3	7603.673	30	7605.772	30		

^f Shafter (1983a) algorithm, Gaussian separation 1950 km s⁻¹

Table 9.6. BZ UMa – Derived Orbital Parameters^a

Object	P_{orb} (days)	K_{em} (km s ⁻¹)	γ_{em} (km s ⁻¹)	T_0 (HJD – 2440000)	σ (km s ⁻¹)
1988 Raw Orbit ^g	0.0679 ± 0.0001	30 ± 11	21 ± 7	7169.987 ± 0.004	32
QPV ^h	0.292 ± 0.001	36 ± 7	-12 ± 5	7170.035 ± 0.009	21
Orbit Only	0.06791 ± 0.00009	31 ± 7	21 ± 5	7169.989 ± 0.002	20
1989 Raw Orbit ^g	0.0679 ± 0.0001	36 ± 6	22 ± 4	7603.960 ± 0.002	39
QPV 1 ^h	0.743 ± 0.004	42 ± 4	3 ± 3	7604.11 ± 0.01	17
QPV 2	1.60 ± 0.02	27 ± 4	1 ± 2	7603.33 ± 0.03	17
[QPV 3	0.1306 ± 0.0005	9 ± 3	0 ± 2	7603.945 ± 0.007	17]
Orbit Only	0.06793 ± 0.00004	36 ± 3	22 ± 2	7603.8247 ± 0.0008	17
He I $\lambda 6678$ ^g	0.0679 ± 0.0001	43 ± 9	20 ± 7	7603.976 ± 0.003	65
1991 Raw Orbit ^g	0.0680 ± 0.0002	42 ± 14	1 ± 10	8319.899 ± 0.004	44
QPV	0.1271 ± 0.0004	36 ± 11	-3 ± 8	8319.849 ± 0.006	36
Orbit Only	0.0679 ± 0.0001	39 ± 11	1 ± 8	8319.897 ± 0.003	35

^g Measured for individual variations with Shafter (1983a) algorithm, separation 970 km s⁻¹

^h QPV \equiv Quasi-periodic variation: velocity variation, not strictly periodic (note changes between epochs), that can fit a sinusoid and is not a time series sampling artifact (see text)

Figure 9.1.

Rectified sum of the 1989 BZ UMa spectra, comprising over 24 hours' exposure time. The emission lines are unusually strong, H α having an equivalent width of nearly 200 Å. Spurious features at $\lambda\lambda$ 5577 and 6300 are bad night-sky line subtractions.

BZ UMa - 1989 Grand Sum Spectrum

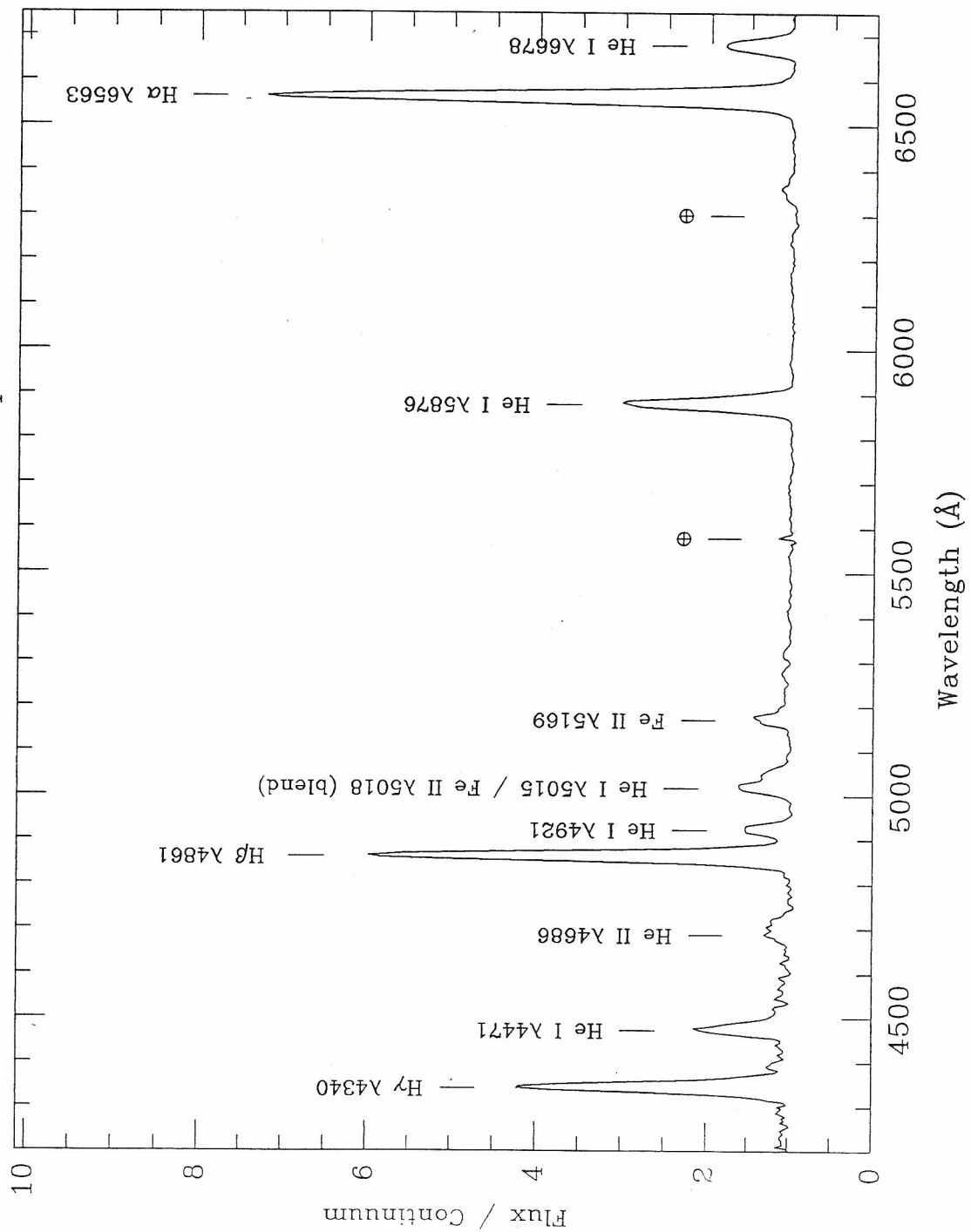


Figure 9.2.

(Top)

Average of the 1991 spectra of BZ UMa, in the red region and sky subtracted. A low-*z* sdF spectrum was used to measure the profiles of the telluric atmospheric bands, subsequently scaled and subtracted with some residual absorption near $\lambda\lambda 6870$ and 7600 .

(Middle)

Same spectrum, with a scaled M5 dwarf spectrum subtracted (see text). The strong anomalous emission bump at $\lambda 8200$ obscures any trace of the Na I or He II features. This deconvolved spectrum is displaced downward by $1.4 \times 10^{-16} \text{ erg cm}^{-2} \text{ s}^{-1} \text{ \AA}^{-1}$ for clarity.

(Bottom)

Scaled M5 dwarf spectrum, displaced upward by $6.4 \times 10^{-16} \text{ erg cm}^{-2} \text{ s}^{-1} \text{ \AA}^{-1}$ for clarity.

BZ UMa - 1991 Grand Sum Spectrum

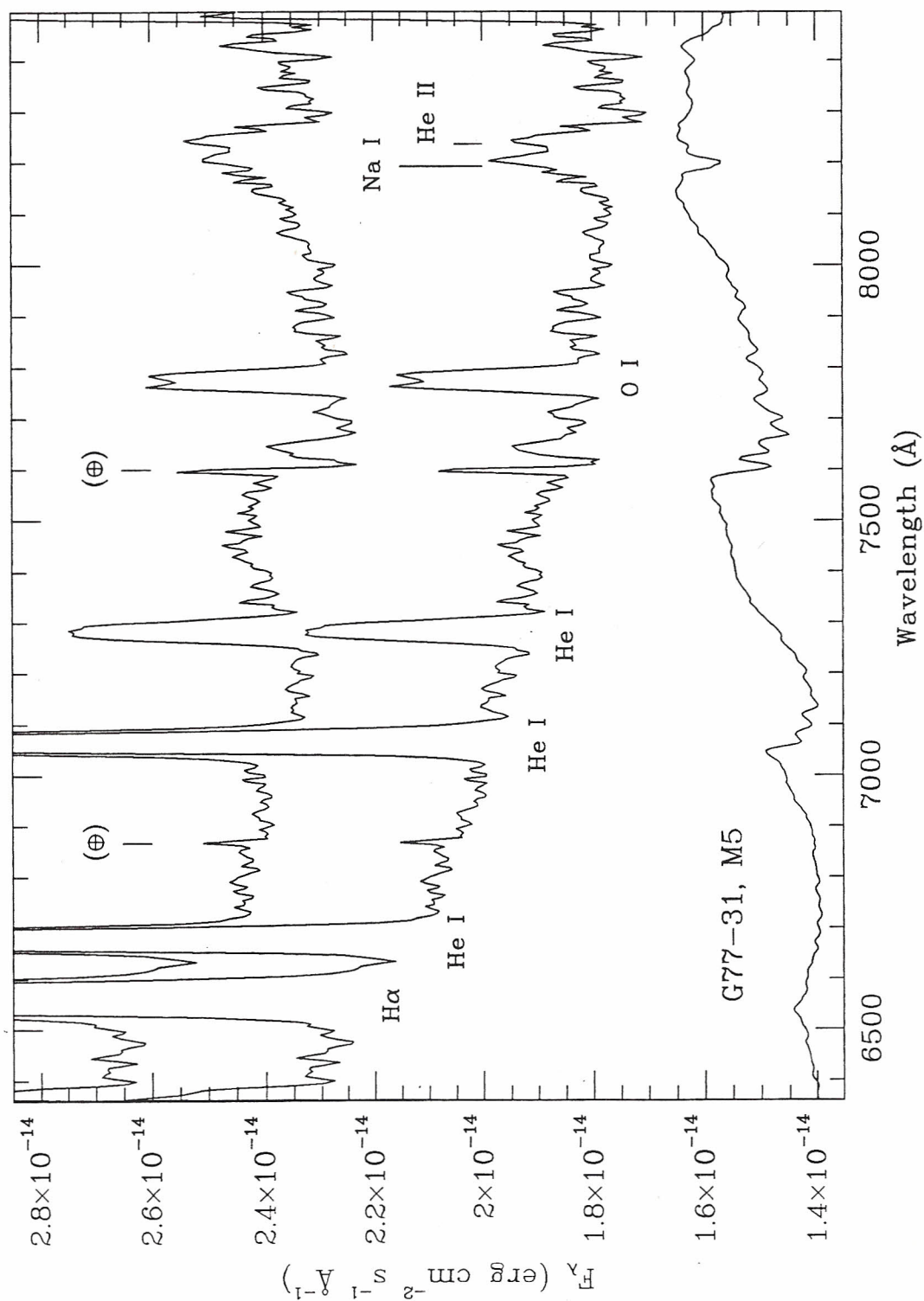


Figure 9.3.

Rectified red end of the 1991 spectra, shown both corrected and uncorrected for telluric absorption. The emission bump at $\lambda 8200$ never goes away.

BZ UMa - 1991 Far Red Spectrum

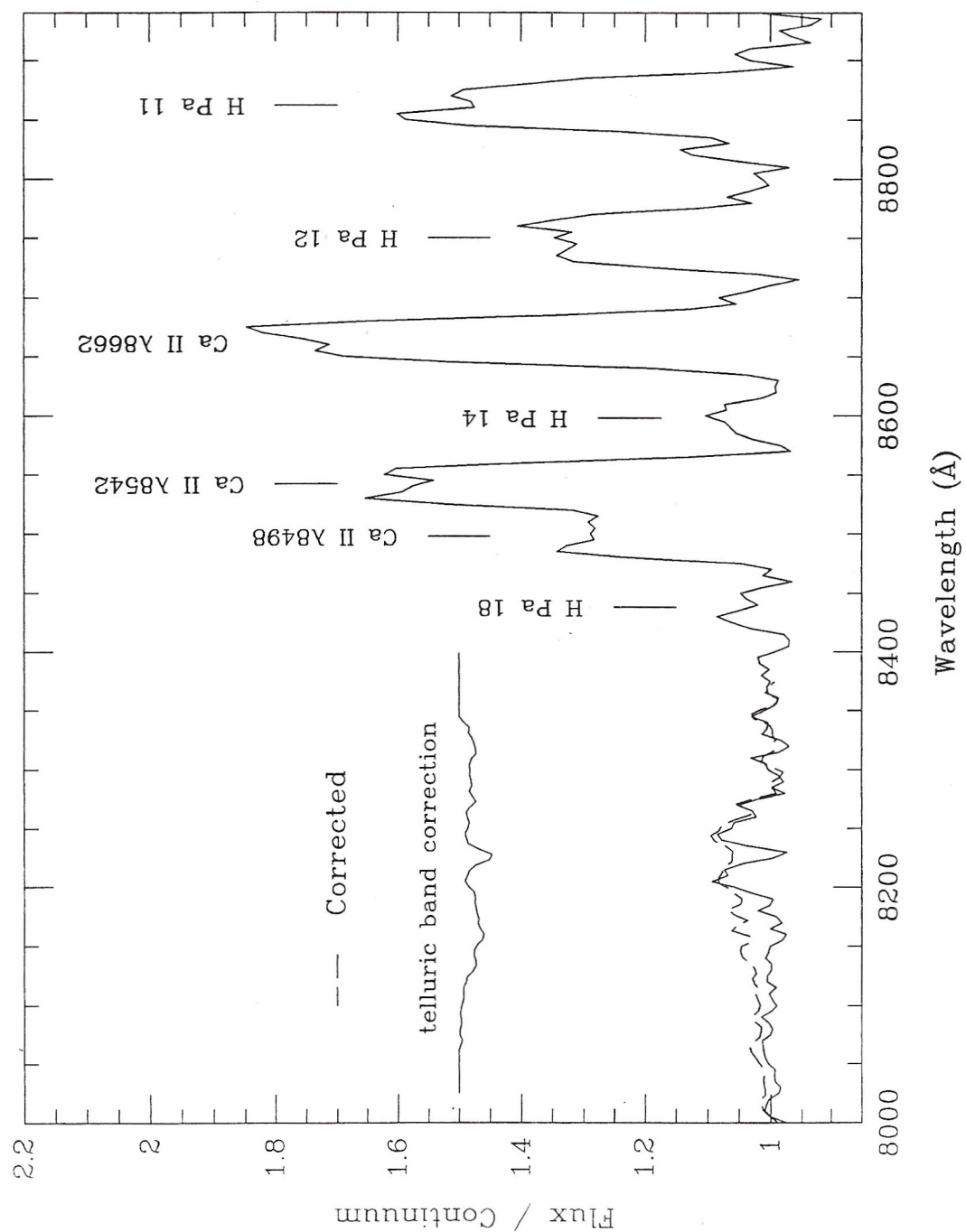


Figure 9.4.

That the 97.8-minute periodicity is the orbital period is shown by this *S*-wave in the profile of $H\alpha$. These spectra are binned over a 97.8-minute period, co-added to reduce noise, and rectified, normalized in height, and given arbitrary offsets in height, for clarity.

BZ UMa - H α profiles (1988)

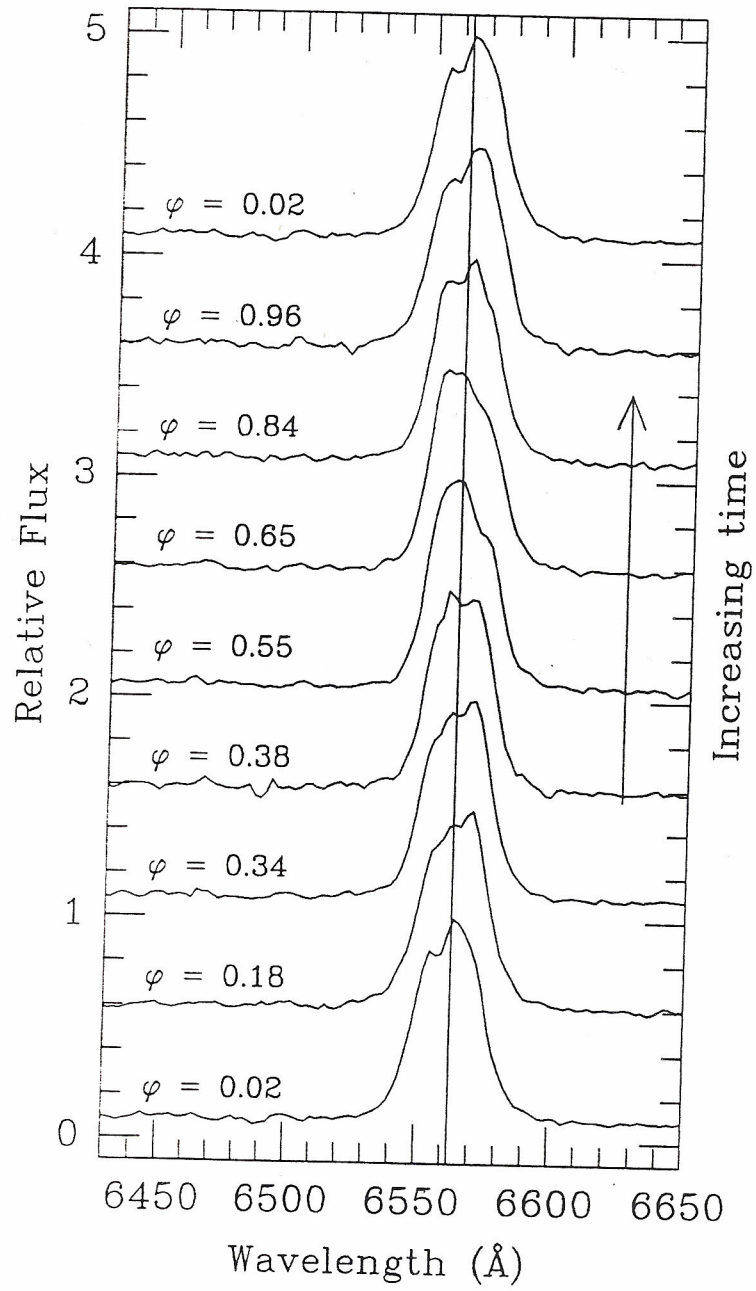


Figure 9.5.

(*Top and Middle-top, -bottom*)

Periodograms of H α velocities, measured by double-Gaussian algorithm. Gaussian separations range from 650 km s⁻¹ (marked *Core*), to 1300 km s⁻¹, to 1950 km s⁻¹ (*Wings*). The low-frequency velocity variations become stronger in the line wings.

(*Bottom*)

Periodogram of an artificial (“fake”) sinusoid with parameters similar to the orbit’s, given random noise with $\sigma = 30$ km s⁻¹, and sampled identically in time to how the real data are sampled. No low-frequency variations are present, so they cannot arise from the sampling of the time series.

BZ UMa - Periodograms of H α Velocities

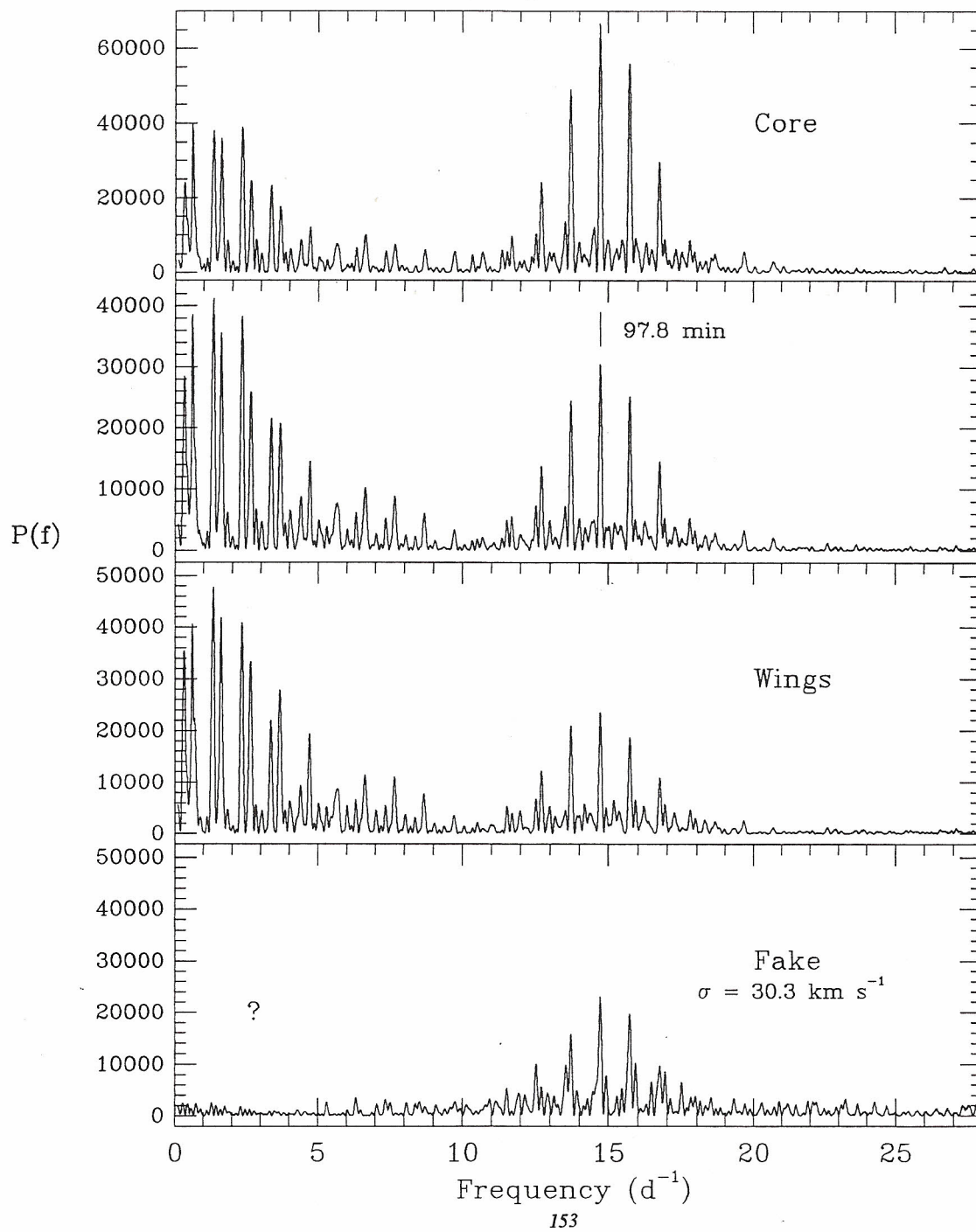


Figure 9.6.

(Top, Middle)

For velocities measured with a Gaussian separation of 1300 km s^{-1} , I fit low-frequency sinusoids to the velocities, subtract them, and generate these periodograms. This suggests at least two low-frequency quasi-periodic variations (QPVs) are present.

(Bottom)

Fig. 9.5, *Middle-top*, expanded to show only the low-frequency quasi-periodicities. There are at least two, attended by forests of 1 cycle/day aliases.

BZ UMa - Periodograms of H α Velocities

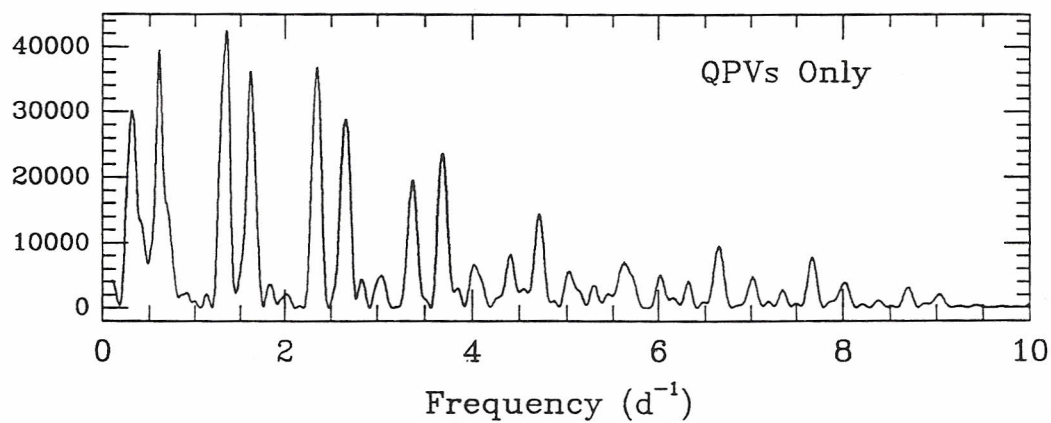
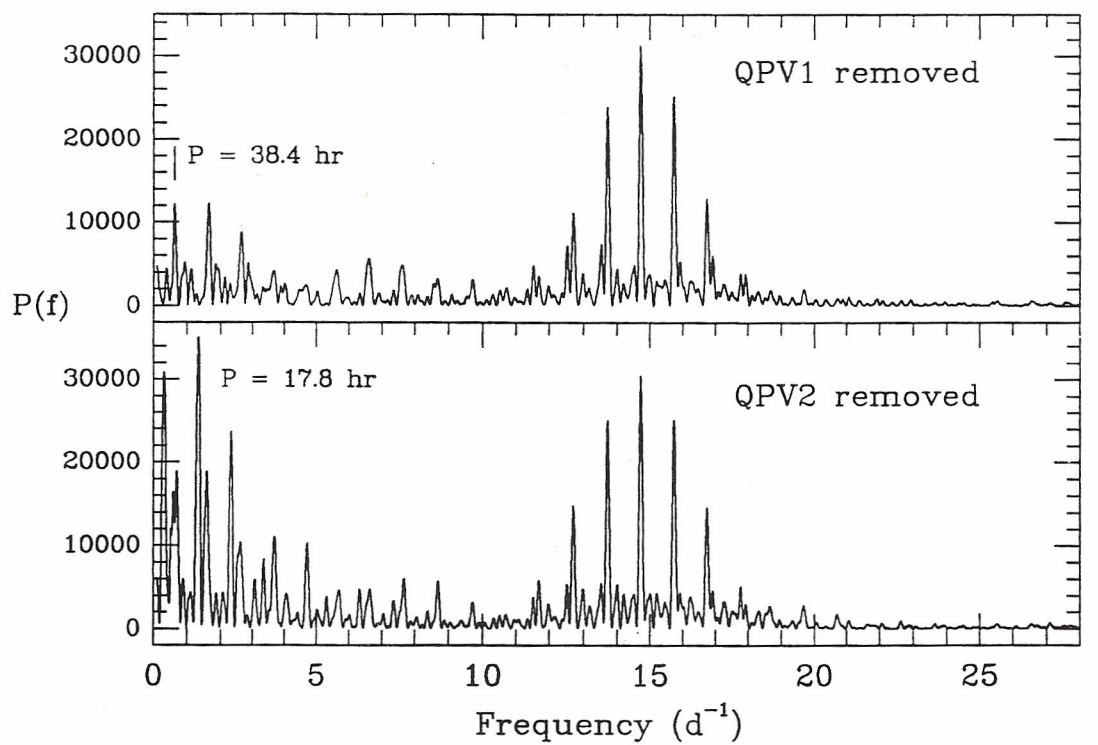


Figure 9.7.

(Top)

After subtracting both the strong low-frequency quasi-periodic variations from the velocities, another periodogram suggests a weak third one is present.

(Middle, Bottom)

With three sinusoids subtracted, the periodogram strongly resembles that of a sinusoid with the orbital parameters (labeled “Fake”).

BZ UMa - Periodograms of H α Velocities

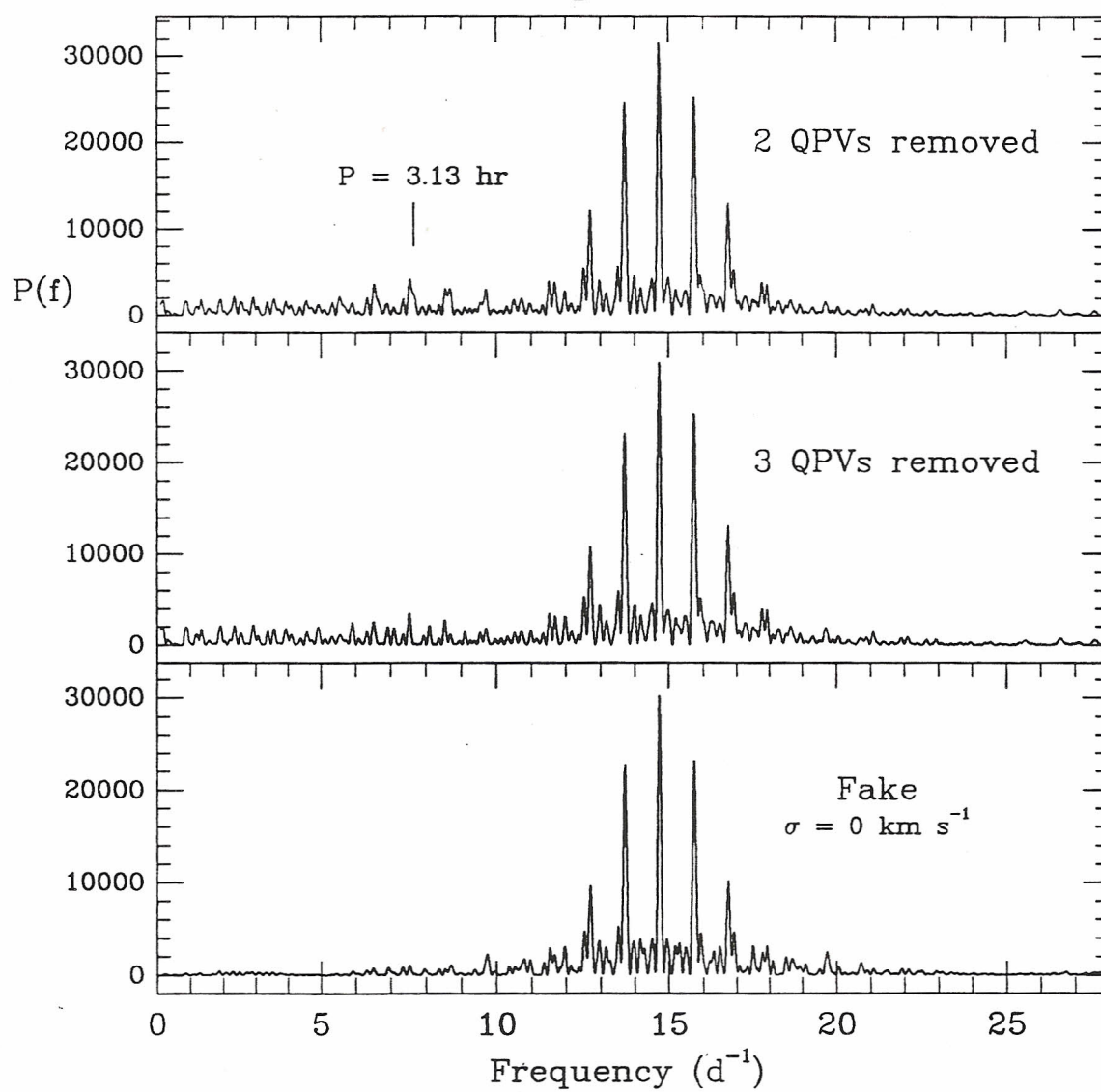


Figure 9.8.

(Top)

The radial velocities for BZ UMa, plotted about the orbital phase. All data are plotted twice for continuity, with different nights plotted with different symbols: for HJD – 2440000, 7600 = diagonal crosses, 7601 = crosses, 7602 = squares, 7603 = triangles, 7604 = five-pointed stars, 7705 = four-pointed stars, 7607 = circles.

(Middle-top, -bottom and Bottom)

When low-frequency sinusoids, corresponding to the quasi-periodic variations, are fitted to and subtracted from the radial velocity curve, its fit to a sinusoid improves.

BZ UMa - H α Radial Velocities

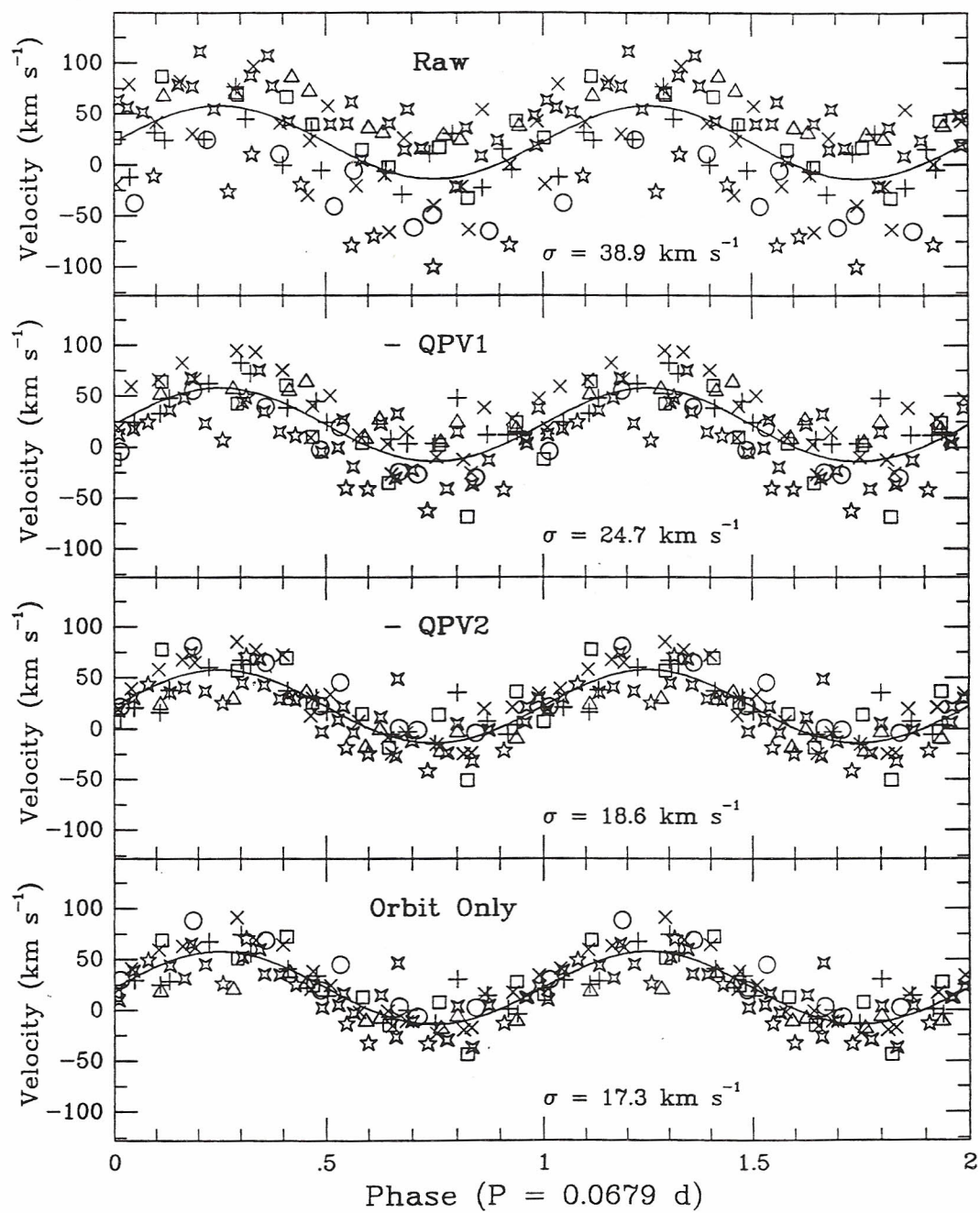


Figure 9.9.

Periodograms of velocities of the He I $\lambda 6678$ line, measured by double-Gaussian algorithm. Separations range from 650 km s^{-1} (*Top*, marked *Core*), to 1300 km s^{-1} (*Middle-top*), to 1950 km s^{-1} (*Middle-top*), to 2600 km s^{-1} (*Bottom*, marked *Wings*). For the middle traces, note the pattern's overall similarity to Fig. 9.5, featuring both orbital and low-frequency variations. The noise level is probably higher since the line is weaker.

BZ UMa - Periodograms of He I λ 6678 Velocities

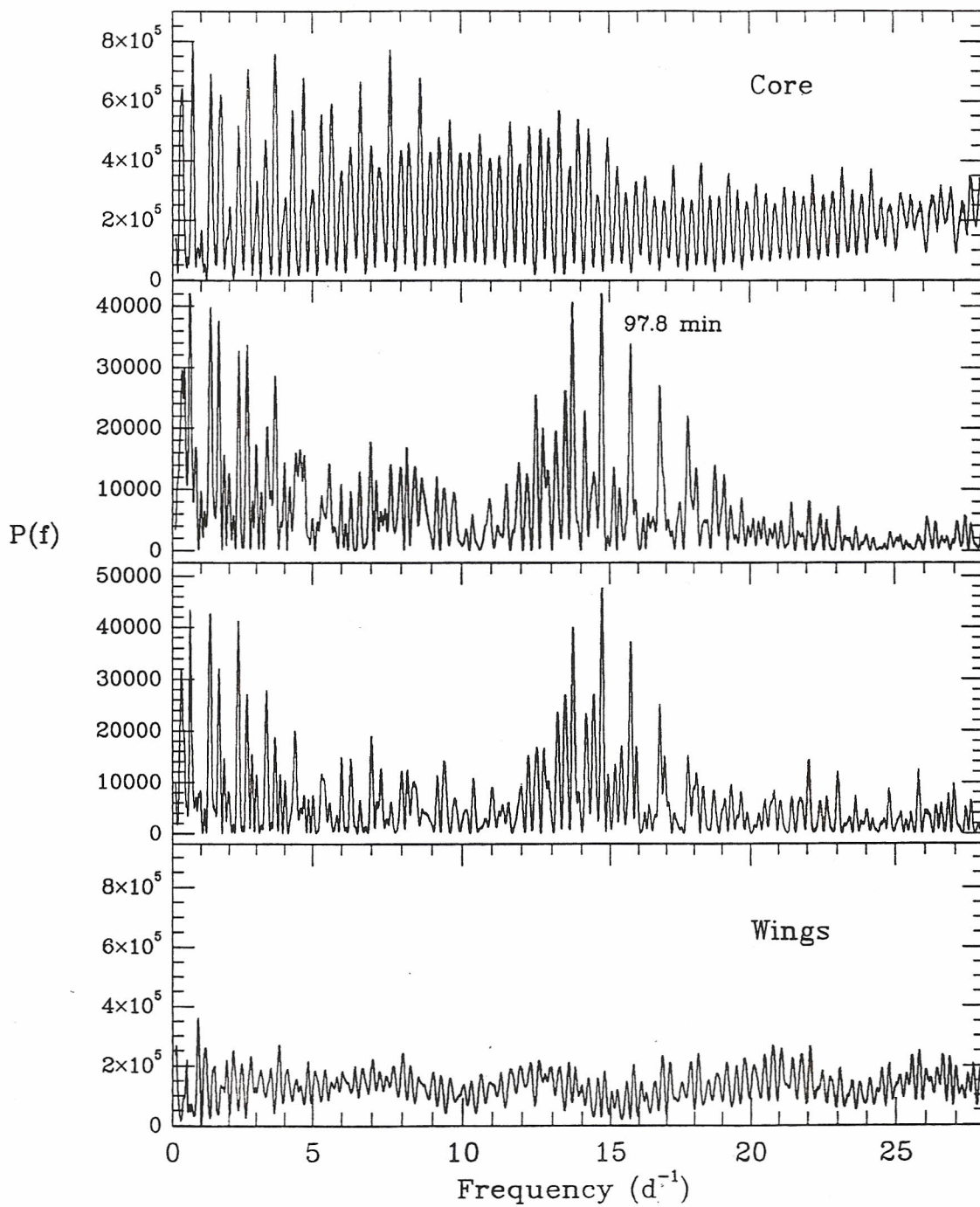


Figure 9.10.

The lightcurve of BZ UMa from Kaluzny (1986), phase-binned about the orbital period. Only the barest trace of an orbital hump is visible, if at all. One discrepant point, perhaps fortuitously at the right place in the cycle, suggests an eclipse, although it seems too narrow to be real.

Kaluzny's BZ UMa photometry (in B)

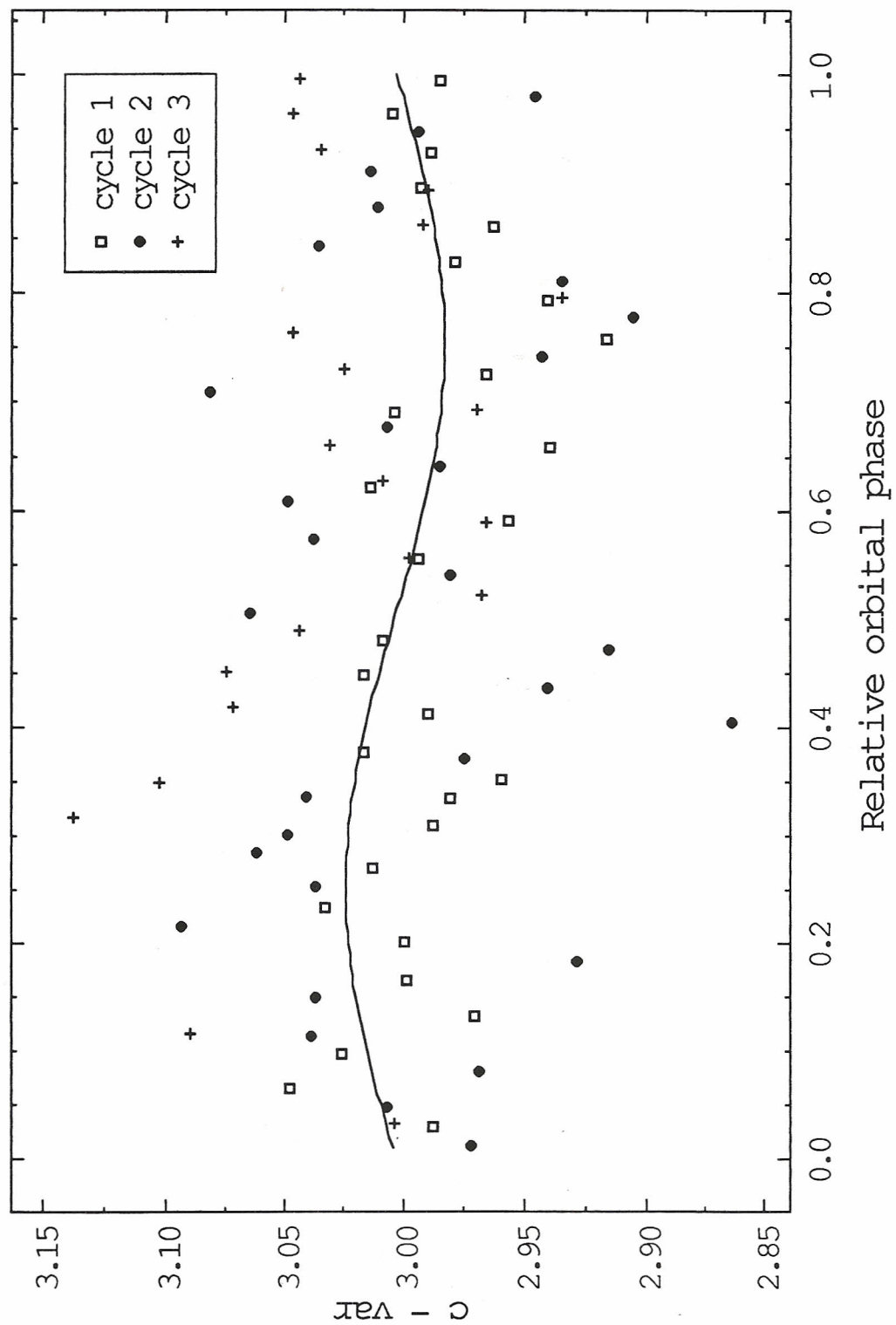


Figure 9.11.

(Top)

The reality of the quasi-periodic variations is supported by subtracting the orbit from the radial velocity curve and plotting the residual velocities, which vary throughout each of the nights, and not just from night to night.

(Connected filled squares)

I also plot velocities of the night sky line O I $\lambda 5577$. As they should be zero, they show the quality of the measured velocities: the deviations of the night-sky lines are of order $\pm 10 \text{ km s}^{-1}$, typical for a Cassegrain spectrograph. Those of the H α line easily exceed $\pm 40 \text{ km s}^{-1}$.

(Middle and Bottom)

The residual velocities also vary continuously, as the individual nights' velocities show.

BZ UMa - H α Radial Velocities (orbit subtracted)

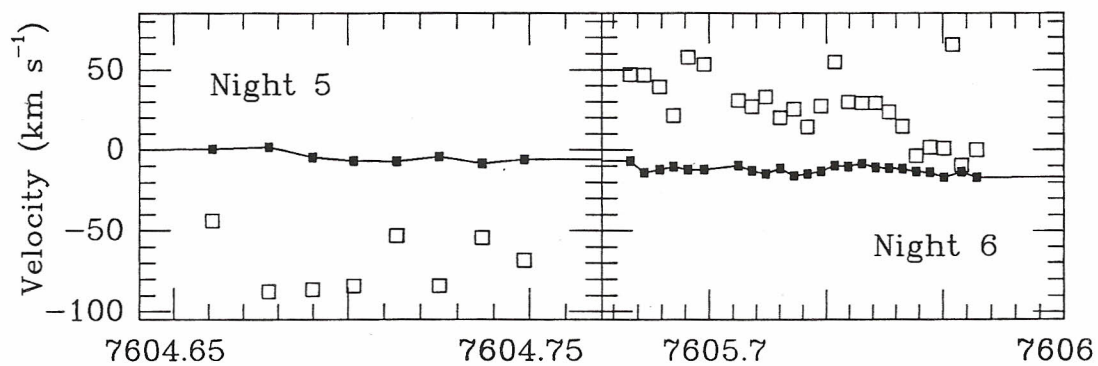
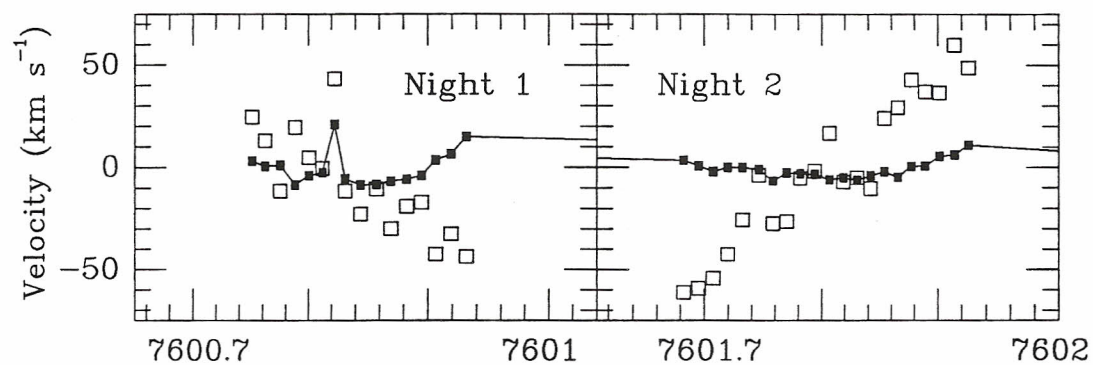
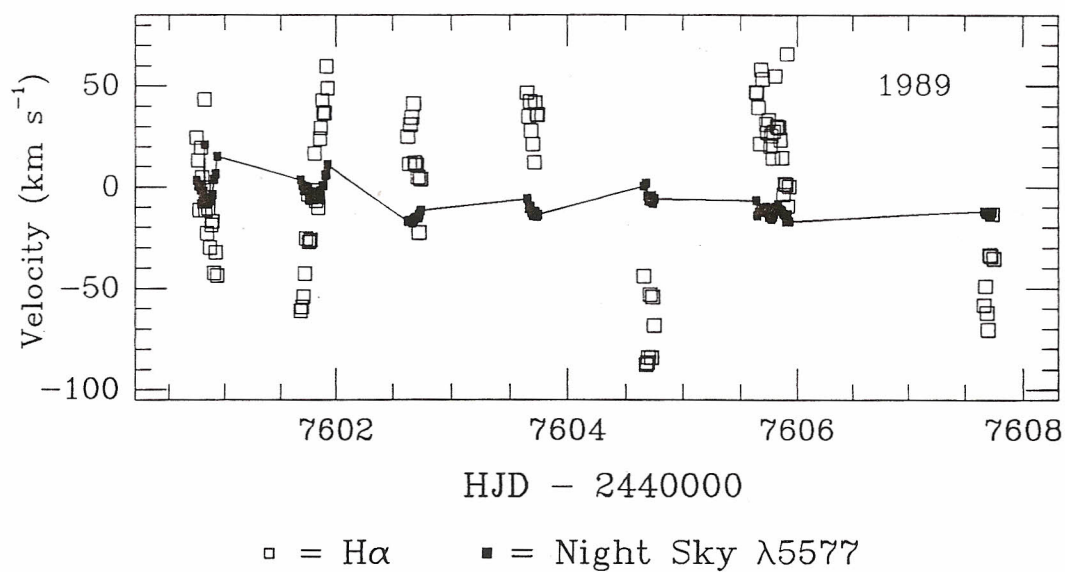
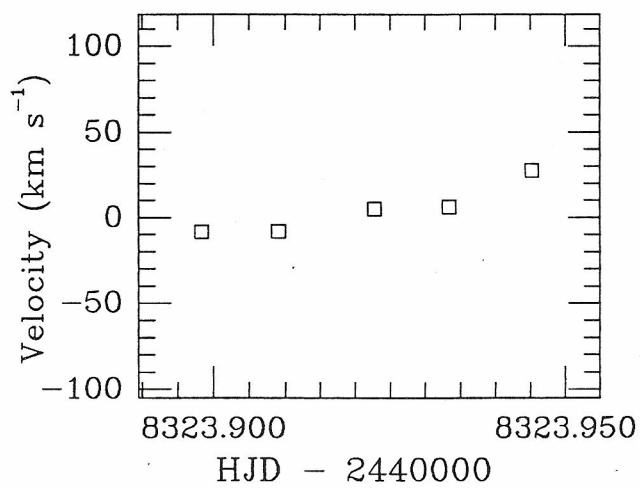
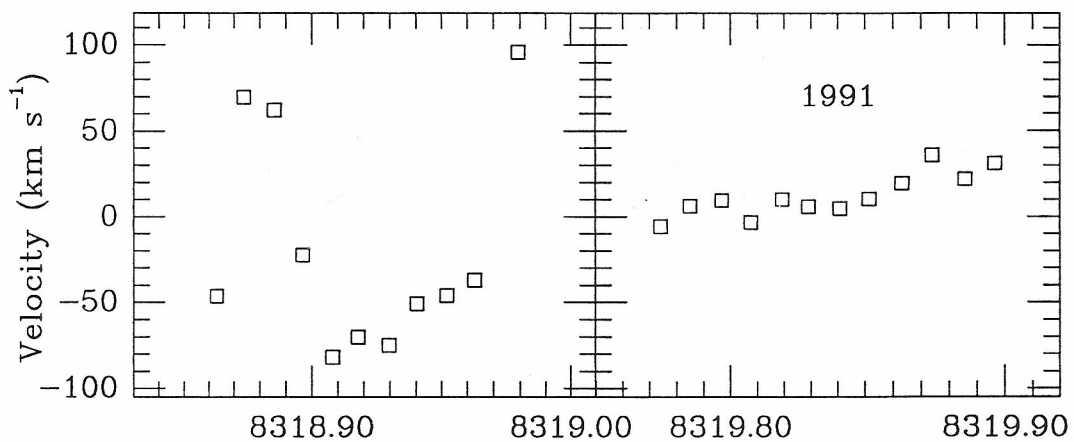
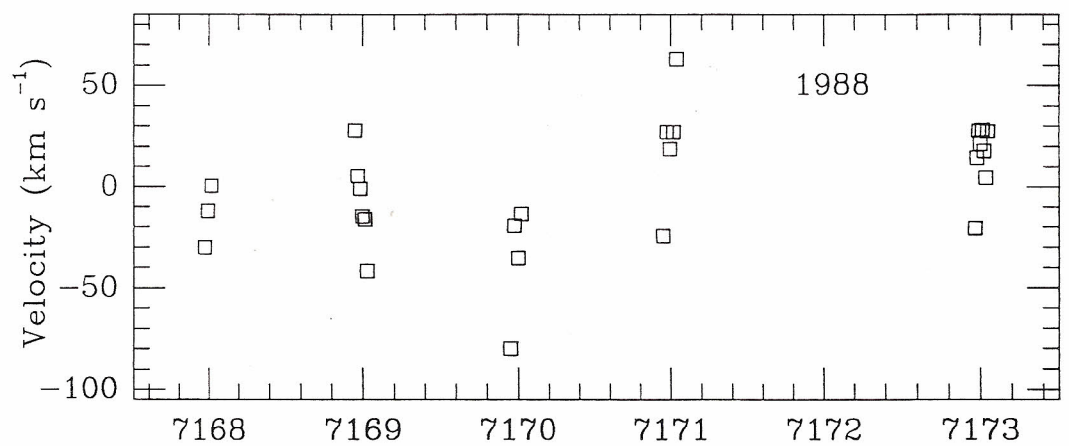


Figure 9.12.

Similar diagram to Fig. 9.11, except plotting the 1988 and 1991 velocities.

Unfortunately, the wavelength coverage did not permit night sky measurements, but still, the H α velocities appear to wander by over $\pm 10 \text{ km s}^{-1}$ in all three epochs.

BZ UMa - H α Radial Velocities (orbit subtracted)



Chapter 10

HX Pegasi, Caught on the Rise to a Dwarf Nova Outburst

You sure must live right having HX Peg sit up and perform for you like that.

W. Liller (private communication)

10.1. Introduction

Dwarf novæ are a subclass of cataclysmic variables showing outbursts that typically peak 2 – 5 magnitudes above quiescent brightness. These last for days to weeks, and recur over weeks to months. Observing these outbursts is complicated by their being only quasi-periodic: there is a large dispersion in their recurrence times, outburst durations, and amplitudes (e.g., Szkody & Mattei 1984; Warner 1987). Dwarf nova outbursts are thought to be accretion-powered, in contrast to the nuclear-powered eruptions of classical novæ, although the mechanism for dwarf nova outbursts has long been controversial. The two most widely-regarded models are still disk thermal instabilities (Osaki 1974) or modulated mass transfer from the red star (Bath 1973). For reviews on theory and phenomenology, see Smak (1984) and Mattei (1990).

While investigating CVs found by the Palomar-Green survey (Green, Schmidt, & Liebert 1986), I performed a radial velocity study of HX Pegasi = PG 2337+123 = “A Blue Variable at High Latitude” (Green, Greenstein, & Boksenberg 1976; hereafter GGB76). The first night, it was near $R = 15$, estimated by its appearance on the TV monitor, and with strong emission lines. Halfway through the second night, the continuum rose rapidly, overwhelming the lines. On the third night, HX Peg was near $R = 12 - 13$, with weak emission lines. Initially, I took this behavior to be that of a nova-like similar to VY Scl, coming out of a characteristic low state (e.g., Shafter et al. 1985). Later, with the radial velocity study finished, I ascertained from the orbital period I found that HX Peg is

probably a dwarf nova, and that it had gone into outburst just as I was observing it. This is the second-ever such time-resolved spectroscopy of a dwarf nova caught on the rise to outburst, after that of Mansperger & Kaitchuck (1990) (hereafter MK90), and the first in the red, to document the behavior of the O I $\lambda 7773$ line. One might hope to use these spectra to find where the outburst occurs in the disk, and how it propagates.

Table 10.1 is a journal of all observations. The observations are described in § 10.2. I find what may be an unusual red star in the quiescent spectrum in § 10.3, and estimate absolute magnitude and distance. The radial velocity study is presented in § 10.4, with results summarized in Table 10.2. I describe the outburst in § 10.5, with overall discussion in § 10.6.

10.2. Observations

The discovery and photometric properties of this CV were described by GGB76, who include a finding chart, and note spectrum variability on a timescale of minutes. Greenstein, Arp, & Sackett (1977; hereafter GAS77) show spectra with variability on timescale of months. When the star is faint, the Balmer and He I lines show up in strong, broad emission, and when the star is bright, these lines weaken considerably, perhaps even going into absorption. This variability is consistent with that of either dwarf nova or anti-dwarf nova activity. So is irregular photometric variability over days to years, between $m_{pg} = 13.5$ and 16.5, noted in a study with the Harvard College Observatory plate archive (Liller & Eachus 1976). This range might be larger than three magnitudes, too, since few HCO archive plates go fainter than $m_{pg} = 16.5$.

I observed HX Peg on 1991 October 18 – 20 UT. Observational procedure is similar to that of Thorstensen & Freed (1985) and this work (Chapter 2), with exceptions noted. Data reductions were carried out as by Thorstensen et al. (1989). Only the first night was clear, perhaps even photometric, although volcanic dust from Mt. Pinatubo was

lighting up the sunset. Instrument rotation on the 1.3-m McGraw-Hill telescope is difficult, so spectrophotometry with the Mark IIIa (black) spectrograph will probably suffer from the effects of differential refraction through the 2.2" slit. Nevertheless, this setup has worked well for radial velocity studies of other CVs (Thorstensen, Davis, & Ringwald 1991a; Beuermann et al. 1992), and the long, narrow slit does provide for accurate digital sky subtraction. The detector was a TI-4849 CCD, mounted inside the BRICC camera (Luppino 1989). A 300 line/mm grism, blazed at $\lambda 6400$, was used, along with a Hoya Y-50 order-blocking filter, to prevent overlap with the red setup, which covered $\lambda\lambda 6200 - 9000$. At 5 Å/pixel along the dispersion, this gave 11-Å resolution FWHM. The wavelength scale was calibrated to within 0.1 Å and reproducible to 0.05 Å with fifth-order polynomial fits to the wavelengths of the lines of Ne, Ar, and Xe lamps, taken at the beginning of each night. Wavelength stability was assured with Ne lamps, taken nominally every 30 minutes while observing, between target exposures. Object exposures were 15 minutes long. Flux standards (Oke 1974) were taken, to remove the instrumental signature from the spectra. Hot, metal-deficient stars (Oke & Gunn 1983) were also observed, to map and calibrate out the telluric absorption features (see Wade & Horne 1988). Sometimes these bands do not divide out perfectly, causing the wrinkles near $\lambda 7600$ in Fig. 10.1.

10.3. Quiescent Spectrum and Red Star

The bottom trace of Fig. 10.1 depicts the average spectrum during the first night. This quiescent spectrum resembles that of a dwarf nova, with strong, broad H α and He I lines, all in emission. The He I $\lambda\lambda 6678, 7065$ lines are also in broad emission, with double peaks of separation 750 km s⁻¹ and 900 km s⁻¹, respectively. The O I $\lambda 7773$ feature is not obvious in the quiescent spectrum. This is not uncommon, although in many quiescent dwarf novæ, it appears weakly in emission (Friend et al. 1988).

There are a few features from this CV's red star, the most obvious being the K I

$\lambda\lambda 7665, 7699$ lines. These lines are deeper than the TiO band at $\lambda 7600$, suggesting a spectral type earlier than M1. The TiO bandhead at $\lambda 7150$ is present, and is stronger than that at $\lambda 7600$. All the flux-deficit ratios of Wade & Horne (1988) indicate a spectral type earlier than M0.5, for example, $d_v(\lambda 7165)/c_v(\lambda 7500) = d_v(\lambda 7165)/c_v(\lambda 7165) = 0.062$. I also had difficulty in deconvolving the red star from the spectrum (see Chapter 9, BZ UMa). None of the spectra, dwarfs ranging from M0 to M6, worked well. An M0 dwarf did permit the subtraction of the absorption features, particularly the TiO band at $\lambda 7600$, while at the same time distorting the He I $\lambda 7065$ line the least.

But, with the orbital period found in § 4, an M2 dwarf should fit inside the Roche lobe of this star (Patterson 1984). If one finds a CV red star with the wrong spectral type, one should expect to find an anomalously later type, from an evolved red star (see e.g., Friend et al. 1990), not an earlier type. An early-K main sequence red star can be ruled out, as one would clearly be too large for the Roche lobe (Patterson 1984). All this supports the conclusion of GAS77 that the red star in HX Peg is a K-subdwarf, based on a spectrophotometric trace during a deep minimum. They find an $M_V = 7.5 \pm 0.2$ in quiescence. This is similar to an absolute magnitude in R_{KC} of 8.0, which is what HX Peg would have if its red star were an M2 dwarf, given the fraction of the light of the red star (about 23%) at $\lambda 6750$ (see Chapter 9, BZ UMa). Even so, at this absolute magnitude, and assuming a quiescent apparent magnitude of $m_V = 16.6$ (GAS77), this star is in the halo, at 660 ± 60 parsecs. This might explain the novelty of its having a subdwarf red star, even though HX Peg has no detectable proper motion (GGB76).

10.4. Radial Velocities and Orbital Period

I measure radial velocities with the method of Shafter (1983a), in which a positive and a negative Gaussian of specified width and separation are convolved with the H α emission line. The centroid of this convolution is taken to be the radial velocity. This

method has the advantage of being able to ignore erratic low-velocity variations, perhaps coming from poorly-understood gas motions in the accretion disk. Instead, attention is focused on the overall motion of the system, to find the orbital period.

Throughout the first night, the lines were in strong emission, with $I_{\text{peak}}/I_{\text{cont}} \approx 1.8$, similar to the minimum spectrum of GAS77. Strong lines make measuring radial velocities easier, so I observed this CV throughout the night, in order to build up a long time baseline for an orbital period determination. The next night, I continued time-resolved observations, to obtain enough velocities to resolve the phase unambiguously and avoid cycle-count aliasing. (For a general discussion of how to measure CV orbital periods, see Thorstensen & Freed 1985.) The lines were still strong enough to allow velocity measurements with no problem, even though the continuum had brightened considerably during the intervening day, with $I_{\text{peak}}/I_{\text{cont}} \approx 1.6$ at the beginning of this night.

Fig. 10.2 is a Lomb-Scargle periodogram (see Press et al. 1992) of the first 39 H α velocities taken, up to HJD = 2448548.706. About two hours after this, the steadily brightening continuum made velocities difficult to measure, so I stopped using the velocities for orbital period determination here. The measurements used a Gaussian width of 2.8 channels, or 640 km s⁻¹, and a Gaussian separation of 1370 km s⁻¹, which maximized K_{em}/σ . The preferred period is clearly 0.2008 days (4.82 hours), with this peak towering over the other one cycle/day aliases. A “fake” sinusoid test (see Chapter 5) is shown below this. Here, an artificial sinusoid with the same parameters as the orbit is given some random noise (here, $\sigma = 34$ km s⁻¹), and then sampled in time identically to how the orbit was sampled and used to generate a periodogram. The time series sampling is sound, as this “fake” periodogram is nearly identical with the real one. A least-squares fit to a sinusoid (Fig. 10.3) gives the parameters listed in Table 10.2, with errors estimated internally with the likelihood ratio test of Cash (1979). This orbital period is much more likely to belong to a dwarf nova, since all orbital periods known securely for VY Scl stars

are between 3.2 and four hours (Ritter 1990), exactly the period regime where dwarf novæ are rare, for unknown reasons (Shafter, Wheeler, & Cannizzo 1986).

CV emission lines do not reliably trace the motion of the white dwarf: I will not attempt to use them to solve the dynamics of this system, as previous attempts have met with bizarre results (e.g., O'Donoghue et al. 1989). With an orbital period from the emission lines, though, the spectra may be binned in phase to build up S/N, to make possible a radial velocity study using the K I $\lambda 7665$ absorption line. The results appear in Table 10.2. The line was measured using the method of Schneider & Young (1980), in which the line is convolved with the derivative of a Gaussian and this centroid of this convolution is taken as the radial velocity. With a narrow Gaussian, of 640 km s^{-1} FWHM, this should sense the bottom of the V-shaped profile of this absorption line. A full dynamical study will have to await time-resolved photometry, though, to search for eclipses to constrain the orbital inclination. Using the weaker K I $\lambda 7699$ line did not result in a significant fit, but it might in higher S/N spectra, since it is farther from the atmospheric A-band and so may better avoid contamination from it.

10.5. Outburst

Halfway through the second night, at HJD = 2448548.787, I noticed the line had dramatically changed in profile and strength, due to the brightening continuum. These changes were obvious in the raw spectra, as well as in spectra calibrated for relative flux (see Fig. 10.1).

Beginning with this rapid rise, the He I lines disappeared completely. $\text{H}\alpha$, during rapid rise, had a pronounced blue wing, which quickly turned into absorption wings. After the rapid rise, the $\text{H}\alpha$ emission core is still present, weakly. This shows that the high-velocity region of the disk where the wings form quickly became optically thick.

The differences in the radial velocity curve during the entire first night, October 18,

and the radial velocity curve of the first 39 velocities is not significant, as Table 10.2 shows. Fitting a sinusoid to the velocities for all subsequent velocities produces a curve differing in velocity semi-amplitude, zero-offset, and phase (see Table 10.2). Seven points fell substantially off the shifted radial velocity sinusoid, by over 100 km s^{-1} . These were the velocities taken at $\text{HJD} - 2448540 = 8.775, 8.798, 8.833, 8.856, 8.879, 8.890,$ and 9.609 . All seven of these velocities occurred during or after the rapid rise to outburst, and are attributable to either line profile changes or the brightened continuum interfering with radial velocity measurements. If these seven velocities are deleted, the radial velocity curve's fit to a sinusoid improves considerably (see Table 10.2).

Reduction of the velocity semi-amplitude (K_{em}) of the radial velocity curve has been seen in dwarf novæ in outburst before (Robinson, Zhang, & Stover 1986; Hessman 1989). The shift in velocity zero-point (γ_{em}) may not be significant. Such a phase shift during outburst would be novel, though: the zero-epoch of the velocity curve changed, after the rapid rise, with a phase shift of $0.025 \pm 0.005 \text{ days} = 0.125 \pm 0.02 \text{ cycles} = 45 \pm 8^\circ$. Such phase shifts have been blamed on brightness asymmetries or velocity field distortions of the disk (Marsh, Horne, & Shipman 1987), and differences in the brightness profiles of a dwarf nova disk in quiescence and in outburst have been observed (Rutten et al. 1992b). Since the error on the zero-epoch is smaller than 0.016 days, this phase shift is present at a level of 1.6 sigma, or at a confidence level exceeding 87%. This means there is slightly less than a 13% chance that this phase shift is just a statistical fluctuation.

Since the night of the rapid rise was not photometric, one cannot derive reliable fluxes, but instead must be content with equivalent widths (see Fig. 10.4). The average variation in the equivalent widths decreased greatly from quiescence to outburst, the fractional variation having reduced by a factor of three and the standard deviation to a linear fit by a factor of two. This is reminiscent of the behavior of the approximate *B* lightcurve of TW Vir observed by MK90 (see their Fig. 1). It may be from the increased mass-flow

through the disk during outburst masking the bright spot, where the gas stream hits the disk. Even so, the equivalent widths in quiescence do not fit a sinusoid with the orbital period well, to less than 38% confidence, with the ratio of the equivalent width semi-amplitude to the standard deviation of the fit equal to only 0.43.

Importantly, the equivalent widths show a kink, just at the rapid rise, at HJD = 2448548.787 (see Fig. 10.5). The equivalent width variations present in quiescence are reduced throughout the second night, allowing linear fits to the equivalent width curve. If there had been an *S*-wave present, it disappeared completely. If a line is fit to all 28 equivalent widths of this second night, the standard deviation of the fit is 1.39 Å. If two different lines are fit, to the first 19 and to the last nine equivalent widths, the standard deviation of these fits are 1.34 and 0.3 Å, respectively, with a significant change in slope at this kink.

About 2.2 hours before the kink (HJD = 2448548.695), a blue emission wing became noticeable on H α . This wing protruded to about 1500 km s⁻¹ from the line center, and it shows up in the average spectrum of the rapid rise (see Fig. 10.1). Soon after the rapid rise, absorption wings developed about H α , with cores ± 750 km s⁻¹ from the line center. These remained for the rest of the night and for the next night, and are also noticeable in Fig. 10.1. In contrast to MK90, the H α emission line did not become appreciably narrower, until immediately after the outburst, when it went from 1100 km s⁻¹ to 800 km s⁻¹ FWHM. This might be an artifact of the low spectral resolution, as it was really the only significant change measurable. H α never completely disappeared, either: the closest it ever came to this was in the one spectrum immediately after the blue wing disappeared and before the absorption wings became recognizable. This was about 100 minutes after the rapid rise (HJD = 2448548.856). The center of the line went into absorption extending below the continuum level, at -650 km s⁻¹ relative to the rest frame, but still with emission wings -400 and +530 km s⁻¹ to either side of it.

The behavior of the continuum slope in F_λ (see Fig. 10.6) contrasts with that of

TW Vir (MK90), which was fairly constant until the rapid rise, and then kinked to blue. To measure the continuum slope, I fit a line by eye on a log-log plot of a spectrum at $\lambda\lambda 6400$ and 6800 . These points were chosen to avoid $H\alpha$, telluric absorption, and strong night sky emission lines, which can leave a ripple even after a precise digital sky subtraction. In the red, this does not leave one with much, so this approximate method probably does not lose much accuracy compared to a rigorous power law fit, which would involve pruning out the $H\alpha$ emission line, an arbitrary process in itself, or with a linear fit, as used by MK90.

Nevertheless, the continuum slope in my spectra was bluest on the night of the rapid rise. It returned to where it had been during the beginning of the night before, so that during this last night, the outburst might have already been in decline, and the maximum was missed. Curiously, during the night before the outburst, the continuum slope reddened suddenly and then became blue. Could this have been the onset of the warm phase? If this were solely due to an atmospheric refraction effect through the unrotated slit, one might expect to see it the next night, too. It was not, even though the hour angles (H) the observations swept through were similar, from $H = -3:24$ to $+3:53$ hours on the first night, and from $H = -3:38$ to $+3:48$ hours on the second night. There is also no obvious correlation between equivalent widths and continuum slopes, on the first night, however, except in for the sudden decrease in both on the first night (see Fig. 10.7).

Fig. 10.8 is the same as Fig. 10.6, on an expanded scale, to show the behavior of the continuum slope on the night of the outburst. Just at the rapid rise, the continuum slope suddenly became blue, and then red. This wiggle might suggest a sudden heating and cooling, and comes from a blue wing suddenly emerging from the $H\alpha$ line, and then disappearing.

10.6. Discussion

Overall, these observations resemble those of MK90, in that a dwarf nova outburst

was vividly caught showing a rapid rise from a warm phase to a hot phase. Both showed a gradual brightening of the continuum before the outburst, and this had also been seen by Clarke, Capel, & Bowyer (1984) and Kaitchuck, Mansperger, & Hantzios (1988). Such a brightening is consistent with the theory of warm and hot phases of the dwarf nova outburst (Mineshige 1988), originally intended to explain the well-known UV delay of dwarf nova outbursts (e.g., Hassal et al. 1983) within the context of the disk instability model.

There are differences, however. The observed kink in the H α equivalent widths contrasts with the smooth transition of the line fluxes of MK90. The continuum slope of MK90 showed an abrupt transition at the rapid rise, whereas mine also showed a sudden jump in an already blue continuum. This slope may also have become bluer after the rapid rise, but daylight forced an end of that observing session before it could be confirmed.

Two important timescales to constrain are the time between the onset of the warm phase and the onset of the hot phase, and the time between the onset of the hot phase and maximum light. I take the time of the kink in the equivalent width curve as the onset of the hot phase. If the drop and rise in the equivalent width curve seen shortly after the beginning of the first night is the onset of the warm phase, I find an impressively precise interval of 25.65 hours. The models of Mineshige (1988) and the observations of MK90 suggest a timescale of about 24 hours, tantalizingly close to this. The onset of the warm phase has never been seen before, though, so caution is advisable here, especially since care should always be taken whenever dealing with any 24-hour timescale. This is the diurnal timescale, after all, and since one cannot observe in the daytime, the diurnal timescale will be imposed onto the data, by the convolution theorem (see Press et al. 1992). If the onset of the warm phase was missed in the intervening daytime, a lower limit of at least 7.2 hours can be set, by the beginning of observations during the second night.

A measurement of the interval between the onset of the hot phase and maximum light is impeded by not having observed HX Peg at maximum light: at the end of the

second night, it was still brightening, and at the beginning of the third night, it was already in decline. These times may be used to constrain this interval, however, to between 4.4 and 21.7 hours. This longer timescale is also consistent with the models of Mineshige and the observations of Mansperger and Kaitchuck.

Detailed modeling is outside the scope of this work, however, and I must express some skepticism toward the good fits found so far. They involve five adjustable parameters, plus system parameters such as stellar masses, radii, and inclinations that are hard to measure even in the most careful analyses (e.g., Wade & Horne 1988), plus also assumptions known to be incorrect, such as that an accretion disk spectrum can be calculated with a stellar atmospheres code applied to summed disk annuli (Wade 1988). Nevertheless, the overall behavior is consistent with the models and with previous observations, and although my spectral resolution was not as good, the red spectral coverage allowed the red star to be seen and fundamentally new observations to be made.

The O I $\lambda 7773$ quintuplet probably forms in the accretion disk, since it is sensitive to CV outburst state (Friend et al. 1988), much as the higher Balmer lines are (e.g., Szkody, Piché, & Feinswog 1990). In the Sun, this line forms at the boundary between the chromosphere and the photosphere, as shown by the Solar flash spectrum (Bray & Loughhead 1974). This might explain its sensitivity to surface gravity: it has long been used as a luminosity-class indicator (Keenan & Hynek 1950), especially for supergiants, and has been used over a wide range of spectral types, from B to K (Thomas, Morton, & Murdin 1979). Its sensitivity to CV outburst state might be explained by accretion disks becoming optically and geometrically thick during outburst (Smak 1992). There is some evidence it forms in the outer disk (Marsh 1990), at least for one quiescent dwarf nova. Interestingly, O I $\lambda 7773$ was in absorption during the warm phase, before the rapid rise to outburst. If this feature really does form in the outer disk, this is consistent with a brightening in the outer disk at in the early stages of the outburst. This outburst may

therefore have started in the outer disk and moved inward.

The CH absorption feature at $\lambda\lambda 4290 - 4314$, widely used as a spectral type indicator for G stars and called the G-band, was seen in absorption by GGB76. This is curious, as the Balmer lines in the same spectra were in shallow, broad absorption, usually as they are at maximum, the least likely time to see spectral features from the red star. The present paper has shown this star can vary in brightness rapidly, so I think it likely that HX Peg was in a high state when the spectra of GGB76 were obtained, and that the G-band absorption came from the disk. More evidence of this comes from their noting that their G-band was variable in profile. If this G-band really does form in the accretion disk, this may provide a constraint on temperature and metallicity for disk models.

This is also the first case of a CV with a red star identified as being a subdwarf K, interesting since this CV is probably in the halo. A search for halo CVs has been undertaken by Howell & Szkody (1990), and although it has turned up many interesting objects, none so far have shown a red star that is a cool subdwarf. I recommend this CV for inclusion as an AAVSO program star, since a lightcurve more detailed than the HCO patrol plates can provide would be of interest, especially since it is now known to be rapidly variable over several magnitudes. A dwarf nova which goes from quiescence to decline in two days is unusually rapid (Szkody & Mattei 1984). Might this be related to metallicity?

Table 10.1. H α Emission Radial Velocities

HJD ^a	V	HJD ^a	V	HJD ^a	V	HJD ^a	V
(km s ⁻¹)	(km s ⁻¹)	(km s ⁻¹)	(km s ⁻¹)	(km s ⁻¹)	(km s ⁻¹)	(km s ⁻¹)	(km s ⁻¹)
HX Peg (1991 October) ^b							
8547.603	54	8547.783	134	8548.638	-33	8548.821	92
8547.614	18	8547.795	124	8548.649	-88	8548.833	-186
8547.625	7	8547.806	111	8548.660	-63	8548.844	72
8547.637	-57	8547.817	3	8548.672	-137	8548.856	195
8547.648	-51	8547.828	-11	8548.683	-116	8548.867	-80
8547.660	-42	8547.840	-30	8548.695	-20	8548.879	-236
8547.670	-66	8547.851	-105	8548.706	16	8548.890	319
8547.682	-84	8547.862	-142	8548.718	-15	8549.609	242
8547.693	-102	8547.873	-66	8548.729	45	8549.622	143
8547.704	-2	8547.884	-114	8548.741	-17	8549.634	166
8547.715	68	8547.895	-119	8548.752	48	8549.644	110
8547.727	48	8548.581	158	8548.764	94	8549.656	31
8547.738	140	8548.592	75	8548.775	-9	8549.667	-57
8547.750	170	8548.604	125	8548.787	124		
8547.760	128	8548.615	77	8548.798	330		
8547.772	102	8548.627	26	8548.810	126		

^a Heliocentric Julian Date of mid-integration, minus 2 440 000

^b Shafter (1983a) algorithm, Gaussian separation 1370 km s⁻¹

Table 10.2. HX Peg – Derived Orbital Parameters^a

Object	P_{orb} (days)	K_{em} (km s ⁻¹)	γ_{em} (km s ⁻¹)	T_0 (HJD – 2440000)	σ (km s ⁻¹)
1991 October ^b					
H α					
October 18 only	(0.2008)	125 ± 10	27 ± 7	8548.721 ± 0.004	34
Before rapid rise ^c	0.2008 ± 0.0005	125 ± 8	29 ± 6	8548.721 ± 0.002	34
After rapid rise ^d	(0.2008)	81 ± 1	58 ± 30	8548.746 ± 0.016	138
After, points deleted	(0.2008)	109 ± 20	43 ± 11	8548.747 ± 0.004	42
K I λ 7665 ^e	(0.2008)	214 ± 78 – 188 ± 55		8548.64 ± 0.01	141

^a Velocities fit to $V(t) = \gamma_{em} + K_{em} \sin[2\pi(t - T_0)/P_{orb}]$; all errors are to 68% confidence (see Thorstensen & Freed 1985)

^b Measured with Shafter (1983a) algorithm, Gaussian separation 1370 km s⁻¹

^c First 39 velocities

^d Velocities 40 – 61

^e Fit to absorption line, Schneider-Young (1980) algorithm, Gaussian width 640 km s⁻¹

Figure 10.1.

Outburst spectra of HX Peg. All spectra are normalized to $\lambda 7500$. The bottom trace is offset downward by 0.25 flux units, and the third, fourth, and fifth from bottom are offset upwards by 0.25, 0.5, and 1.0 units, respectively, for clarity. Wrinkles from imperfect removal of the telluric A band near $\lambda 7600$ are marked by an Earth symbol.

The bottom trace is from 1991 October 18 UT, with this dwarf nova in quiescence. Progressing upward are the next nights' spectra, with UTs of mid-exposure shown. The trace at 3:52 UT, marked "Rapid Rise," represents a drastic and sudden change in the spectrum, over about 90 minutes. Before this, it had been similar to the spectrum before it, and afterward, it resembled the spectrum after it. Note O I $\lambda 7773$ going in broad absorption, during the gradual brightening before the rapid rise.

HX Peg - Spectra of rise to outburst

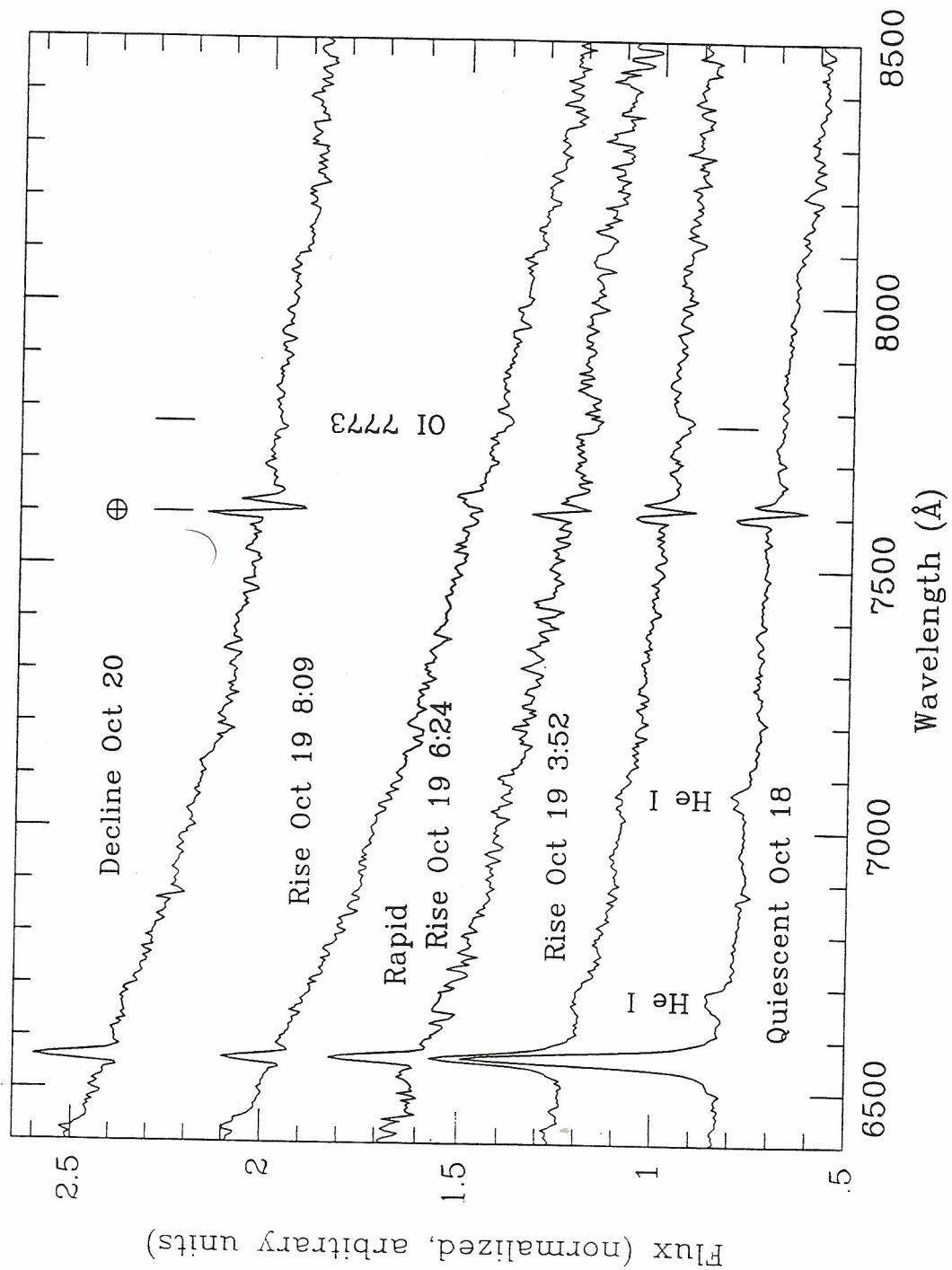


Figure 10.2.

(Top)

Periodogram of the first 39 H α radial velocities, measured by double-Gaussian algorithm (Shafter 1983a) with a separation of 1370 km s⁻¹. The periodicity at 0.2009 days (4.82 hours) is obvious, the peak corresponding to it at 4.98 cycles / day towering over the 1 cycle/day aliases.

(Bottom)

Identically-sampled artificial sinusoid with the derived orbital parameters and random noise ($\sigma = 38$ km s⁻¹) added. The similarity between real and fake periodograms shows that the sampling of the time series was nearly optimal. This diminishes spurious alias peaks, even the unavoidable 1 cycle/day aliases due to daylight.

HX Peg - Periodogram of H α Radial Velocities

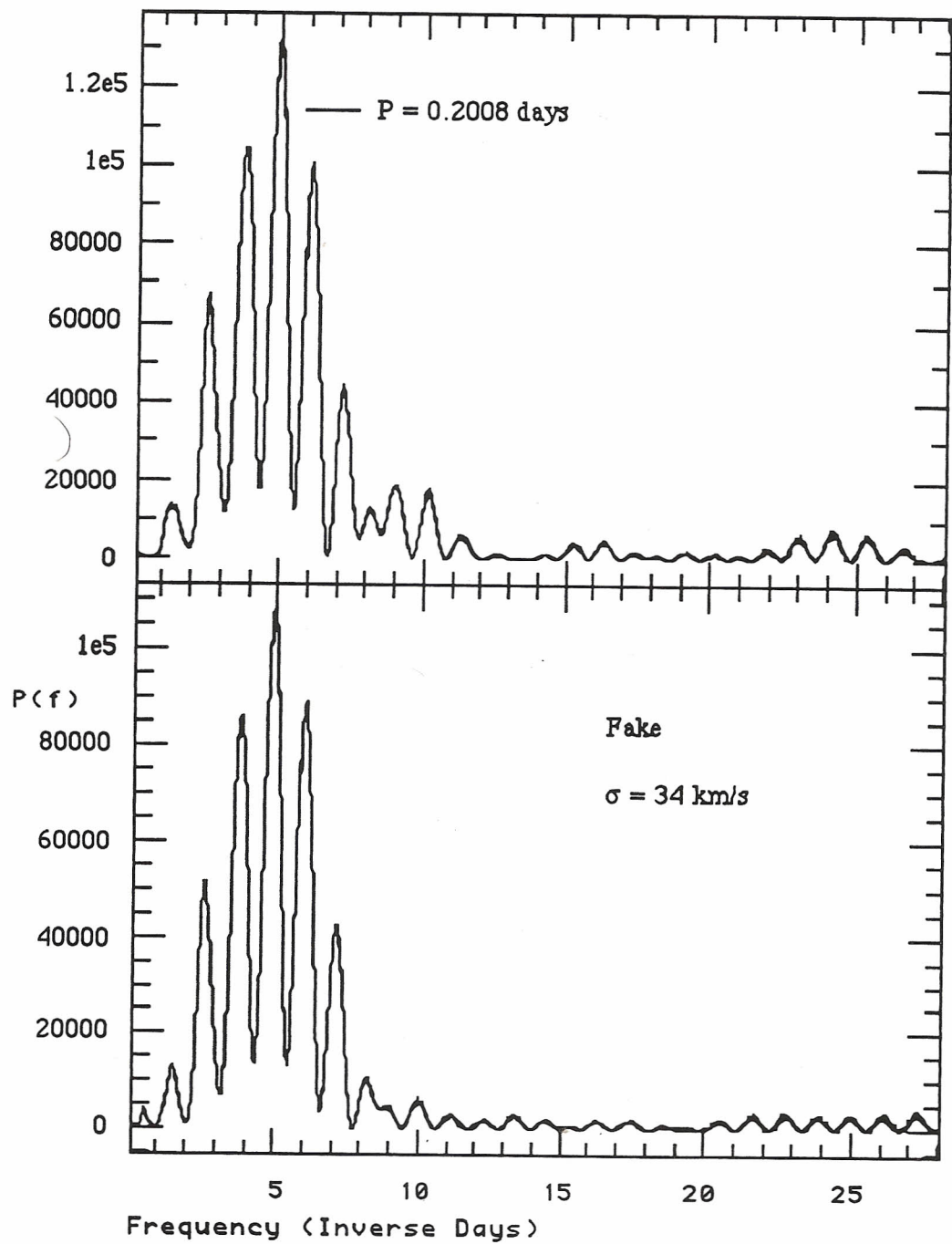


Figure 10.3.

The $H\alpha$ radial velocities for HX Peg, plotted about the orbital phase. All points are plotted twice, for clarity.

HX Peg - H α Radial Velocities

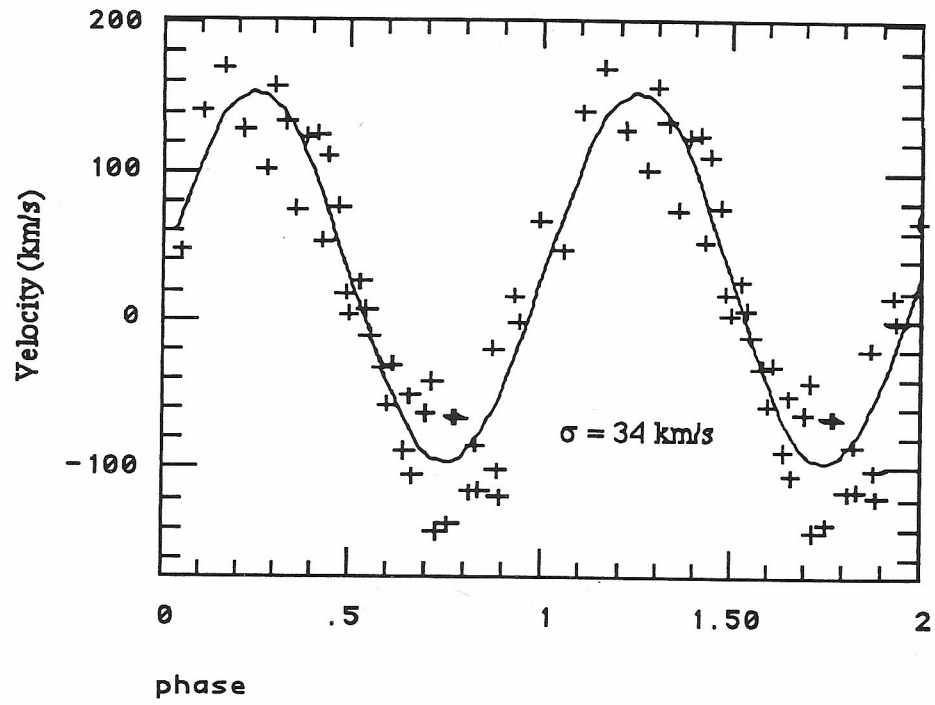


Figure 10.4.

Equivalent widths of $H\alpha$ plotted against $MHJD = HJD - 2440000$. The observations on 1991 October 18, 19, and 20 UT readily indicate quiescence, rise to outburst, and outburst maximum.

HX Peg outburst - H alpha equivalent widths

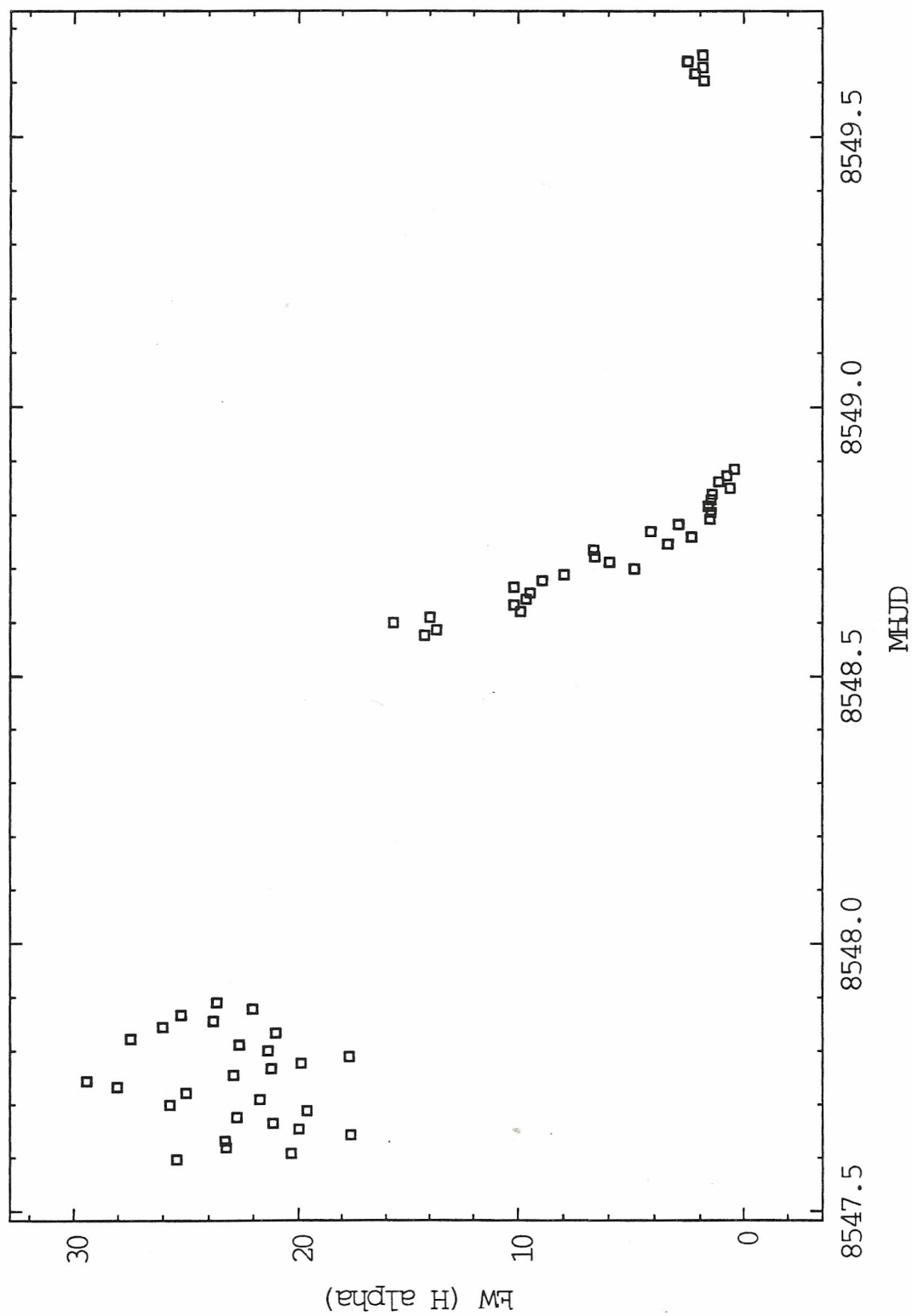


Figure 10.5.

Same as Fig. 10.4, with the night of 1991 October 19 UT on an expanded time scale. Note the kink in the equivalent width curve near $\text{MHJD} = 8548.8$, corresponding to 6:24 UT . It was just then that I noticed the rapid rise to outburst.

HX Peg outburst - H alpha equivalent widths

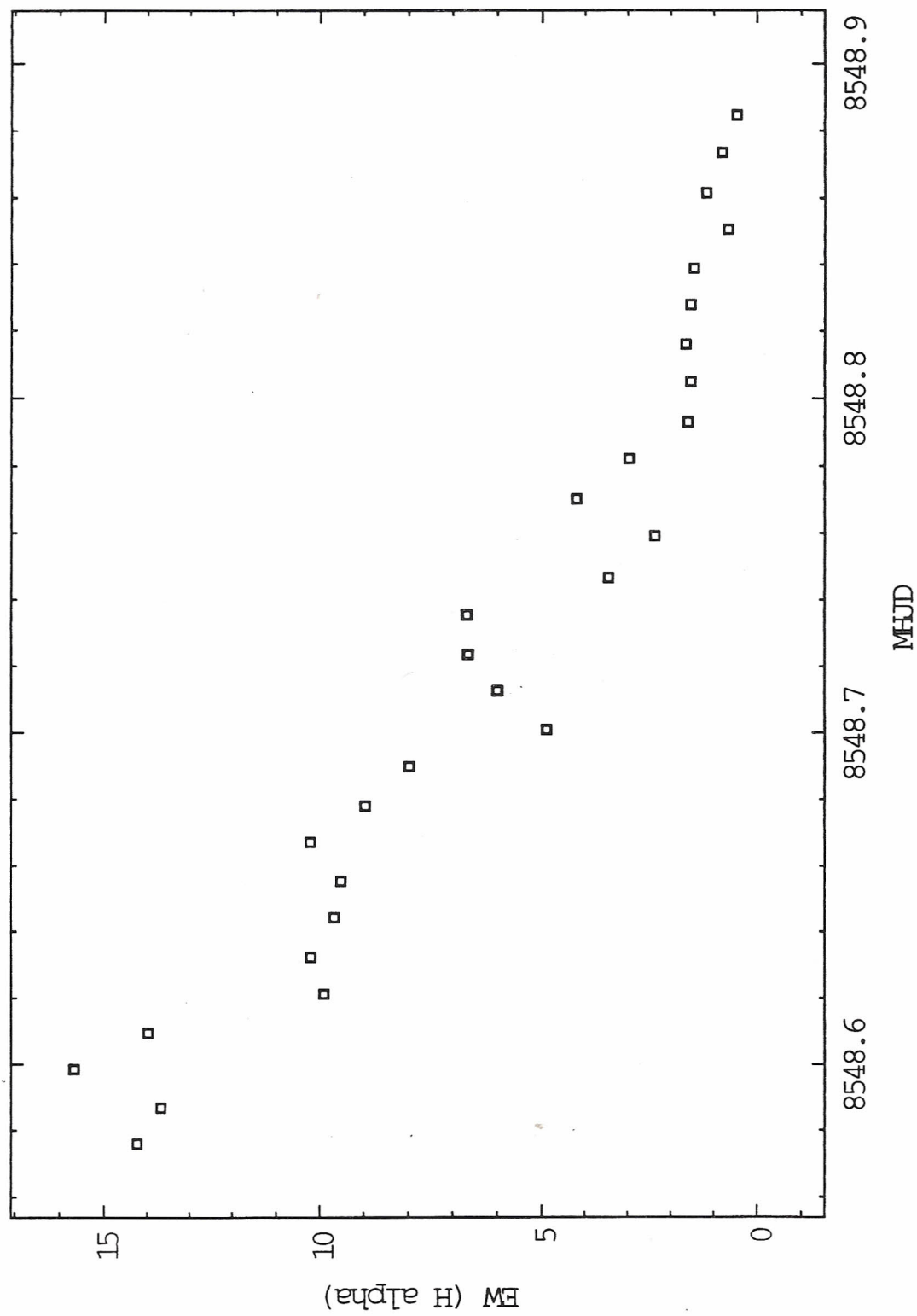


Figure 10.6.

Continuum slope, measured by index α by fitting a power law $F_\lambda = k \lambda^{-\alpha}$ to the continuum at $\lambda\lambda 6400$ and 6800 , plotted against MHJD.

HX Peg power law continuum fits (6400 - 6800 Angstroms)

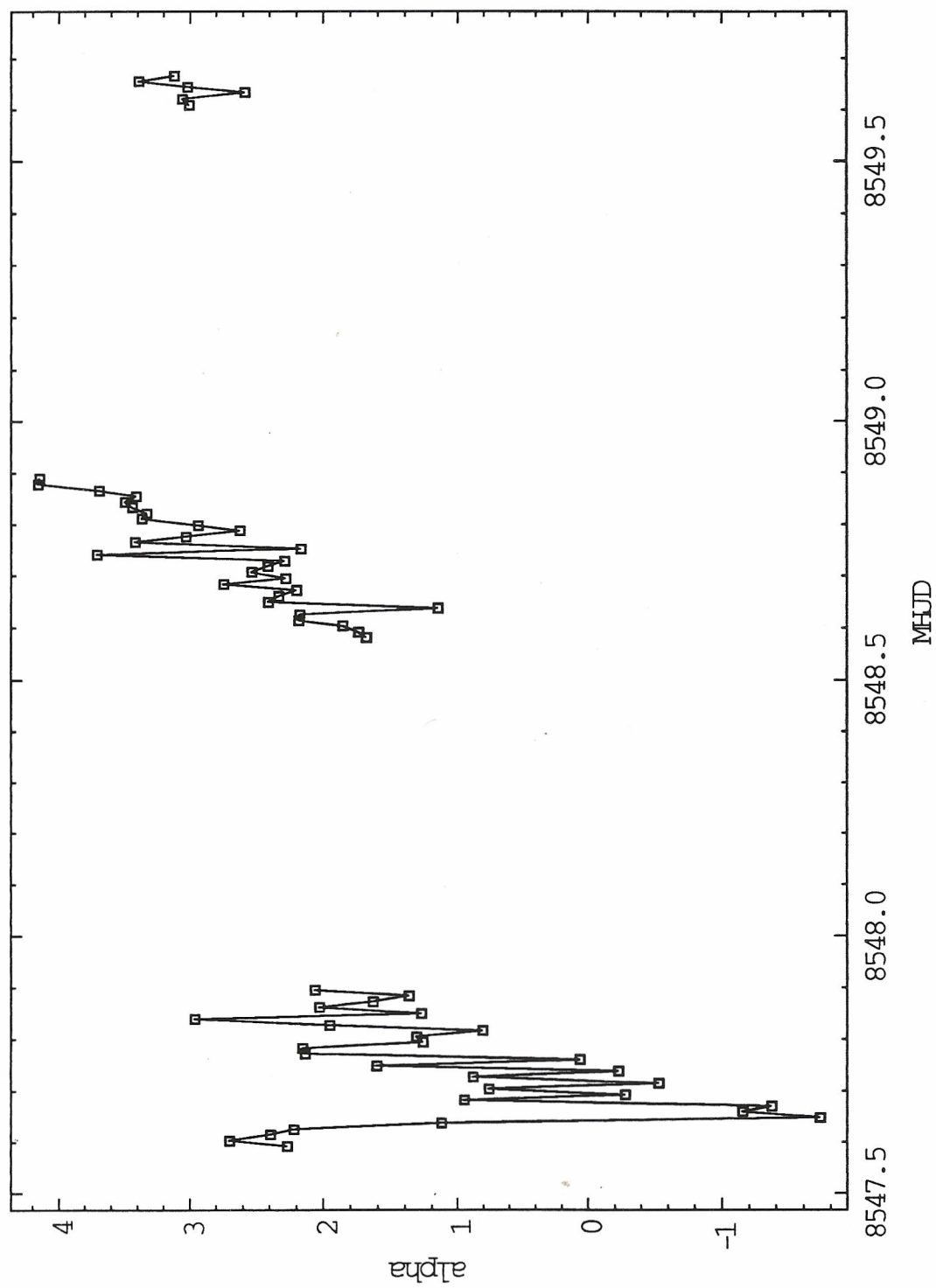


Figure 10.7.

Equivalent width of $H\alpha$ (above) and continuum slope, as in Fig. 10.6, for the first night. No obvious correlation is evident, except perhaps the drop in both during the first night.

HX Peg EWs and continuum fits

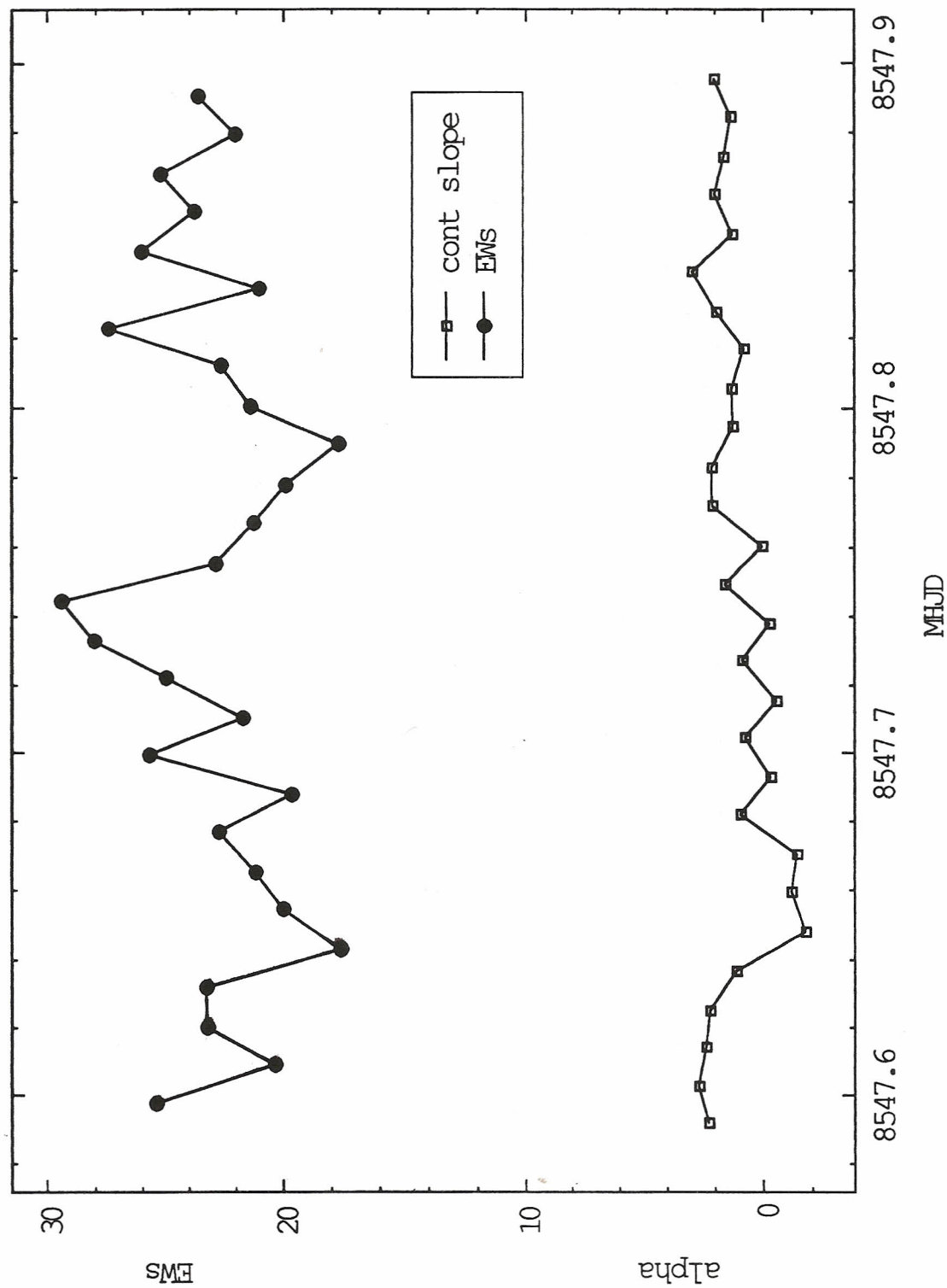
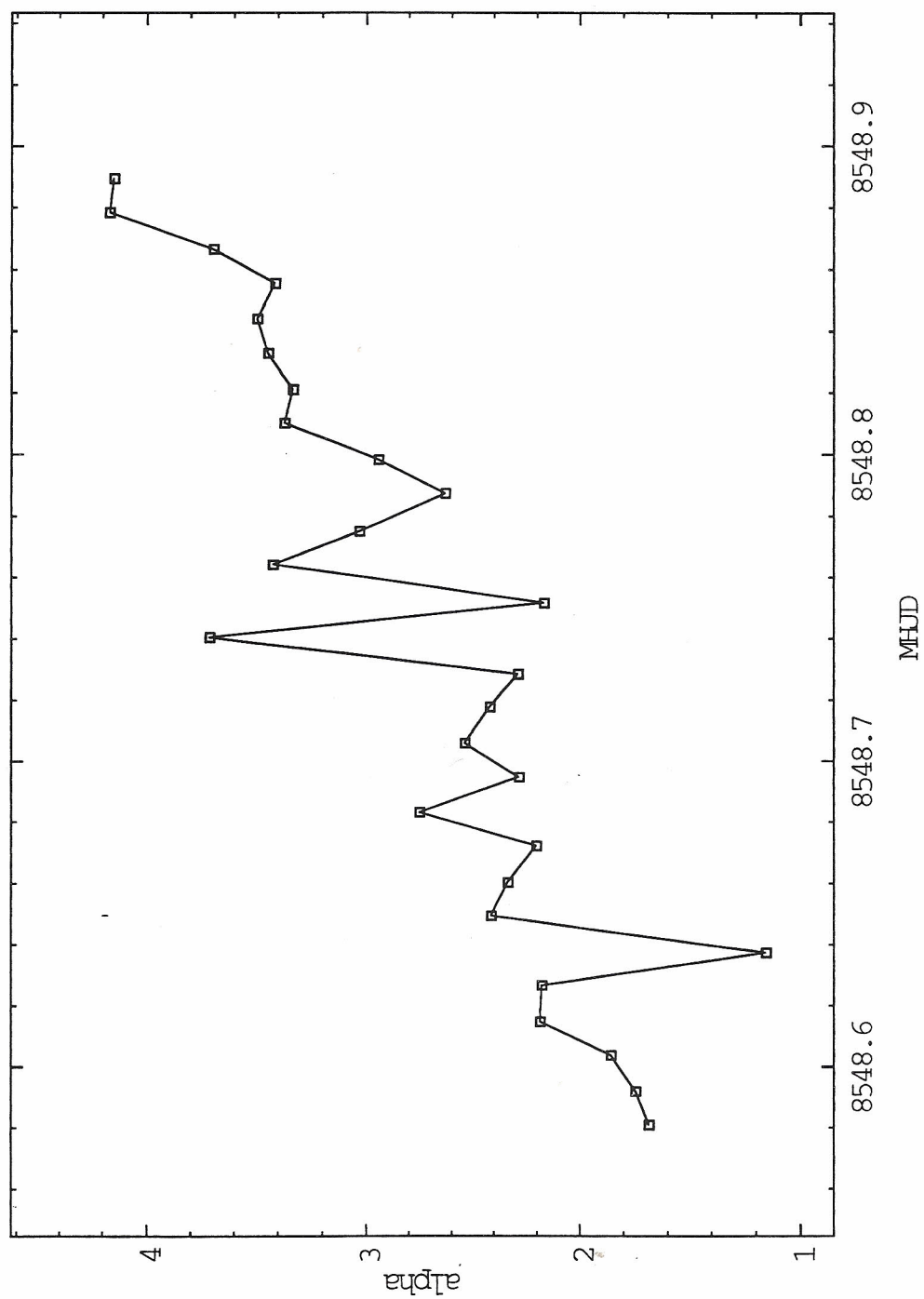


Figure 10.8.

Same as Fig. 10.6, with the night of 1991 October 19 UT on an expanded time scale. There is also a kink in the curve near $\text{MHJD} = 8548.8$, corresponding to 6:24 UT, the rapid rise to outburst.

HX Peg power law continuum fits (6400 - 6800 Angstroms)



Appendix A

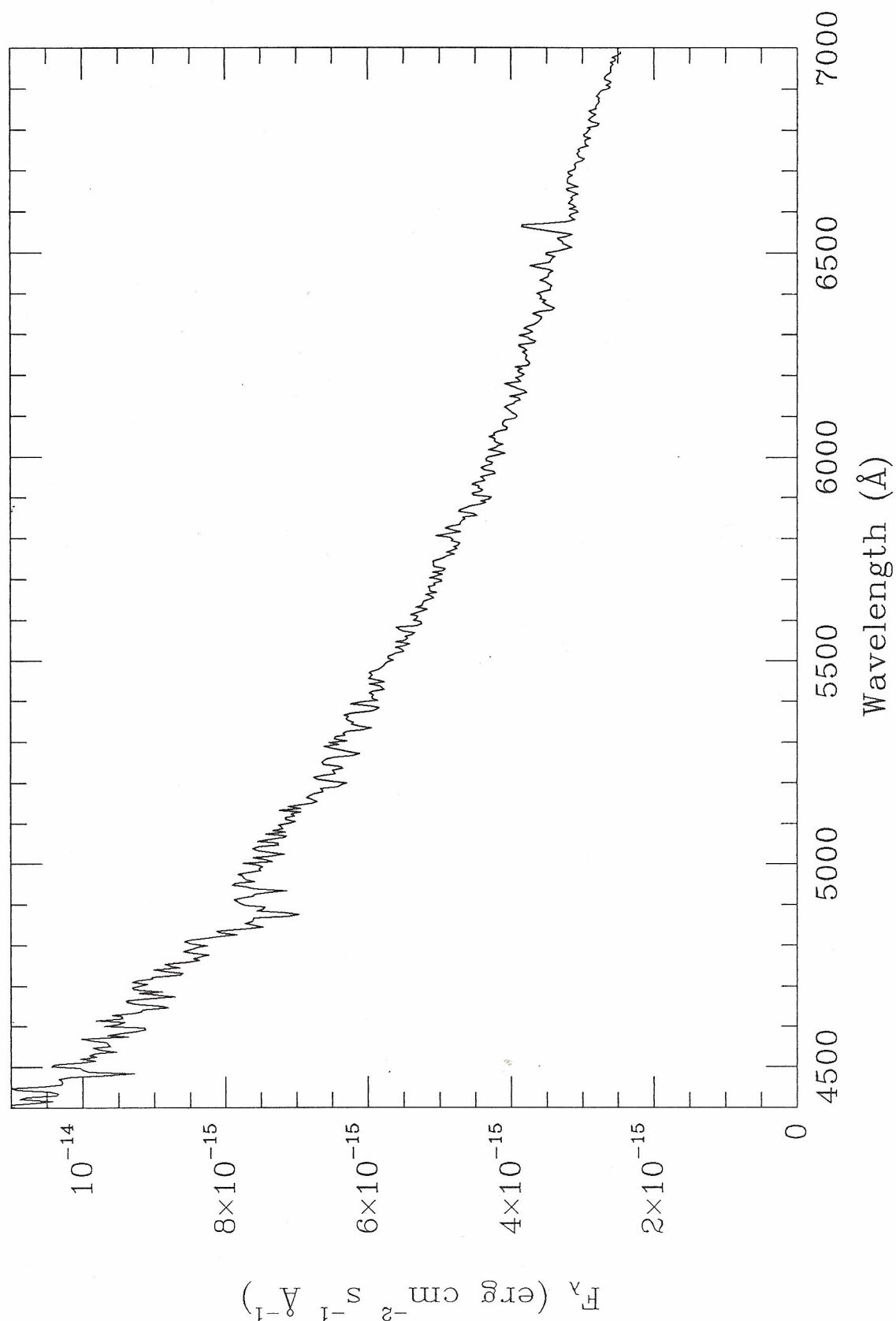
Cataclysmic Variable Spectra

presented in order of Right Ascension

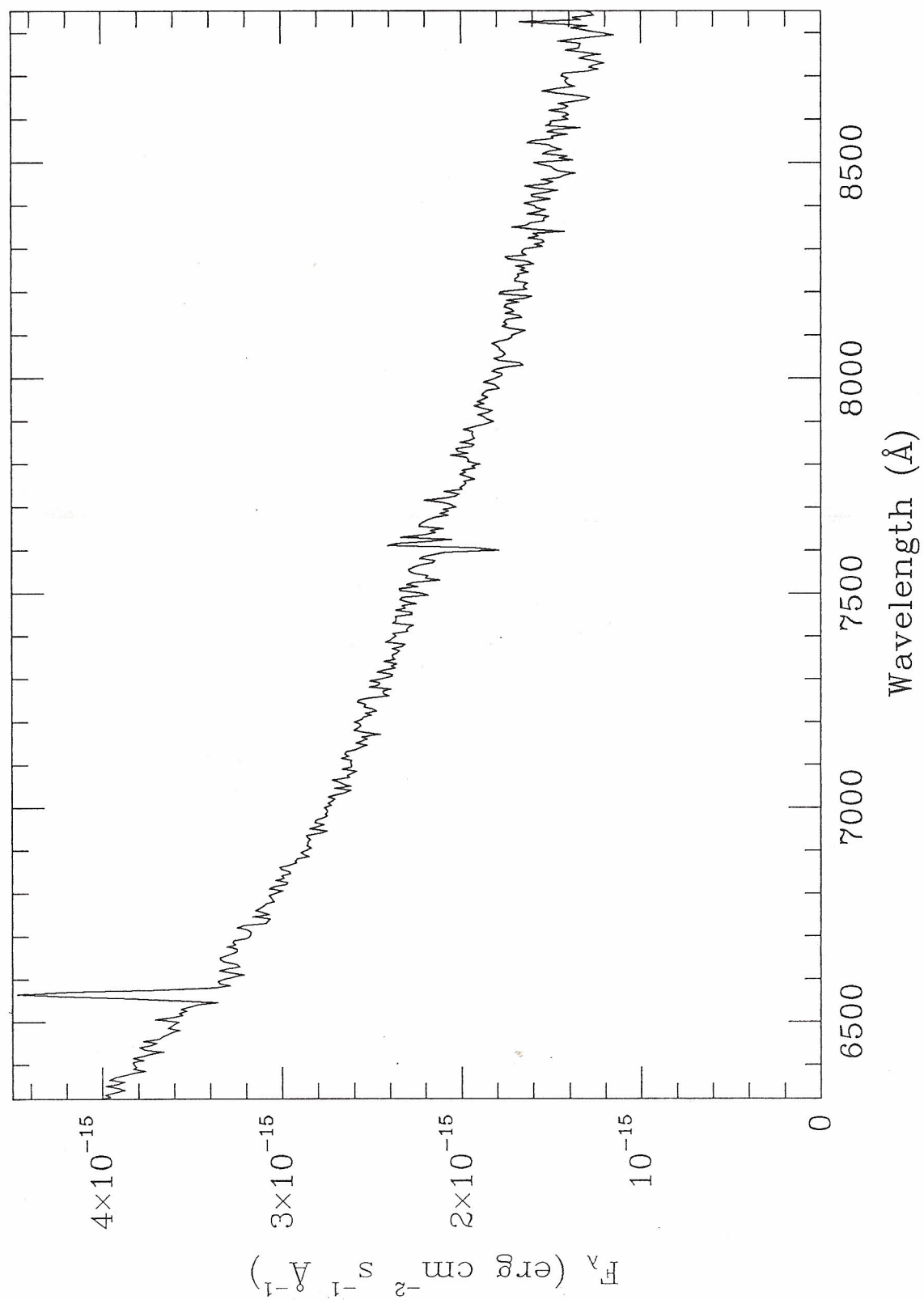
All spectra are in F_λ , are sky-subtracted, and have the telluric absorption bands divided out:
see Chapter 2.

For descriptions of the individual objects, see Chapter 6.

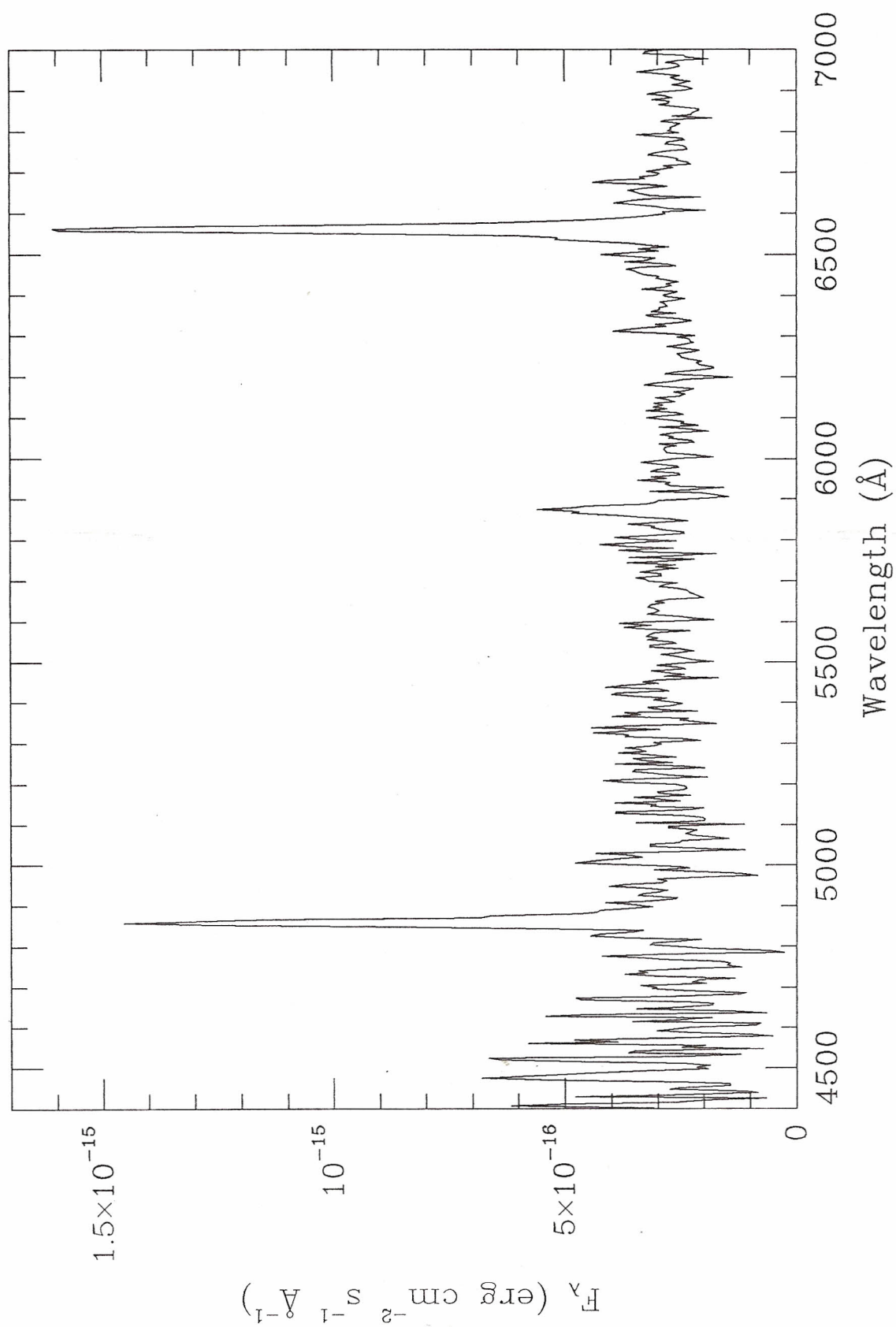
PG 0917+342 - 1990 April 28 04:58 UT



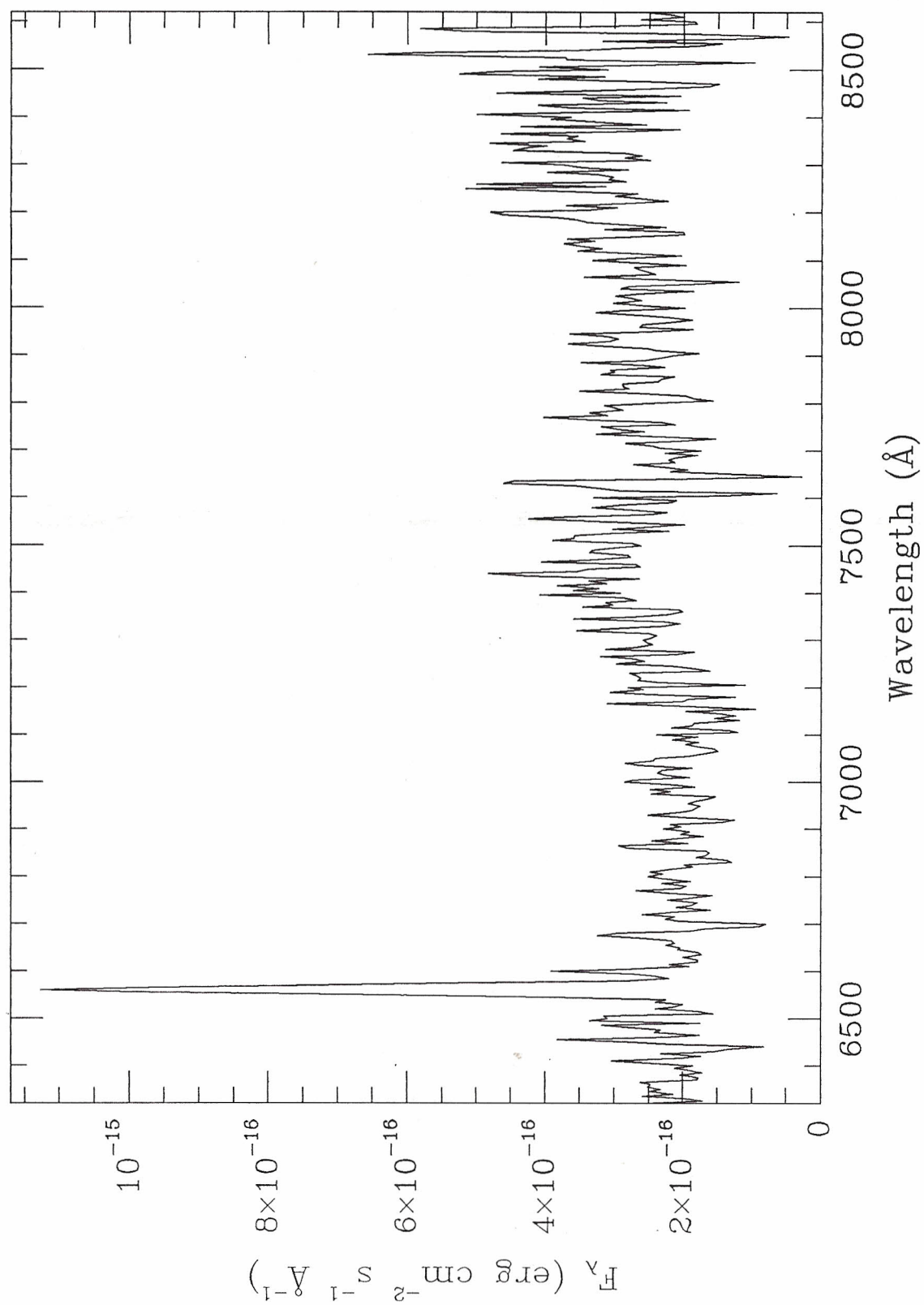
PG 0917+342 - 1990 May 5 05:36 UT



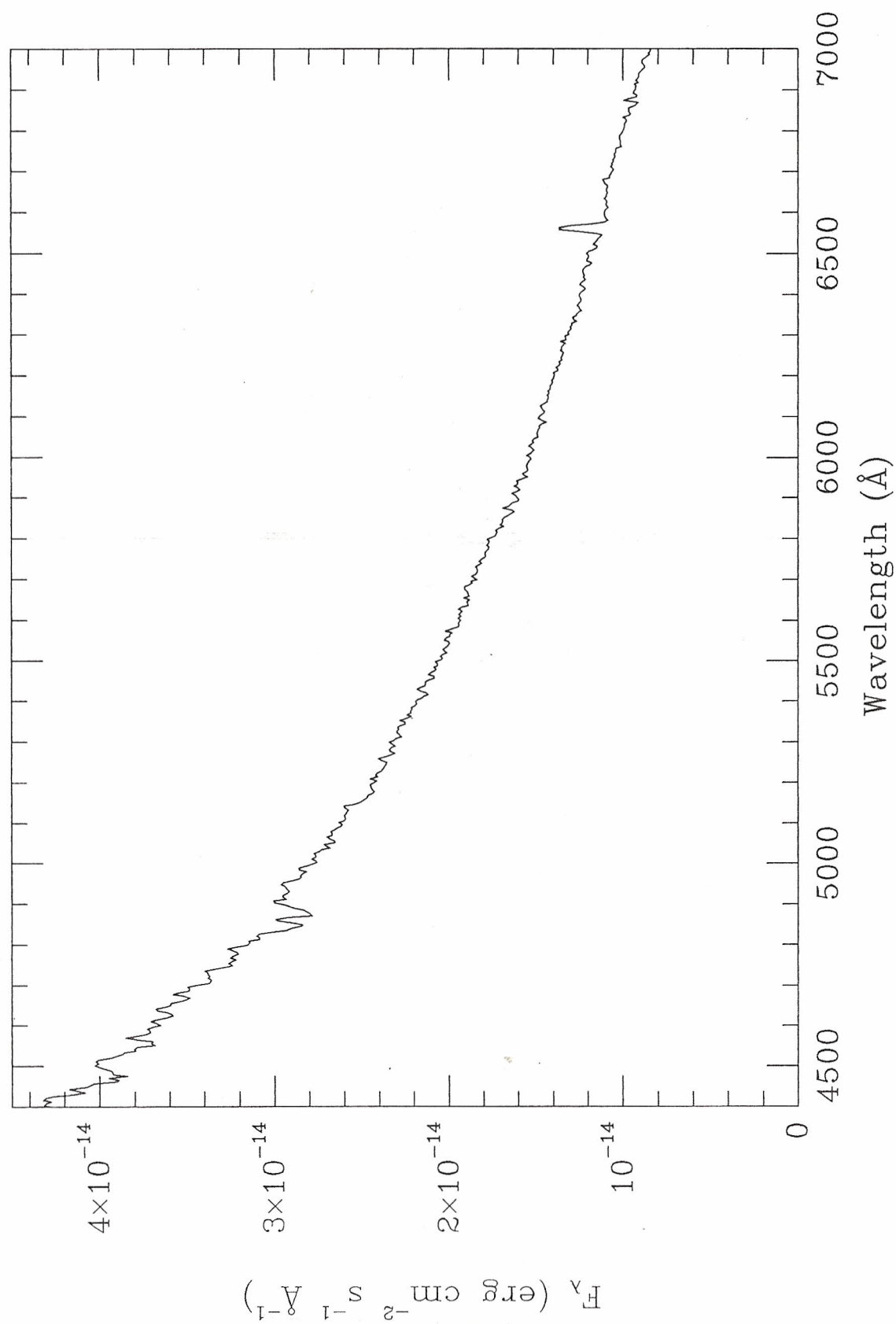
PG 0935+075 - 1990 April 27 05:07 UT



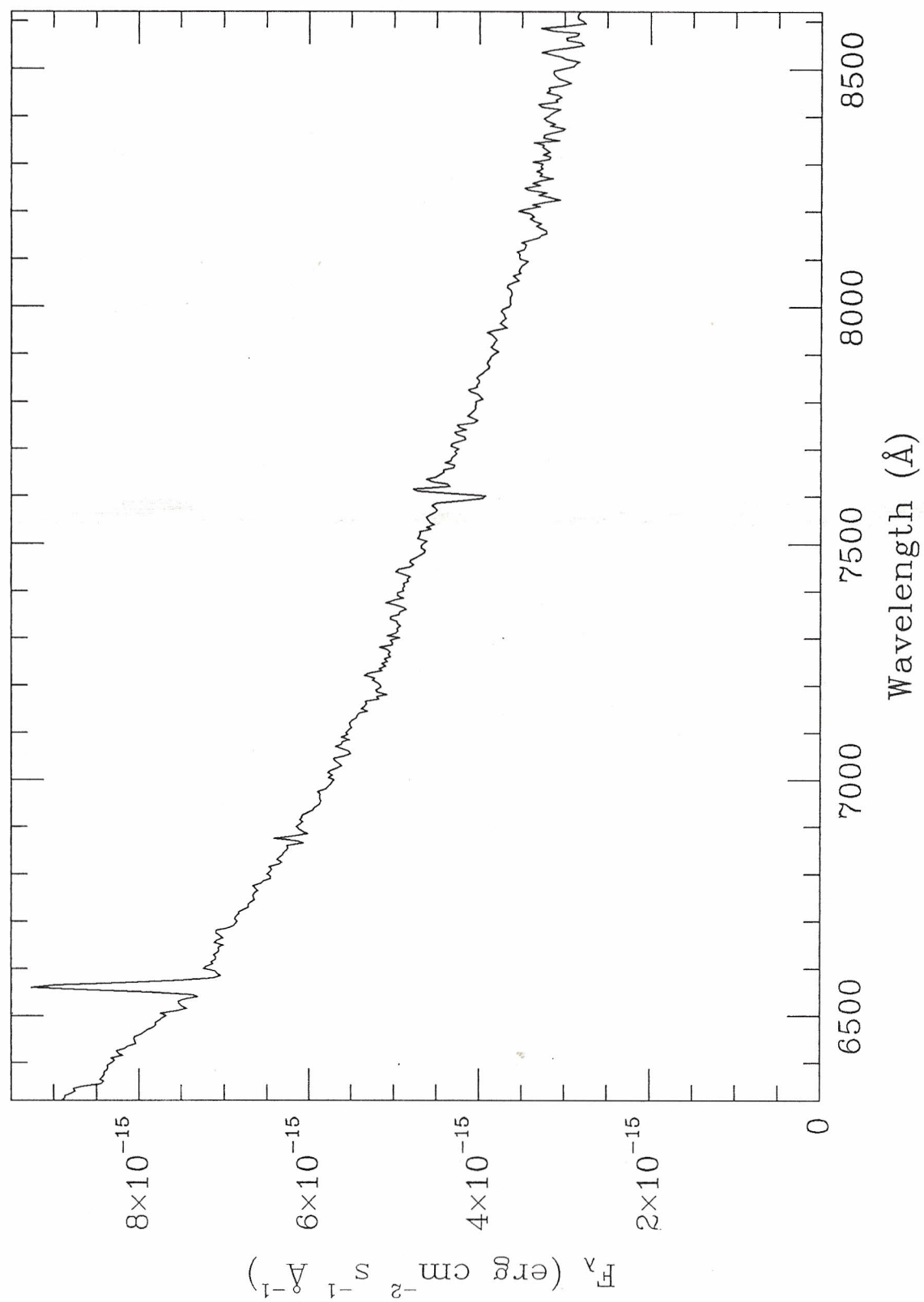
PG 0935+075 - 1990 May 6 3:40 UT



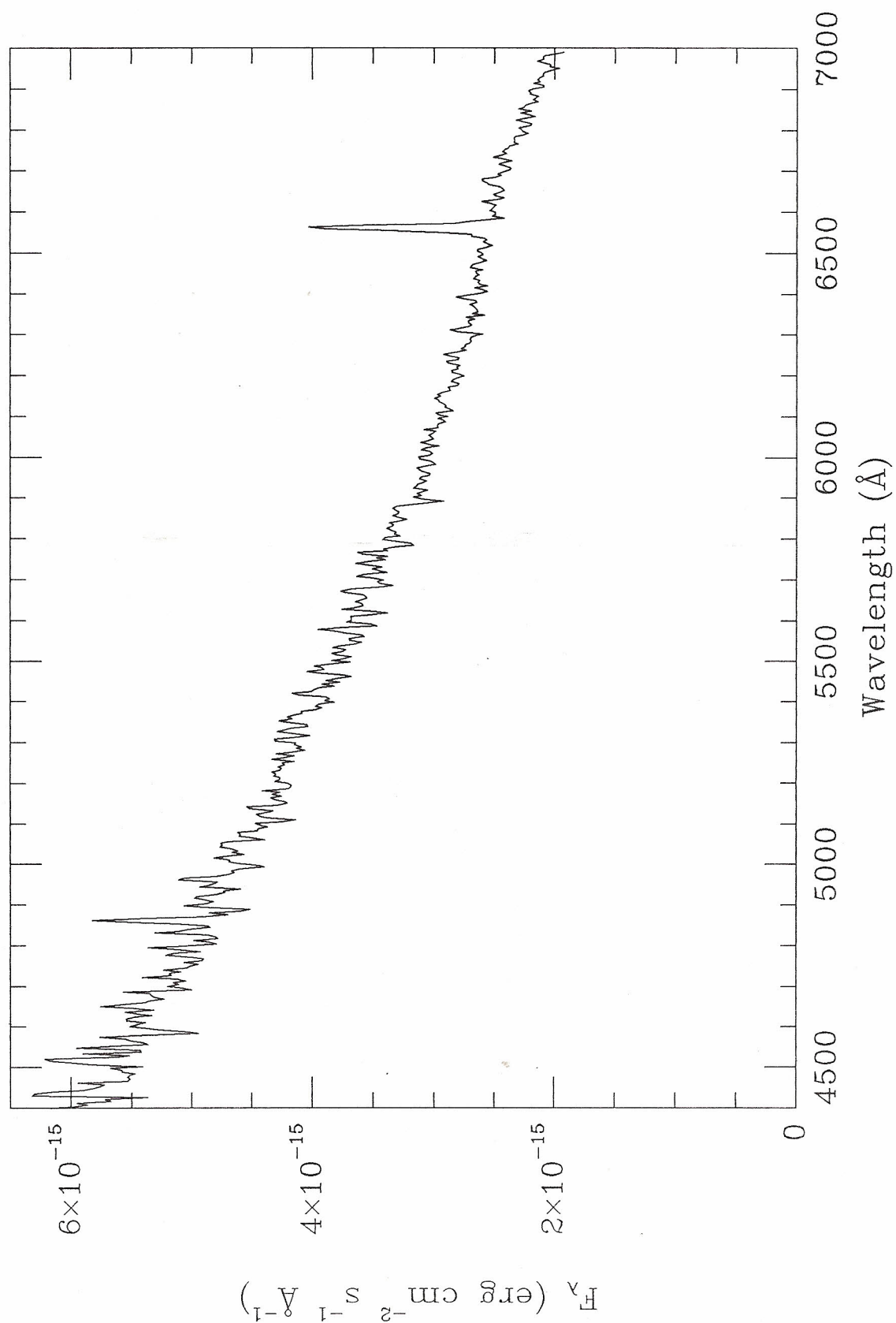
PG 0943+521 - 1990 April 27 05:29 UT



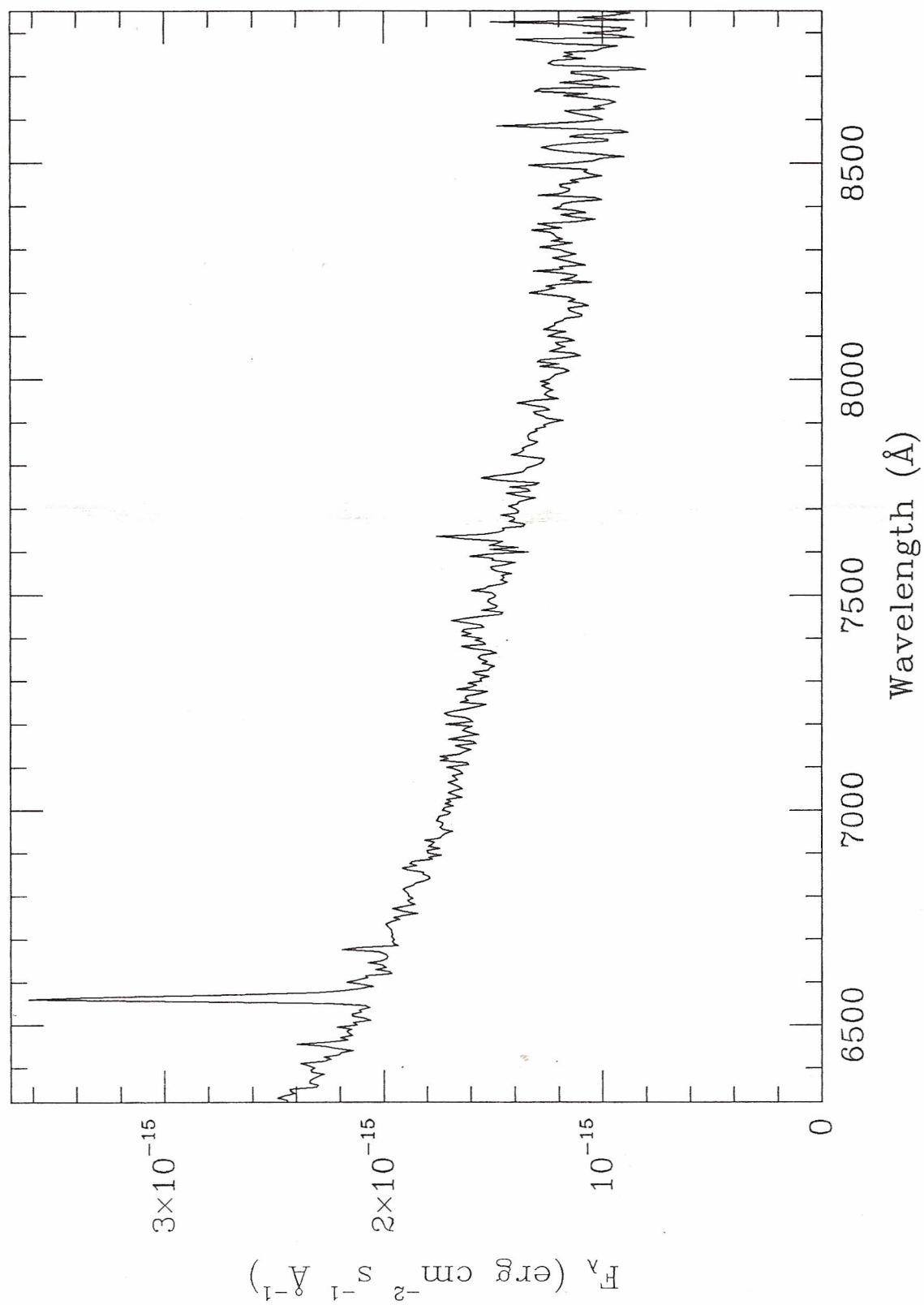
PG 0943+521 - 1990 May 6 4:56 UT



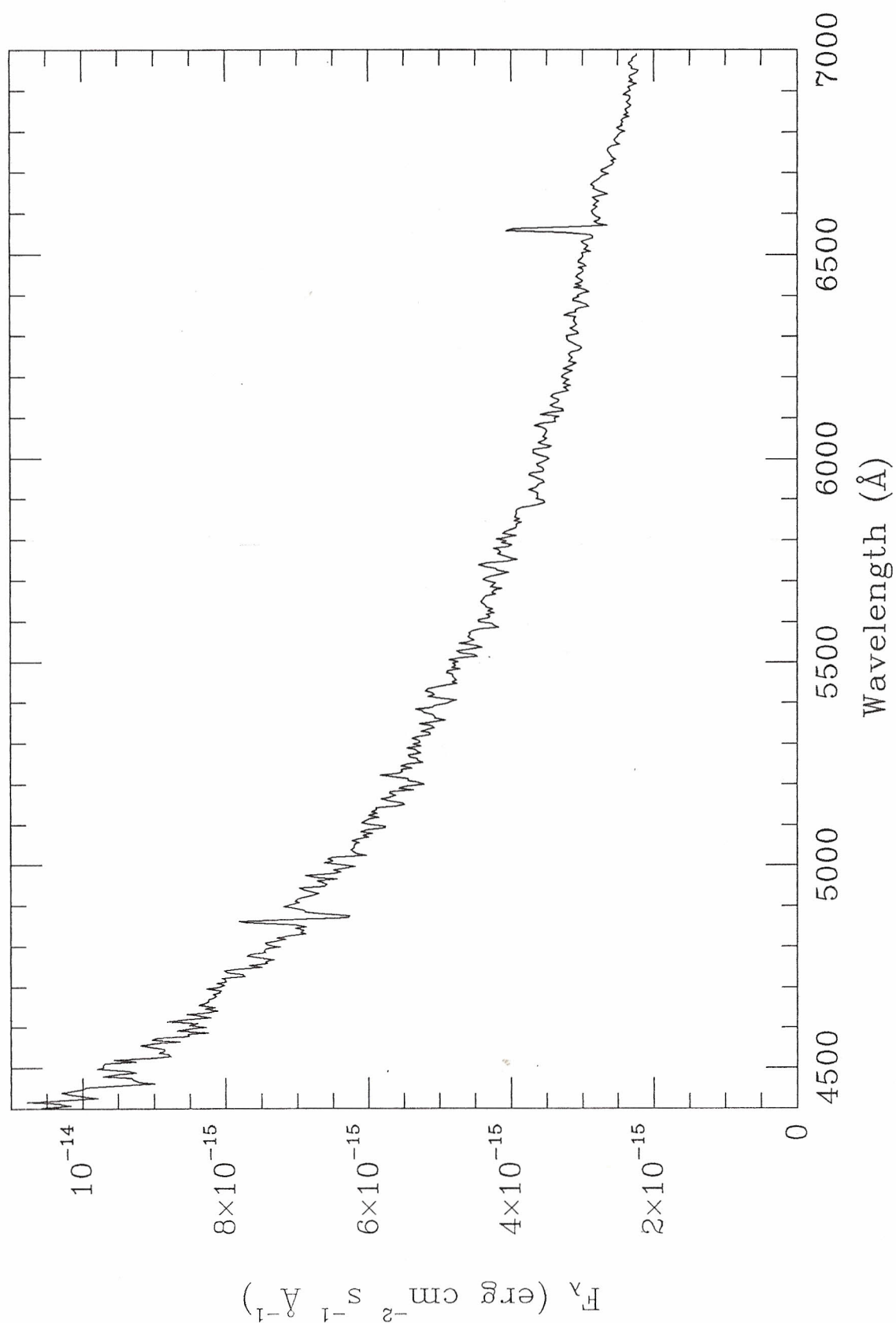
PG 1000+667 - 1990 April 28 05:40 UT



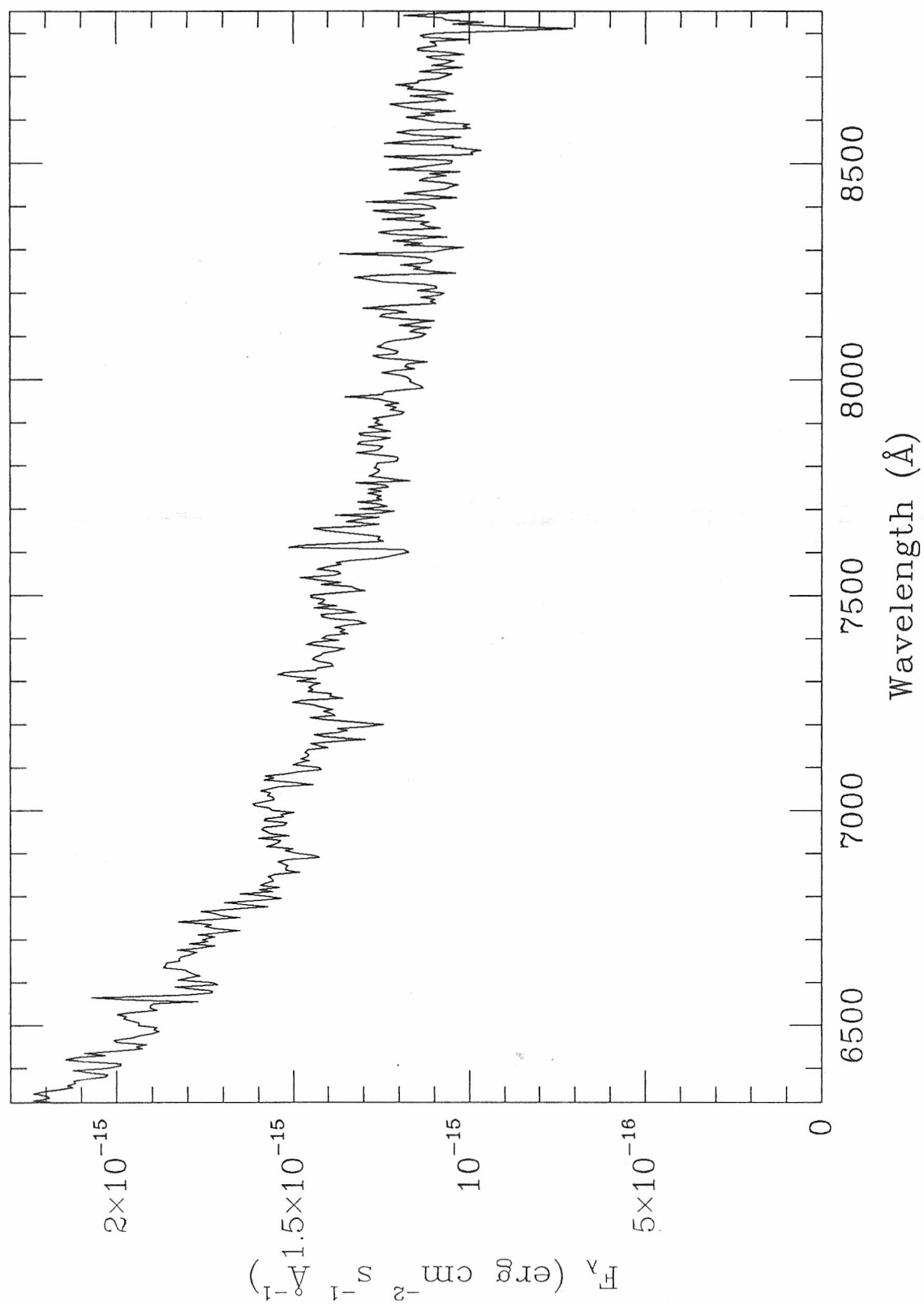
PG 1000+667 - 1990 May 6 5:17 UT



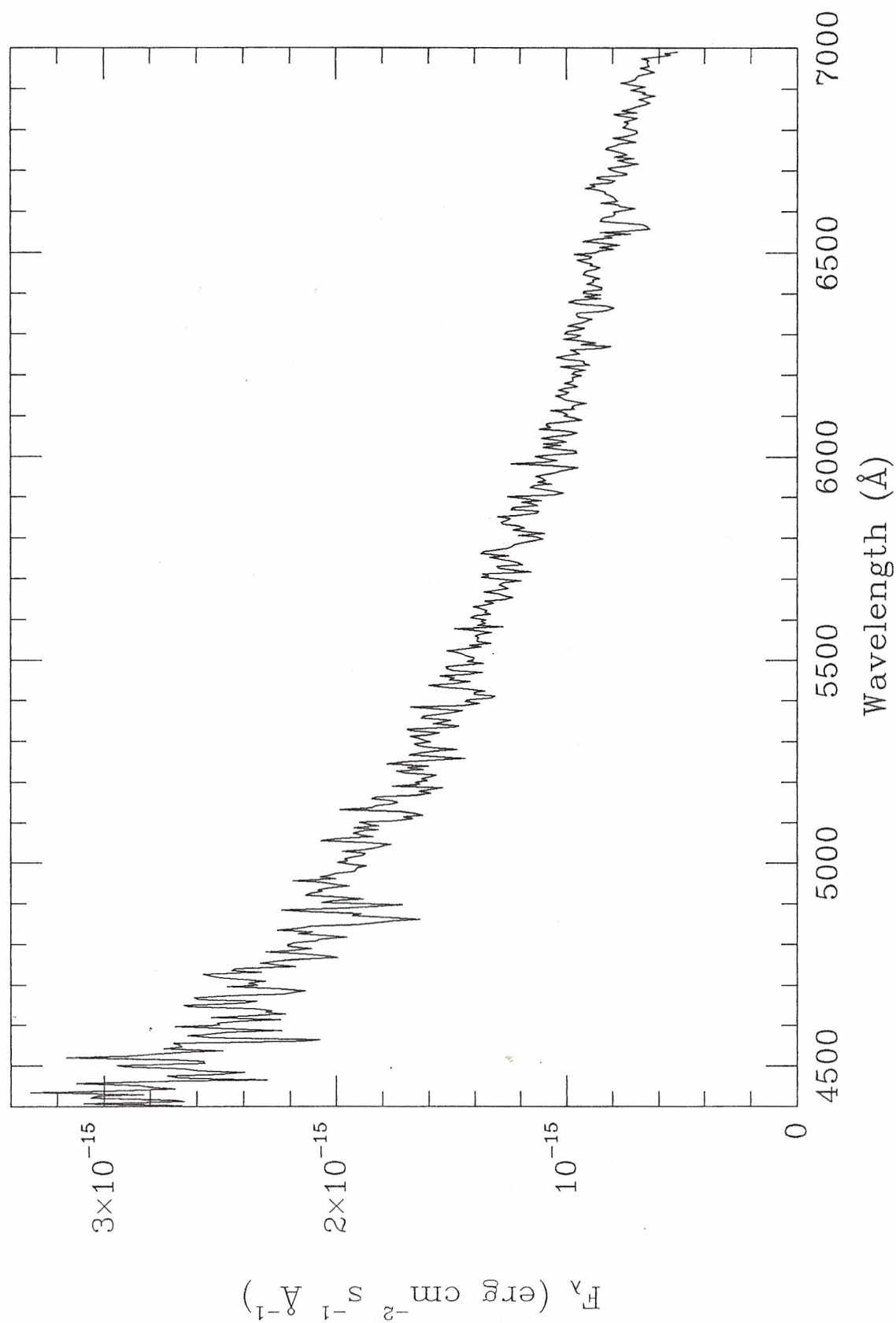
PG 1114+187 - 1990 April 28 06:58 UT



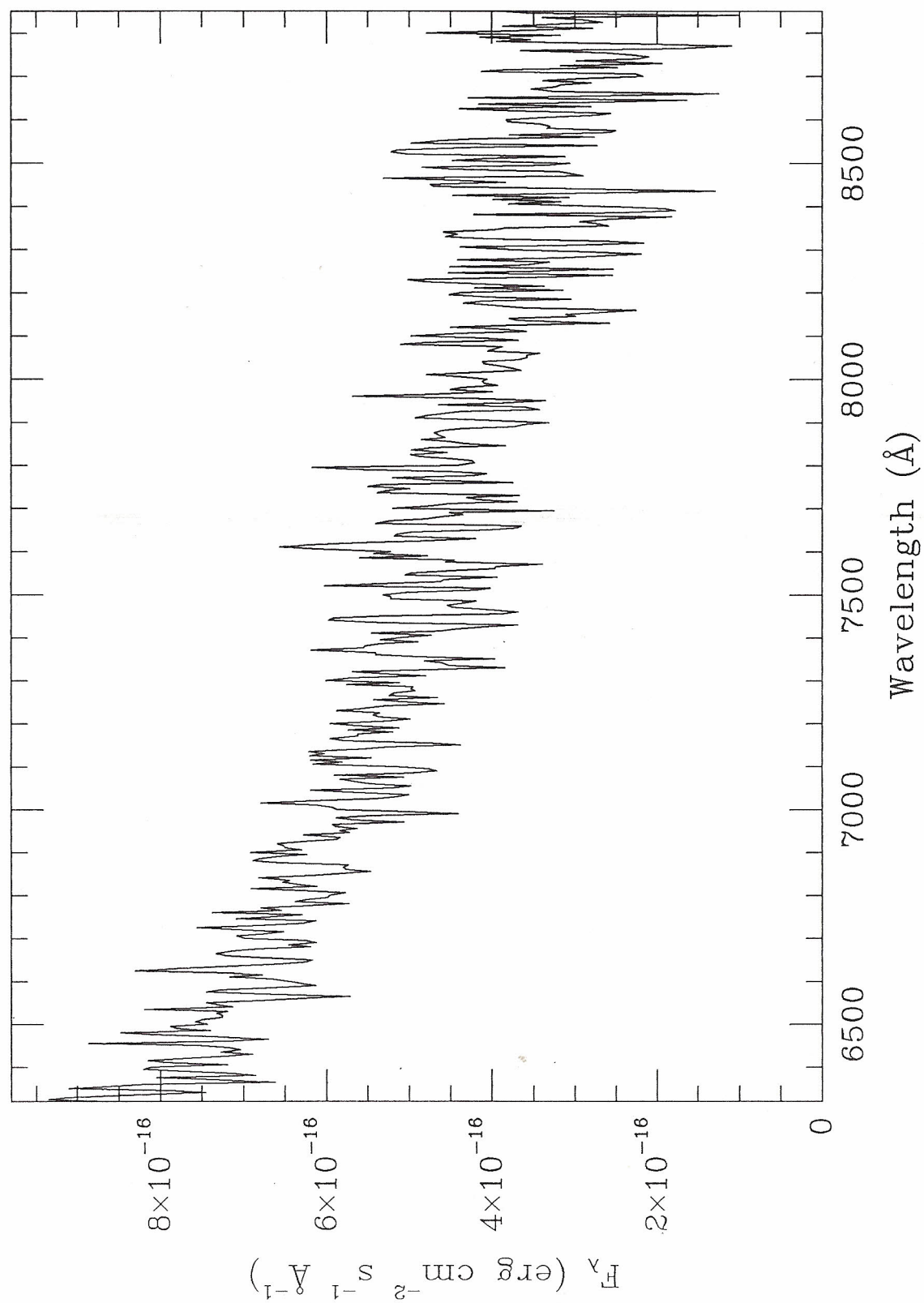
PG 1114+187 - 1990 May 4 7:29 UT



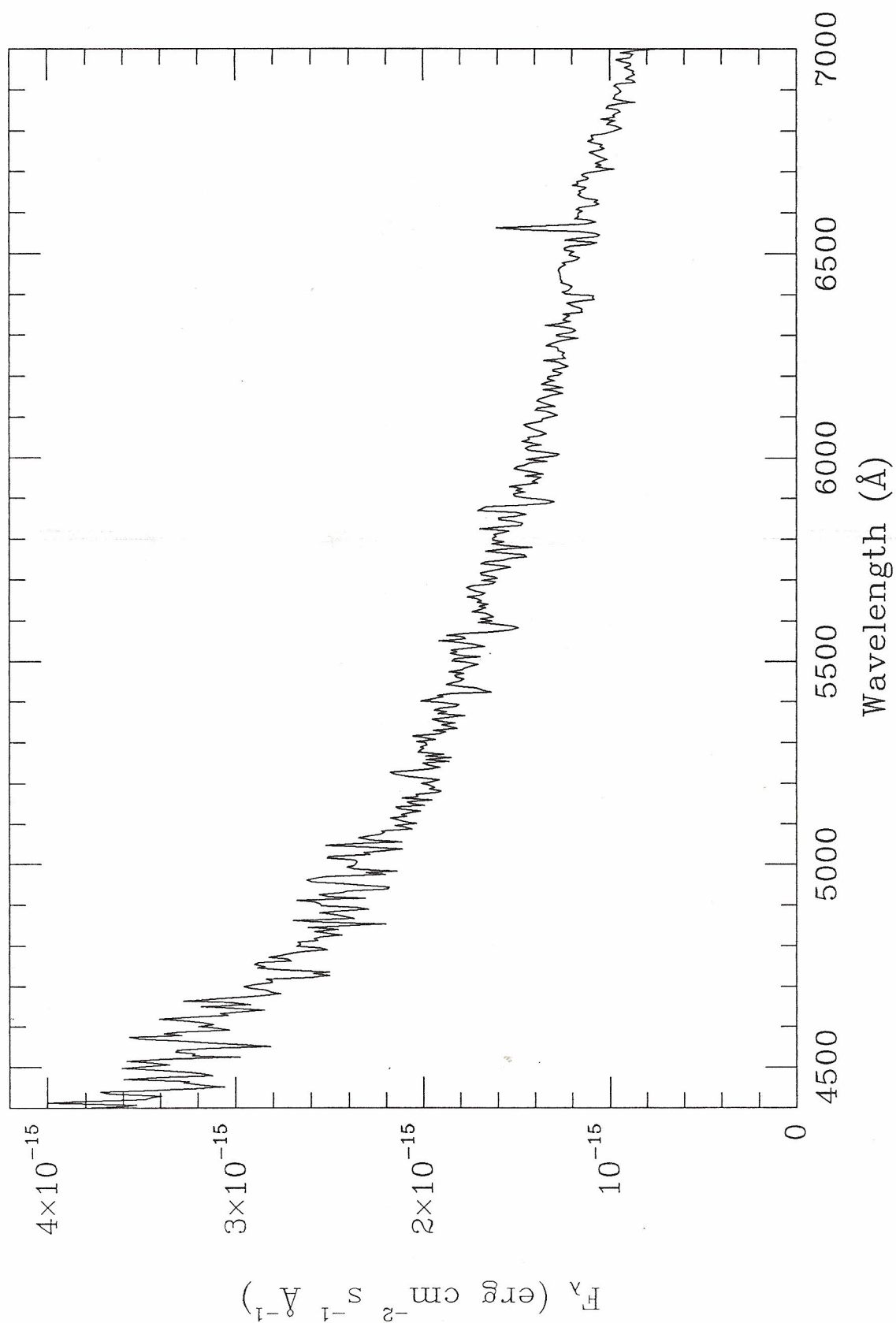
PG 1119+147 - 1990 April 28 07:20 UT



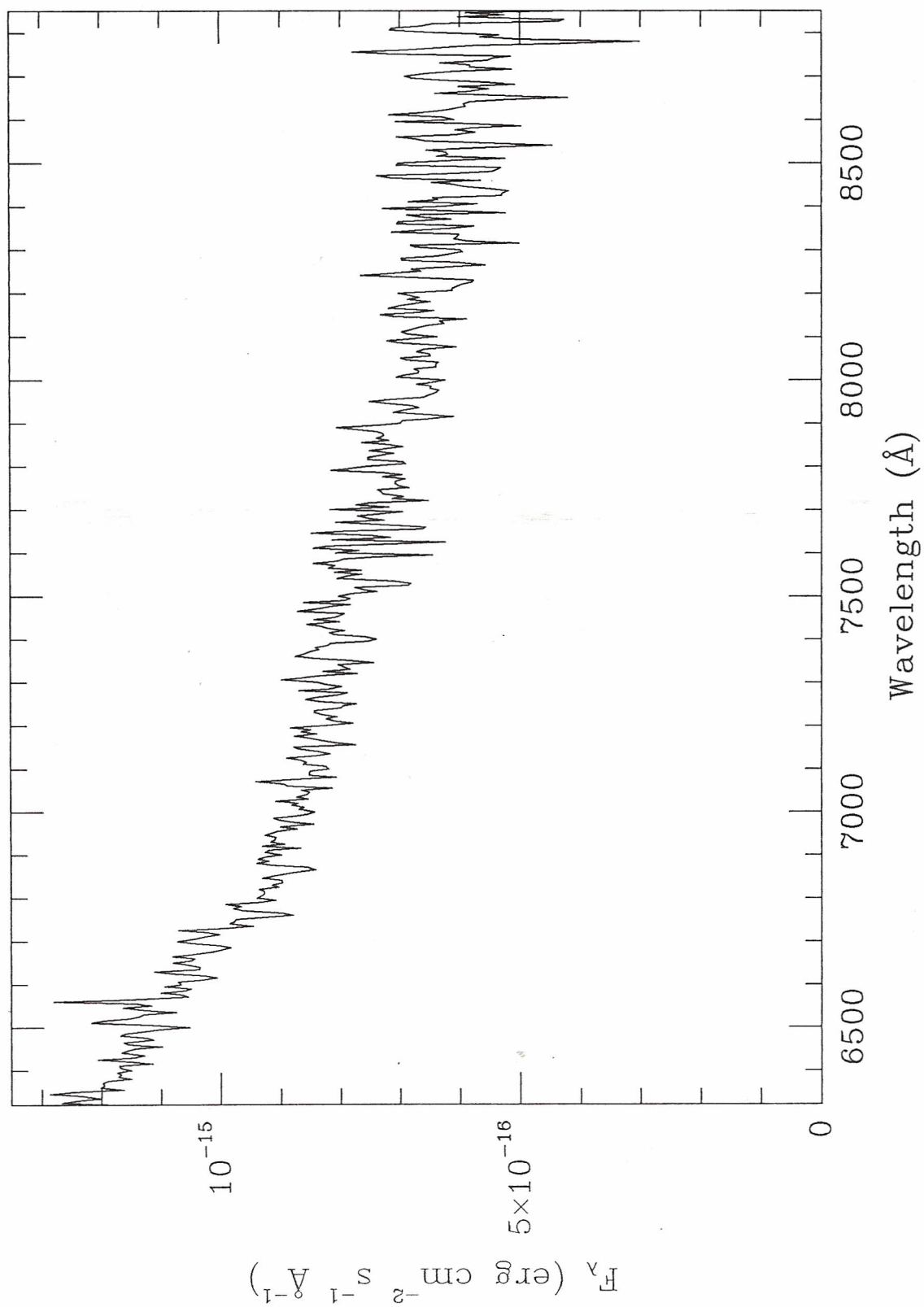
PG 1119+147 - 1990 May 5 6:00 UT



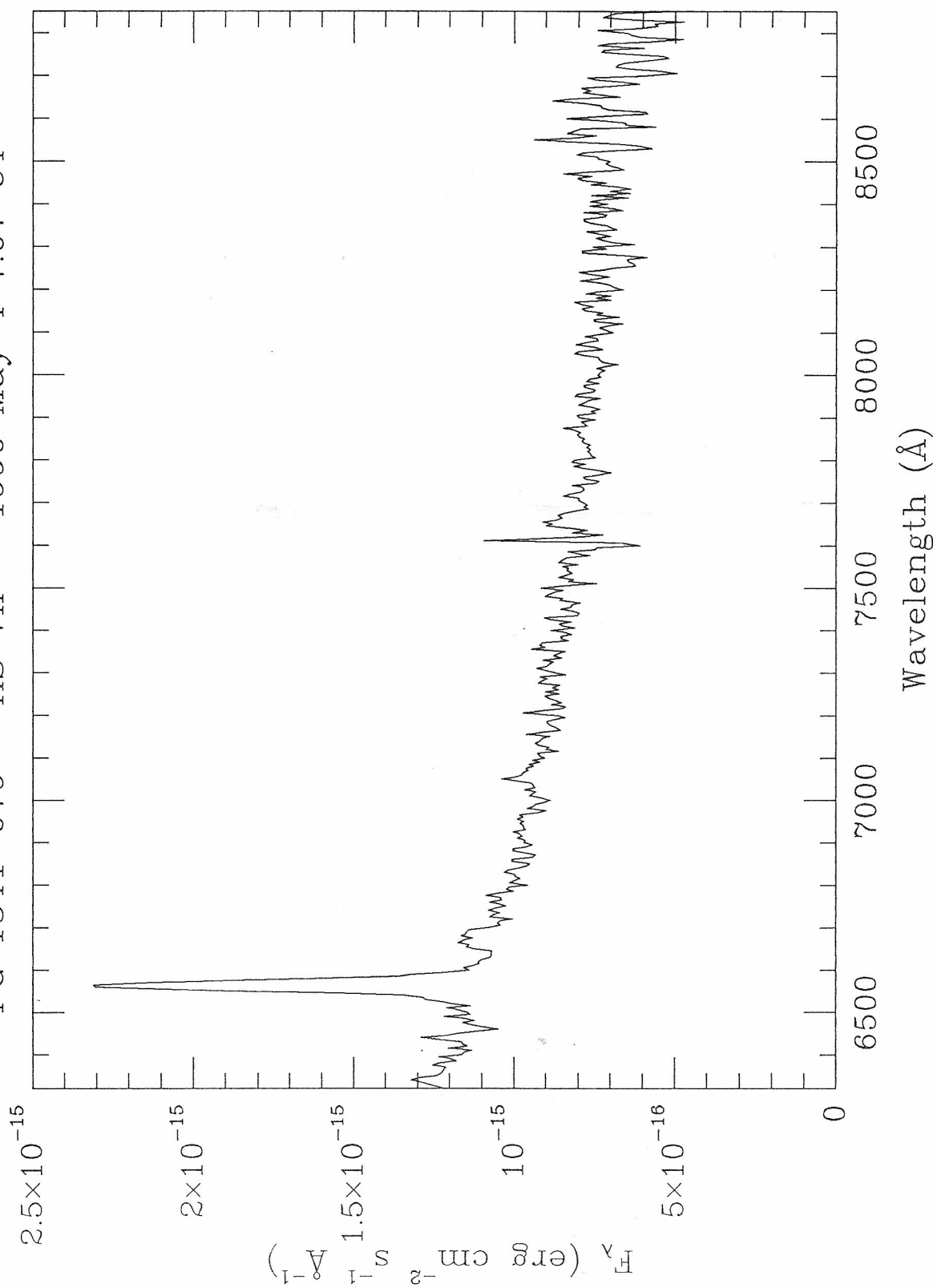
PG 1316+678 - 1990 April 27 07:18 UT



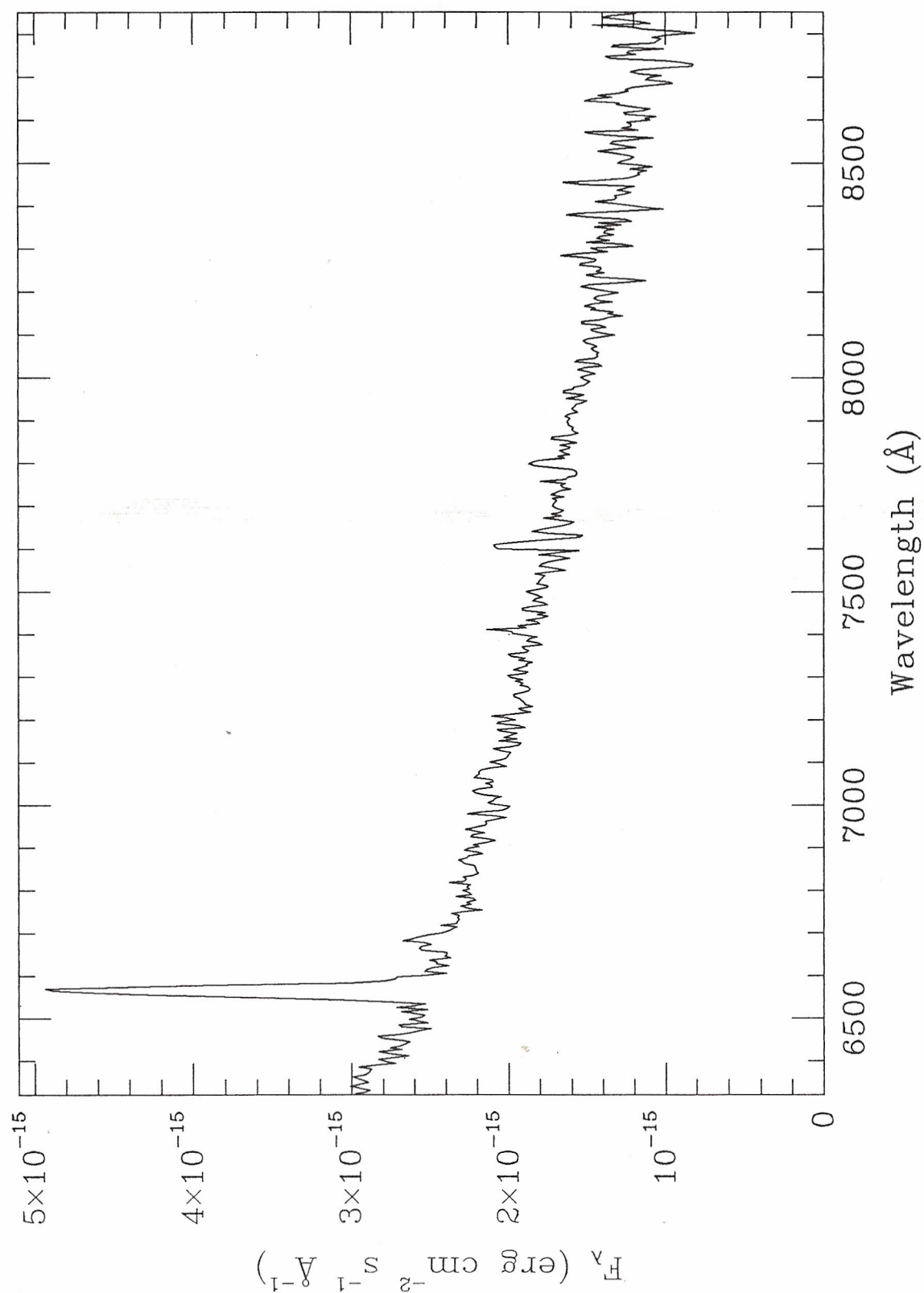
PG 1316+678 - 1990 May 5 8:12 UT



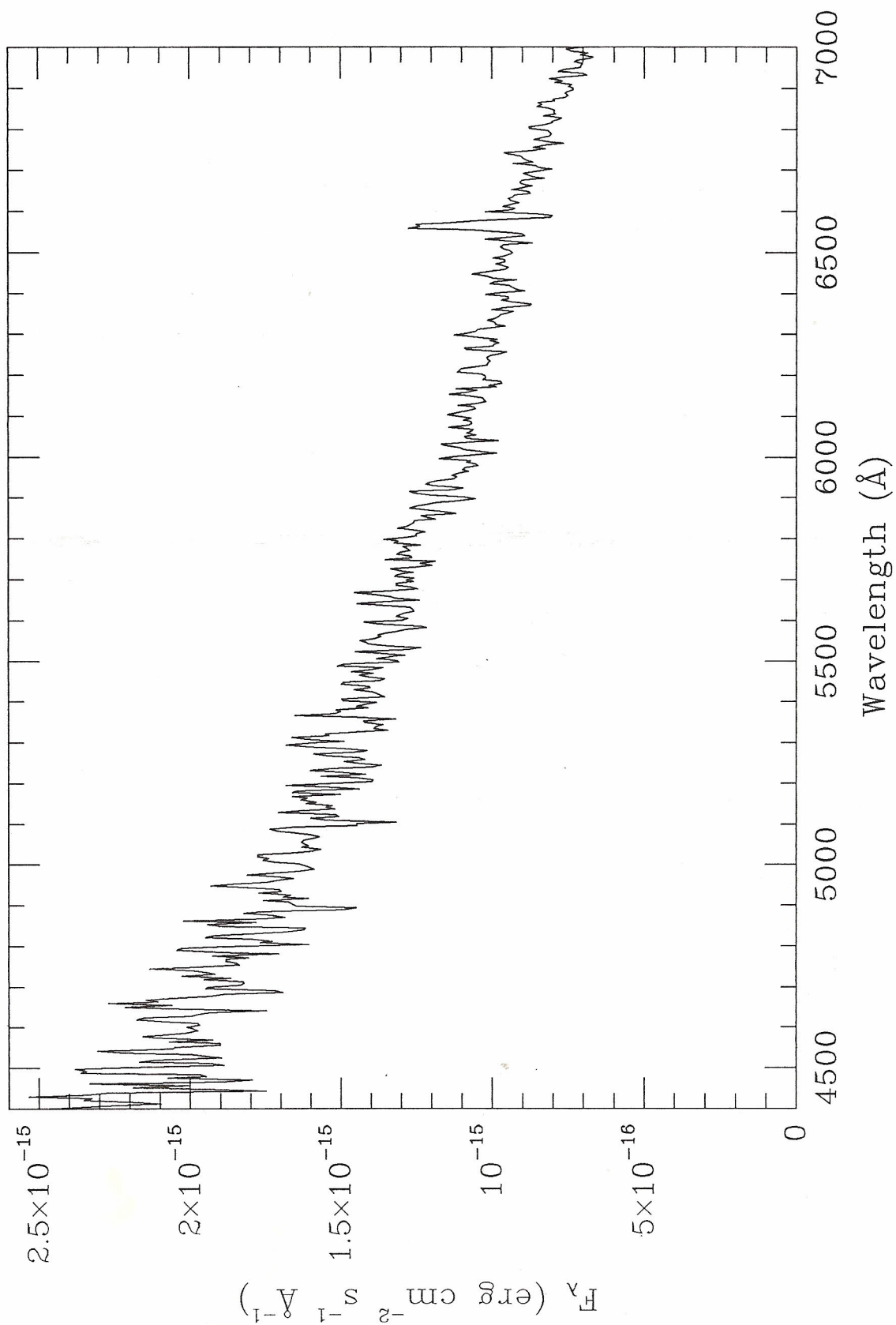
PG 1341-079 = HS Vir - 1990 May 4 7:07 UT



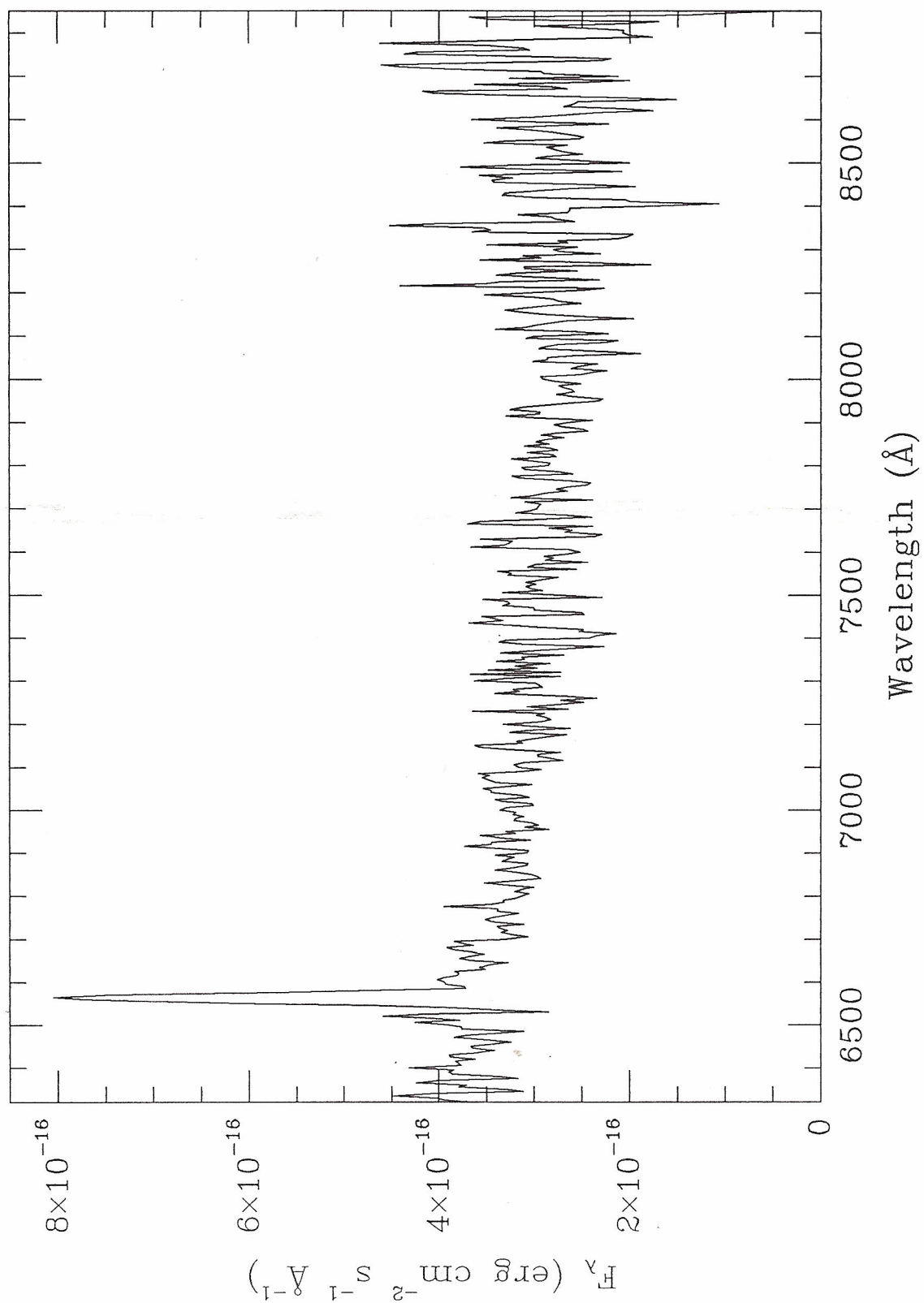
PG 1341-079 = HS Vir - 1990 May 7 6:06 UT



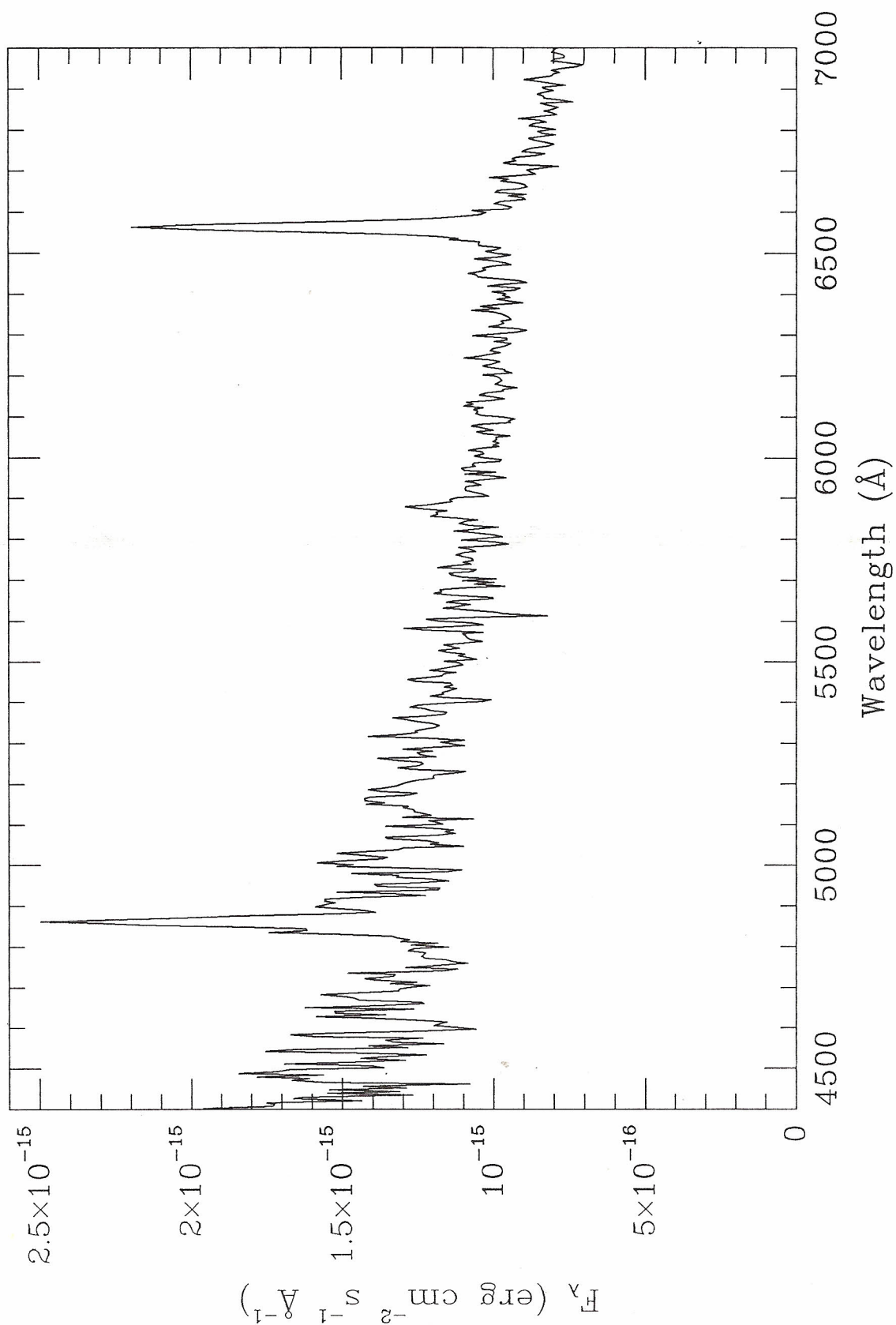
PG 1510+234 - 1990 April 27 09:26 UT



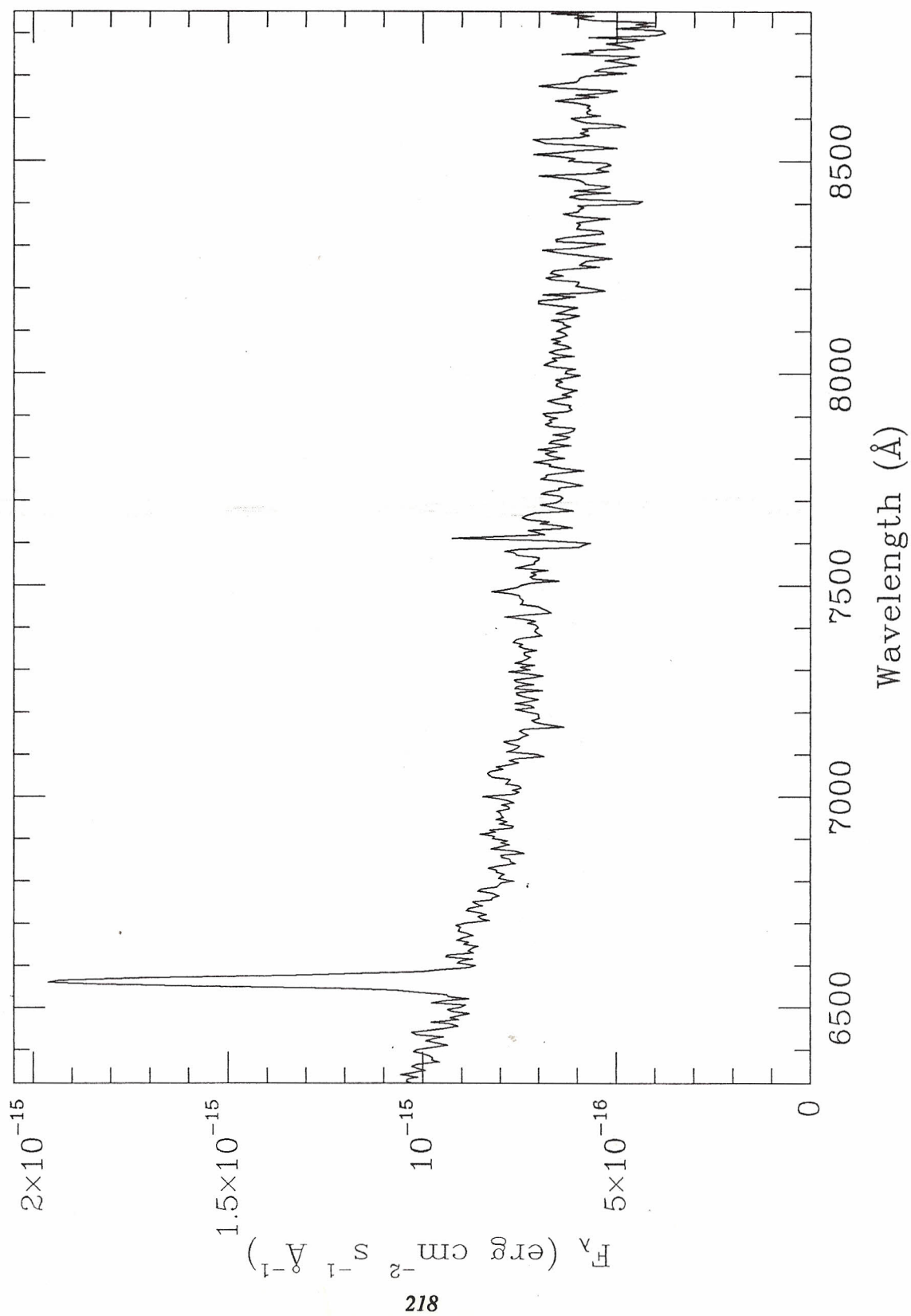
PG 1510+234 - 1990 May 5 9:28 UT



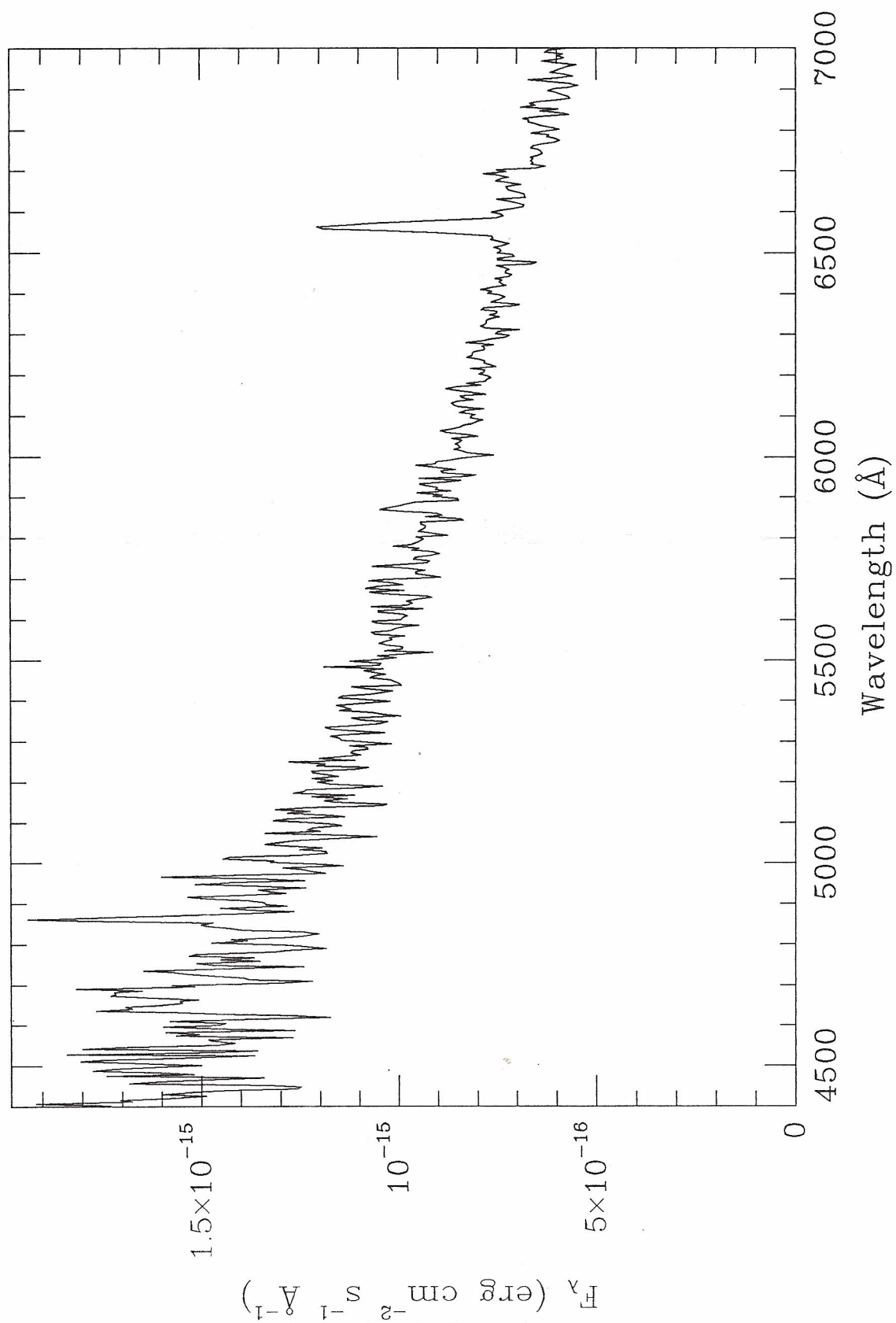
PG 1524+622 - 1990 April 27 10:34 UT



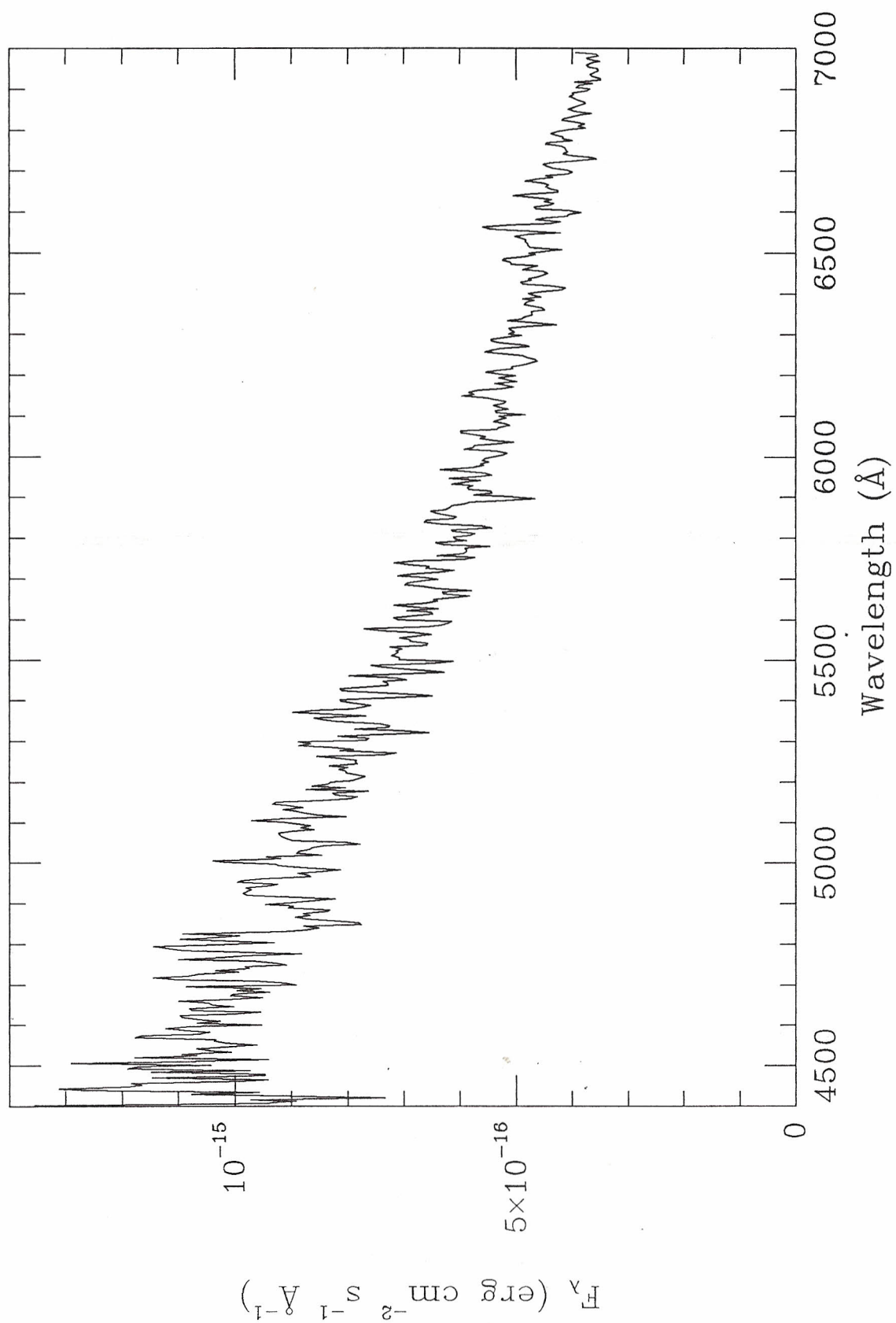
PG 1524+622 - 1990 May 4 9:14 UT



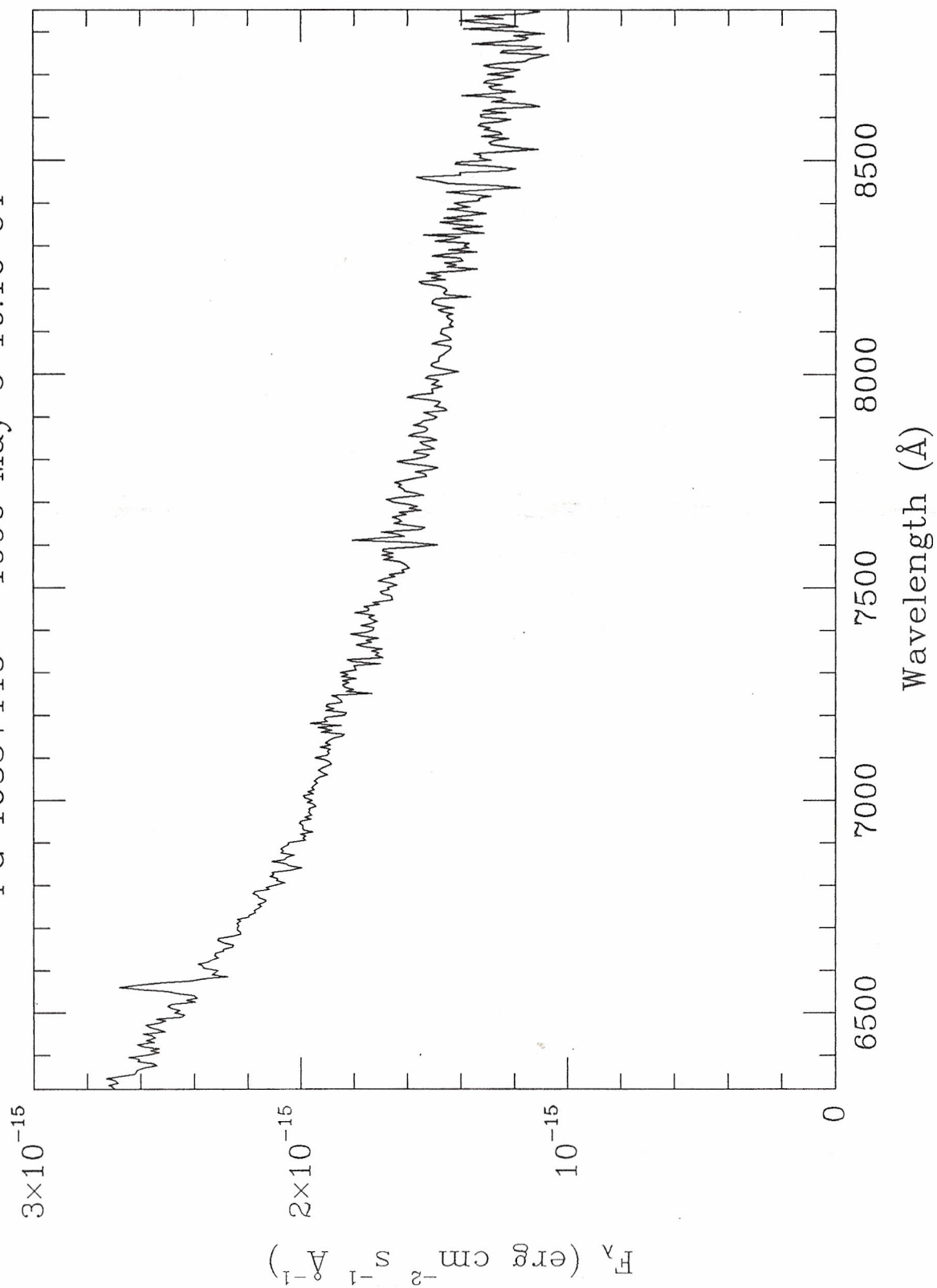
PG 1543+145 = CT Ser - 1990 May 3 10:20 UT



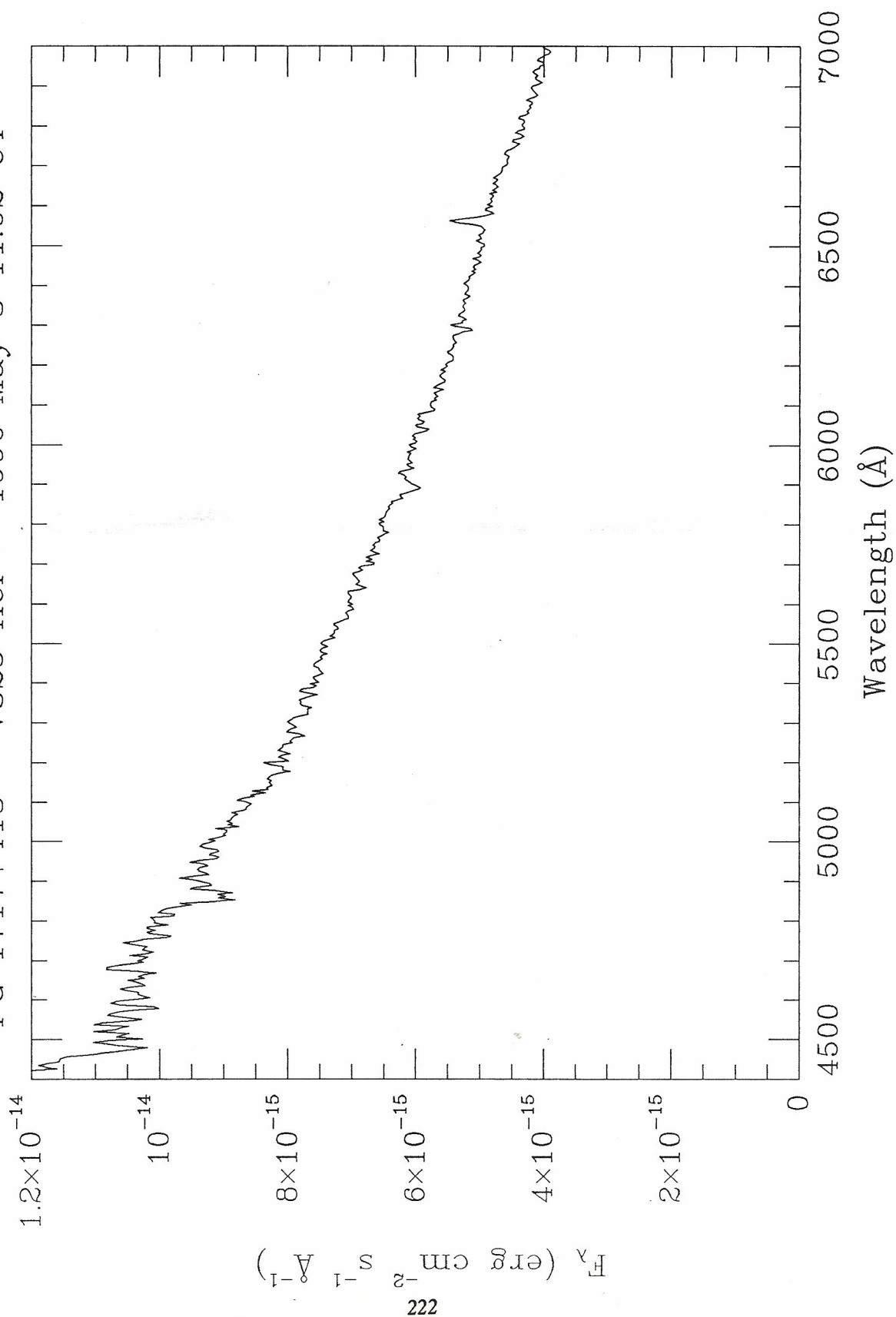
PG 1633+115 - 1990 April 29 10:49 UT



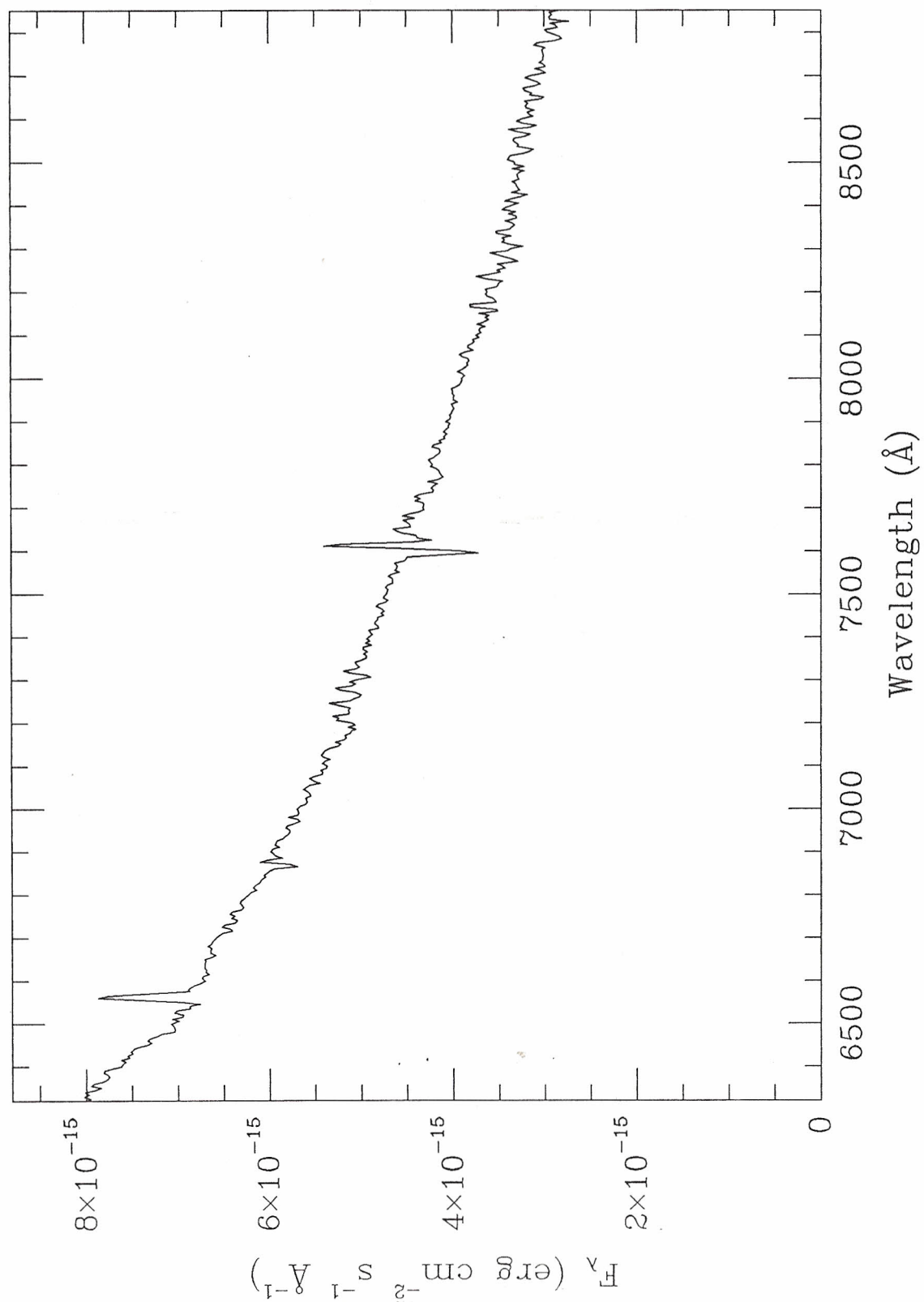
PG 1633+115 - 1990 May 5 10:16 UT



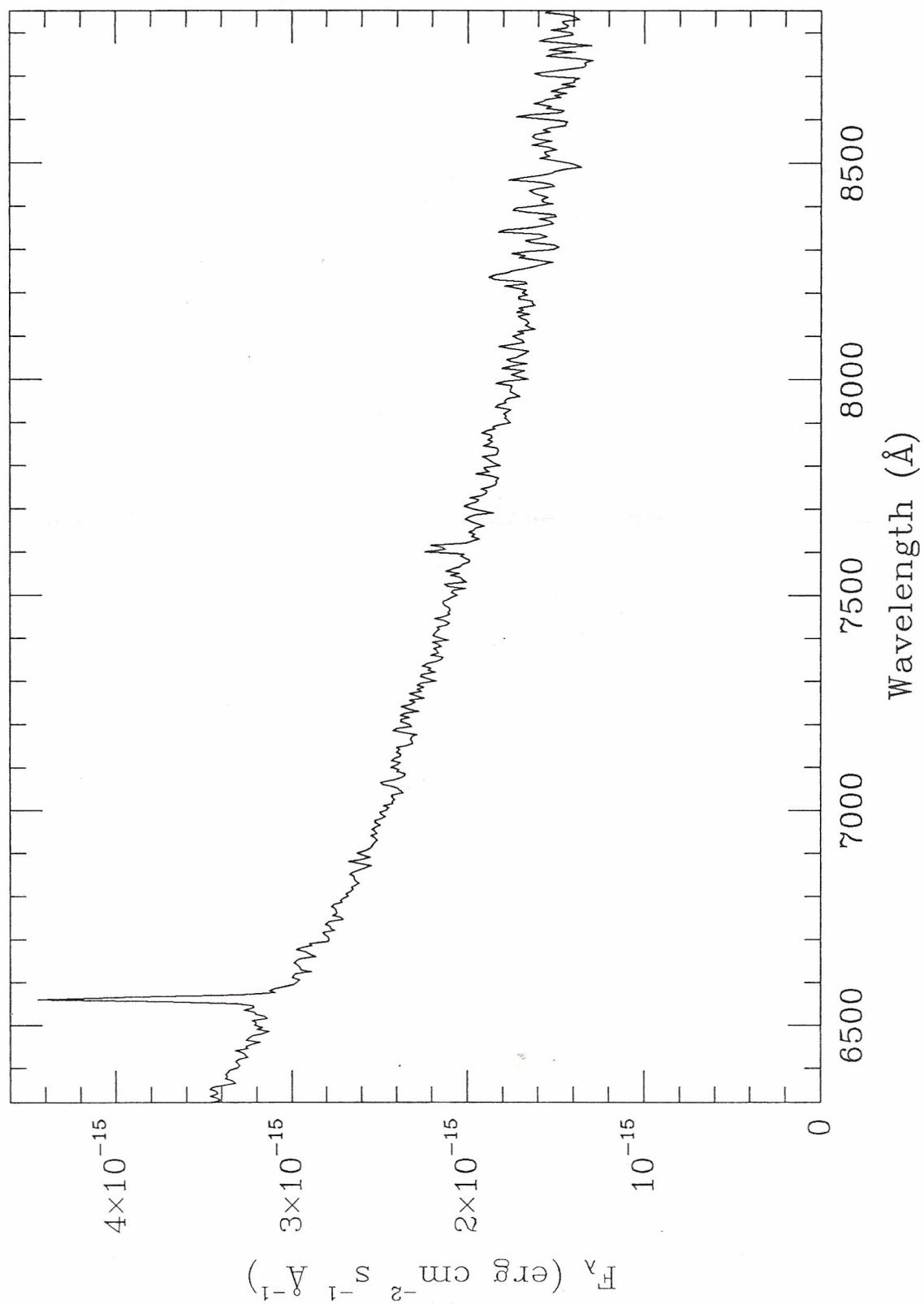
PG 1717+413 = V825 Her - 1990 May 3 11:02 UT



PG 1717+413 = V825 Her - 1990 May 4 11:19 UT



PG 2133+115 - 1990 May 5 10:49 UT



Appendix B

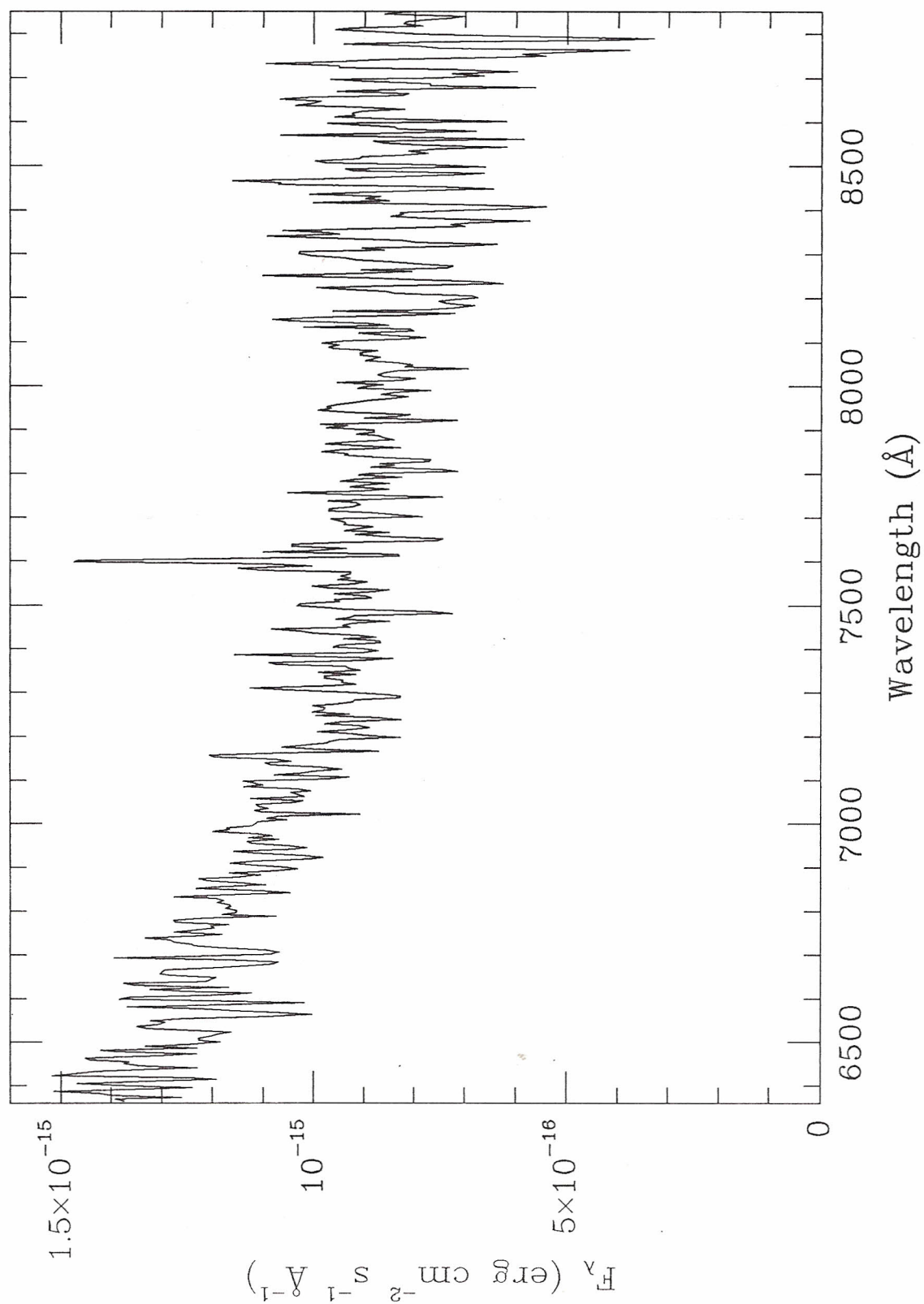
Spectra of Other Objects

presented in order of Right Ascension

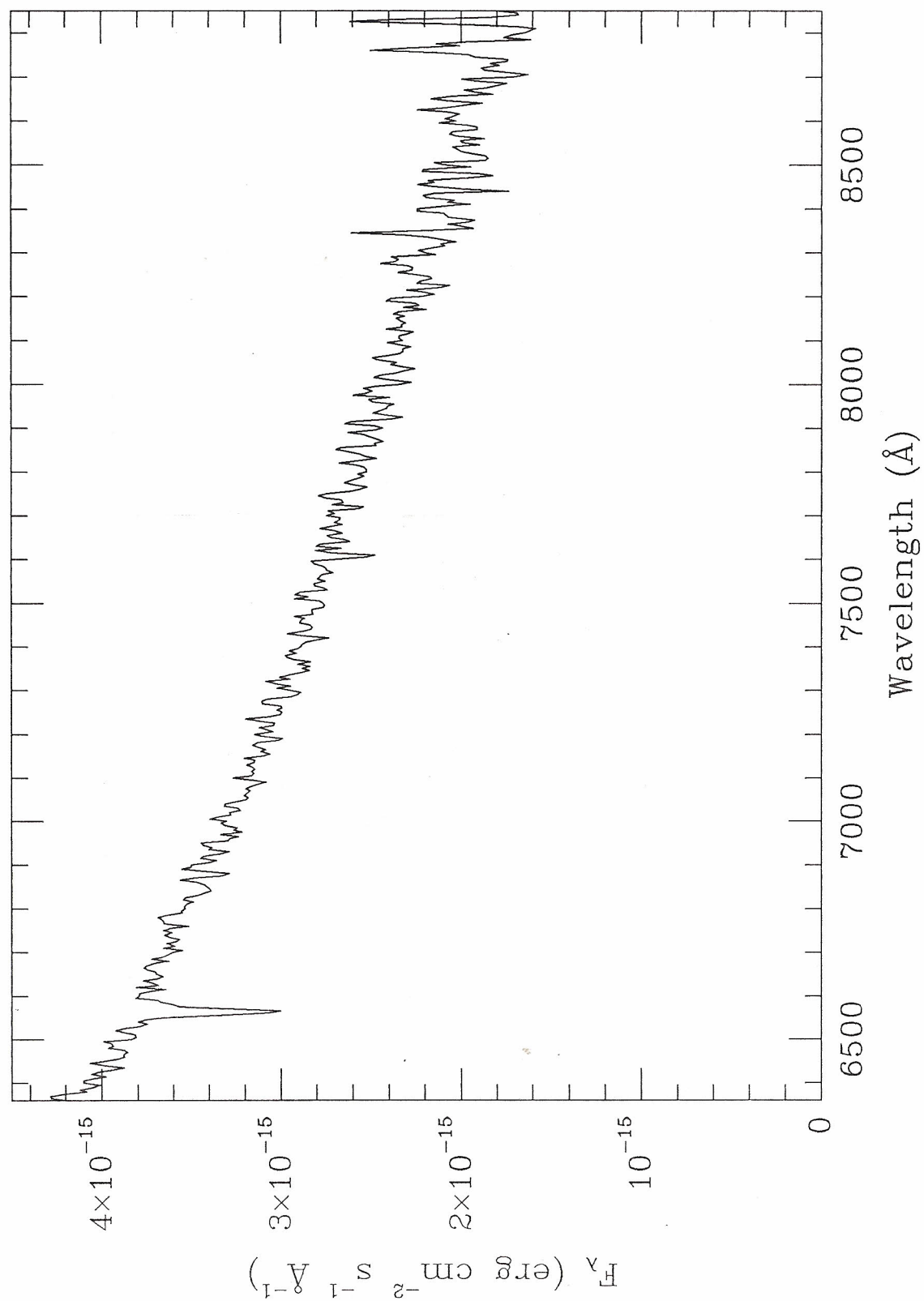
All spectra are in F_λ , are sky-subtracted, and have the telluric absorption bands divided out:
see Chapter 2.

For descriptions of the individual objects, see Chapter 6.

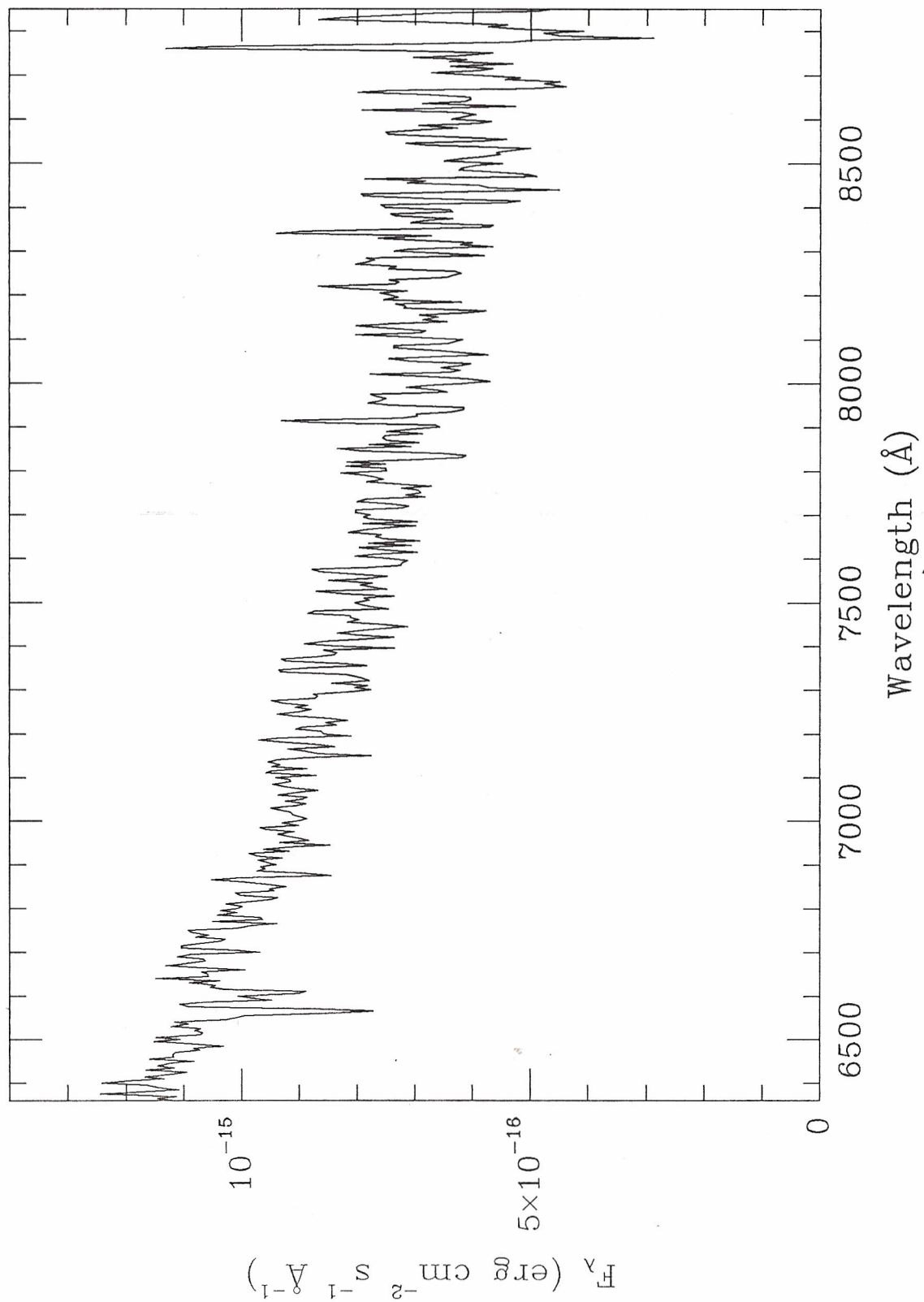
PG 0023+298 - 1991 October 21 03:19 UT



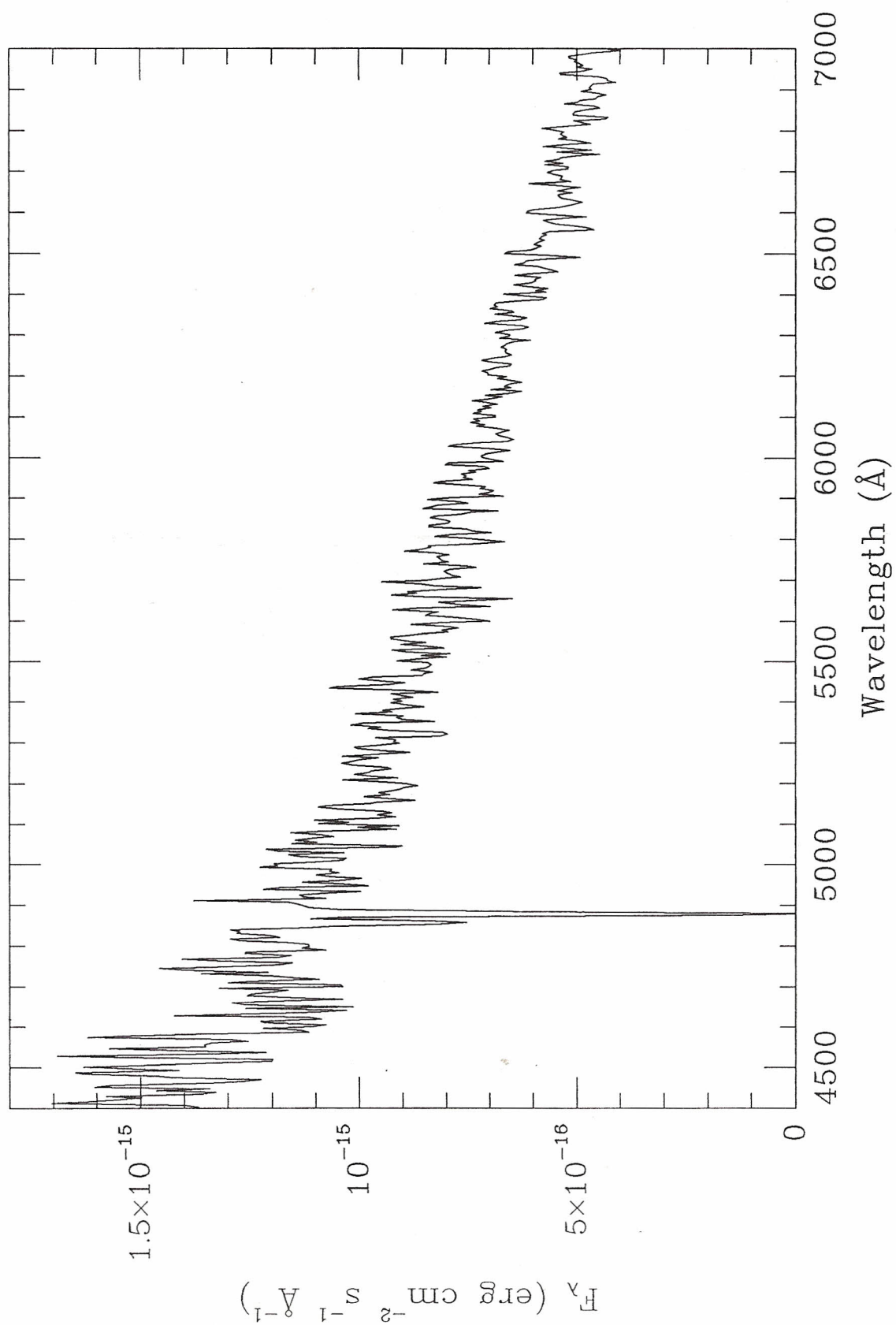
PG 0048+091 - 1991 October 27 06:08 UT



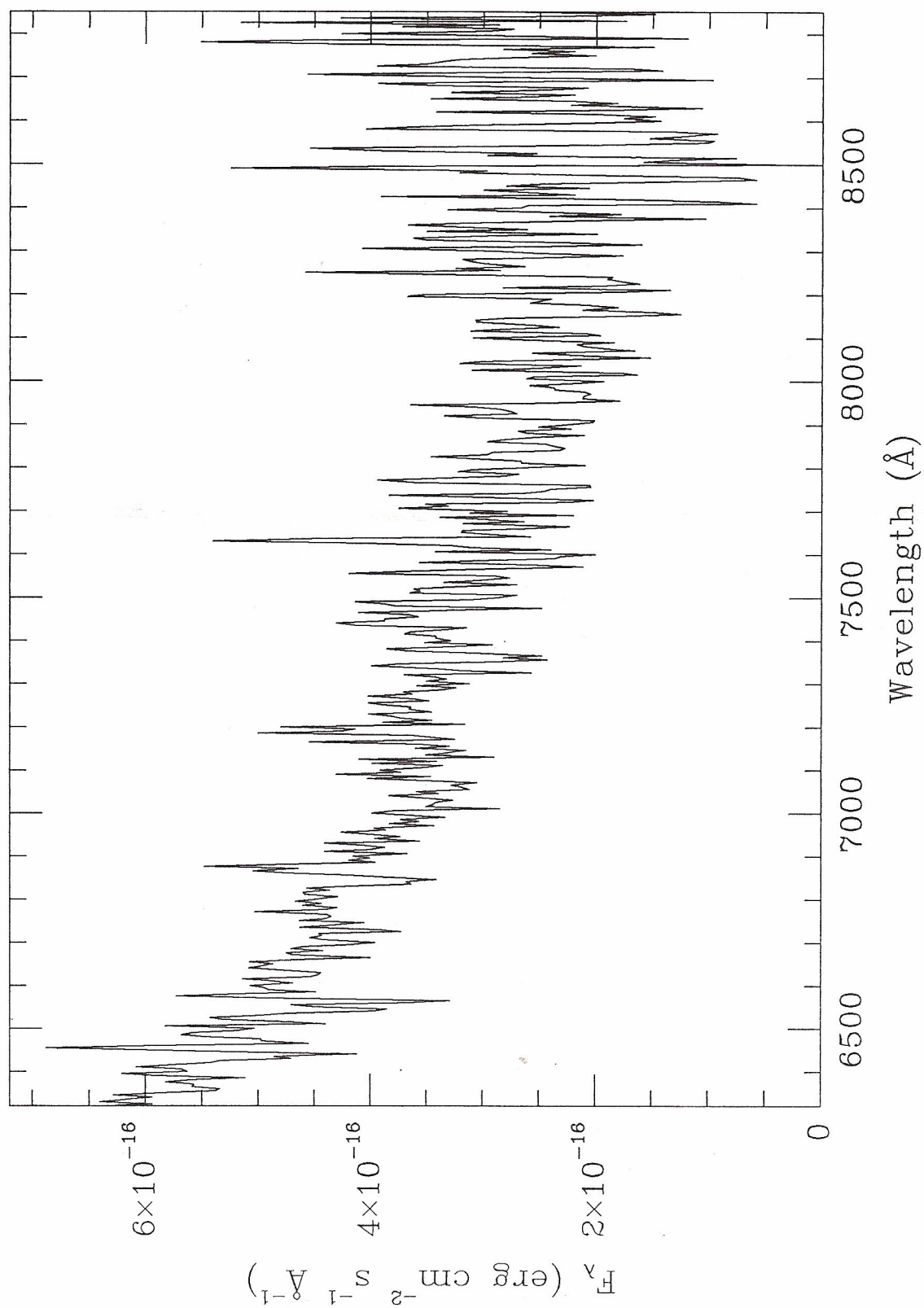
PG 0051+169 - 1991 October 27 06:35 UT



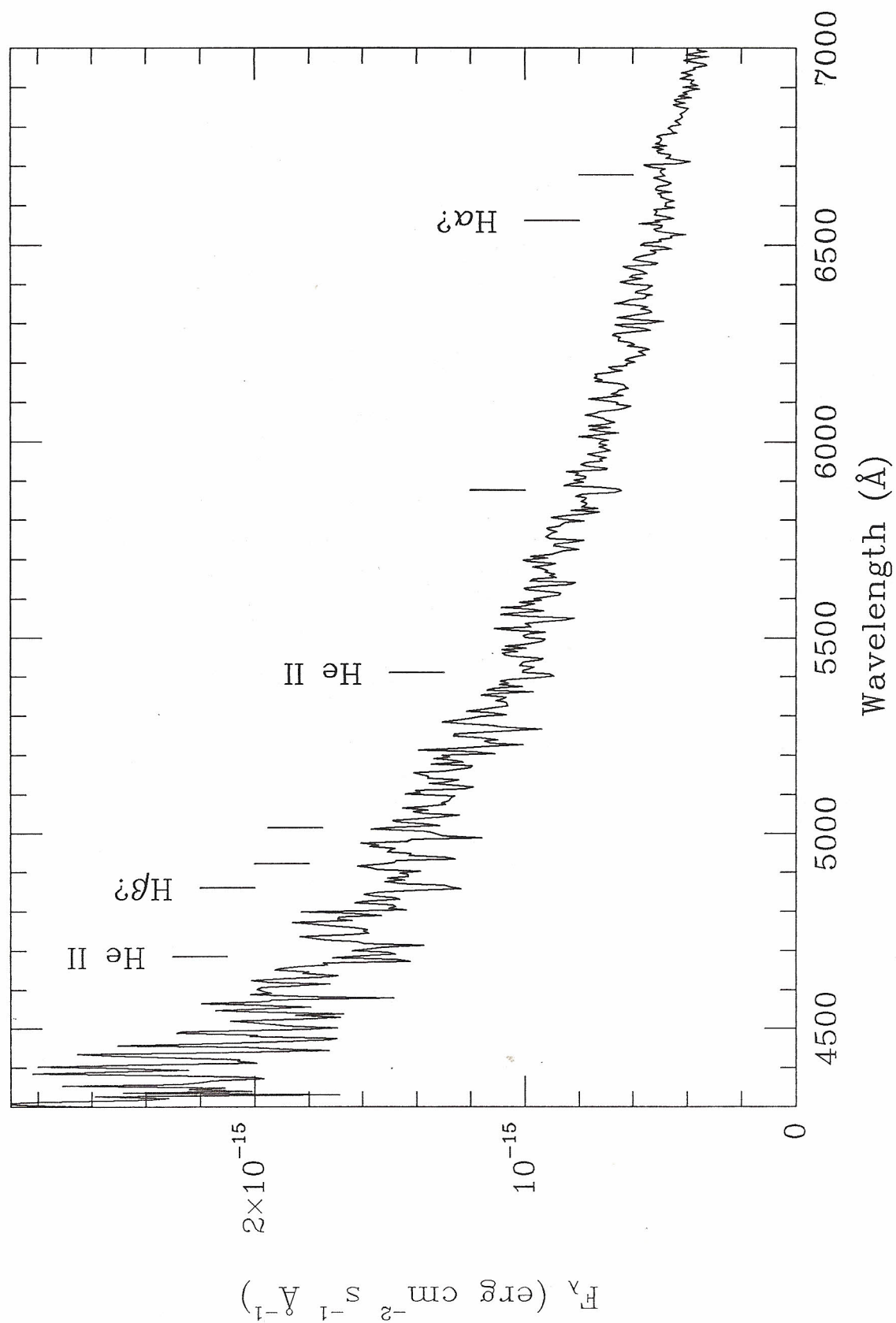
PG 0914+120 - 1990 April 27 04:22 UT



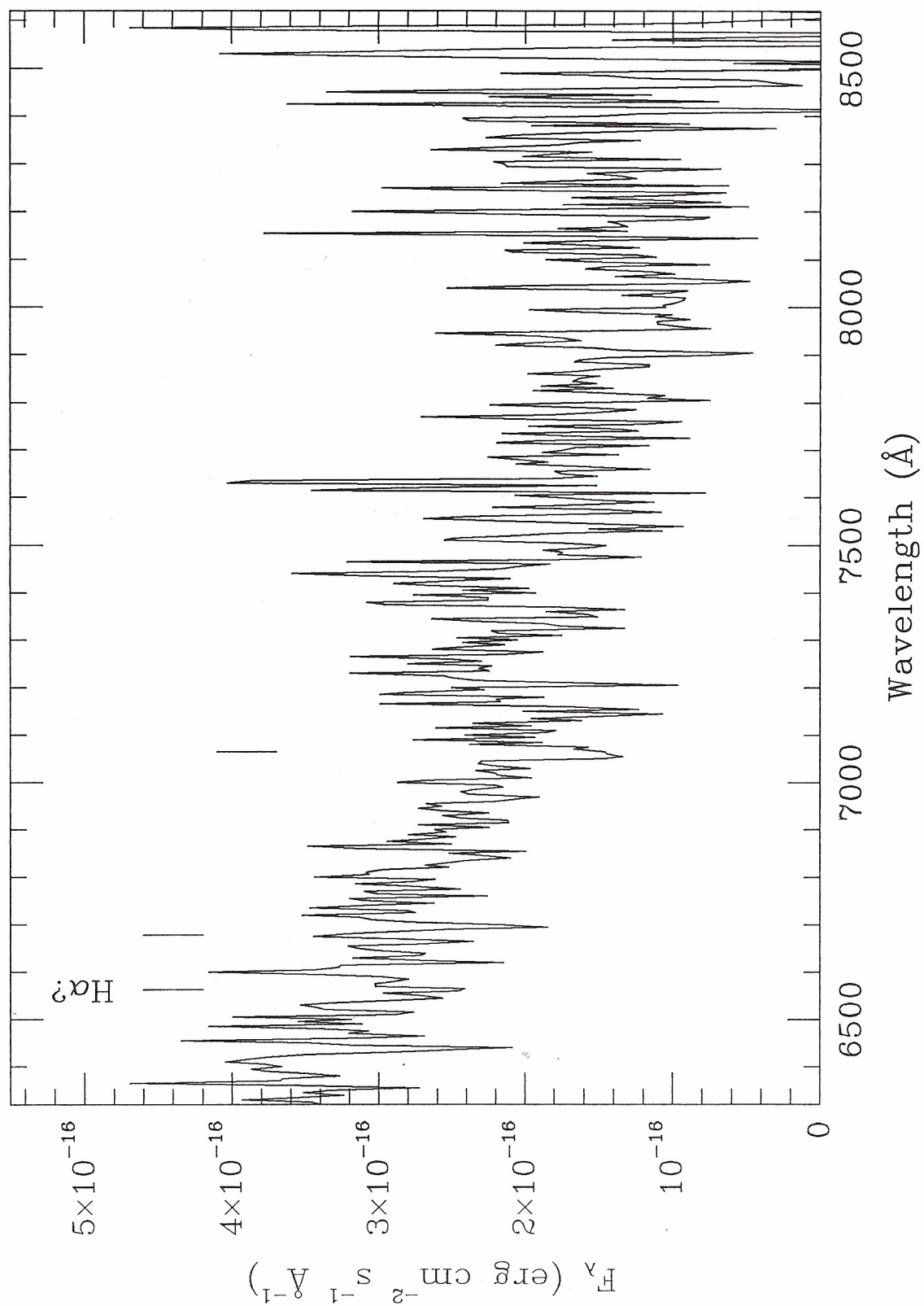
PG 0914+120 - 1990 May 6 04:35 UT



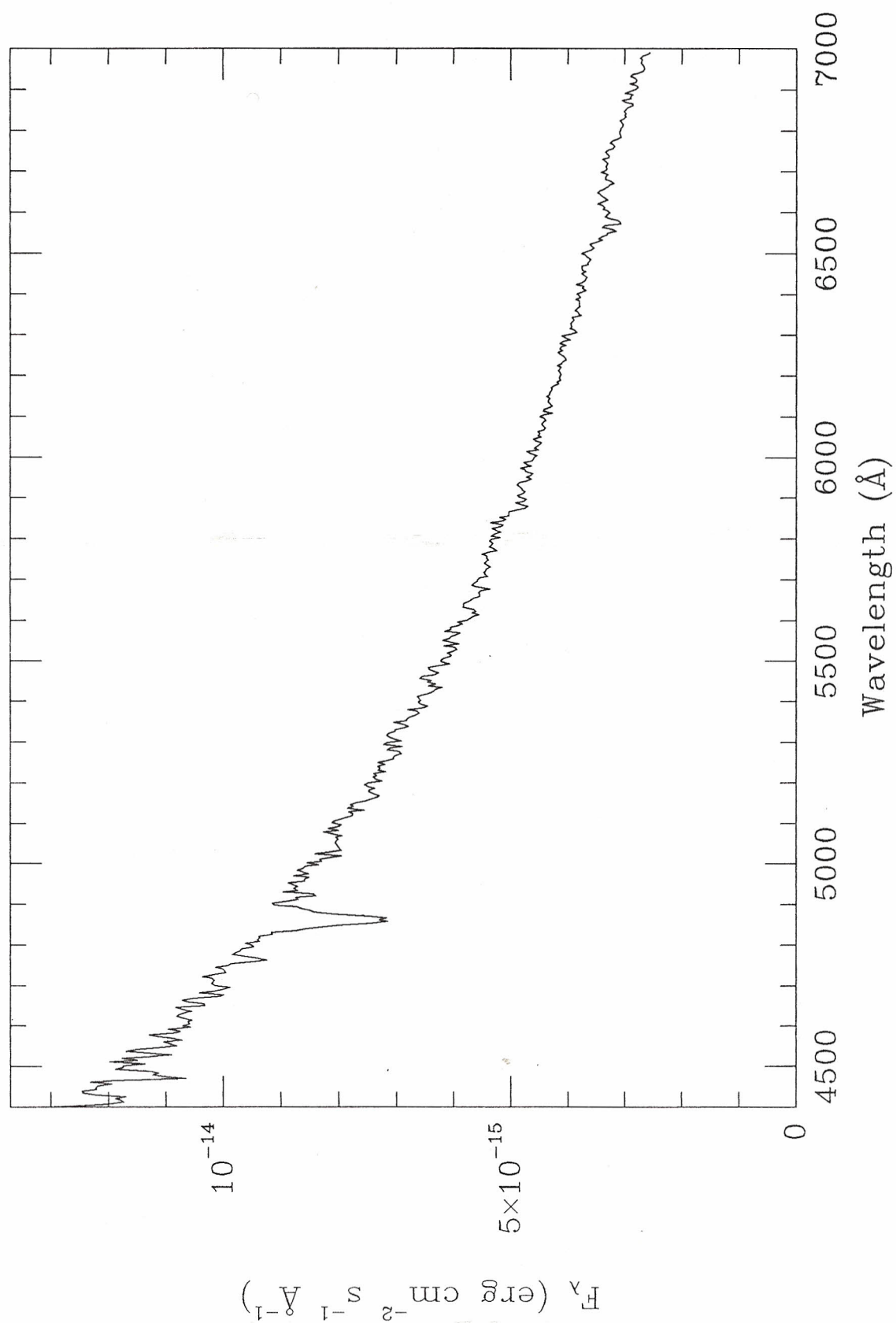
PG 0935+087 - 1990 April 27 04:44 UT



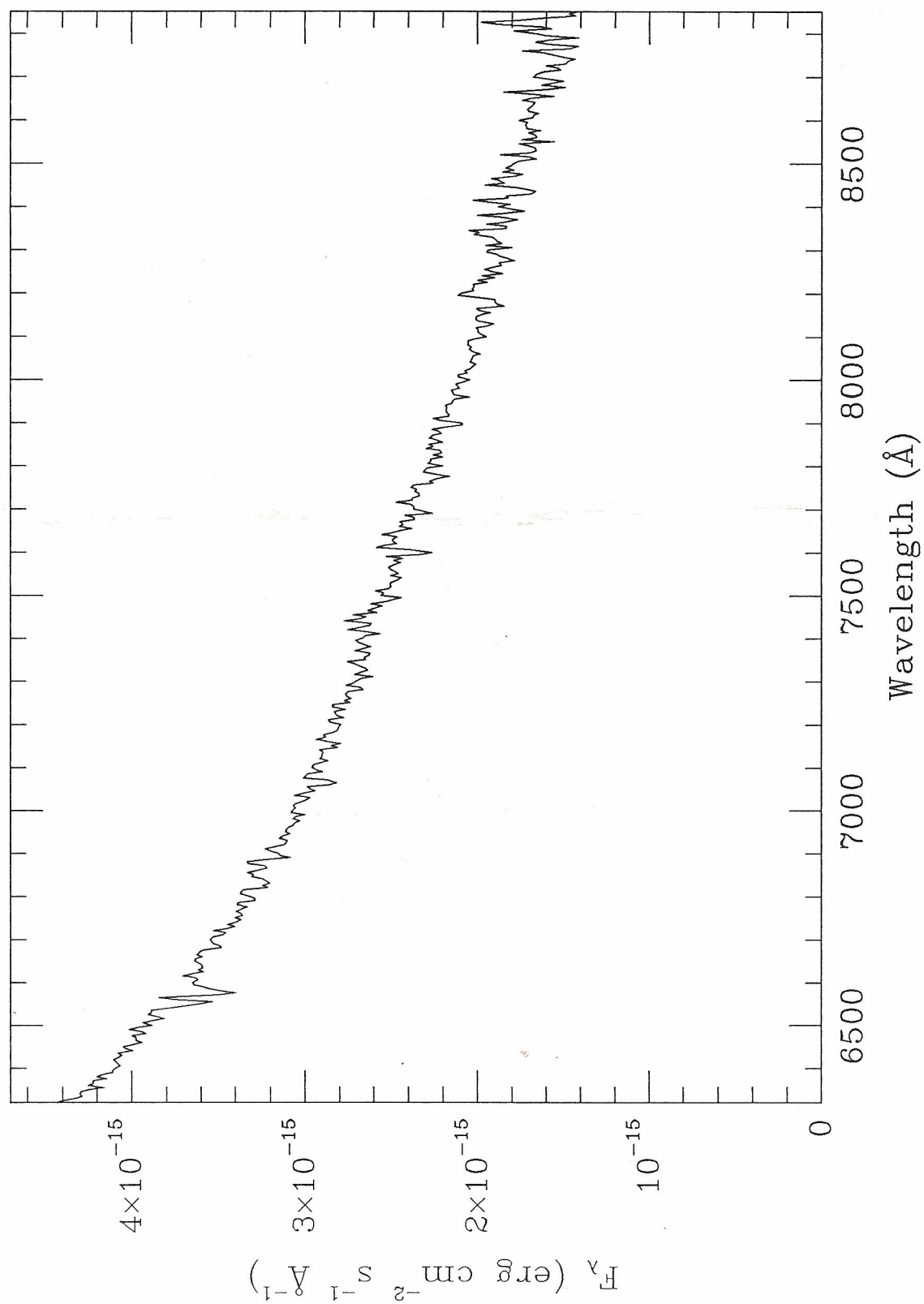
PG 0935+087 - 1990 May 6 4:04 UT



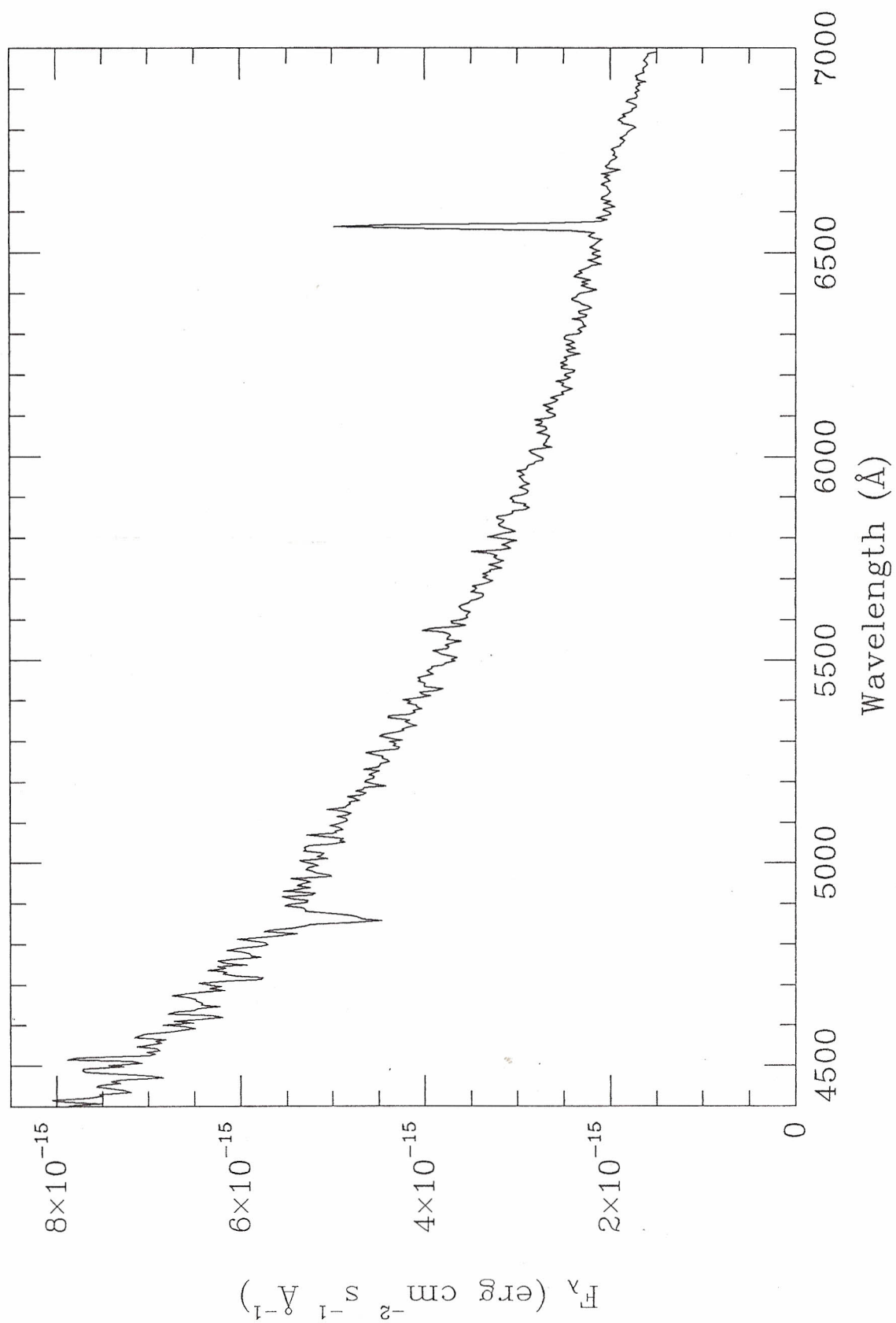
PG 0948+344 = RZ LMi -- 1990 April 28 05:17 UT



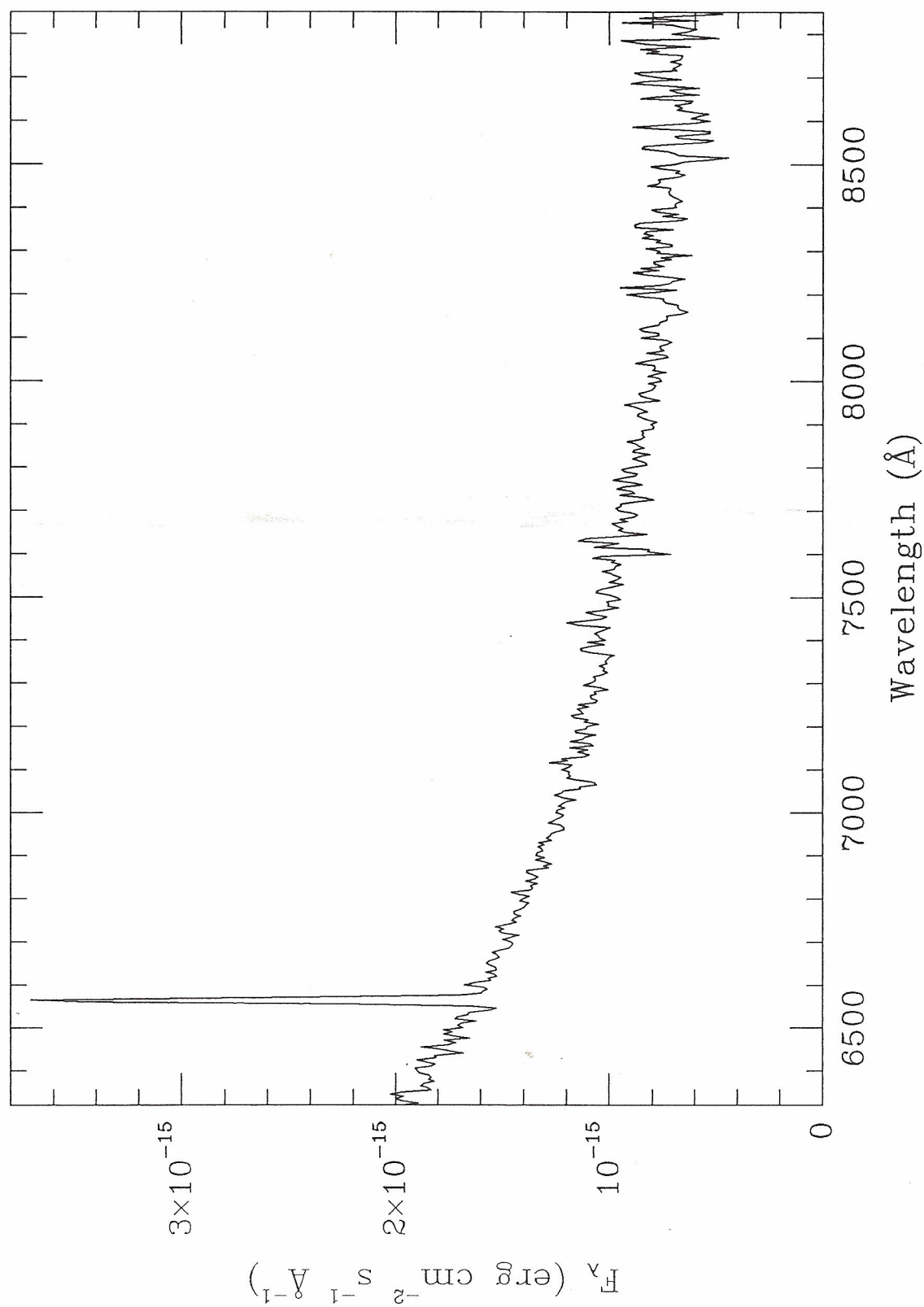
PG 0948+344 = RZ LMi - 1990 May 5 5:02 UT



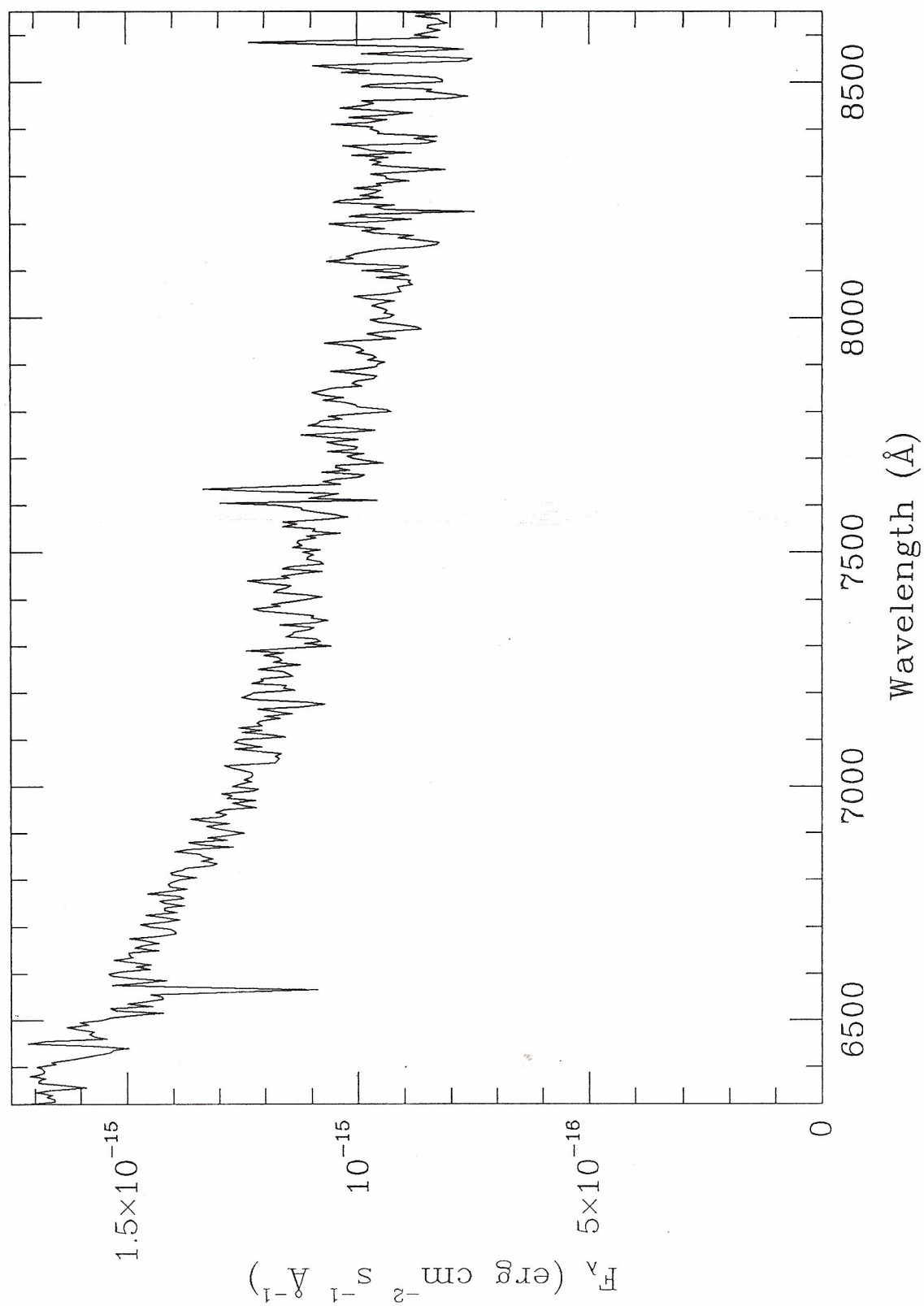
PG 1002+506 - 1990 April 28 06:00 UT



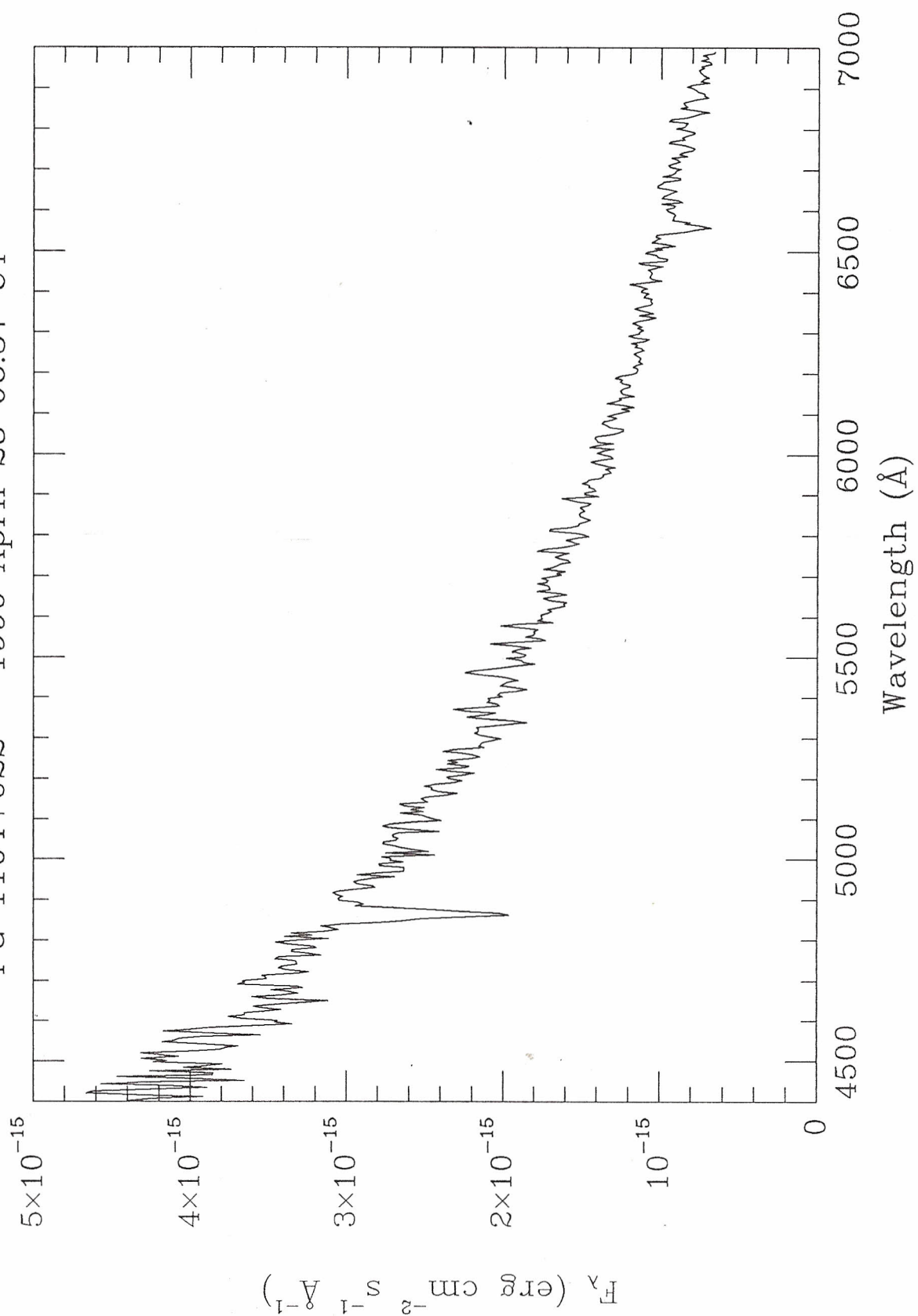
PG 1002+506 - 1990 May 6 5:47 UT



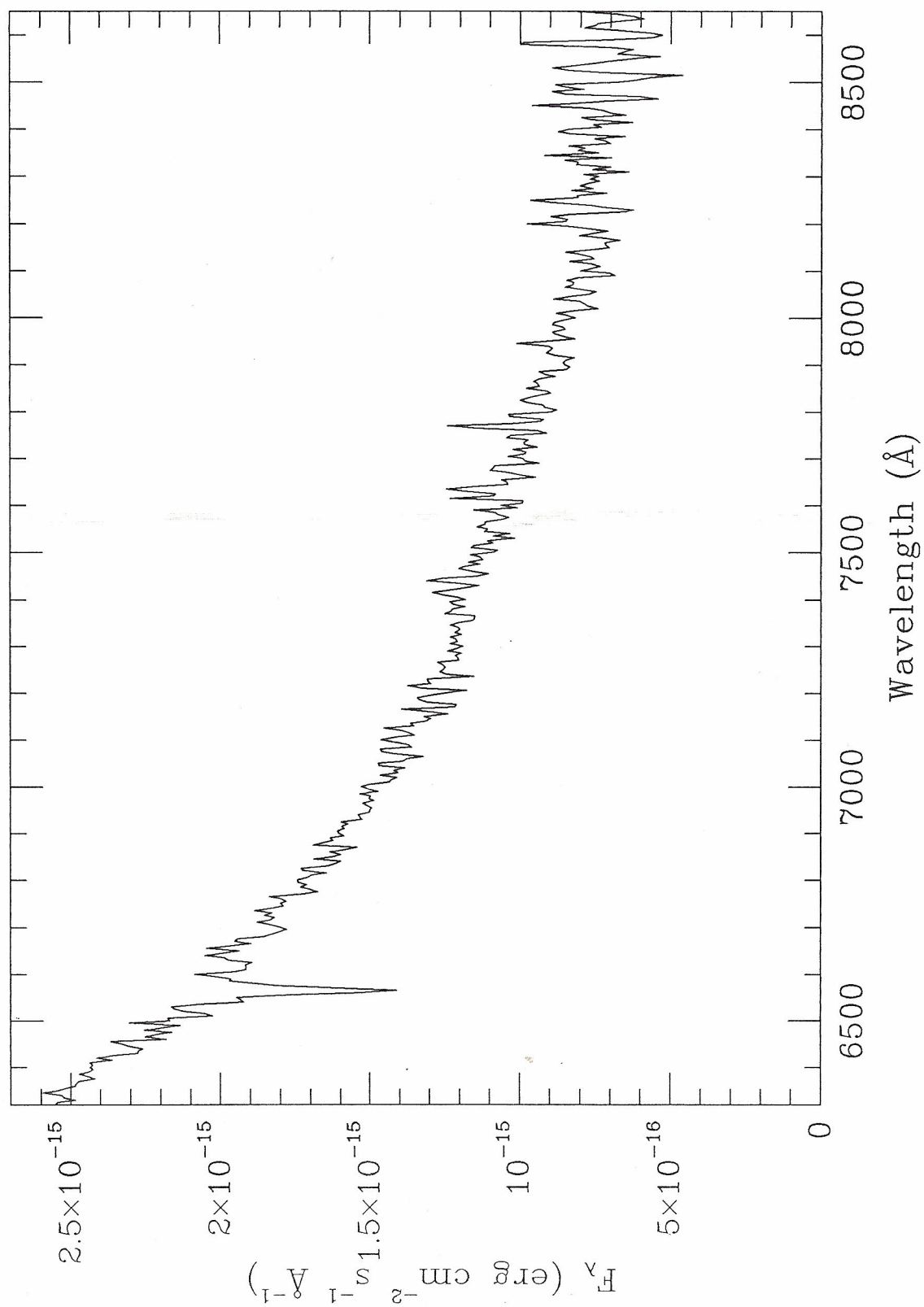
PG 1038+270 - 1990 May 6 6:12 UT



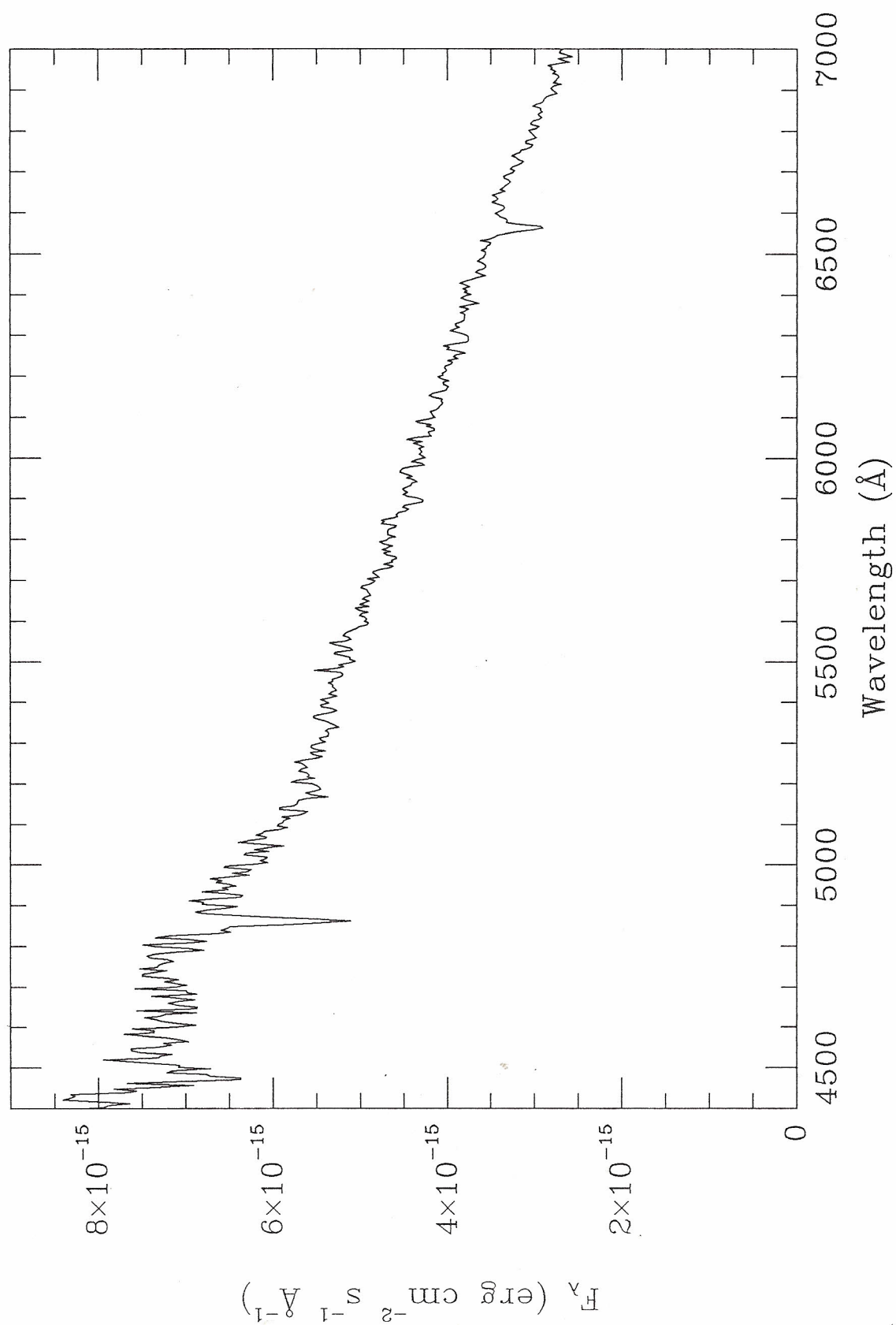
PG 1104+022 - 1990 April 28 06:37 UT



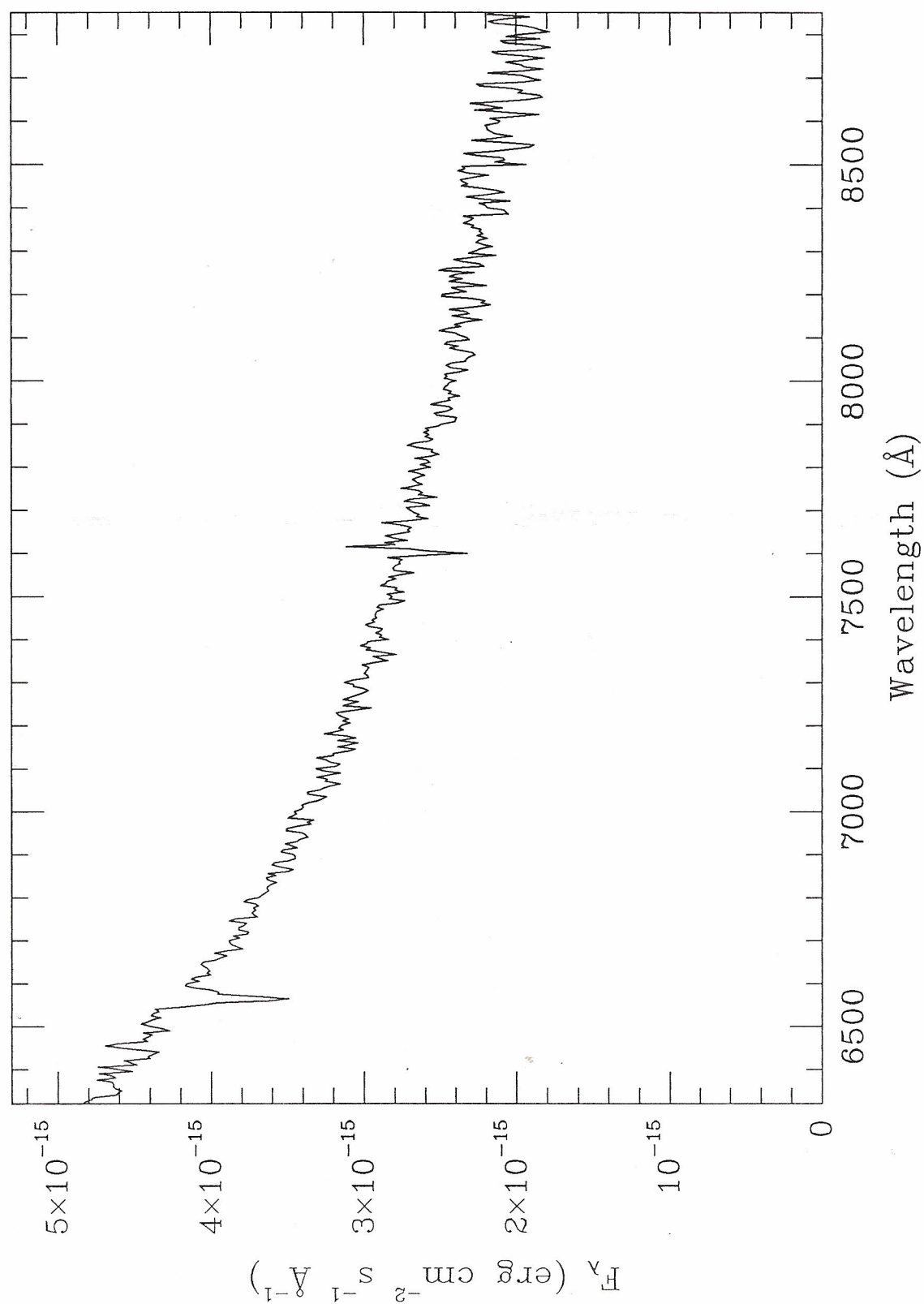
PG 1104+022 - 1990 May 6 6:32 UT



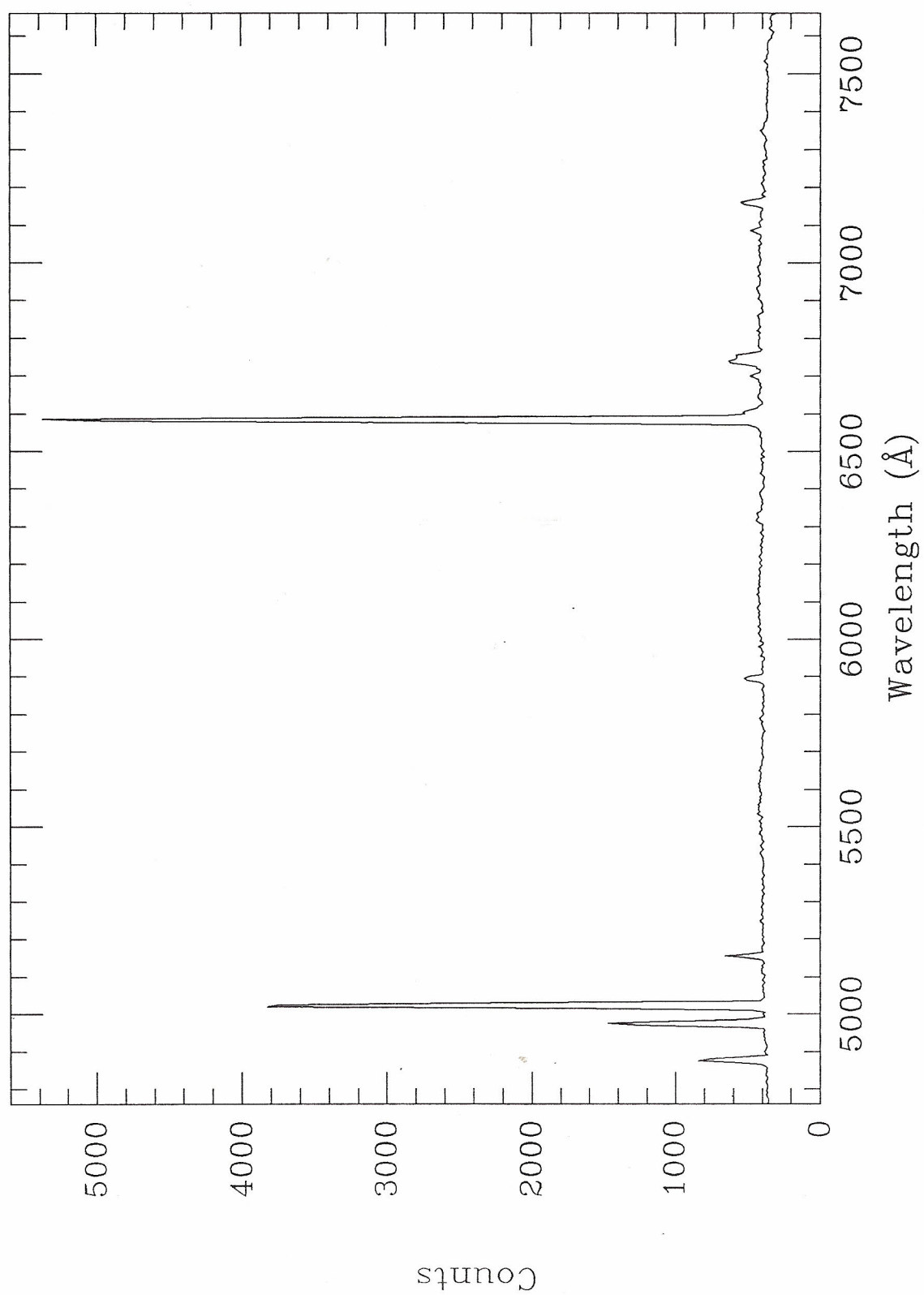
PG 1128+098 - 1990 May 3 05:16 UT



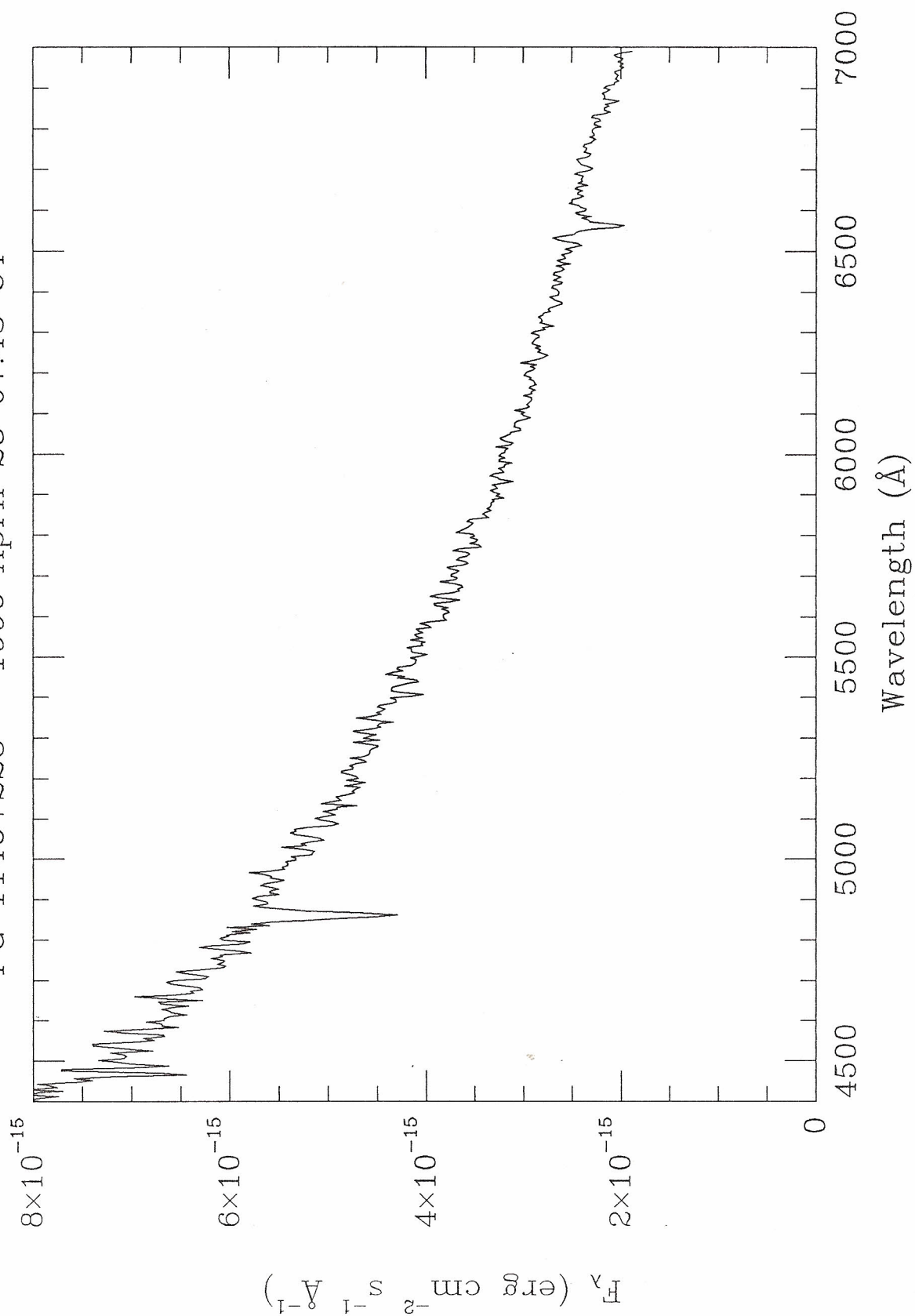
PG 1128+098 - 1990 May 5 6:26 UT



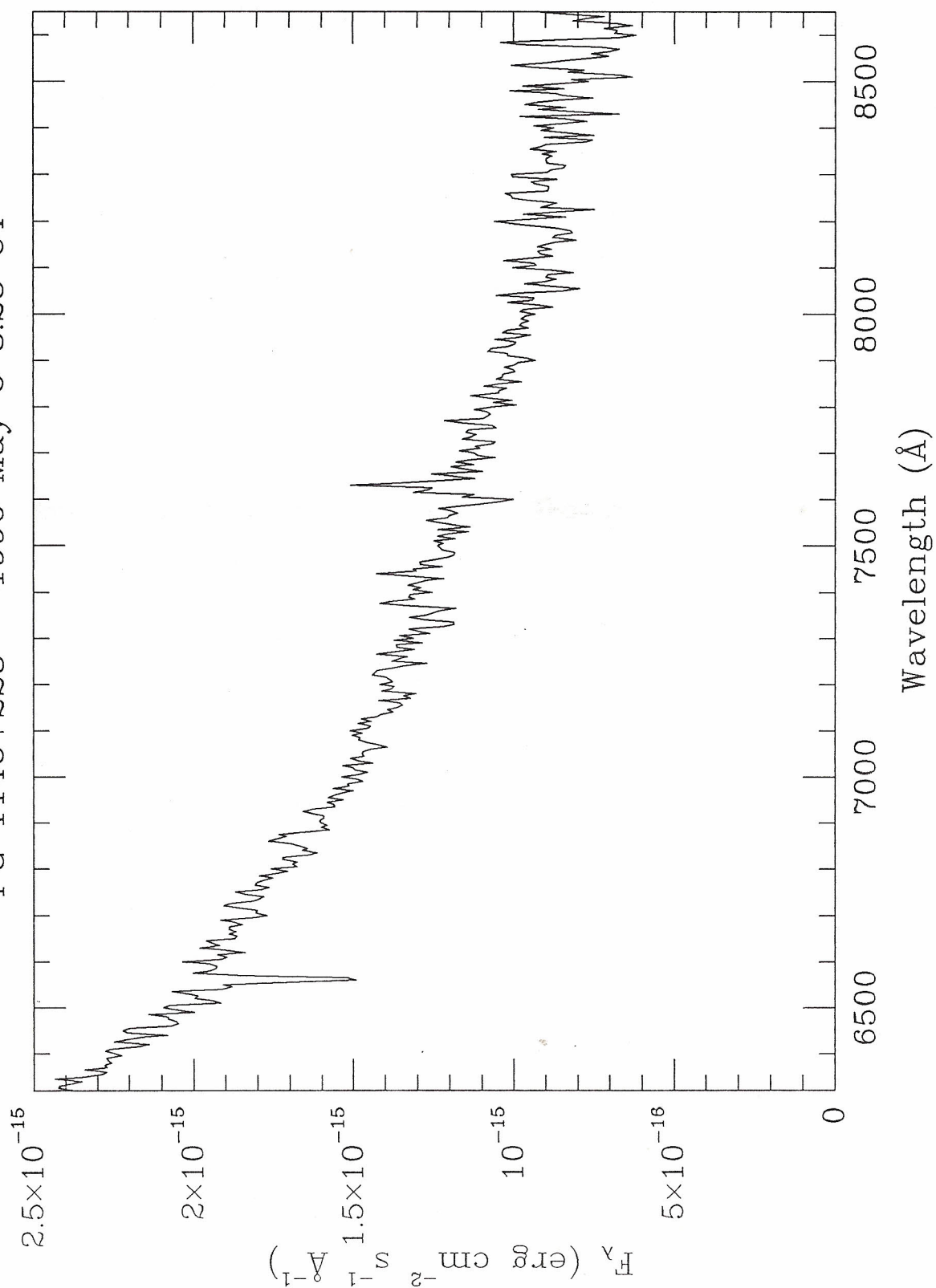
PG 1136+581 - 1990 February 6 11:18 UT



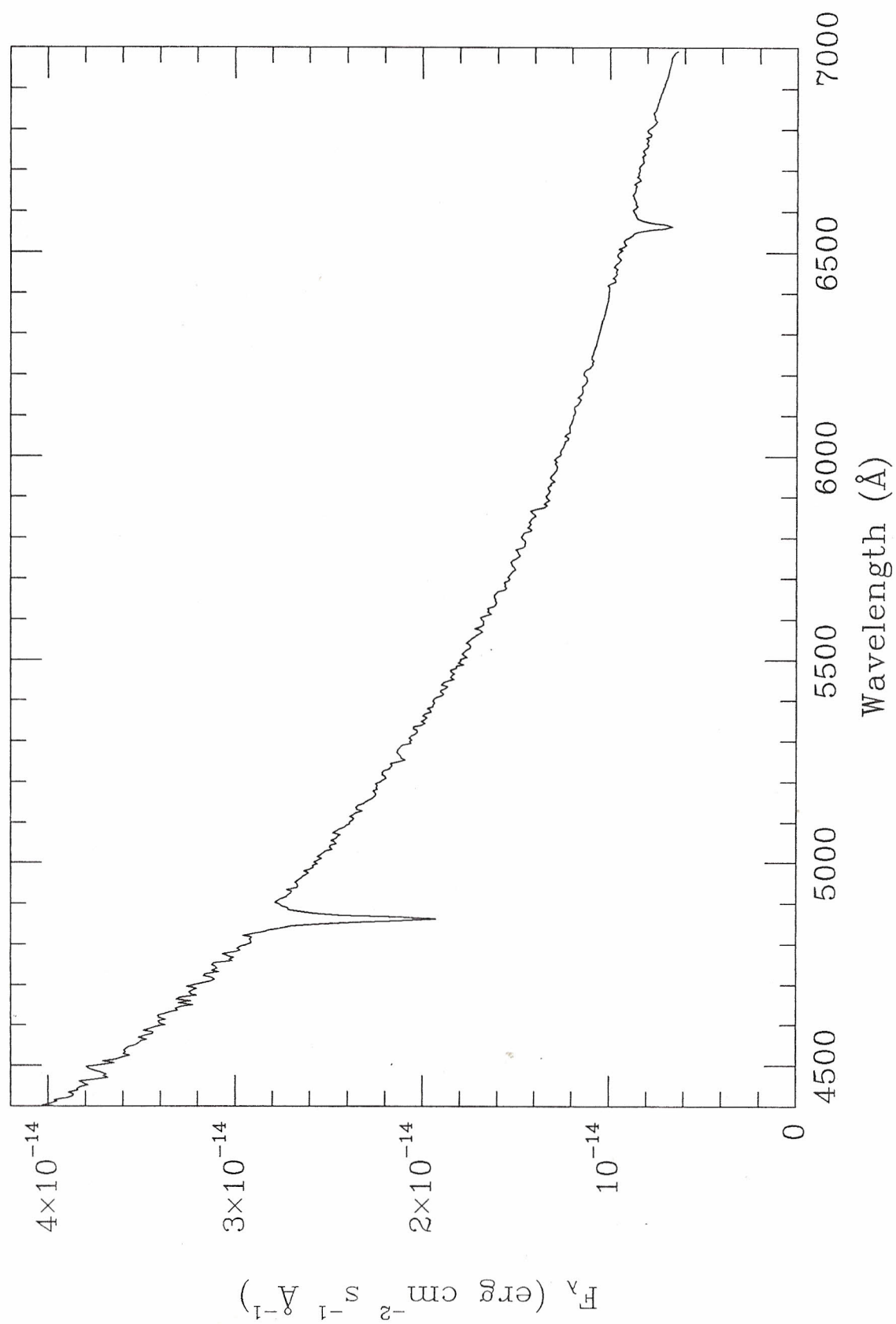
PG 1146+228 - 1990 April 28 07:43 UT



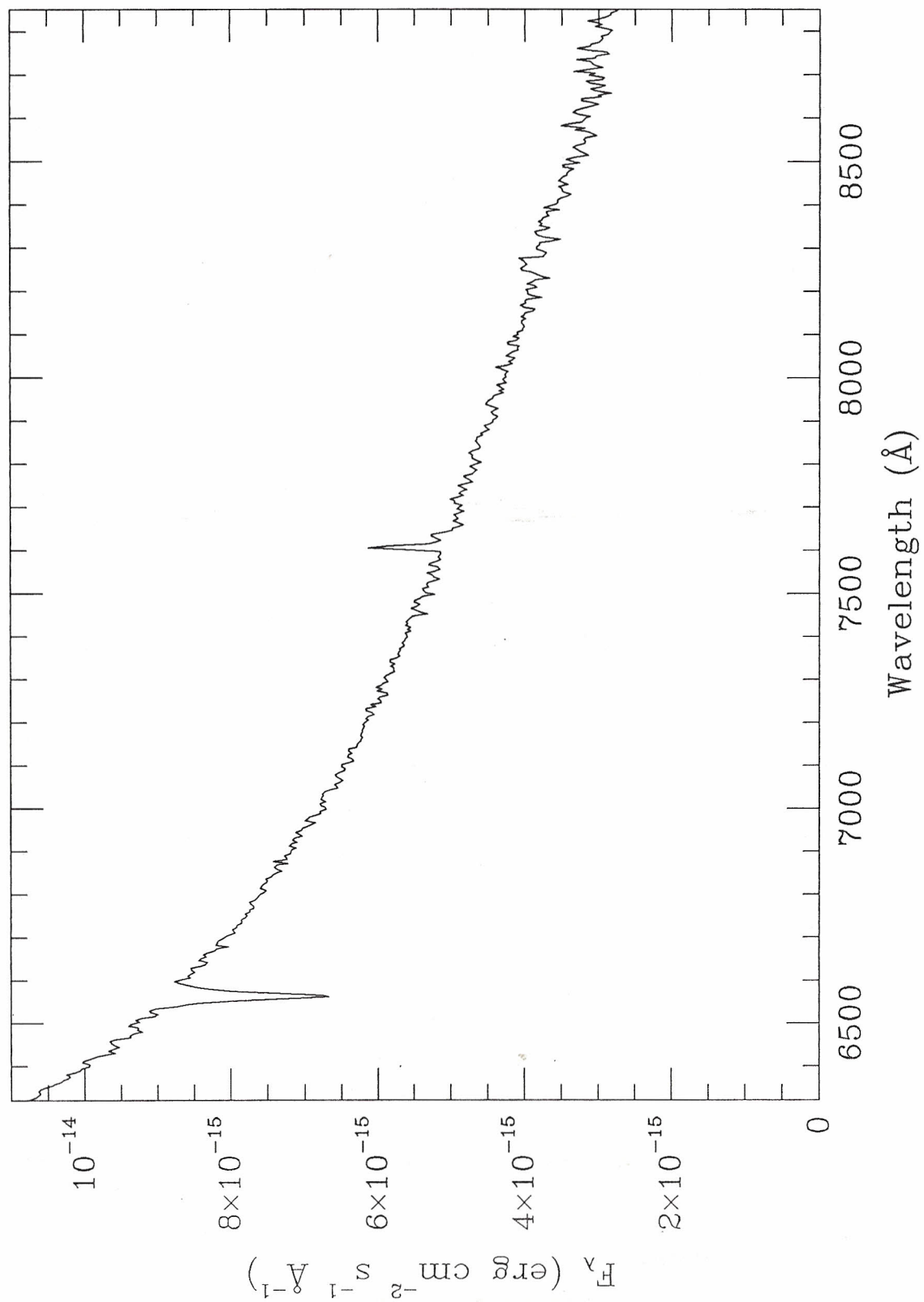
PG 1146+228 - 1990 May 6 8:28 UT



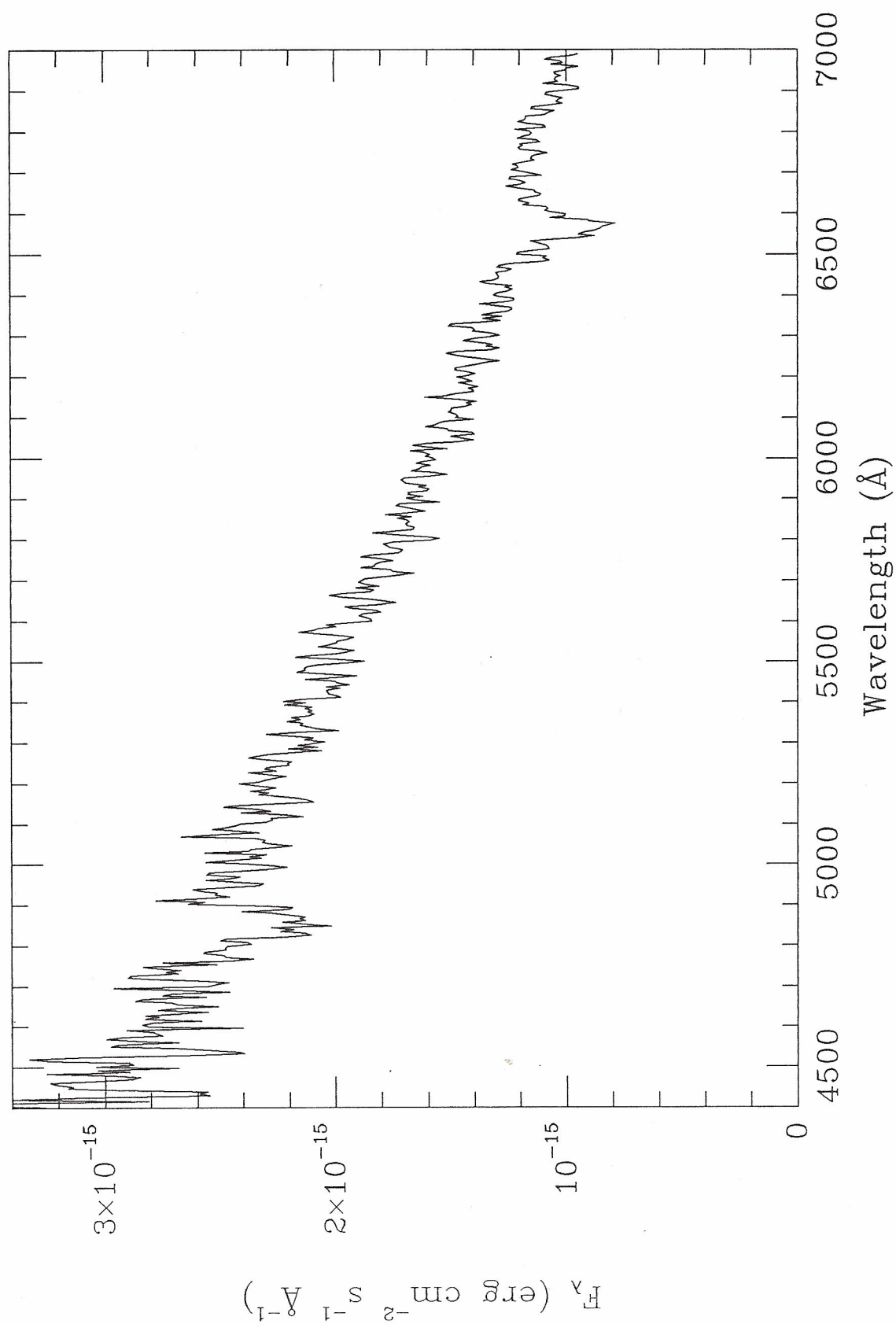
PG 1156-037 - 1990 April 28 08:02 UT



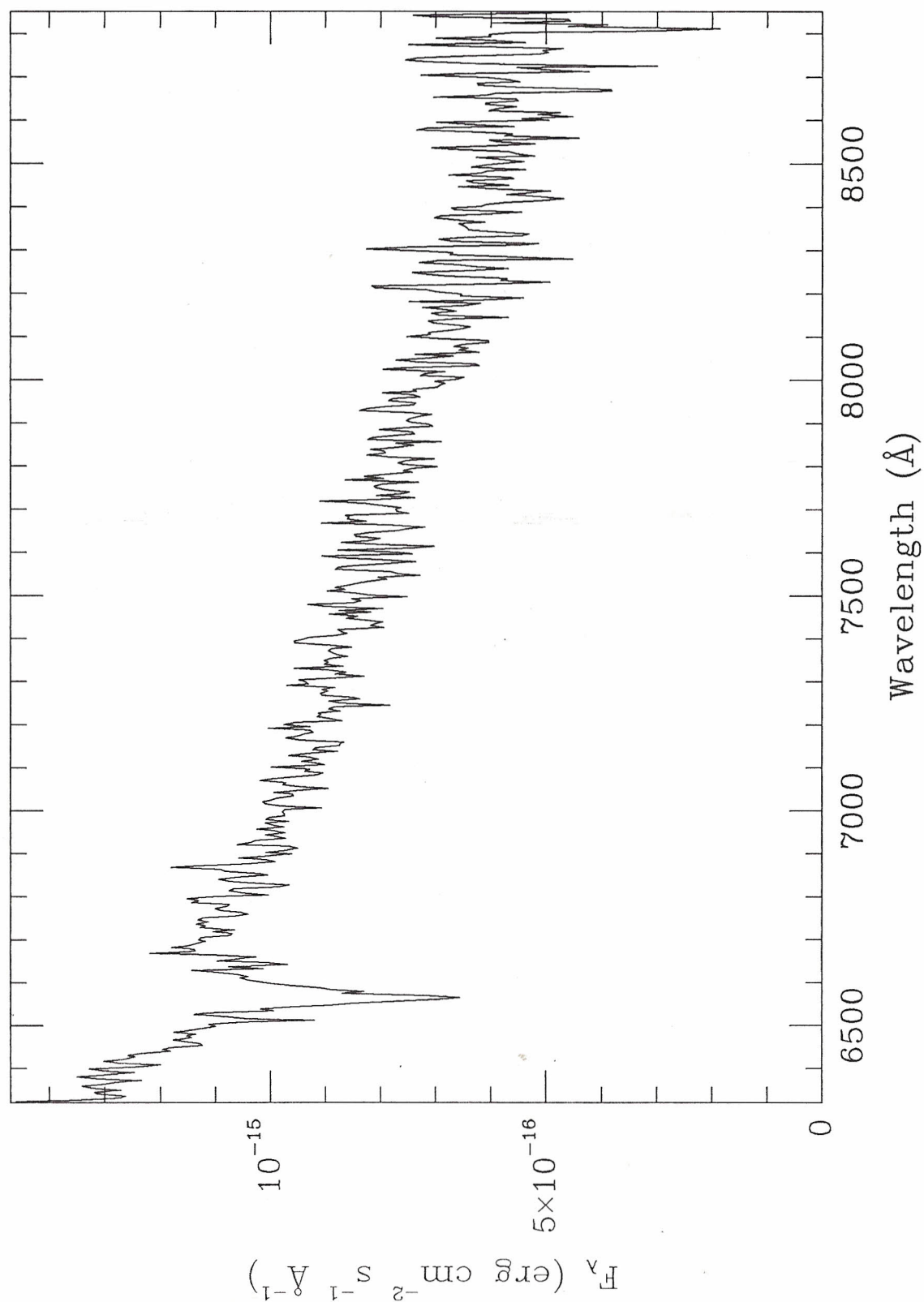
PG 1156-037 - 1990 May 7 4:14 UT



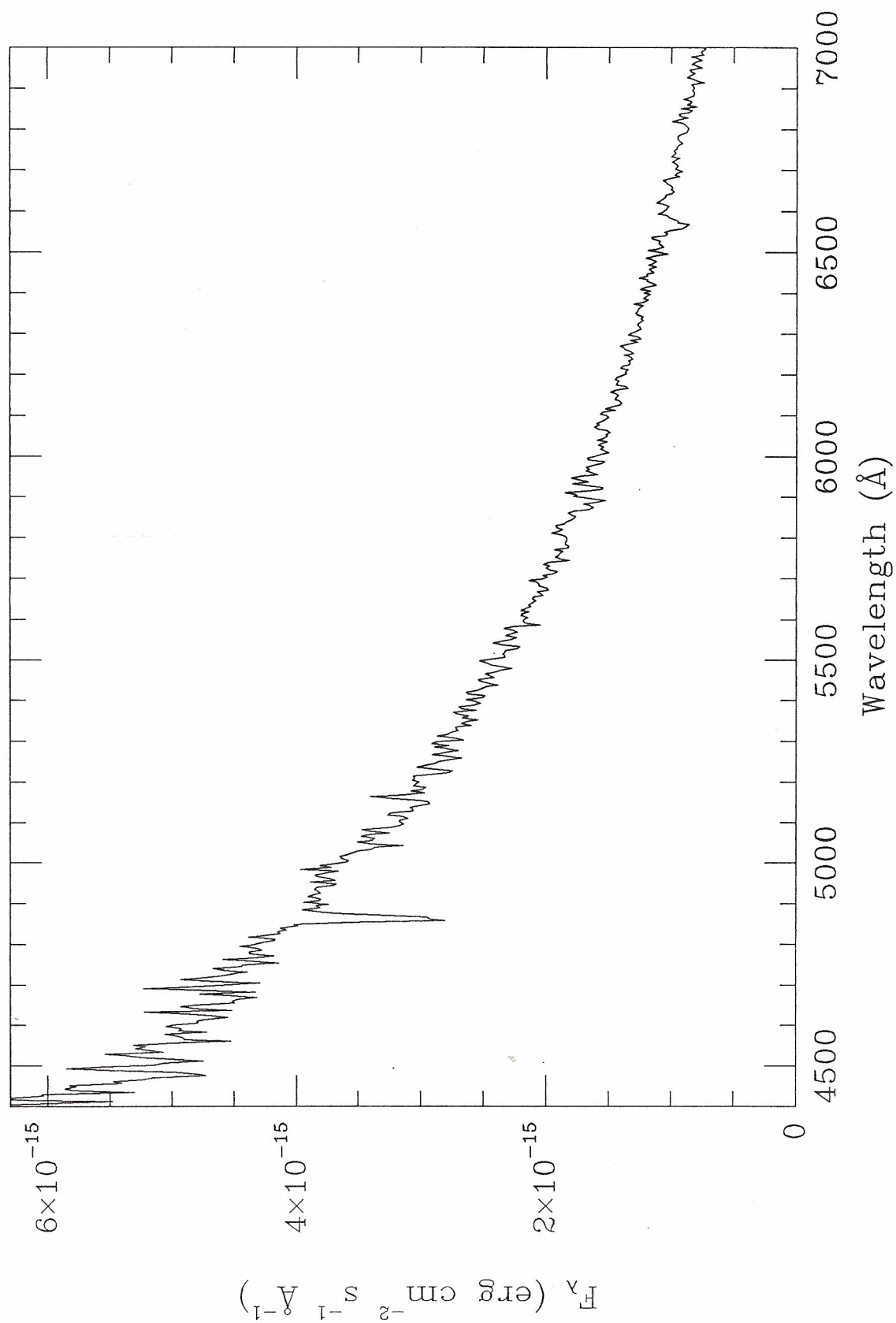
PG 1157+004 - 1990 April 28 08:27 UT



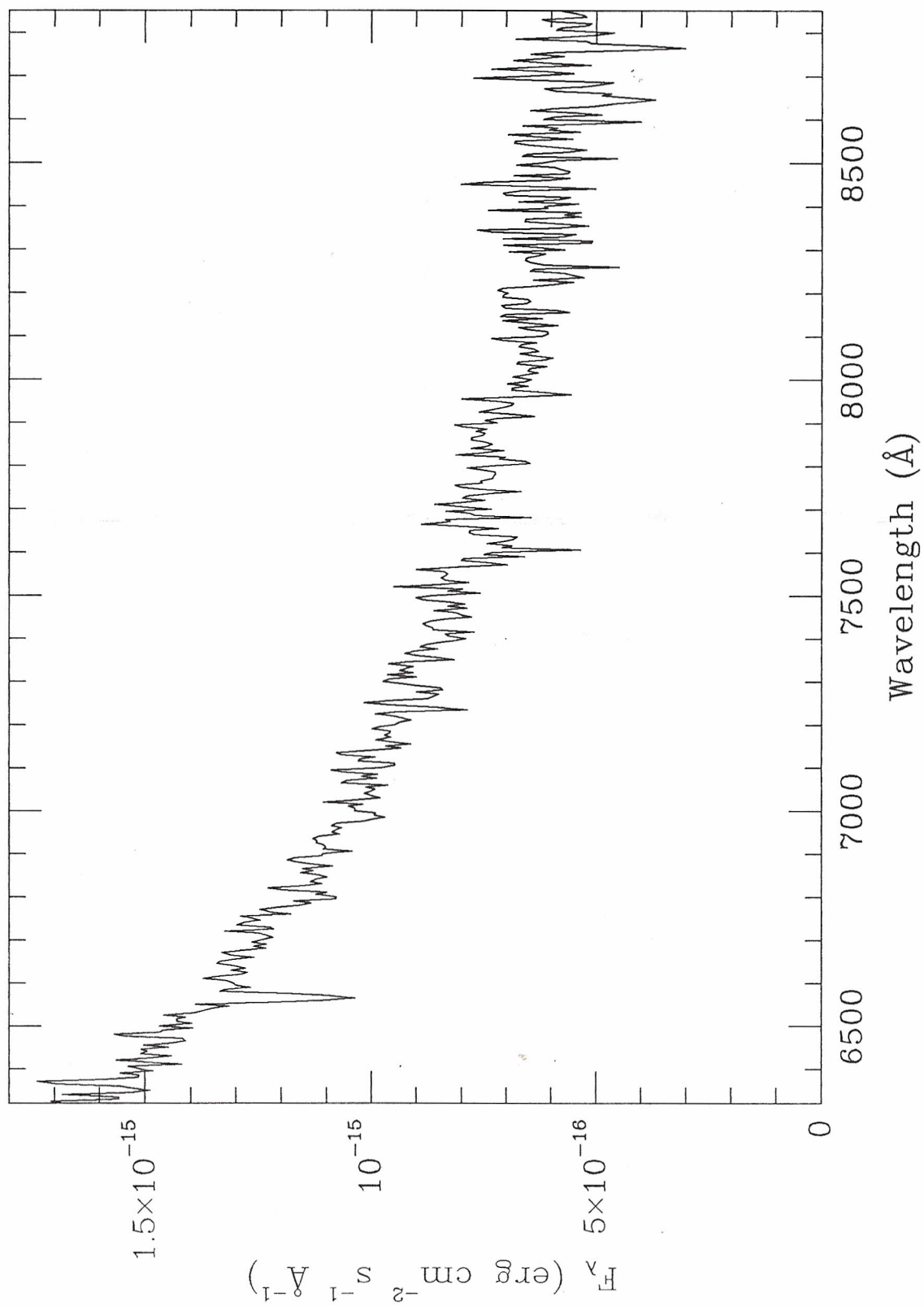
PG 1157+004 - 1990 May 7 4:34 UT



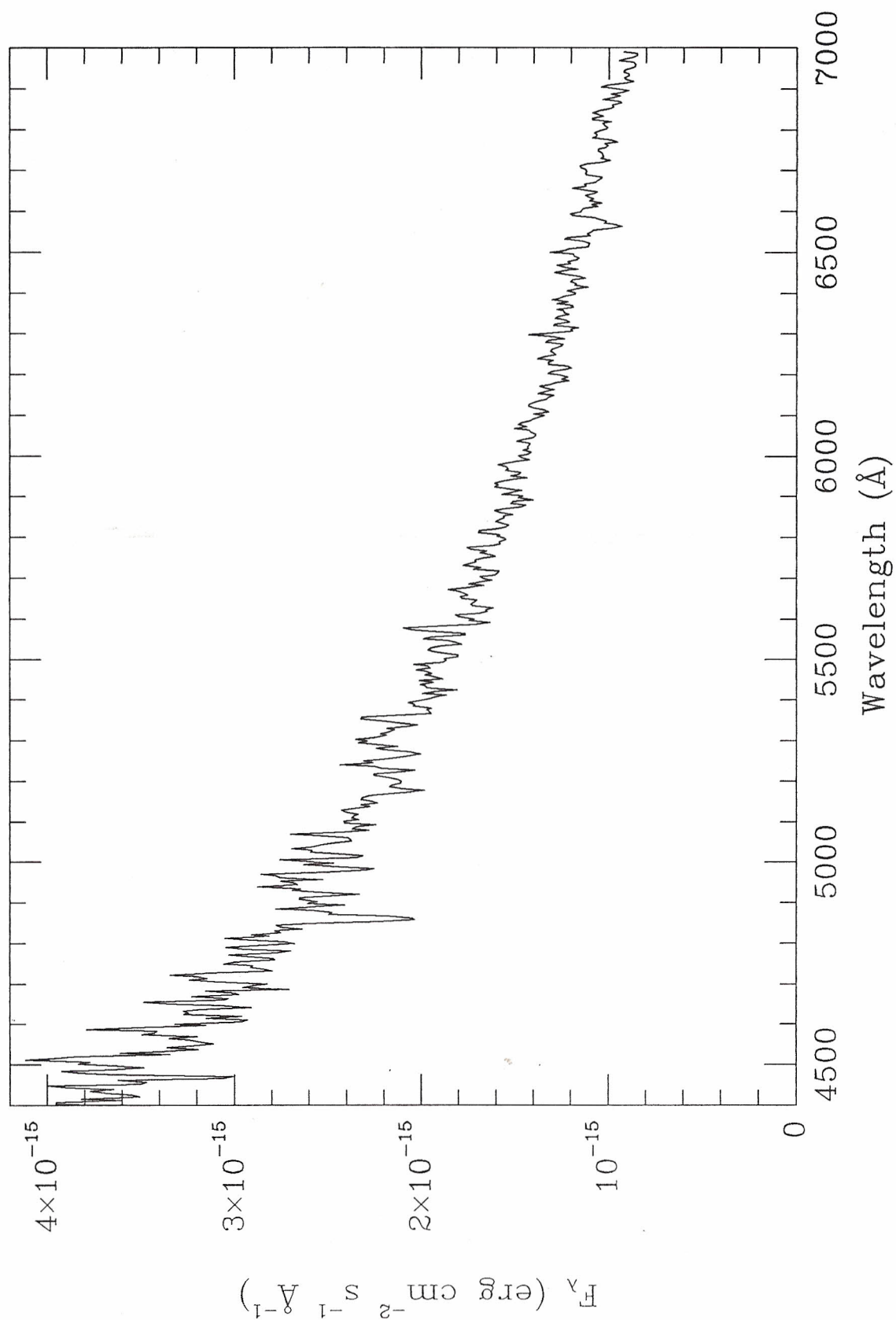
PG 1217-067 - 1990 May 3 07:40 UT



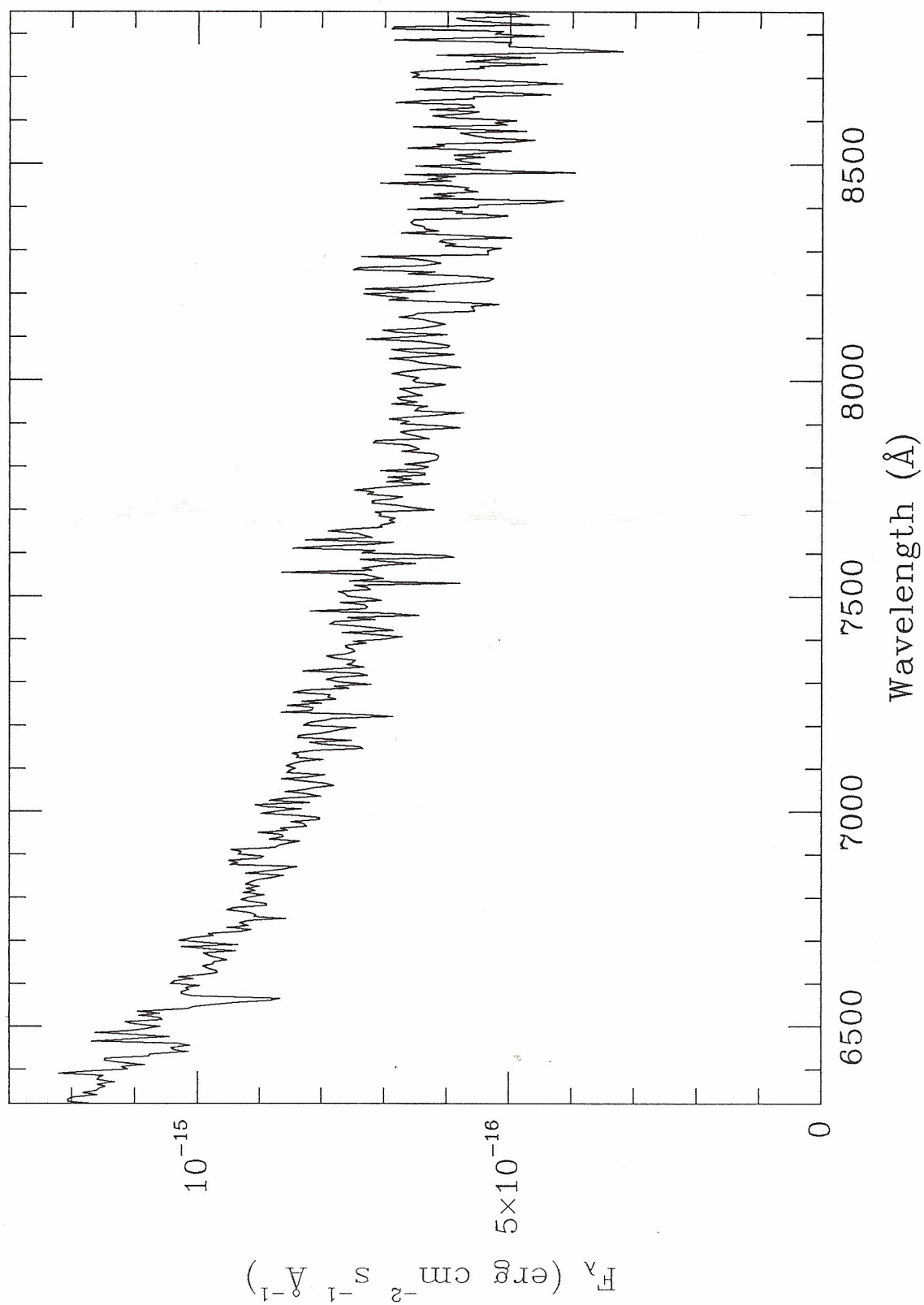
PG 1217-067 - 1990 May 5 6:59 UT



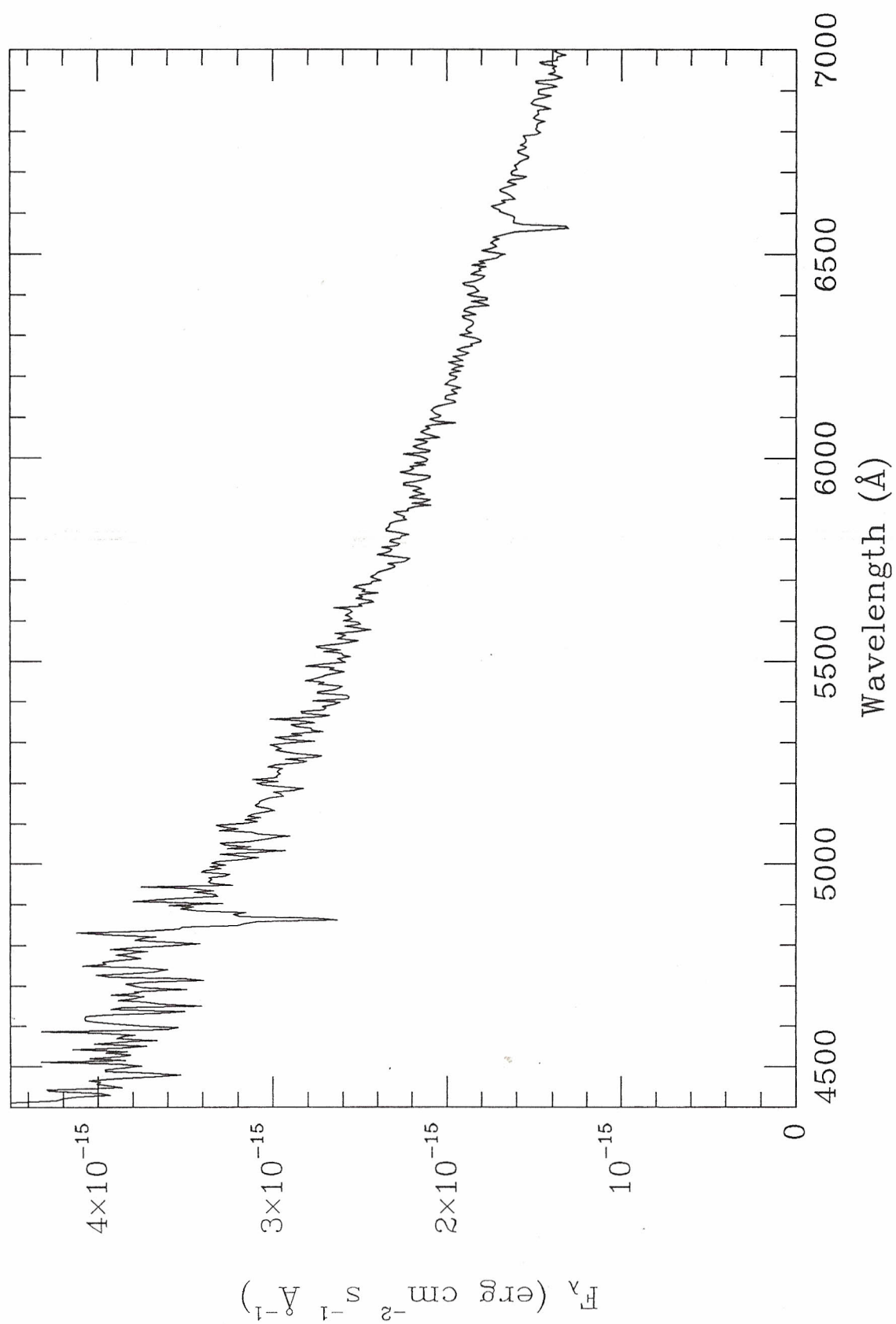
PG 1314+041 - 1990 April 28 08:45 UT



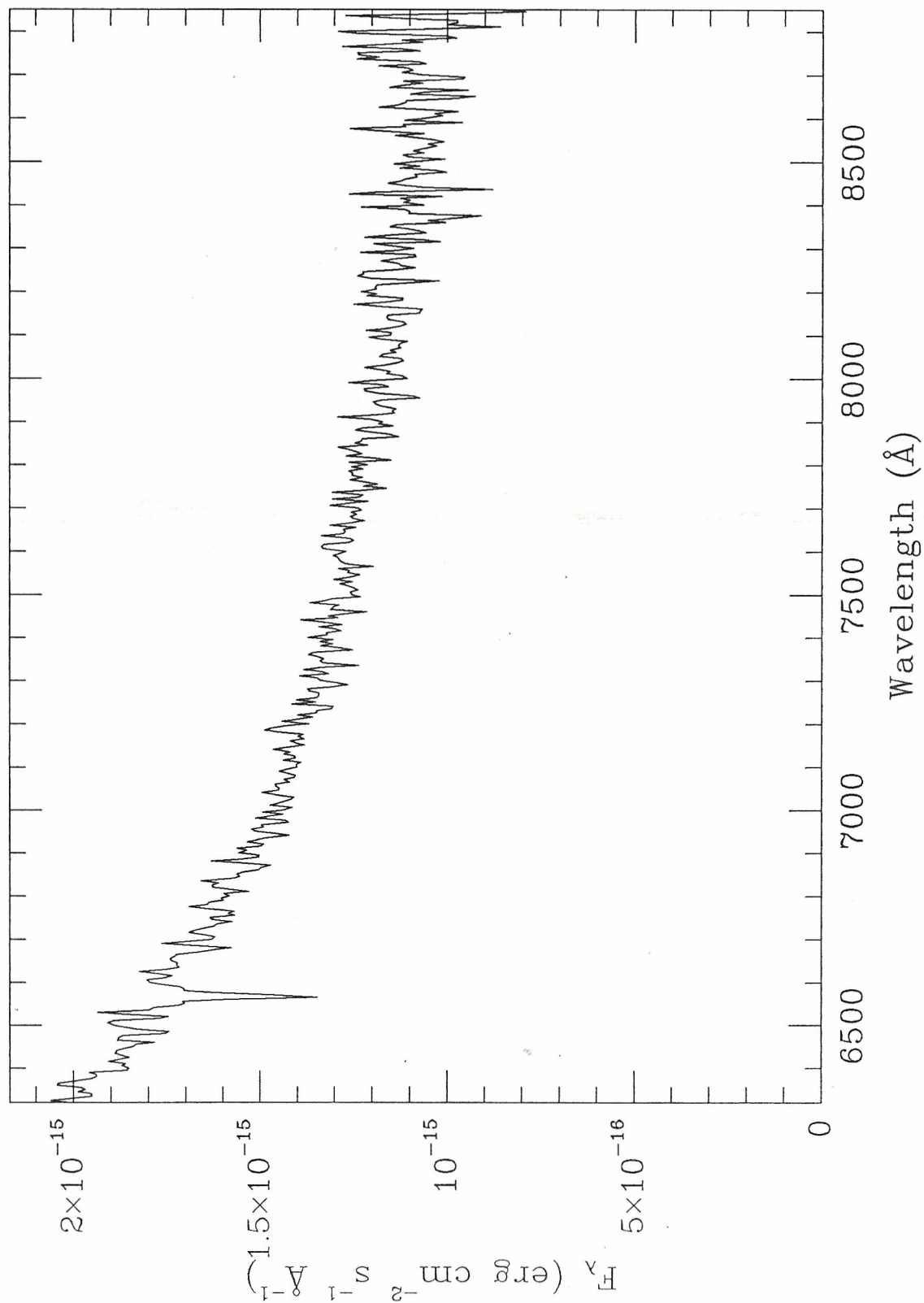
PG 1314+041 - 1990 May 5 7:19 UT



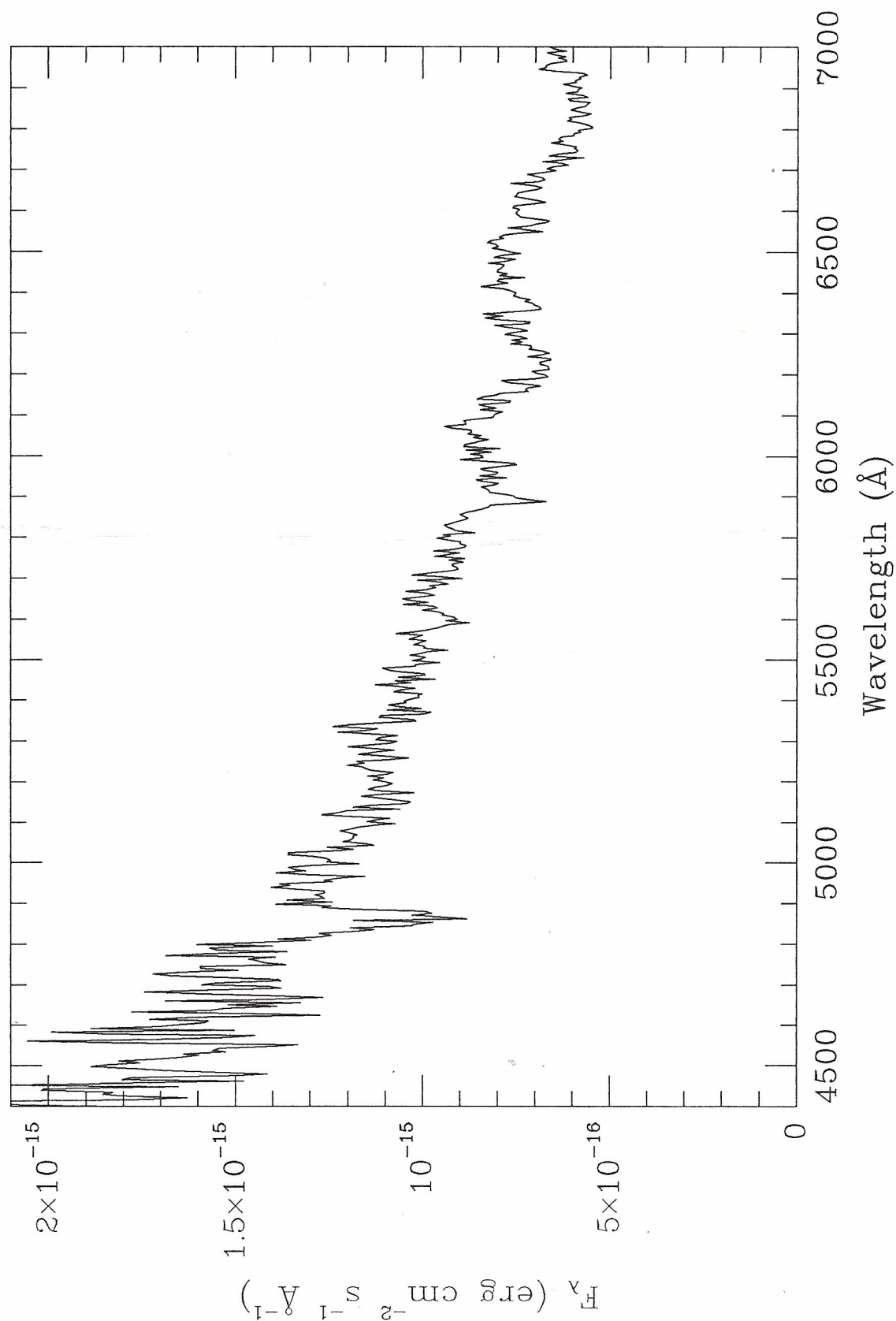
PG 1315-123 - 1990 May 3 08:06 UT



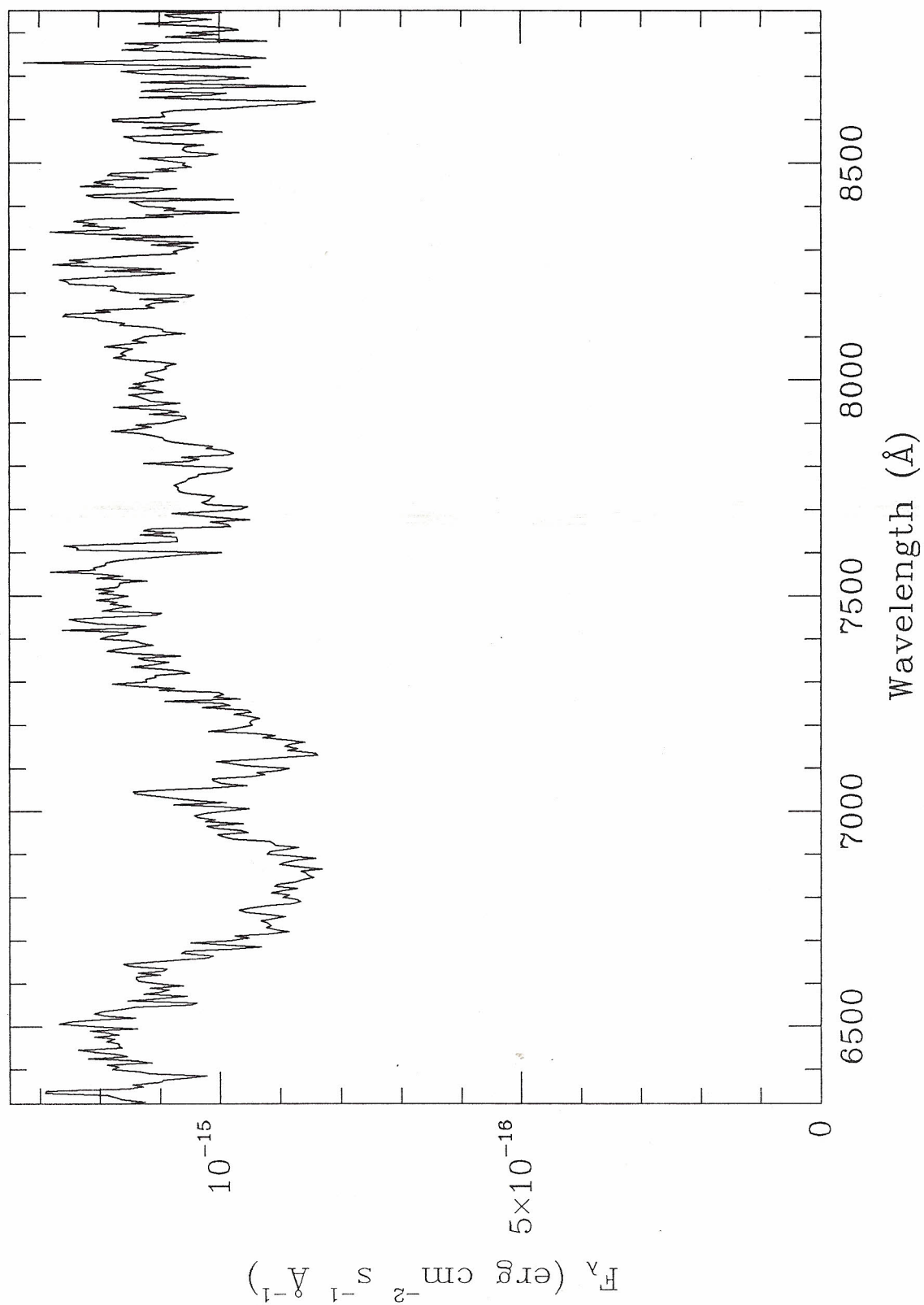
PG 1315-123 - 1990 May 5 7:41 UT



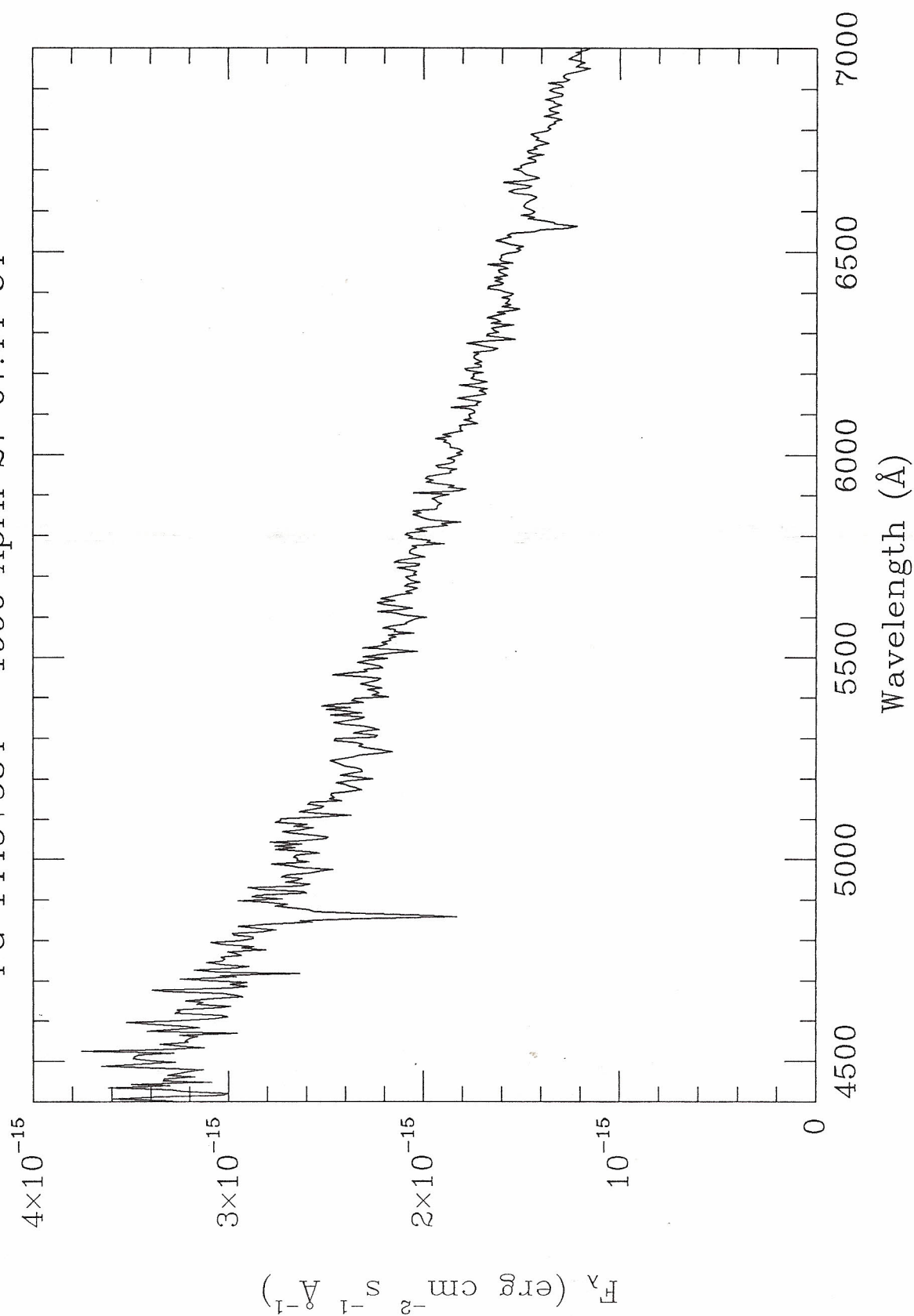
PG 1443+337 - 1990 May 3 08:52 UT



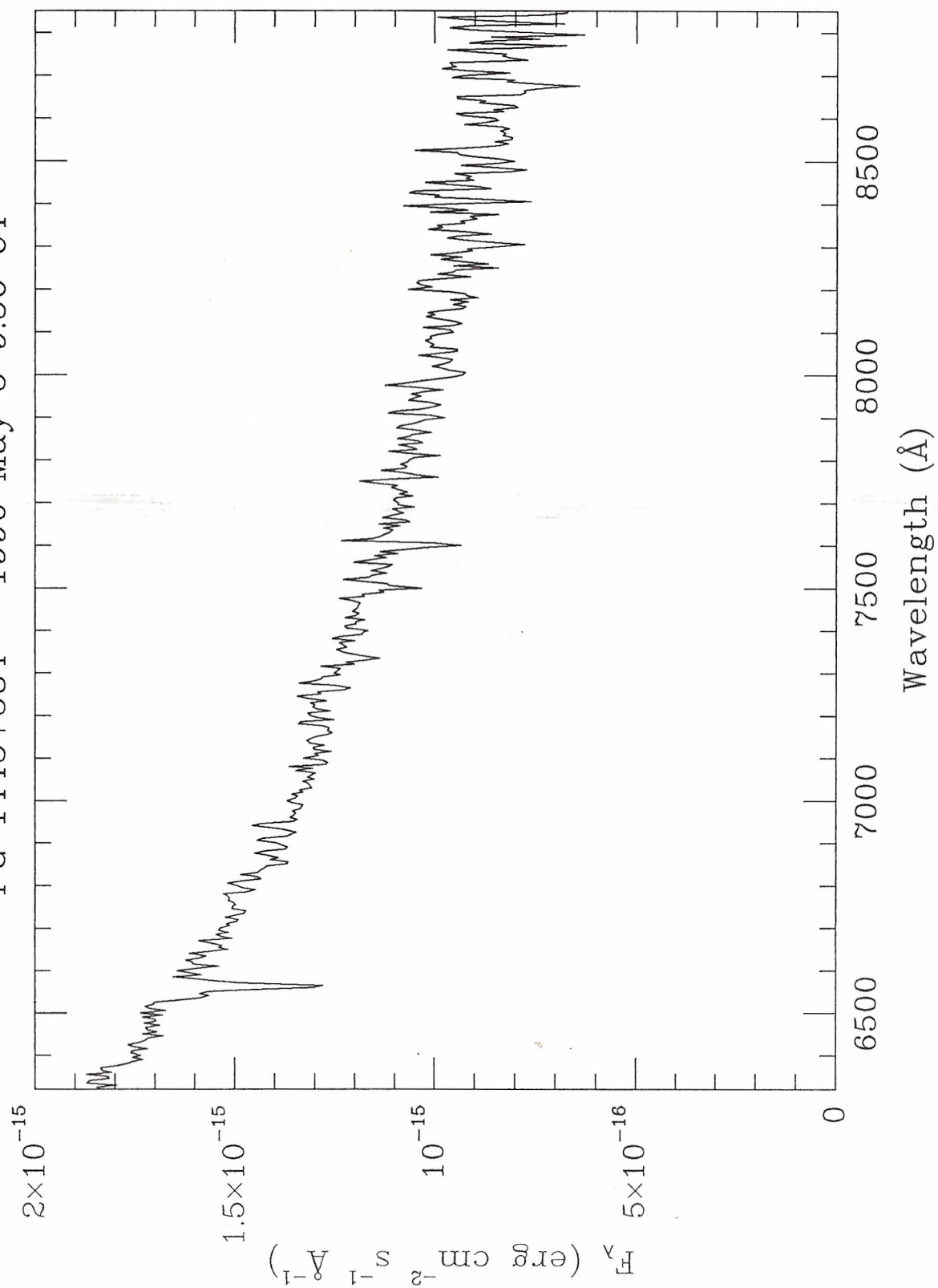
PG 1443+337 - 1990 May 5 9:07 UT



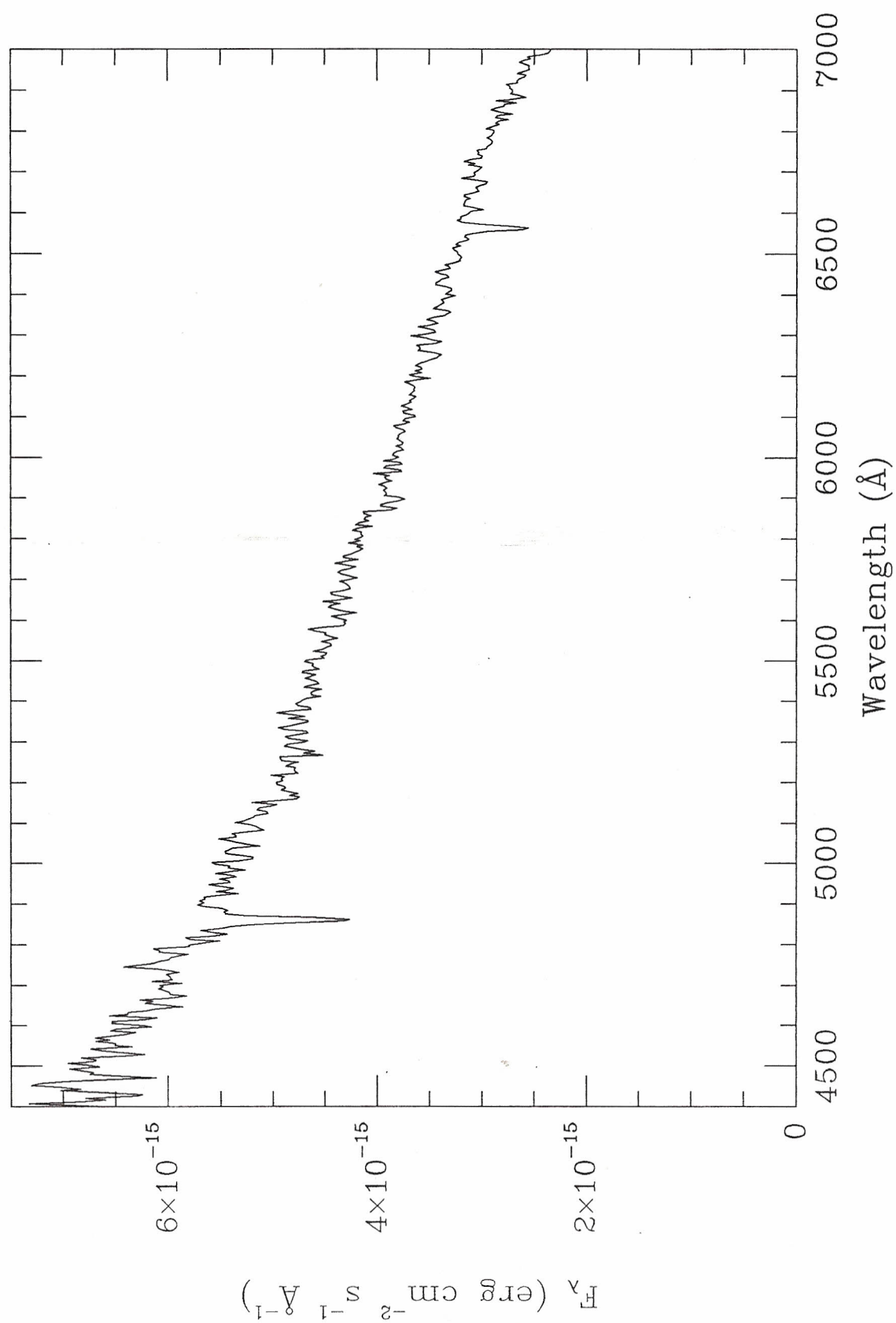
PG 1445+584 - 1990 April 27 07:44 UT



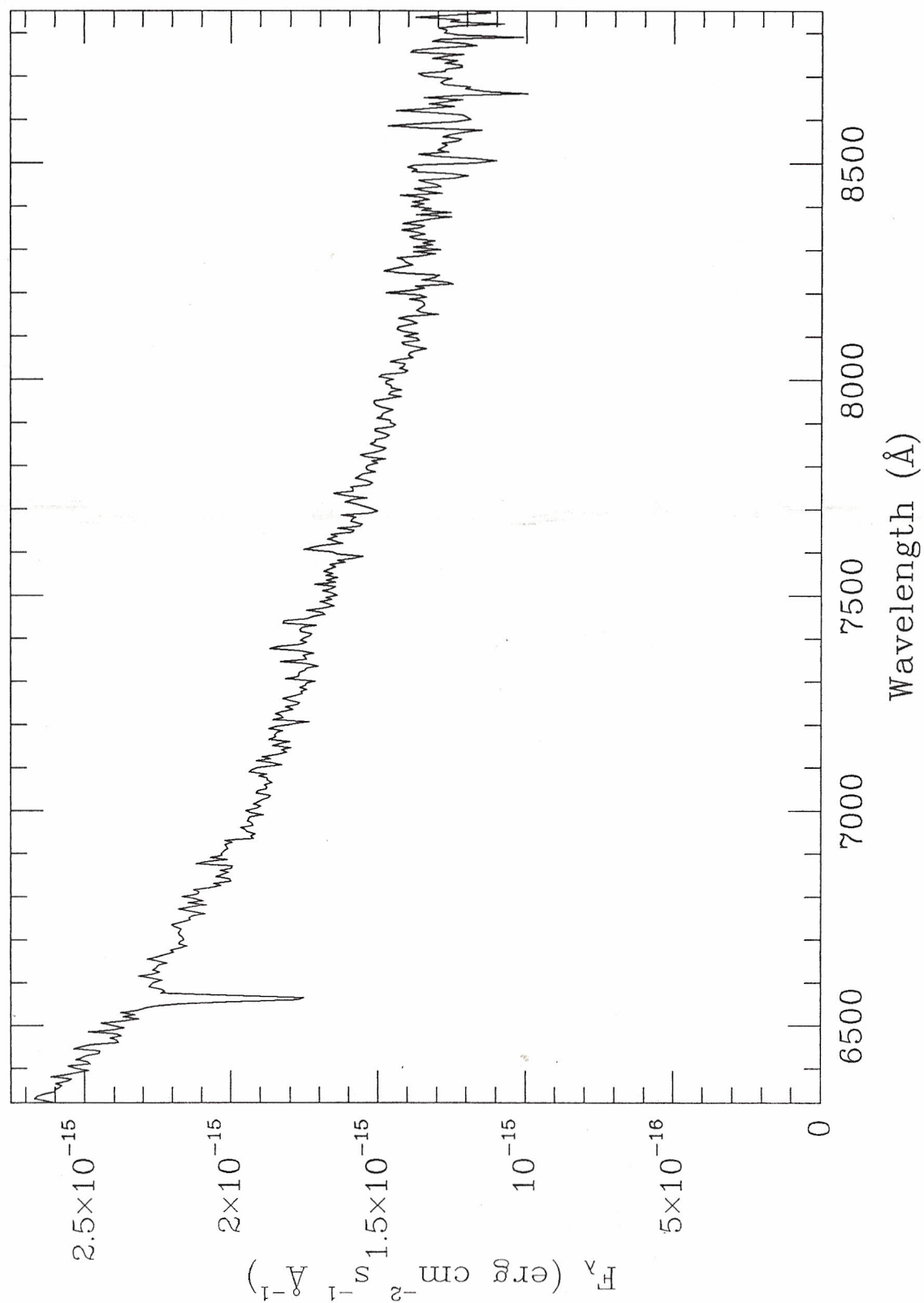
PG 1445+584 - 1990 May 5 9:56 UT



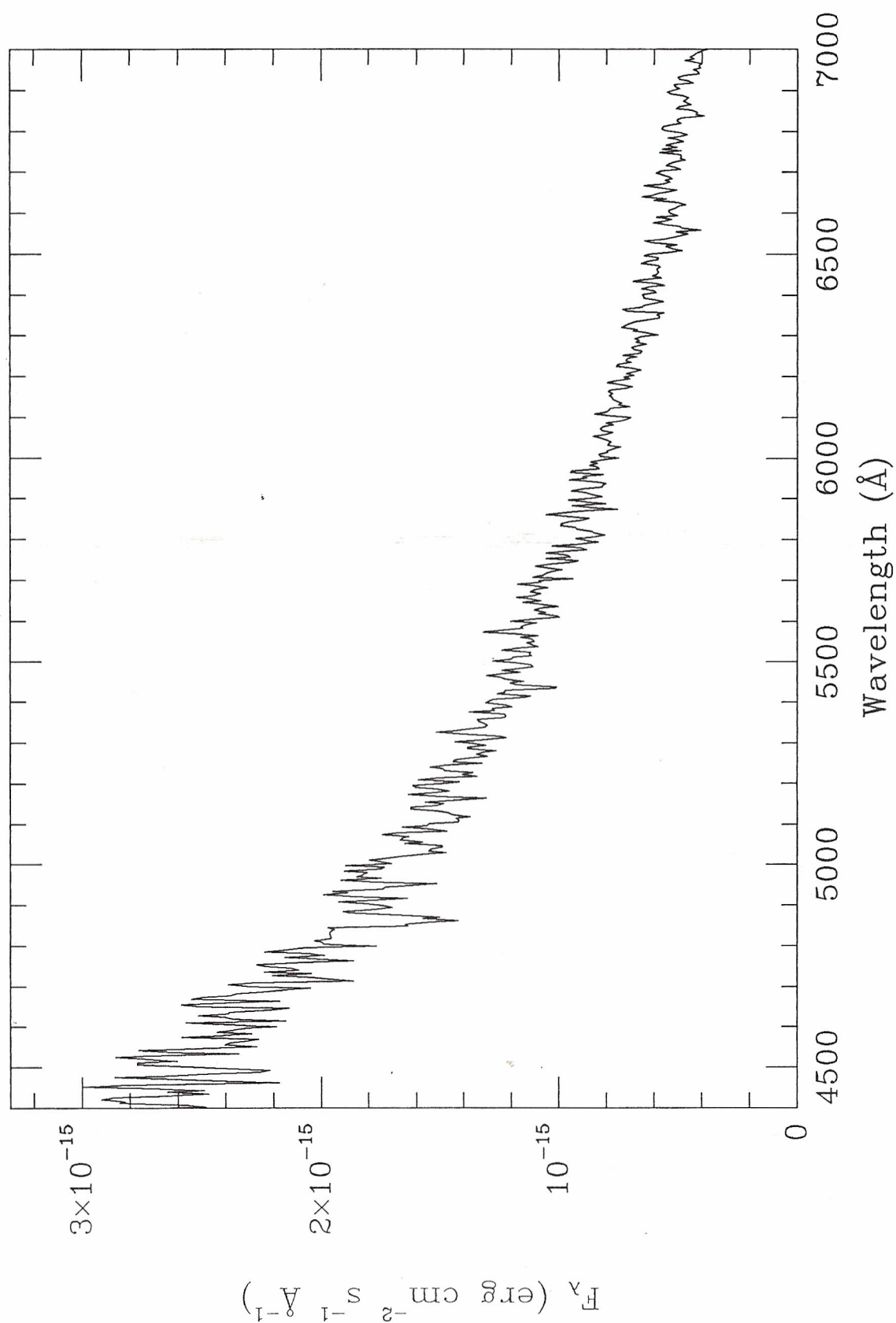
PG 1459-026 - 1990 April 27 09:05 UT



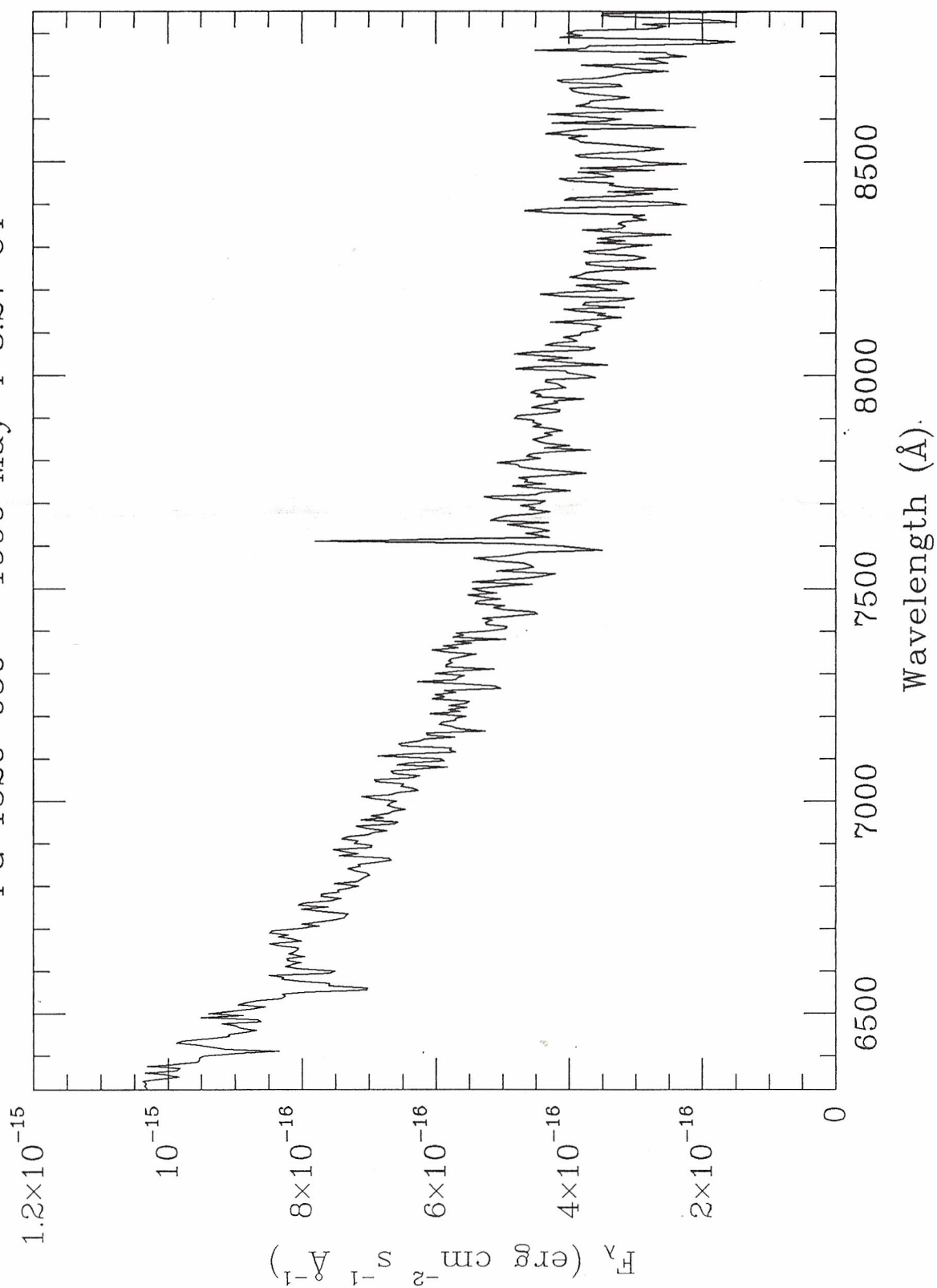
PG 1459-026 - 1990 May 6 8:47 UT



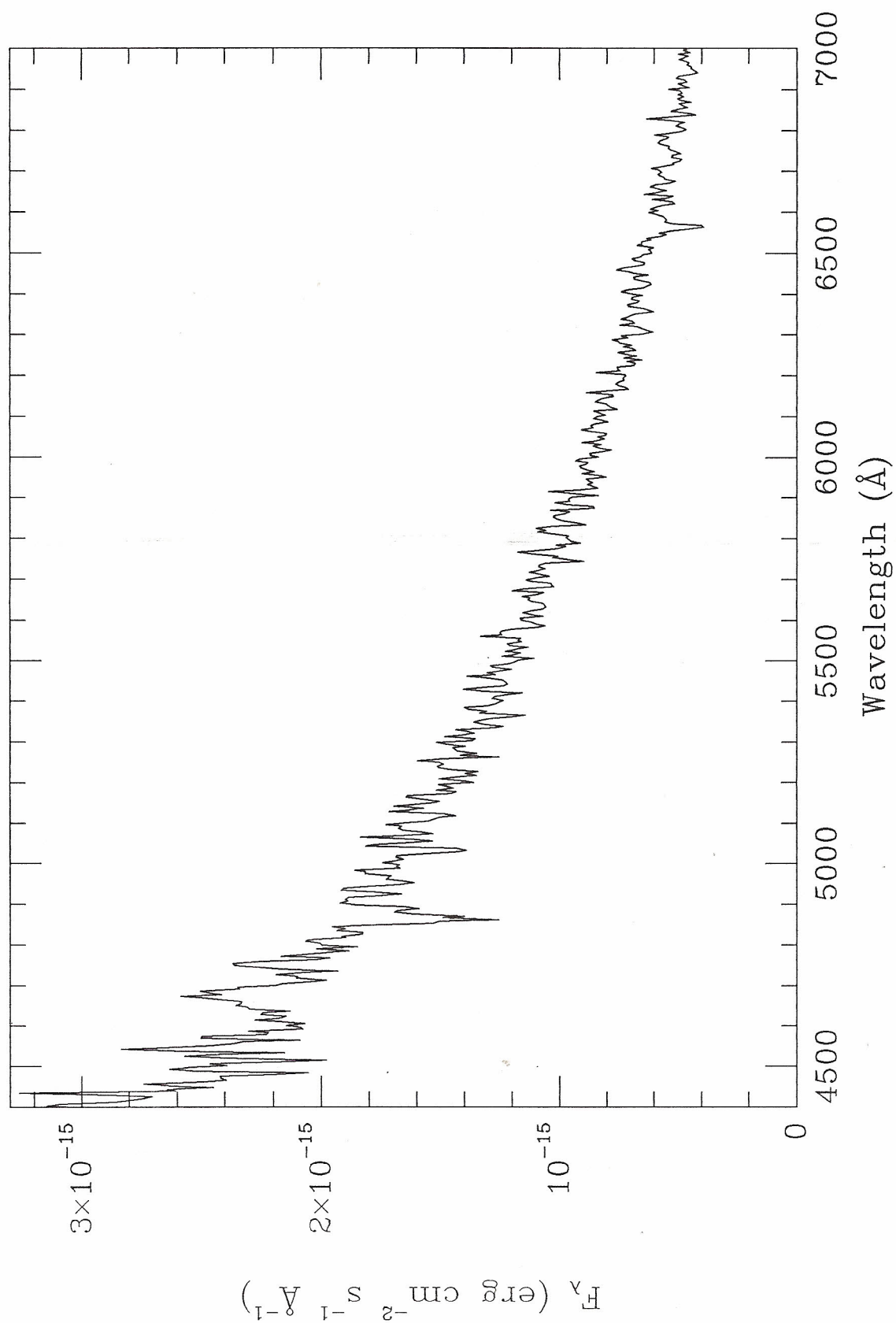
PG 1520-050 - 1990 April 27 09:49 UT



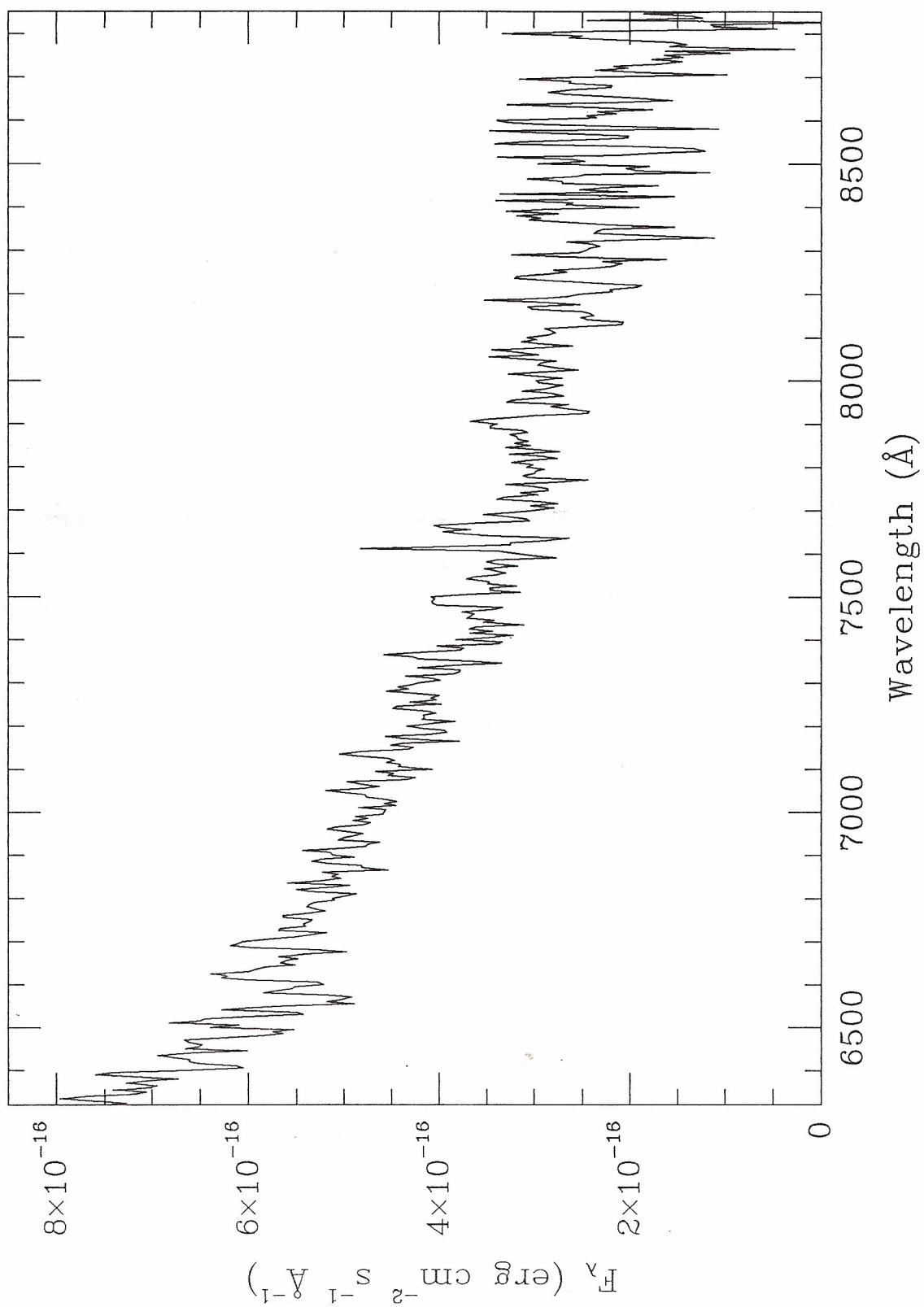
PG 1520-050 - 1990 May 4 8:27 UT



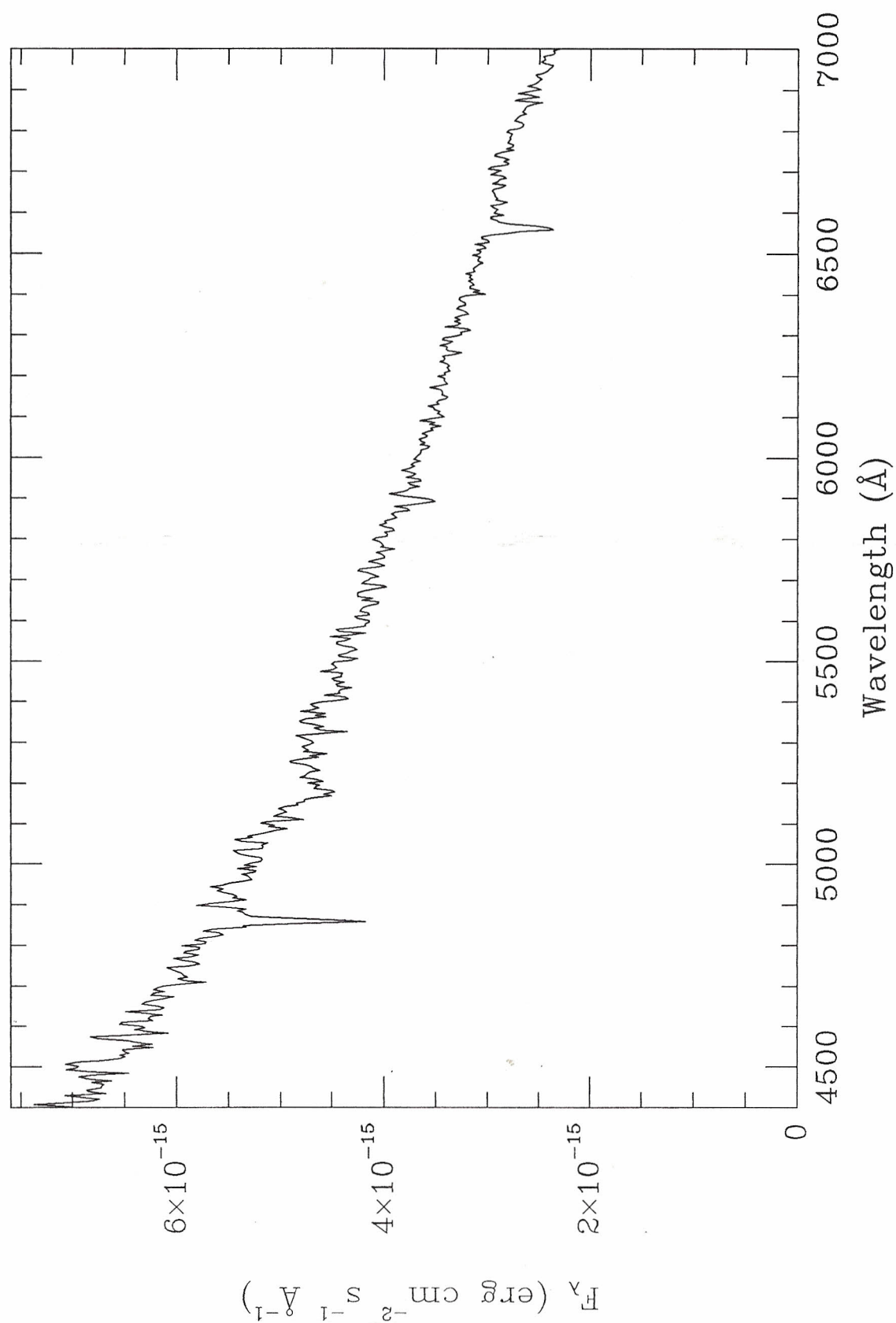
PG 1522+122 - 1990 April 27 10:12 UT



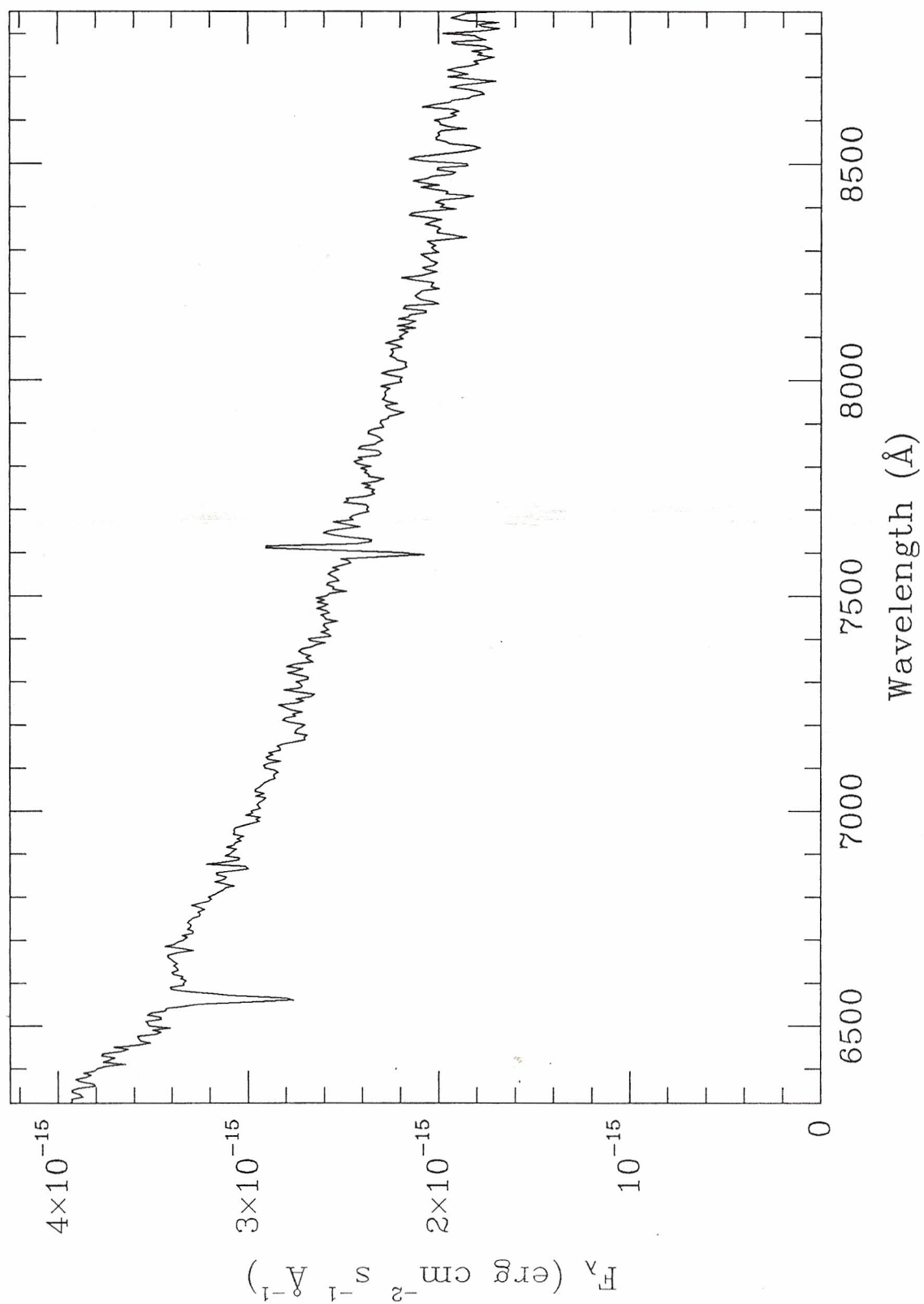
PG 1522+122 - 1990 May 4 8:53 UT



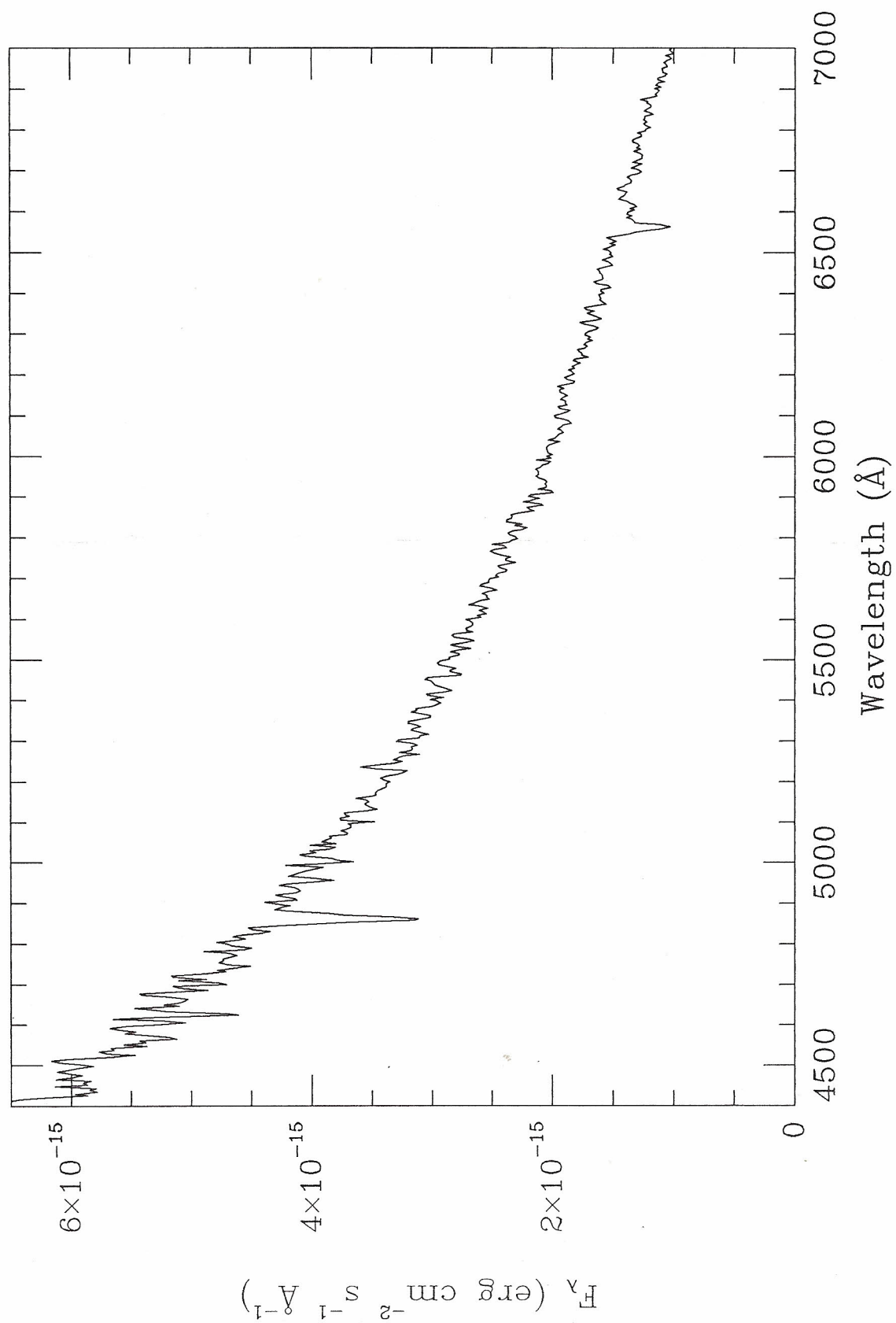
PG 1617+150 - 1990 April 27 10:54 UT



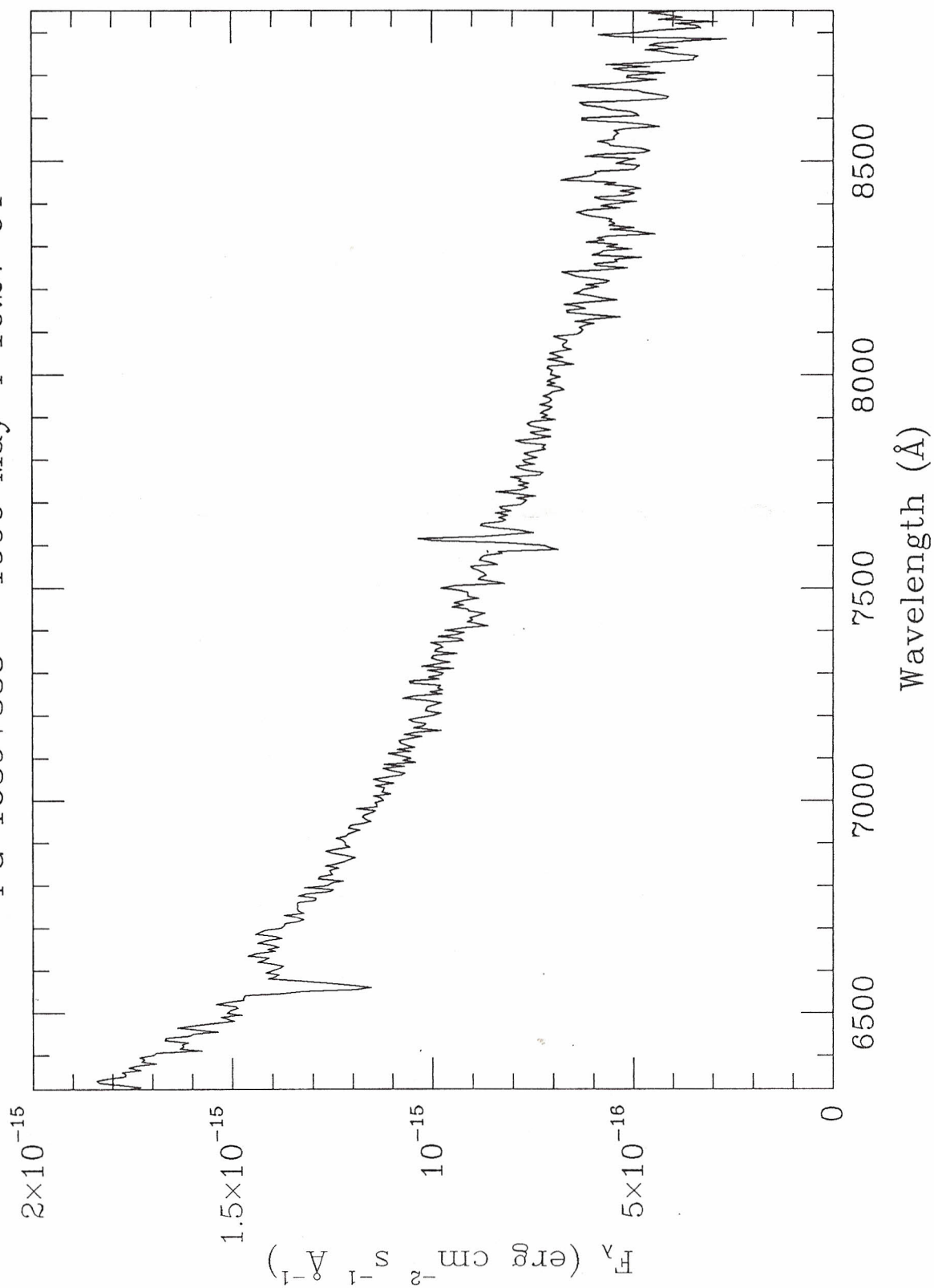
PG 1617+150 - 1990 May 4 9:34 UT



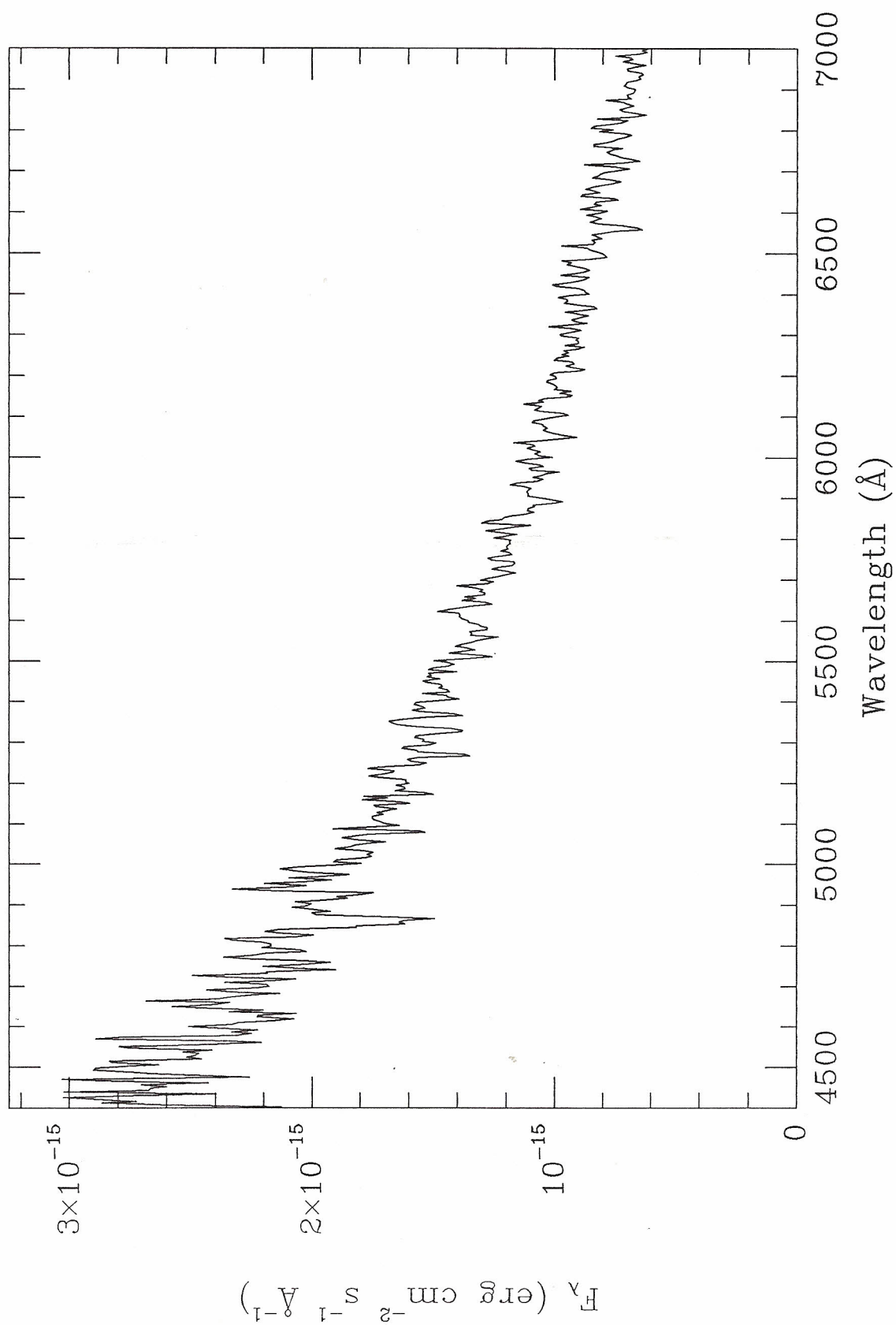
PG 1639+338 - 1990 April 27 11:15 UT



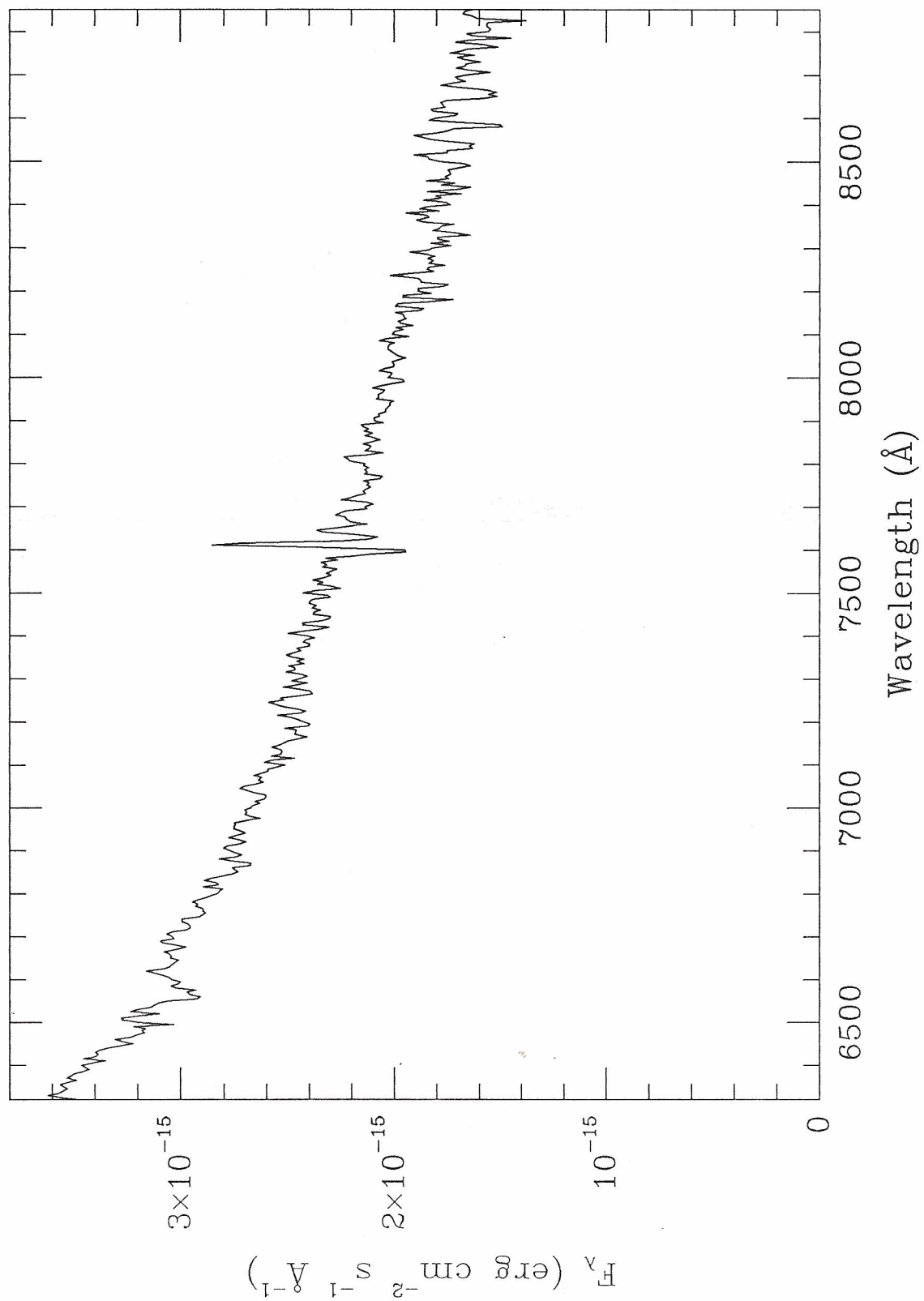
PG 1639+338 - 1990 May 4 10:27 UT



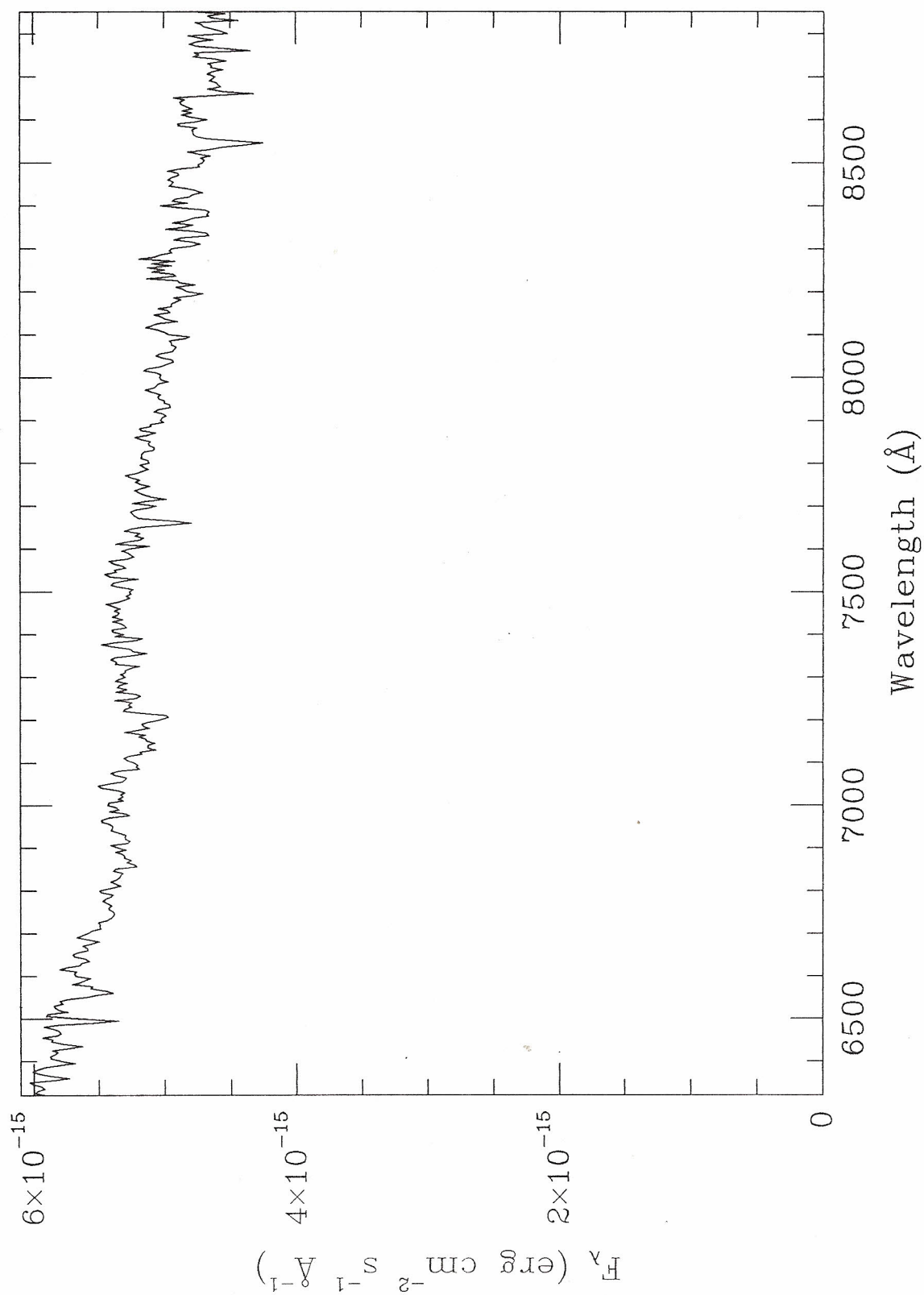
PG 1657+656 - 1990 April 27 11:42 UT



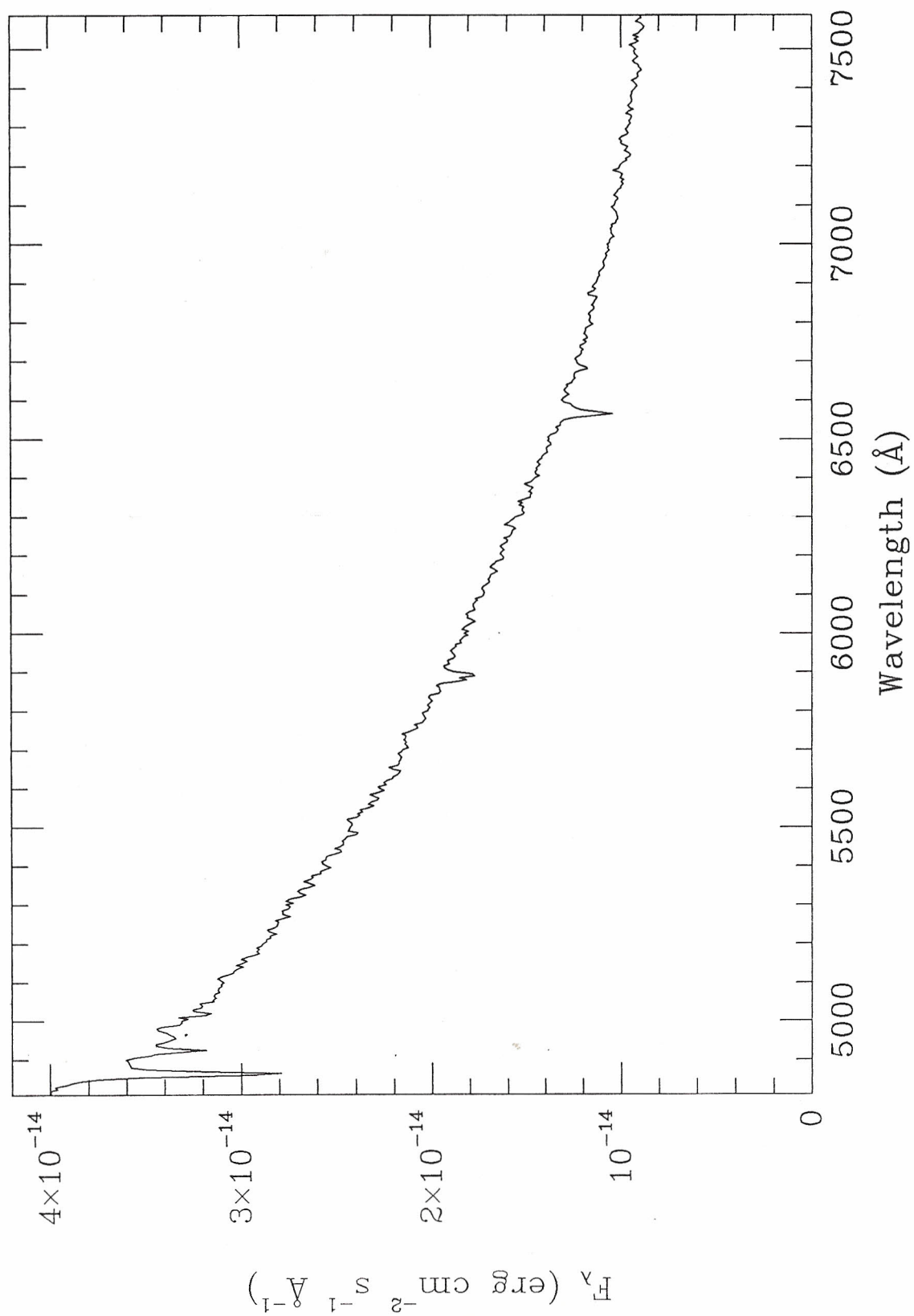
PG 1710+566 - 1990 May 4 11:39 UT



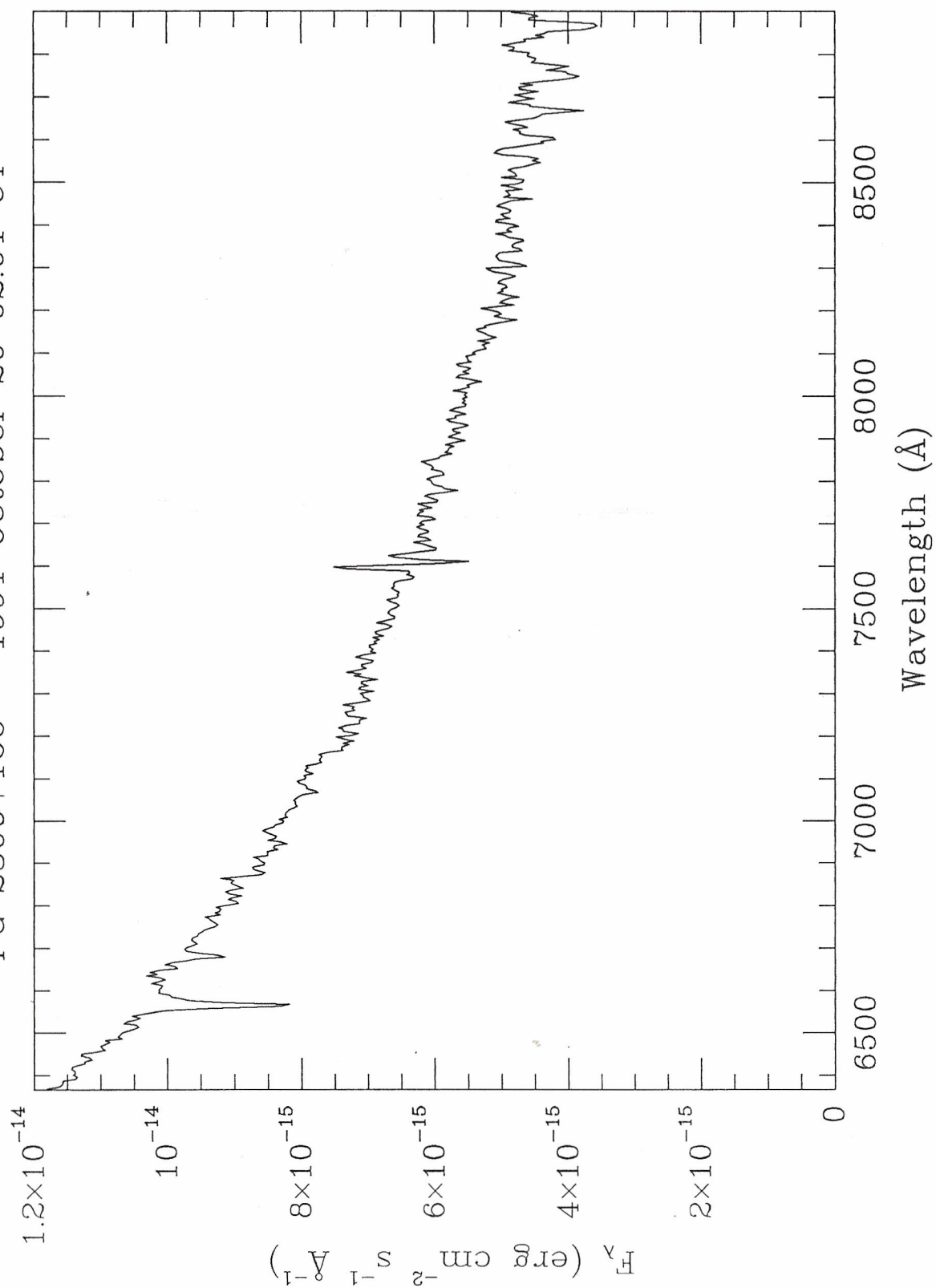
PG 2200+085 - 1990 May 6 11:41 UT



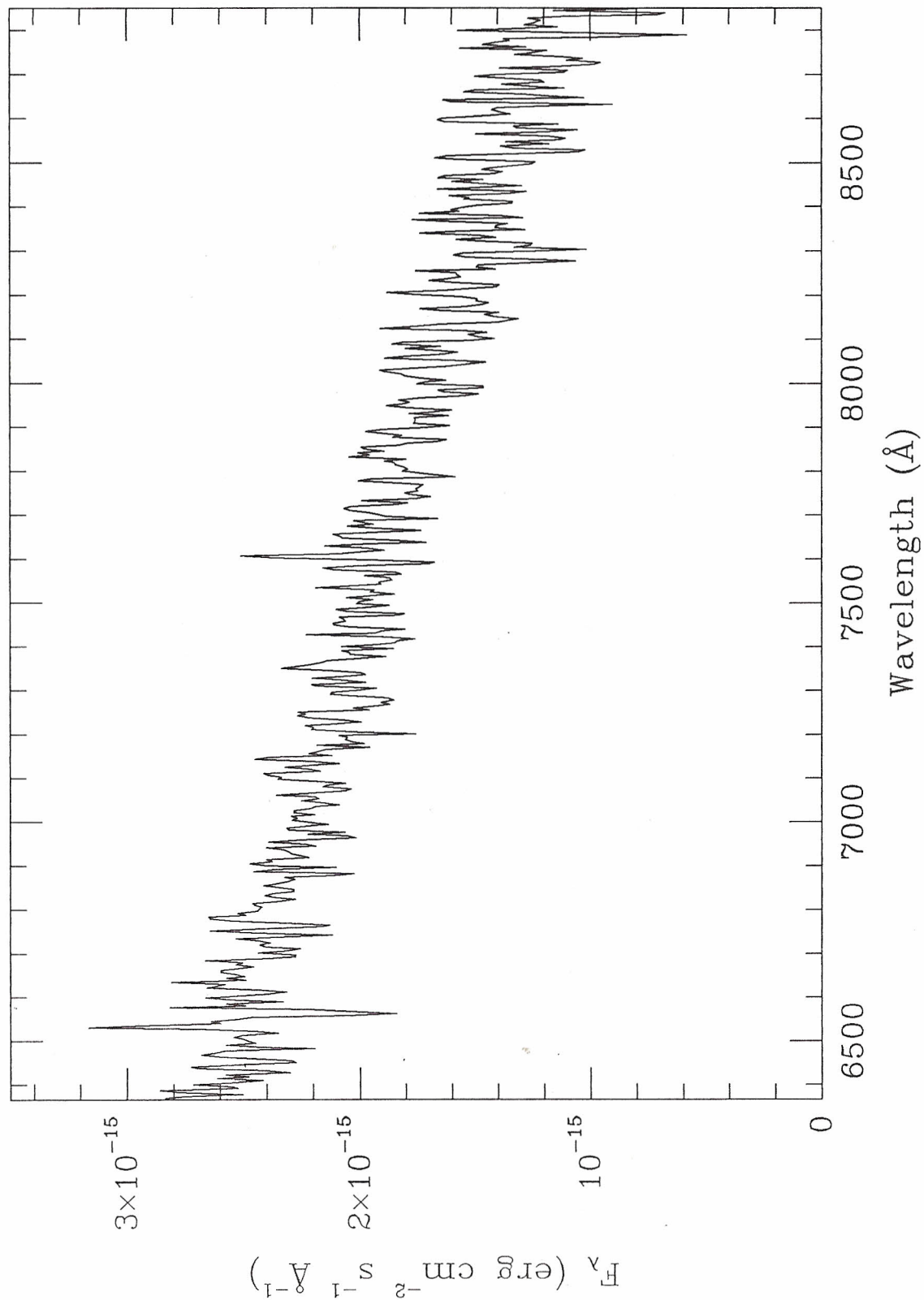
PG 2300+166 - 1989 November 9 04:25 UT



PG 2300+166 - 1991 October 20 02:01 UT



PG 2315+071 - 1991 October 21 02:42 UT



References

- Abbott, T. M. C., Shafter, A. W., Wood, J. H., Tomaney, A. B., & Haswell, C. A. 1990, *PASP*, 102, 558
- Adam, J. 1990, *A&A*, 240, 541
- Adam, J., Innes, D. E., Shaviv, G., Störzer, H., & Wehrse, R. 1989, in *Theory of Accretion Disks*, ed. F. Meyer, W. J. Duschl, J. Frank, & E. Meyer-Hofmeister (Kluwer), 173
- Ando, H., Okazaki, A., & Nishimura, S., 1982, *PASJ*, 34, 141
- Andronov, I. L. 1986a, *Astron. Tsirk.*, 1417, 5
- _____. 1986b, *Astron. Tsirk.*, 1432, 7
- _____. 1991, *IBVS No.* 3645
- Andronov, I. L., Kimeridze, G. N., Richter, G. A., & Smykov, V. P. 1989, *IBVS No.* 3388
- Bailey, J. 1979, *MNRAS*, 189, 41p
- Bailey, J. 1981, *MNRAS*, 197, 31
- Bath, G. T. 1973, *Nat. Phys. Sci.*, 246, 84
- Bath, G. T., & Shaviv, G. 1978, *MNRAS*, 183, 515
- Berg, C., Wegner, G., Foltz, C. B., Chaffee, F. H. & Hewett, P. C. 1992, *ApJS*, 78, 409
- Berriman, G. 1987, *A&AS*, 68, 41
- Bessell, M. S. 1986, *PASP*, 98, 1303
- _____. 1991, *AJ*, 101, 662
- Beuermann, K., & Thomas, H. C., 1990, *A&A*, 230, 326
- Beuermann, K., Thorstensen, J. R., Schwope, A. D., Ringwald, F. A., & Sahin, H. 1992, *A&A*, 256, 442
- Bianchini, A. 1990, *AJ*, 99, 1941

- Biermann, P., Schmidt, G. D., Liebert, J., Stockman, H. S., Tapia, S., Kuhr, H.,
Strittmatter, P. A., West, S., & Lamb, D. Q. 1985, *ApJ*, 293, 303
- Bode, M. F., Duerbeck, H. W., & Evans, A. 1989, in *Classical Novae*, ed. M. F. Bode &
A. Evans (Wiley), 249
- Boeshaar, P. C. 1976, Ph.D. thesis, Ohio State University
- Böhm-Vitense, E., Nemec, J., & Proffitt, C. 1984, *ApJ*, 278, 726
- Bray, R. J., & Loughhead, R. E. 1974, *The Solar Chromosphere* (Chapman & Hall), 165
- Bruch, A. 1984, *A&AS*, 56, 441
- _____. 1989, *A&AS*, 78, 145
- Bruch, A., Fischer, F.-J., & Wilmsen, U. 1987, *A&AS*, 70, 481
- Buckley, D. A. H., Sullivan, D. J., Remillard, R. A., Tuohy, I. R., & Clark, M. 1990,
ApJ, 355, 617
- Cash, W. 1979, *ApJ*, 228, 939
- Chen, J.-S., Liu, X.-W., & Wei, M.-Z. 1991, *A&A*, 242, 397
- Ciardullo, R., Ford, H. C., Neill, J. D., Jacoby, G. H., & Shafter, A. W. 1987, *ApJ*,
318, 520
- Clarke, J. T., Capel, D., & Bowyer, S. 1984, *ApJ*, 287, 845
- Claudi, R., Bianchini, A., & Munari, U. 1990, *IAU Circ. No.* 4975
- Cohen, J. 1985, *ApJ*, 292, 90
- Cook, M. C. 1985, *MNRAS*, 215, 81p
- Córdova, F. A., & Howarth, I. D. 1987, in *Exploring the Universe with the IUE Satellite*,
ed. Y. Kondo (D. Reidel), 395
- Cropper, M. 1990, *Space Sci. Rev.* 54, 195
- Cropper, M., Mason, K. O., Allington-Smith, J. R., Branduardi-Raymont, G.,
Charles, P. A., Mittaz, J. P. D., Mukai, K., Murdin, P. G., Smale, A. P. 1989,
MNRAS, 236, 29p

- Davey, S., & Smith, R. C. 1992, MNRAS, 257, 476
- de Kool, M., & Ritter, H. 1993, A&A, 267, 397
- Demers, S., Fontaine, G., Wesemael, F., Lamontagne, R. & Irwin, M. J. 1987, in The
Second Conference on Faint Blue Stars, ed. A. G. Davis Philip, D. S. Hayes, &
J. W. Liebert (L. Davis Press), 497
- Dhillon, V. S., Jones, D. H. P., Marsh, T. R., & Smith, R. C. 1992, MNRAS, 258, 225
- Dhillon, V. S., Marsh, T. R., & Jones, D. H. P. 1990, in Accretion-Powered Compact
Binaries, ed. C. W. Mauche (Cambridge Univ. Press), 127
- _____. 1991, MNRAS, 252, 342
- Diaz, M. P., & Steiner, J. E. 1990, A&A, 238, 170
- Dobrzycka, D., & Howell, S. B. 1992, ApJ, 388, 614
- Downes, R. A. 1986a, ApJS, 61, 569
- _____. 1986b, ApJ, 307, 170
- _____. 1987, ApJ, 316, 763
- Duerbeck, H. W. 1984, Ap&SS, 99, 363
- Eason, E. L. E., Worden, S. P., Klimke, A., & Africano, J. L. 1984, PASP, 96, 372
- Echevarría, J. 1984, Rev. Mex. Astron. Astrofis., 9, 99
- Eddington, A. S. 1940, MNRAS, 100, 354
- Eggleton, P. P. 1983, ApJ, 268, 368
- Feibelman, W. A. 1987, PASP, 99, 270 1987
- Feibelman, W. A., & Bruhweiler, F. C. 1989, ApJ, 347, 901
- Ferguson, D. H., Green, R. F., & Liebert, J. 1984, ApJ, 287, 320
- Ferguson, D.H., Liebert, J., Cutri, R., Green, R. F., Willner, S. P., Steiner, J. E.,
Tokarz, S. 1987, ApJ, 316, 399
- Ferguson, D.H., Liebert, J., Green, R. F., McGraw, J. T., & Spinrad, H. 1981, ApJ,
251, 205

- Fleming, T. A., Liebert, J., & Green, R. F. 1986, *ApJ*, 308, 176 (FLG86)
- Frank, J., King, A., & Raine, D. 1992, *Accretion Power in Astrophysics*, Second Edition (Cambridge Univ. Press), Ch. 5
- Friend, M. T., Martin, J. S., Smith, R. C., & Jones, D. H. P. 1988, *MNRAS*, 233, 451
- _____. 1990, *MNRAS*, 246, 654
- Ford, H. C. 1978, *ApJ*, 219, 595
- Garnavich, P. M., Szkody, P., Mateo, M., Feinswog, L., Booth, J., Goodrich, B., Miller, H. R., Carini, M. T., & Wilson, J. W. 1990, *ApJ*, 365, 696
- Garrison, R. F. 1987, in *Physics of Be Stars*, ed. A. Slettebak & T. P. Snow (Cambridge Univ. Press), 460
- Grauer, A. D., Ringwald, F. A., Wegner, G., Liebert, J., Schmidt, G., & Green, R. F. 1993, in preparation
- Green, R. F. 1980, *ApJ*, 238, 685
- _____. 1991, private communication
- Green, R. F., Greenstein, J. L., & Boksenberg, A. 1976, *PASP*, 88, 598 (GGB76)
- Green, R. F., Ferguson, D. H., Liebert, J., & Schmidt, M. 1982, *PASP*, 94, 560 (GFLS82)
- Green, R. F., & Morrill, M. E. 1978, *PASP*, 90, 601
- Green, R. F., Schmidt, M., & Liebert, J. 1986, *ApJS*, 61, 305 (GSL86)
- Greenstein, J. L., Arp, H. C., & Shectman, S. 1977, *PASP*, 89, 741 (GAS77)
- Haefner, R. 1989, *A&A*, 213, L15
- Hameury, J. M., King, A. R., & Lasota, J. P. 1991, *A&A*, 248, 525
- Hameury, J. M., King, A. R., Lasota, J. P., & Ritter, H. 1988, *MNRAS*, 231, 535
- Hantzios, P. P. 1992, Ph.D. thesis, Ohio State University
- Harrison, T., & Gehrz, R. D. 1992, *AJ*, 103, 243

- Hassal, B. J. M., Pringle, J. E., Schwarzenberg-Czerny, A., Wade, R. A.,
 Whelan, J. A. J., & Hill, P. W. 1983, MNRAS, 203, 865
- Hazen, M. L. 1986, IBVS No. 2880
- Heber, U. 1986, A&A, 155, 33
- Hertzog, K. P. 1986, Observatory, 106, 38
- Hessman, F. V. 1989, AJ, 98, 675
- _____. 1990, IAU Circ. No. 4971
- Honey, W. B., Charles, P. A., Whitehurst, R., Barrett, P. E., & Smale, A. P., 1988,
 MNRAS, 231, 1
- Honeycutt, R. K., Kaitchuck, R. H., & Schlegel, E. M., 1987, ApJS, 65, 451
- Honeycutt, R. K., Schlegel, E. M., & Kaitchuck, R. H. 1986, ApJ, 302, 388
- Horne, J. H., & Baliunas, S. L., 1986, ApJ, 302, 757
- Horne, K., & Marsh, T. R. 1986, MNRAS, 218, 761
- Horne, K., Wade, R. A., & Szkody, P. 1986, MNRAS, 219, 791
- Howell, S. B., & Szkody, P. 1990, ApJ, 356, 623
- Howell, S. B., Szkody, P., Kreidl, T. J., & Dobrzycka, D. 1991, PASP, 103, 300
- Howell, S. B., Szkody, P., Kreidl, T. J., Mason, K. O., & Puchnarewicz, E. M. 1990,
 PASP, 102, 758
- Hurst, G. M., & Lubbock, S. 1988, IAU Circ. 4691
- Hutchings, J. B., & Cowley, A. P. 1985, PASP, 97, 328
- Kaitchuck, R. H., Mansperger, C. S., & Hantzios, P. P. 1988, ApJ, 330, 305
- Kaluzny, J., 1986, IAU Circ. No. 4287
- Kato, S., 1989, in Theory of Accretion Disks, ed. F. Meyer, W. J. Duschl, J. Frank, &
 E. Meyer-Hofmeister (Kluwer), 173
- Kawaler, S. D. 1988, ApJ, 333, 236
- Keenan, P. C., & Hynek, J. A. 1950, ApJ, 111, 1

- Kenyon, S. J. 1986, *The Symbiotic Stars* (Cambridge Univ. Press)
- Kholopov, P. N. et al. 1985, *General Catalogue of Variable Stars*, 4th ed. (Nauka)
- King, A. R. 1988, *QJRAS*, 4, 1
- _____. 1989, *MNRAS*, 241, 365
- Kirkpatrick, J. D., Henry, T. J., & McCarthy, D. W., Jr., 1991, *ApJS*, 77, 417
- Kojoian, G., Chute, P. A., & Aumann, C. E. 1984, *AJ*, 89, 332
- Kondo, M., Noguchi, T., & Maehara, H. 1984, *Ann. Tokyo Astron. Obs.*, 20, 130
- Kondo, M., Wantanabe, E., Yutani, M., & Noguchi, T. 1982, *PASJ*, 34, 541
- Kopylov, I. M., Lipovetskii, V. A., Somov, N. N., Somova, T. A., & Stepanyan, Dzh. A.
1988, *Astrofizika*, 8, 33
- Kraft, R. P. 1963, *ApJ*, 135, 408
- Kraft, R. P., & Luyten, W. J. 1965, *ApJ*, 142, 1041
- Kroupa, P., Tout, C. A., & Gilmore, G. 1990, *MNRAS*, 244, 76
- la Dous, C. 1991, *A&A*, 252, 100
- Liebert, J., & Stockman, H. S., 1980, *PASP*, 92, 657
- Liebert, J., Stockman, H. S., Williams, R. E., Tapia, S., Green, R. F., Rautenkrantz, D.,
Ferguson, D. S., & Szkody, P. 1982, *ApJ*, 256, 594
- Liller, W., & Eachus, L. 1976, *IAU Circ.* 2907
- Linsky, J. L. 1988, in *Multiwavelength Astrophysics*, ed. F. A. Córdova (Cambridge Univ. Press), 49
- Livio, M. 1992, STScI preprint 659, in the proceedings of the 22nd "SAAS FEE"
Advanced Course, Interacting Binaries. In press
- Lomb, N. R. 1976, *ApSS*, 39, 447
- Luppino, G. A. 1989, *PASP*, 101, 931
- Maceroni, C., Bianchini, A., Rodonò, M., Van't Veer, F. & Vio, R. 1990, *A&A*, 237, 395
- Mansperger, C. S., & Kaitchuck, R. H. 1990, *ApJ*, 358, 268 (MK90)

- Margon, B., Downes, R. A., & Katz, J. I. 1981, *Nature*, 293, 200
- Markarian, B. E. 1968, *Astrofizika*, 4, 144
- _____. 1969, *Astrofizika*, 5, 443
- Markarian, B. E., Lipovetskii, V. A., & Stepanyan, Dzh. A. 1981, *Astrofizika*, 17, 619
- Marsh, T. R. 1990, *ApJ*, 357, 621
- Marsh, T. R., Horne, K., & Shipman, H. L. 1987, *MNRAS*, 225, 551
- Mason, K. O., Reichert, G. A., Bowyer, S. & Thorstensen, J. R. 1982, *PASP*, 94, 521
- Mateo, M., Szkody, P., & Bolte, M. 1985, *ApJ*, 97, 45
- Mateo, M., Szkody, P., & Garnavich, P. 1991, *ApJ*, 370, 370
- Mattei, J. A. 1989, Observations from the International AAVSO Database, private communication
- _____. 1990, in *Active Close Binaries*, ed. C. Ibanoglu (Kluwer), 611
- _____. 1991, List of AAVSO Program Stars, private communication
- McClure, R. D. 1983, *ApJ*, 268, 264
- McClure, R. D., Fletcher, J. M., & Nemec, J. M. 1980, *ApJ*, 238, L35
- McCook, G. P., & Sion, E. M. 1984, Villanova Univ. Obs. Contr., No. 3 (Villanova)
- McDermott, P. N. & Taam, R. E. 1989, *ApJ* 342, 1019
- McNaught, R. H. 1986, IBVS No. 2926
- Meyer, F., & Meyer-Hofmeister, E. 1983, *A&A*, 121, 29
- Mineshige, S. 1988, *A&A*, 190, 72
- Moehler, S., Richtler, T., de Boer, K. S., Dettmar, R. J., & Heber, U. 1990, *A&AS*, 86, 53
- Molnar, L. A., & Kobulnicky, H. A. 1992, *ApJ*, 392, 678
- Mukai, K., & Charles, P. A. 1986, *MNRAS*, 222, 1p
- Mukai, K., Mason, K. O., Howell, S. B., Allington-Smith, J., Callanan, P. J., Charles, P. A., Hassall, B. J. M., Machin, G., Naylor, T., Smale, A. P., &

- van Paradijs, J. 1990, MNRAS, 245, 385.
- Noguchi, T., Maehara, H., & Kondo, M. 1980, Ann. Tokyo Astron. Obs., 18, 55
- O'Donoghue, D., Chen, A., Marang, F., Mittaz, J. P. D., Winkler, H., & Warner, B. 1991, MNRAS, 250, 363
- O'Donoghue, D., Warner, B., Wargau, W., & Grauer, A. D. 1989, MNRAS, 240, 41
- Oke, J. B. 1974, ApJS, 27, 21
- Oke, J. B., & Gunn, J. E. 1983, ApJ, 266, 713
- Oke, J. B., & Wade, R. A. 1982, AJ, 87, 670
- Osaki, Y. 1974, PASJ, 26, 429
- _____. 1989, PASJ, 41, 1005
- Osminkin, E. Yu. 1985, Perem. Zvezdy, 22, 261
- Paczynski, B., & Schwarzenberg-Czerny, A. 1980, Acta Astr., 30, 127
- Patterson, J. 1984, ApJS, 54, 443
- _____. 1986, private communication to Downes (1986a)
- Patterson, J. & Eisenmann, N. 1987, IBVS No. 3079
- Patterson, J., & Richman, H. 1991, PASP, 103, 735
- Patterson, J., Schwartz, D. A., Pye, J. P., Blair, W. P., Williams, G. A., & Caillault, J.-P. 1992, ApJ, 392, 233
- Penning, W. R., Ferguson, D. H., McGraw, J. T., Liebert, J., & Green, R. F. 1984, ApJ, 276, 233
- Pesch, P., & Sanduleak, N. 1989, ApJS, 70, 163
- Peterson, S. D. 1973, AJ, 78, 811
- Plavec, M., & Kratochvil, P., 1964, Bull. Astron. Inst. Czech., 15, 165
- Press, W. H., Teukolsky, S. A., Vetterling, W. T., & Flannery, B. 1992, Numerical Recipes in FORTRAN, Second Edition (Cambridge Univ. Press)
- Politano, M. J. 1988, Ph.D. thesis, University of Illinois

- Rappaport, S., Verbunt, F., & Joss, P. C. 1983, *ApJ*, 275, 713
- Reid, N. 1987, *MNRAS*, 225, 873
- Reid, N., Wickramasinghe, D. T., & Bessell, M. S. 1983, *Proc. Astr. Soc. Australia*, 5, 230
- Remillard, R. A., Bradt, H. V., McClintock, J. E., & Tuohy, I. R., 1992, preprint
- Richter, G. A. 1989, *Astron. Nachr.*, 310, 143
- Ringwald, F. A. 1991, *BAAS*, 23, 1463
- Ringwald, F. A., Thorstensen, J. R., & Hamwey, R. M. 1993, in preparation
- Ritter, H. 1986a, *A&A*, 168, 105
- _____. 1986b, *A&A*, 169, 139
- _____. 1990, *A&AS*, 85, 1179
- Ritter, H., & Özkan, M. T. 1986, *A&A*, 167, 260
- Ritter, H., Politano, M., Livio, M., & Webbink, R. F. 1990, *ApJ*, 376, 177
- Robinson, E. L. 1975, *AJ*, 80, 515
- _____. 1976, *ARA&A*, 14, 119
- _____. 1983, in *Cataclysmic Variables and Related Objects*, ed. M. Livio & G. Shaviv (D. Reidel), 1
- Robinson, E. L., Zhang, E.-H., & Stover, R. J. 1986, *ApJ*, 305, 732
- Rosen, S. R., Branduardi-Raymont, G., Mason, K. O., & Murdin, P. G. 1989, *MNRAS*, 237, 1037
- Russell, H. N. 1945, *ApJ*, 102, 1
- Rutten, R. G. M., Kuulkers, E., Vogt, N., & van Paradijs, J. 1992b, *A&A*, 265, 159
- Rutten, R. G. M., van Paradijs, J., & Tinbergen, J. 1992a, *A&A*, 260, 213
- Sanduleak, N. 1983, *PASP*, 95, 619
- Scargle, J. D. 1982, *AJ*, 263, 835
- Schmeer, P. 1990, *IAU Circ.* 5051

- Schmidt, M. 1968, *ApJ*, 151, 393
- Schneider, D. P., & Young, P. J. 1980, *ApJ*, 238, 946
- Shafter, A. W. 1983a, *ApJ*, 267, 222
- _____. 1983b, Ph.D. thesis, Univ. of California, Los Angeles
- _____. 1991, in *Fundamental Properties of Cataclysmic Variable Stars*, ed. A. W. Shafter (Mount Laguna Obs.), 39
- Shafter, A. W., Hessman, F. V., & Zhang, E. H. 1988, *ApJ*, 327, 248
- Shafter, A. W., Robinson, E. L., Crampton, D., Warner, B., & Prestage, R. M. 1990, *ApJ*, 354, 708
- Shafter, A. W., & Szkody, P. 1984, *ApJ*, 276, 305
- Shafter, A. W., Szkody, P., Liebert, J., Penning, W. R., Bond, H. E., & Grauer, A. D. 1985, *ApJ*, 290, 707
- Shafter, A. W., Szkody, P., & Thorstensen, J. R. 1986, *AJ*, 308, 765
- Shafter, A. W., Wheeler, J. C., & Cannizzo, J. K. 1986, *ApJ*, 305, 261
- Shara, M. M. 1989, *PASP*, 101, 5
- Shara, M. M., Livio, M., Moffat, A. F. J., & Orio, M. 1986, *AJ*, 311, 163
- Shu, F. H., Cuzzi, J. N., & Lissauer, J. J. 1983, *Icarus*, 53, 185
- Silber, A. D. 1992, Ph.D. thesis, Massachusetts Institute of Technology
- Silva, D. R., & Cornell, M. E. 1992, *ApJS*, 81, 865
- Smak, J., 1984, *PASP*, 86, 5
- _____. 1992, in *Evolutionary Processes in Interacting Binary Stars*, ed. Y. Kondo, R. Sistero, & R. S. Polidan (Kluwer), 83
- Stobie, R. S., Morgan, D. H., Bhatia, R. K., Kilkenny, D., & O'Donoghue, D. 1987, in *The Second Conference on Faint Blue Stars*, ed. A. G. Davis Philip, D. S. Hayes, & J. W. Liebert (L. Davis Press), 493
- Stockman, H. S., Schmidt, G. D., Berriman, G., Liebert, J., Moore, R. L., &

- Wickramasinghe, D. T., 1992, *ApJ*, 401, 628
- Stone, R. P. S. 1977, *ApJ*, 218, 767
- Szkody, P. 1985, *AJ*, 90, 1837
- _____. 1987, *AJ*, 94, 1055
- _____. 1988, *PASP*, 100, 791
- _____. 1991, in *Fundamental Properties of Cataclysmic Variable Stars*, ed. A. W. Shafter (Mount Laguna Obs.), 56
- Szkody, P., Downes, R., & Mateo, N. 1988, *PASP*, 100, 362
- Szkody, P., & Feinswog, L. 1988, *AJ*, 334, 422
- Szkody, P., & Howell, S. B. 1992, *ApJS*, 78, 537
- _____. 1993, *ApJ*, 403, 743
- Szkody, P., Howell, S. B., Mateo, M., & Kreidl, T. J. 1989, *PASP*, 101, 899
- Szkody, P., & Mateo, M. 1983, *PASP*, 95, 596
- Szkody, P., & Mattei, J. A. 1984, *PASP*, 96, 988
- Szkody, P., & Piché, F. 1990, *ApJ*, 361, 235
- Szkody, P., Piché, F., & Feinswog, L. 1990, *ApJS*, 73, 441
- Taam, R. E., & Spruit, H. C. 1989, *AJ*, 345, 972
- Thomas, R. M., Morton, D. C., & Murdin, P. G. 1979, *MNRAS*, 188, 19
- Thorstensen, J. R. 1986, *AJ*, 91, 940
- Thorstensen, J. R., & Freed, I. W. 1985, *AJ*, 90, 2082.
- Thorstensen, J. R., Charles, P. A., Margon, B., & Bowyer, S. 1987, *ApJ*, 223, 260
- Thorstensen, J. R., Davis, M.K., & Ringwald, F. A. 1991a, *AJ*, 102, 683
- Thorstensen, J. R., Ringwald, F. A., Wade, R. A., Schmidt, G. D., & Norsworthy, J. E.
1991b, *AJ*, 102, 272
- Thorstensen, J. R., Wade, R. A., & Oke, J. B. 1986, *ApJ*, 309, 721
- Thorstensen, J. R., Wegner, G. A., Hamwey, R., Boley, F., Geller, M. J., Huchra, J. P.,

- Kurtz, M. J., & McMahan, R. K. 1989, *AJ*, 98, 1143
- Udalski, A. 1990a, *AJ*, 100, 226
- _____. 1990b, *IBVS* No. 3425
- Veilleux, S., & Osterbrock, D. E. 1987, *ApJS*, 63, 295
- Verbunt, F., & Zwann, C. 1981, *A&A*, 100, L7
- Vogt, N. 1989, in *Classical Novae*, ed. M. F. Bode & A. Evans (Wiley), 225
- Wade, R. A. 1988, *ApJ*, 335, 394
- Wade, R. A., & Horne, K. 1988, *ApJ*, 324, 411
- Wade, R. A., & Ward, M. J. 1985, in *Interacting Binary Stars*, ed. J. E. Pringle & R. A. Wade (Cambridge Univ. Press), 129
- Warner, B. 1974, *M.N.A.S. So. Africa*, 33, 21
- _____. 1976, *Observatory*, 96, 49
- _____. 1985, in *Interacting Binaries*, ed. P. P. Eggleton & J. E. Pringle. (D. Reidel), 367
- _____. 1987, *MNRAS*, 227, 23
- _____. 1988, *High Speed Astronomical Photometry* (Cambridge Univ. Press)
- Warner, B., & Nather, R. E. 1971, *MNRAS*, 152, 219
- Webbink, R. F. 1989, in *Critical Observations Versus Physical Models for Close Binary Systems*, ed. K. C. Leung (Gordon & Breach), 403
- _____. 1990, unpublished
- Webbink, R. F., Livio, M., Truran, J. W., & Orio, M. 1987, *ApJ*, 314, 653
- Wegner, G., & McMahan, R. K. 1985, *AJ*, 90, 1511
- _____. 1986, *AJ*, 91, 139
- _____. 1988, *AJ*, 96, 1933
- Wegner, G., & Swanson, S. R. 1990a, *AJ*, 99, 330
- _____. 1990b, *AJ*, 100, 1274
- _____. 1991, *ApJS*, 75, 507

- Wegner, G., McMahan, R. K., & Boley, F. I. 1987, AJ, 94, 1271
- Wenzel, W. 1982, IBVS No. 2256
- Wesemael, F., Green, R. F., & Liebert, J. 1985, ApJS, 58, 379
- Whitehurst, R. 1988, MNRAS, 232, 35
- Wickramasinghe, D. T. 1988, in Polarized Radiation of Circumstellar Origin,
ed. G. V. Coyne et al. (Vatican Obs.), 3
- Williams, G. A. 1983, ApJS, 53, 523
- Williams, R. E. 1989, AJ, 97, 1752
- Williams, R. E., & Ferguson, D. H. 1982, ApJ, 257, 672
- . 1983, in Cataclysmic Variables & Related Objects, ed. M. Livio & G. Shaviv
(D. Reidel), 97
- Wilson, J. W., Miller, H. R., Africano, J. L., Goodrich, B. D., Mahaffey, C. T., &
Quigley, R. J. 1986, A&AS, 66, 323
- Woltjer, L. 1975, A&A, 42, 109
- Wood, J. H. 1986. Ph. D. thesis, Cambridge University
- Wood, J. H., & Marsh, T. R. 1991, ApJ, 381, 551
- Wood, K. S., Meekins, J. F., Yentis, D. J., Smathers, H. W., McNutt, D. P., Bleach,
R. D., Bryam, E. T., Chubb, T. A., Friedman, H., & Meidaw, M., 1984. ApJS,
56, 507
- Young, P., Schneider, D. P., & Shectman, S. A. 1981, ApJ, 244, 259
- Zhang, E., Robinson, E. L., & Nather, R. E. 1986, ApJ, 305, 740
- Zhang, E., Robinson, E. L., Ramseyer, T. F., Shetrone, M. D., & Stiening, R. F. 1991,
ApJ, 381, 534

(What are you looking here for? Get back to work!)